SEISMIC HAZARD ANALYSIS OF NEPAL

A THESIS SUBMITTED TO THE

CENTRAL DEPARTMENT OF GEOLOGY

INSTITUTE OF SCIENCE AND TECHNOLOGY

TRIBHUVAN UNIVERSITY

NEPAL

FOR THE AWARD OF DOCTOR OF PHILOSOPHY

IN GEOLOGY

BY

SUDHIR RAJAURE

JUNE 2019

SEISMIC HAZARD ANALYSIS OF NEPAL

A THESIS SUBMITTED TO THE

CENTRAL DEPARTMENT OF GEOLOGY

INSTITUTE OF SCIENCE AND TECHNOLOGY

TRIBHUVAN UNIVERSITY

NEPAL

FOR THE AWARD OF DOCTOR OF PHILOSOPHY

IN GEOLOGY

BY

SUDHIR RAJAURE

JUNE 2019

DECLARATION

Thesis entitled "**Seismic Hazard Analysis of Nepal**" submitted to the Central Department of Geology, Institute of Science and Technology (IOST), Tribhuvan University, Nepal for the award of the degree of Doctor of Philosophy (Ph.D.), is a research work carried out by me under the supervision of Prof. Dr. Lalu Prasad Paudel, Central Department of Geology, Tribhuvan University, Nepal and co-supervised by Senior Seismologist. Dr. Susan Hough, United States Geological Survey, USA.

This research is original and has not been submitted earlier in part or full in this or any other form to any university or institute, here or elsewhere, for the award of any degree.
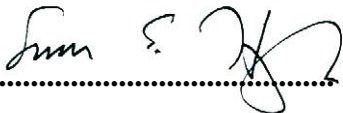
Sudhir Rajaure

June 2019

RECOMMENDATION

This is to recommend that **Sudhir Rajaure** has carried out research entitled "**Seismic Hazard Analysis of Nepal**" for the award of Doctor of Philosophy (Ph.D.) in **Geology** under my/our supervision. To my/our knowledge, this work has not been submitted for any other degree.

He has fulfilled all the requirements laid down by the Institute of Science and Technology (IOST), Tribhuvan University, Kirtipur for the submission of the thesis for the award of Ph.D. degree.

....

Prof. Dr. Lalu Prasad Paudel

Supervisor

Central Department of Geology

Tribhuvan University, Kirtipur, Kathmandu,

Nepal

....

Dr. Susan E. Hough

Co-supervisor

Senior Seismologist

United States Geological Survey

California, USA

June 2019

LETTER OF APPROVAL

06/03/2076 B.S.

On the recommendation of Prof. Dr. **Lalu Prasad Paudel**/Senior Seismologist Dr. **Susan Hough**, this Ph.D. thesis submitted by Mr. **Sudhir Rajaure** entitled "**Seismic Hazard Analysis of Nepal**" is forwarded by Central Department Research Committee (CDRC) to the Dean, IOST, T.U..

....

Prof. Dr. Lalu Prasad Paudel

Professor and Head,

Central Department of Geology

Tribhuvan University

Kirtipur, Kathmandu

Nepal

ACKNOWLEDGEMENTS

Sudhir Rajaure

June, 2019

ABSTRACT

Nepal is situated in the central part of the Himalaya, which is one of the most seismically active zones in the world. Nepal has witnessed several mega-quakes, with magnitude above 8, and thousands of smaller earthquakes. The 2015 Mw 7.8 Gorkha earthquake is the most recent significant event in the country. Large and moderately large earthquakes can have a tragic impact on people and society as a whole. The preparation of seismic hazard map and evaluation of site specific ground motion due to earthquake are recognized as the fundamental steps towards the earthquake risk reduction.

An attempt is made to develop seismic hazard maps of Nepal using available data of earthquakes, recent knowledge of seismotectonics and refined geological features. A comprehensive and magnitude-homogenized earthquake catalogue is prepared from the processing of earthquake catalogues collected from different sources. Thus prepared catalogue contains earthquake data since 1100 AD to 2017 AD. Nine sets of potential earthquake source models are delineated after the analysis of the seismicity distribution, geological structures, results of different geophysical and geodetic surveys and the experience of 2015 Gorkha Earthquake.

Probabilistic technique of seismic hazard analysis is applied to evaluate seismic hazard in Nepal. The result shows high hazard in an east-west elongated belt that runs parallel to the front of the Higher Himalaya. The maximum PGA reaches about 0.45 g in far-west Nepal and about 0.4 g in Kathmandu Valley for 10 % probability of exceedance in 50 years, at engineering rock site.

The effect of the sediments of the Kathmandu sedimentary basin is investigated using strong motion data of earthquakes recorded in the Kathmandu Valley. During the Mw 7.8 (Gorkha) earthquake, the largest PGA (0.25 g) was recorded at Kirtipur (KTP), which is a rock site. The record shows a single and unusual spike, which is attributed to the permanent displacement of the Main Himalayan Thrust. The second largest PGA (0.23 g) was recorded at the Central Department of Geology (Tribhuvan University (TVU)), which is a soil site. During the Mw 7.8 earthquake, the PGAs were

comparatively smaller at all soil sites, whereas the peak ground velocity (PGV) was small at KTP (rock site) and were larger at all other soil sites.

The strong motion records of the earthquakes depict the predominant period being between 3 and 5 seconds at the soil sites. The high frequencies (>2.5 Hz), were strongly damped and the low frequencies (<2.5 Hz) were amplified at the soil sites, therefore tall buildings suffered more and the low rise buildings suffered less when compared. The amplification factor was small during the stronger earthquakes and was large during smaller earthquakes; thus demonstrating non-linear response of soil. The analysis shows that the azimuthal effect of earthquake sources was not observed in the Kathmandu Valley.

Earlier reports on the 1934 Bihar-Nepal Earthquake (Mw 8.2) and 1833 North Kathmandu Earthquake (Mw ~7.6) report localized massive destruction in the Kathmandu valley and attribute the massive destruction to local geology of the basin (Pandey and Molnar, 1988). Contrary to these claims, amplification of ground acceleration was not observed in the Kathmandu valley during the 2015 Gorkha Earthquake but the low frequencies were amplified.

The seismic hazard map and ground response results are mandatorily considered in policy making, planning, formulation and revision of building codes, design of new infrastructures and retrofitting of existing infrastructures. It facilitates the seismic risk assessment, insurance policies and many other related matters.

LIST OF ACRONYMS AND ABBREVIATIONS

DMG   : Department of Mines and Geology

DSHA   : Deterministic Seismic Hazard Analysis

GSHAP   : Global Seismic Hazard Program

IRIS   : Incorporated Research Institutions for Seismology

ISC   : International Seismological Centre

ISC-GEM   : International Seismological Centre-Global Earth Model

Jyb   : Shortest distance between a site and the surface projection of
               the rupture surface

MBT   : Main Boundary Thrust

MFT   : Main Central Thrust

MCT   : Main Central Thrust

MHT   : Main Himalayan Thrust

NEHRP   : National Earthquake Hazard Reduction Program

PGA   : Peak Ground Acceleration

PSA   : Peak Spectral Acceleration

PSHA   : Probabilistic Seismic Hazard Analysis

Rrup   : Rrup is the closest distance to the rupture surface from a site

SA   : Spectral Acceleration

SHA   : Seismic Hazard Analysis

USGS   : United States Geological Survey

LIST OF SYMBOLS

λ : Annual exceedance rate of earthquake

β : 2.303 * b-value

∫ : function of

Δ : increment

∑ : sum

g : Acceleration due to gravity (9.8 m/sec2)

LIST OF TABLES

LIST OF FIGURES

xviii

LIST OF APPENDICES

Appendix 1:   List of publications and full content of the papers

Appendix 2:   List of conference attended and conference abstracts

Appendix 3:   NEHRP soil classification system

Appendix 4:   Local earthquakes relocated using double difference techniques after Rajaure *et al*. (2013)

Appendix 5:   Geological map of Nepal published by the Department of Mines and Geology (1987)

Appendix 6:   Active fault distribution in Nepal

Appendix 7:   Google Earth image of Nepal and surrounding region.

Appendix 8:   Geological structures, fold axis and lineaments in the region

Appendix 9:   Subsurface ridges in north India.

Appendix 10:   Possible segments along the Himalaya and their potential magnitudes at the present

Appendix 11:   Potential earthquake sources, identified in the present study. There are altogether nine source models.

Appendix 12:   Generalized section across the Himalaya (USGS poster).

Appendix 13:   Variation in PGA with variation in depth of source plane.

Appendix 14:   Variation in seismic hazard with variation in maximum potential magnitude. Common model (Appendix 11-1), common attenuation relation and common recurrence parameters were used in this test.

Appendix 15:   Maximum potential magnitude and earthquake recurrence parameters of identified earthquake sources.

Appendix 16:   Variation of seismic hazard with variation in b-value.

Appendix 17:   Variation in seismic hazard with different catalogues and differently estimated a- and b-values.

Appendix 18:   Attenuation relations (also called ground motion prediction equation (GMPE)), which were used in this study.

TABLE OF CONTENTS

CHAPTER 1

INTRODUCTION

1.1. Background

The world faces and suffers from a number of disasters such as floods, droughts, landslides, cyclones, earthquakes, tsunamis and fires every year. A disaster is a serious disruption, occurring over a relatively short time of the functioning of a community or a society involving widespread human, material, economic or environmental loss and impacts, which exceed the ability of the affected community or society to cope using its own resources. Some of the disasters are natural and some are human induced. Earthquake, flood, cyclone etc. are natural disasters caused by the natural processes. Developing countries suffer more when a disaster hits. More than 95 percent of all deaths and casualties caused by hazards occur in developing countries, and losses due to natural hazards are greater (as a percentage of GDP) in developing countries than in developed countries (https://www.usgs.gov/faqs/).

Earthquake is one of the most frightening and destructive phenomena of nature because of its terrible impacts not only to people but also to the society and the nation or beyond. Scientifically speaking, an earthquake is a sudden movement on geological faults, which causes the abrupt release of strain that has accumulated over a long time. The tectonic forces have acted for millions of years and resulted in shaping the Earth as it is at present. Tectonic plates move at certain rate over, under and past each other. During interseismic periods, the plates are locked together, and are unable to release the accumulating energy. When the accumulated energy grows strong enough, the plates break and displacement occurs on geological faults. In general, earthquakes with magnitude smaller than 5 do not cause considerable damage. If the earthquake magnitude is large (usually larger than 5) and occurs in a populated area, the consequences may be very catastrophic. The effect of an earthquake depends on its magnitude, distance between earthquake source and sites, local site effect, construction types, season (rainy or dry), time of occurrence (day, night, and holiday or office hours) and response of people during earthquake. An adverse event will not rise to the level of a disaster if it occurs in an area without vulnerable population. In a

vulnerable area, however, an earthquake can have disastrous consequences with significant damage, which may require years to recover.

Earthquakes in Nepal and the Himalaya region are caused by the release of energy that accumulates on account of the collision between the Indian and the Eurasian Plates (Dewey & Bird, 1970; Powell & Conaghan, 1973). The collision between the two plates is believed to have started about 50 million years ago (Le Fort, 1975; Coward *et al.*, 1986) and it is still active. Collision between these two plates leads to the straining of the crust. This process causes accumulation of energy in the form of elastic deformation in the medium. Continuous collision of tectonic plates and cyclic accumulation and release of elastic energy has been attributed to the development of the Himalayan range.

Nepal is situated in the central part of the Himalaya and has witnessed a number of large earthquakes since the historical times. Earthquakes have occurred more or less in the same regions from pre-historic times. Large earthquakes are rare events in comparison to others. However, the consequences of occasional large earthquakes have remained very painful to the people, society, economy and the nation.

Prediction of earthquakes, till now, is not possible. However, its effects can be minimized by assessing the probability of occurrence of large earthquakes and their probable effects in advance and working out the reduction of earthquake vulnerability. The preparation of a seismic hazard map of an area and the identification of the site-specific response of a ground motion during earthquake could be the fundamental step in mitigating the earthquake risk.

Seismic hazard maps are updated regularly when new findings, knowledge and data become available. Several attempts have been made to assess seismic hazard of Nepal in the past with limited data, limited source models, and limited attenuation relations. A lot of researches have been carried out and the new seismic phenomena have been observed like new seismotectonics of the sources and effects of earthquakes in Nepal. The seismic hazard in Nepal requires a new approach for its investigation utilizing logic tree so that uncertainties in earthquake source geometry, earthquake source location, attenuation relation and maximum potential magnitude could be minimized. Present research incorporates new findings in the field of seismotectonics, source

zonation, size of maximum potential earthquake and observation of 2015 Gorkha Earthquake.

The present research aims to evaluate seismic hazard in Nepal and prepare a seismic hazard map so that the map can be utilized for estimating probable peak ground acceleration of an area during an earthquake. Such data can be used in designing earthquake resistant infrastructures so as to minimize the effect of an earthquake. In addition to the seismic hazard analysis of Nepal, site-specific ground response of the Kathmandu valley was also analyzed using the strong motion data from the 2015 Gorkha Earthquake. Present study, in this regard, is a latest contribution in the field of seismic hazard study of Nepal by considering multiple source models and multiple attenuation relations. Site-specific ground response analysis of the Kathmandu valley using the 2015 Gorkha Earthquake is also a new study for the Kathmandu valley. It is envisaged that, the results of the present study will be very useful for the earthquake-resistant infrastructure development in Nepal.

This thesis is the result of six years continuous work. One paper has been published in an international journal with impact factor and three papers have been published in indexed journal (Appendix 1). Similarly, the results were presented in national and international conferences (Appendix 2). This thesis provides a detailed elaboration of the research questions, objectives, methodology, results and conclusions of the study.

1.2. Geological setting of the Nepal Himalaya

Geologically, Nepal is divided into five major units (Figure 1 and Figure 2), which are the Indo-Gangetic Plain (Terai), the Sub-Himalaya, the Lesser Himalaya, the Higher Himalayan and the Tethys Himalaya, successively from south to the north (Gansser, 1964). These geological units extend approximately parallel to each other and run all along the Nepal Himalaya. The geological units are characterized by their own lithology, tectonics, structures and geological history. Besides the major geological zones, Nepal comprises a number of intermontane basins and dun valleys. The Kathmandu valley is one of the major intermontane basins in Nepal. A brief description of each tectonic zones and geological setting of the Kathmandu valley is given in the following sections.
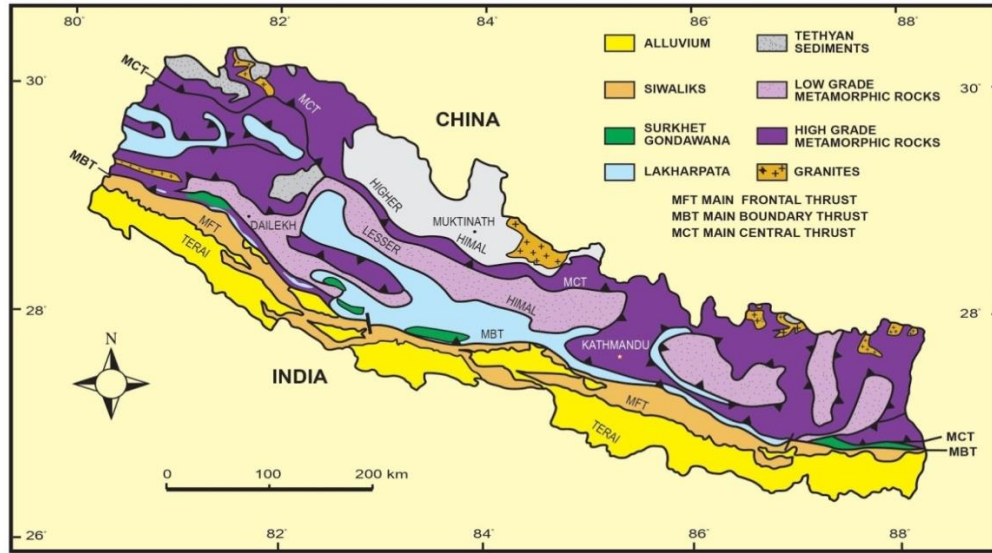
Figure 1: Geological Map of Nepal prepared by Petroleum Exploration Promotion Project, Department of Mines and Geology, Government of Nepal (Source: https://petroleumnepal.gov.np/).
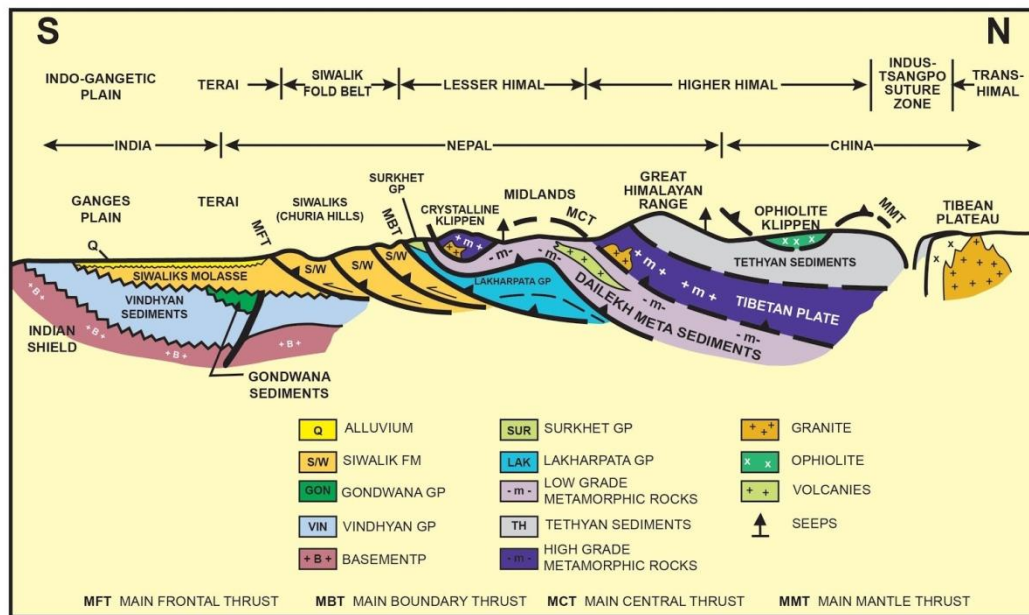
Figure 2: Geological cross section at the longitude of Kathmandu prepared by Petroleum Exploration Project, Department of Mines and Geology, Government of Nepal (Source: https://petroleumnepal.gov.np/).

1.2.1. Indo-Gangetic Plain

It is the southernmost geological unit, which is called Terai in Nepal. It is a foreland basin, which developed after the collision of the Indian and Eurasian Plates, which is directly linked with the rise of the Himalaya. The basin is filled in with by Pleistocene to Recent alluvial deposits. In the north, it is bounded by the Main Frontal Thrust

(MFT). The average thickness of deposit is about 1500 m. The Terai Zone shares a significant proportion of current Himalayan stress accumulation which is evidenced by presence of blind thrusts and thrust-propagated folds beneath the sediments.

1.2.2 Sub-Himalaya (Siwalik)

The foothill ranges of the Himalaya are called the Sub-Himalaya or Siwaliks. It is bounded to the south by the MFT while in the north it is separated by the Main Boundary Thrust (MBT). The Sub-Himalayan rocks represent the Late Tertiary (Middle Miocene to Early Pleistocene) continental molassic sediments deposited within the southern foredeep basin of the Himalaya. The Siwalik succession is 4-6 km thick in Nepal Himalaya and in general represents a coarsening upwards sequence with individual fining up cycles which reflects the rising history of the Himalaya (Gansser, 1964).

1.2.3 Lesser Himalayan Zone

The Lesser Himalaya lies between the Sub-Himalaya and Higher Himalaya. Both the southern and northern boundaries are represented by thrust-faults, i.e., the MBT and the Main Central Thrust (MCT), respectively. It comprises mainly sedimentary to low-grade meta-sedimentary rocks of Late Precambrian to Oligocene (Hashimoto *et al.*, 1973; Stöcklin & Bhattarai, 1977; Sakai, 1983). In the eastern part, it consists of many windows consisting of low grade meta-sedimentary rocks around the crystalline rocks of the thrust sheets.

1.2.4. Higher Himalaya

The Higher Himalaya is bound by the MCT in the South and the South Tibetan Detachment System (STDS) in the north. The Higher Himalaya is composed of about 10 km thick pelitic, psammatic and calcareous para-gneisses, granitic ortho-gneisses and migmatites of amphibolite facies containing kyanite and sillimanite (Le Fort, 1975; Arita, 1983; Colchen *et al.*, 1986). The MCT has transported the high-grade Higher Himalayan rocks over the low-grade meta-sedimentary rocks of the Lesser Himalaya. The Higher Himalayan rocks form nappes (e.g. Kathmandu Nappe,

Dadheldhura Nappe) and klippes (e.g., Jajarkot Klippe, Kahun Klippe) at different places in the Lesser Himalaya.

1.2.5. Tethys Himalaya

The Tethys Himalaya lies between the STDS in the south and the Indus-Tsangpo Suture (ITS) Zone in the north. This zone comprises sedimentary rocks (e.g. shales, limestones, and sandstones), which range in age from Cambrian to Cretaceous from shelf-sediments deposited on the northern margin of the Indian Continent (Hagen, 1968; Bodenhausen & Egeler, 1971; Bordet *et al.*, 1971; Colchen *et al.*, 1981).

1.2.6. Geology of Kathmandu valley

The Kathmandu valley is located within the Lesser Himalaya (Figure 3). The basin falls in the Midland Zone of the Lesser Himalaya, and is bounded by the Mahabharat Lekh in the south and the Shivapuri Lekh in the north. The basement of the Kathmandu basin is interpreted to be a huge nappe (Kathmandu Nappe) formed by thrusting along Mahabharat Thrust (MT), probably the southward extension of the Main Central Thrust (MCT) (Stöcklin, 1980). It is made up of the Precambrian Bhimphedi Group and Paleozoic Phulchoki Group (Stöcklin, 1980). The Kathmandu valley is filled in with young fluvio-lacustrine sediments (Figure 3) of Pliocene to Quaternary age (Yoshida & Igarashi, 1984). The maximum depth to bedrock is more than 500 m at the middle of the basin. Geologically, the Kathmandu valley falls in the Midland zone of the Lesser Himalaya (Dhital, 2015).
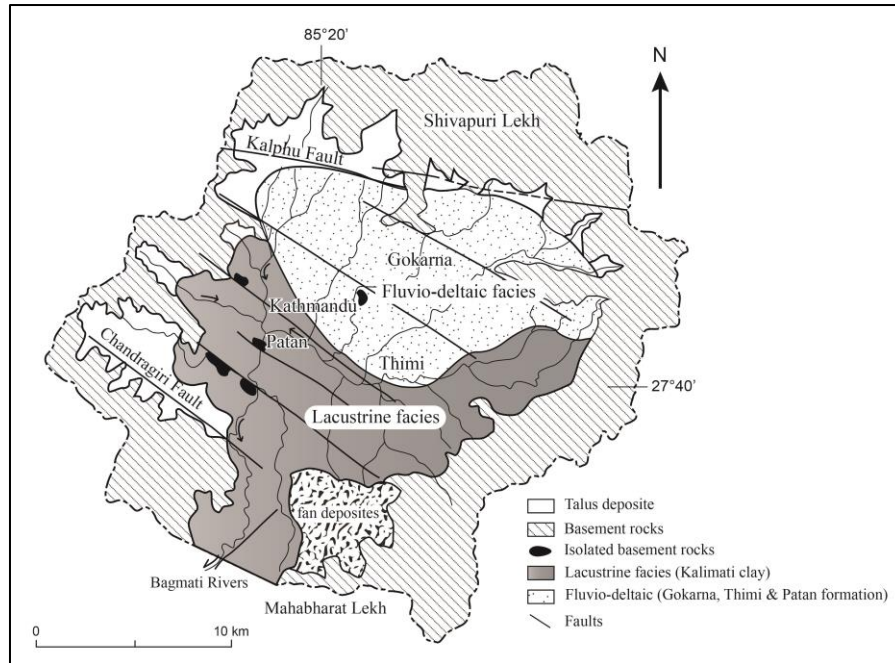
Figure 3: Geological map of Kathmandu valley (Modified from Sakai, 2001).
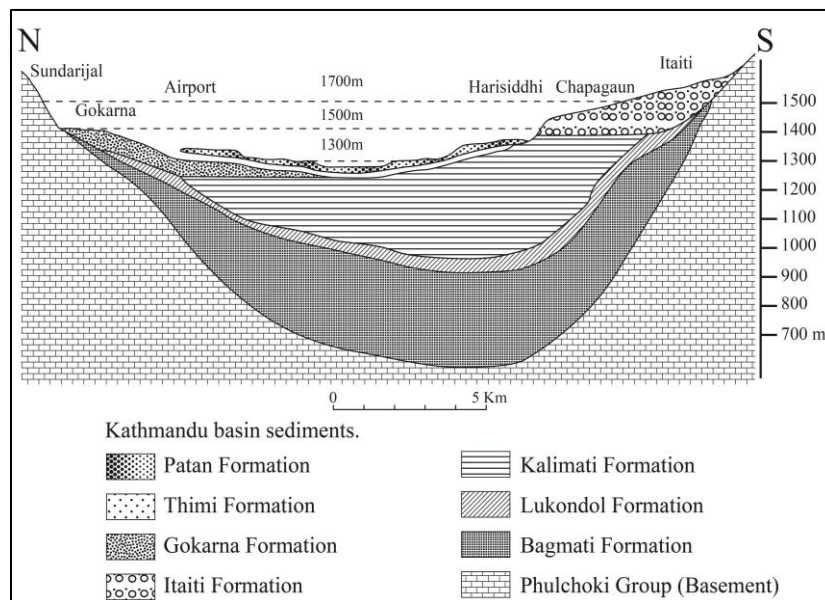
Figure 4: Schematic cross section beneath the Kathmandu valley (Modified after Sakai, 2001).

The sediments of the Kathmandu basin unconformably lie on the Kathmandu Complex rocks (Figure 4). The sediments range in age from 2.5 Ma to about 20 kyr with a total thickness of about 600 m at the central part of the basin.

1.3. Seismicity and seismotectonics of the Nepal Himalaya

The Himalayan range is one of the seismically active regions in the world, which has produced several destructive earthquakes in the past (e.g. Bilham *et al.*, 2001; Bilham, 2004; Szeliga *et al.*, 2010; Ambraseys & Jackson, 2003; Chitrakar & Pandey, 1986; Pant, M. R., 2002).The Himalayan region has witnessed six destructive earthquakes in less than 150 years, which are the 1987 Shillong Earthquake (Mw 8.3), 1905 Kangra Earthquake (Mw 7.8), 1934 Bihar-Nepal Earthquake (Mw 8.4), and 1950 Assam Earthquake (Mw 8.6), 2005 Muzafarabad (Pakistan) Earthquake (Mw 7.6), and the recent 2015 Gorkha Earthquake (Mw 7.8). Historical documentation shows that the region between the 1905 Kangra Earthquake and the 1934 Bihar Nepal Earthquake (between 78°E and 84°E) has not produced any major earthquake since approximately the last five hundred years and is feared as a seismic gap (e. g. Khattri & Tyagi, 1983; Khattri, 1987; Bilham *et al.*, 1995; Pandey *et al.*, 1999), where destructive earthquakes could be overdue.

A belt of seismic activity can be traced all along the Nepal Himalaya (Figure 5) (Pandey *et al.*, 1999). This belt of seismic activity correlates to a zone of maximum uplift rate revealed in leveling data (Jackson & Bilham, 1994; Pandey *et al.*, 1995; Bilham *et al.*, 1997 and Lave & Avouac, 2001), and a zone of maximum horizontal GPS velocity (Cattin & Avouac, 2000) at the geometrical ramp, which is a transition zone between locked southern part of the Main Himalayan Thrust (MHT) and aseismically creeping part in the north, beneath South Tibet. The seismicity of the Himalayan belt is characterized by shallow focus (10<depth<25km) earthquakes (Figure 6). The 1988 Udayapur Earthquake area is an exception, where the earthquakes occur in the upper mantle (Chen *et al.*, 1981; Chen & Molnar, 1983; Pandey, M. R. & Nicolas, M., 1991; Zhao & Helmberger, 1991; Zhu & Helmberger, 1996; Chen & Yang, 2004; Kayal, 2001; Pandey *et al.*, 1999).
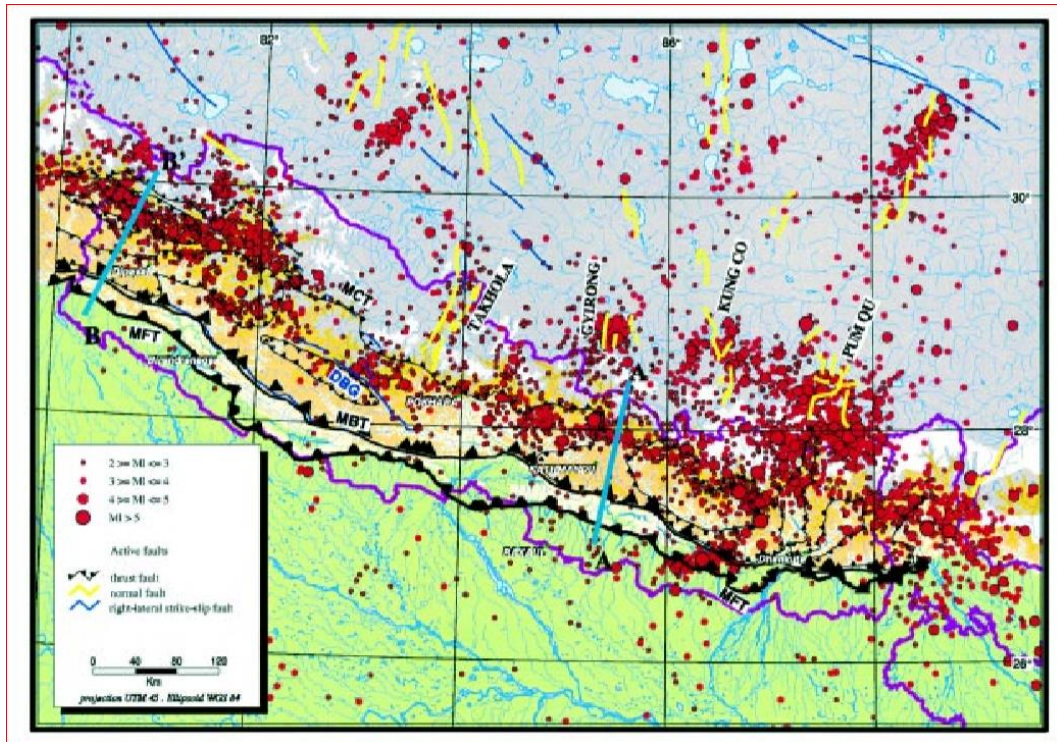
Figure 5: Seismicity map of Nepal (Pandey *et al*., 1999).
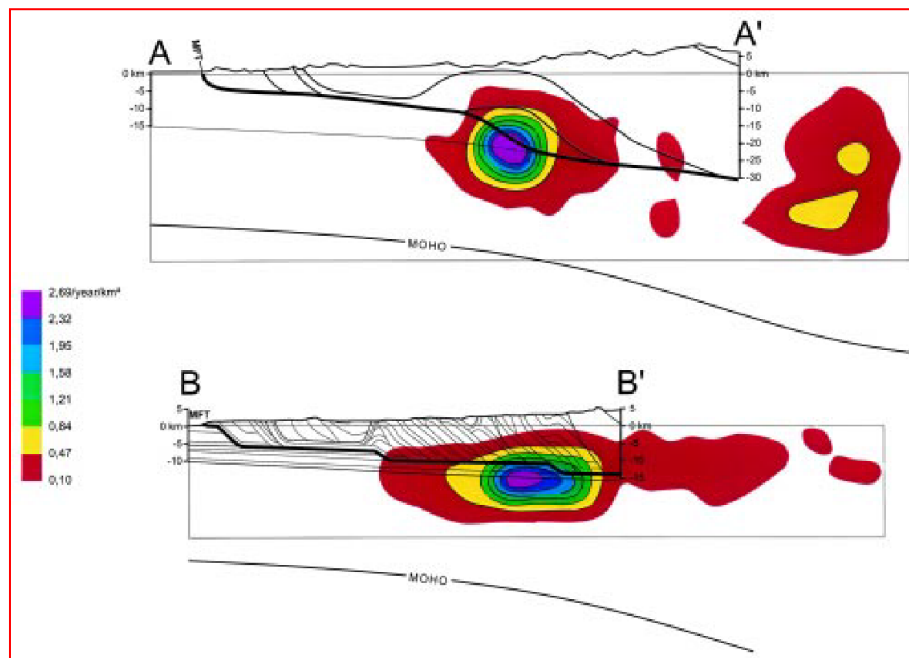
Figure 6: Structural cross sections across the central Himalaya and far-west of Nepal (AA' and BB' in Figure 5) (Pandey *et al*., 1999). The figure shows the density of earthquake foci concentrated at shallow depth.

The MHT is the major geological structure beneath the Himalaya. The MFT, MBT and the MCT are inferred to join this mega thrust at depth (e.g. Avouac, 2003). Most of the crustal deformation in the Himalaya occurs on MHT (Cattin & Avouac, 2000;

9

Lave &Avouac, 2000). The MHT is a detachment thrust and its surface expression is the MFT (Nakata, 1989), where the long term slip rate has been estimated from the study of uplift of Holocene terraces to be 21.5±1.5 mm/yr in central Nepal (Lave & Avouac, 2000) and 19±6 mm/yr in western Nepal (Mugnier *et al.*, 2003).

Geodetic investigations carried out in Nepal show that the MHT absorbs about 20 mm/year of the India-Eurasia convergence (Bilham *et al.*, 1997), which is about 50 percent of the India-Eurasia convergence rate (Bettinelli *et al.*, 2006). Geodetic studies also show that the MHT is nearly fully locked from the surface trace of MFT to a width of about 100 km in the north, beneath the front of the Higher Himalaya (Bilham *et al.*, 1997; Jouanne *et al.*, 1999; Larson *et al.*, 1999; Bettinelli *et al.*, 2006; Ader *et al.*, 2012). This locking decreases towards north abruptly, within a transition zone of smaller than 30 km width. This transition occurs at a depth of about 15-20 km, where the temperature on the MHT is estimated to reach 350°C (Ader *et al.*, 2012). In the north of the locking zone the MHT extends into a sub horizontal shear zone, which is interpreted to be associated with aseismic creep, probably, thermally enhanced by ductile flow (Cattin & Avouac, 2000). At present, the MFT is considered to be the most active fault system regarding the surface deformation of Holocene terraces across it (Lave *et al.*, 2000; Lave *et al.*, 2001). At the time of great earthquakes, it is believed that the nucleation of earthquake occurs at the geometrical ramp and propagates towards the south resulting in surface deformation and surface break close to MFT. Possibly MFT does not rupture during magnitude less than 8.0 earthquakes and leaves the frontal area stressed to be ruptured in next great earthquake or with smaller magnitude local earthquake in the south of the ramp. The other thrusts/faults are not considered very active in comparison to the MFT (Pandey *et al.*, 1999). The shallow earthquakes (depth <20 km) in South Tibet show normal faulting whereas the relatively deeper events (depth >60 km) show strike slip mechanism (Rajaure *et al.*, 2013).

1.4. Seismic hazard and seismic hazard map

Seismic hazard is the hazard associated with potential earthquakes in a particular area, and a seismic hazard map shows the relative hazards in different areas (USGS, 2019). Geology, seismicity and seismotectonic setting of the Himalayan region show that Nepal and its adjoining regions are in seismically high hazard zone. Historical data of

last five centuries show high casualty rate during the earthquakes of more than 6 magnitudes in the Indian subcontinent. More than 1.7 million people have died in the Indian subcontinent in the last two centuries due to earthquake (Bilham, 2004).

Kathmandu valley was destroyed by 9 major earthquakes since 1255 (Chitrakar & Pandey, 1986) and thousands of people were killed, millions of peoples became homeless, many historical monuments including the Dharahara collapsed, and epidemic had spread. Latest in the series of earthquakes is the 25 April 2015 Gorkha Earthquake of Mw 7.8. It occurred at about 80 km in north-west direction from the Kathmandu valley. This earthquake claimed about 9000 lives; injured thousands and hundreds of thousands were made homeless (e.g. http://drrportal.gov.np/).

1.5. Rationale

Geological and seismotectonic settings reveal that Nepal falls in one of the most seismically active zone of the world as discussed earlier. The 2015 Gorkha Earthquake (Mw 7.8), followed by a number of strong aftershocks has once again left us message that destructive earthquakes are less frequent, but can cause unimaginable loss of lives and property leaving the economy of the region in a poor condition, which might sometimes result in social unrest.

Earthquakes cannot be predicted reliably so far. Therefore, in order to minimize loss of lives and property, earthquake resistant structures must be designed and constructed. Assessment of seismic hazard is the primary and crucial input in an effort to make safer structures. Results from seismic hazard assessment can provide input to design earthquake resistant structures as well as to strengthen existing structures at sites of interest. It also helps to formulate national level development policies, planning, upgrade of existing building code and making land use planning. In recent years, growing number of urban centers and construction of high-rise buildings, reservoir-type hydropower projects and road tunnels in Nepal have warranted for more specific and reliable peak ground acceleration (PGA) values for safer design and construction. Seismic hazard assessment map provides PGA values for any construction sites.

Present research was undertaken to develop a new probabilistic seismic hazard map of Nepal utilizing also the lessons from 2015 Gorkha Earthquake and the relevant characteristics, such as, new multiple source models, multiple attenuation relations, different datasets and earthquake recurrence parameters estimated using different methods.

The 2015 Gorkha Earthquake also provided a unique opportunity to study the ground response of the Kathmandu valley using locally recorded strong motion data. The 2015 Gorkha Earthquake and its aftershocks were well recorded by accelerometers operating in the Kathmandu Valley.

1.6. Research gap

There are a number of seismic hazard maps of Nepal published by different researchers in the past. However, the researchers have used limited earthquake data available at that time, limited attenuation relations, less known seismotectonics of the region than at present, and less known earthquake sources. Additionally, in some cases only instrumentally recorded data were used by previous researchers, whereas seismic hazard assessment requires records of historical earthquakes in addition to instrumentally recorded data.

The ground response study of the Kathmandu valley sediments carried out by the previous researchers was based on microtremors. Records of strong earthquakes were not available for such studies in the past. The predominant period and amplification of ground motion in the Kathmandu valley is not properly understood. On the other hand, it is still not clear whether the site-effects are linear or non-linear.

1.7. Research questions

There are a number of research questions related to the seismic hazard assessment of Nepal and ground response of the Kathmandu valley during a large earthquake. They are as follows:

(i)   What are the potential earthquake sources for Nepal?
(ii)   How much is the peak ground acceleration for major cities in Nepal?
(iii)   Are the site-effects in the Kathmandu valley linear or non-linear?

(iv)　What is the predominant period of ground motion in the Kathmandu valley?

(v)　Do the Kathmandu valley sediments amplify the seismic waves? If so, how much is the amplification?

(vi)　Should the existing building code of Nepal be revised or not?

1.8. Objectives

1.8.1 General objectives

The general objectives of the present research are as follows:

(i)　To develop probabilistic seismic hazard map of Nepal

(ii)　To estimate the ground response of Kathmandu valley sediments

1.8.2. Specific objectives

The specific objectives of present research are as follows:

i.　To prepare Earthquake catalogue for Nepal and adjoining areas

ii.　To identify potential earthquake sources for Nepal and adjoining region

iii.　To evaluate peak ground acceleration in major cities in Nepal

iv.　To investigate whether the site-effects are linear or non-linear

v.　To identify the predominant period of ground motion in the Kathmandu valley

vi.　To calculate the seismic wave amplification in Kathmandu valley sediments

vii.　To recommend concerned authorities for building code revision according to new results

1.9. Outputs

The following are the outputs of this research

(i)　Comprehensive, magnitude-homogenized earthquake catalogue for seismic hazard analysis.

(ii)　Probabilistic seismic hazard map of Nepal.

(iii)　Ground response of Kathmandu valley sediments using strong motion records of earthquakes recorded in the valley.

1.10. Applications

Seismic hazard maps are basic input in planning, policy making, formulation and revision of building codes and strengthening of existing structures. Seismic hazard results are therefore very important in the development of any country like Nepal, which requires acceleration of its development works in a sustainable way. Results of present research are useful in the revision of the existing National Building Code prepared by the Government of Nepal.

Similarly, there are several projects of national priority, which require appropriate and reasonable assessment of seismic hazard in Nepal. This thesis provides basic requirements in the revision of building code and design of projects of national priority as well as other development projects.

1.11. Limitations

Seismic hazard assessment requires data recorded for a long period of time. Such a period should cover a complete earthquake cycle of great earthquakes. However, earthquake monitoring started in the early of 20th century with very few seismic stations globally. Because of sparse distribution of seismic stations and early technology, only strong earthquakes only were recorded (Mw >5) in the past. The world saw a revolution in the monitoring of earthquakes after the expansion of existing networks that improved the detection threshold for earthquakes.

The Department of Mines and Geology (DMG) started to operate its nationwide seismic network in 1995. The network was installed in a technical collaboration between DMG and Department Analyze Surveillance Environment (DASE), France. The network has short-period, vertical component seismometers at 21 locations in Nepal and its detection threshold is local magnitude (Ml) 2.0 for earthquakes in Nepal.

Proper seismic hazard analysis is based on available data, understanding of the seismotectonics, experience of strong earthquakes and strong motion records. The following are the limitations in this study:

i. Limited pre-instrumental records of earthquakes and their uncertainties in terms of location and magnitude, which might have partly increased the uncertainties.

ii. Maximum potential magnitude as well as earthquake recurrence parameters of earthquake source zones are important factor in any seismic hazard assessment. The maximum potential magnitude of earthquake sources were adopted from published literatures in some cases. Similarly, the earthquake recurrence parameters were estimated from available data assuming the b-value does not vary with time.

iii. Locally derived attenuation relations for Nepal Himalaya do not exist. In the present study attenuation relations derived for other regions with similar tectonic settings ere used, which might not represent the real situations of the Nepal Himalaya.

iv. Ground response analysis was carried out only for the Kathmandu valley because the strong motion data were not available for other major cities of Nepal.

v. Strong earthquakes occur in many tens to hundreds of years but we have record of earthquakes recorded by instruments that is not longer than one hundred years. Of course, the instrumental record is supplemented from historical record in the form of different types of documents but their uncertainty in terms of location and magnitude is large.

1.12. Layout of the Thesis

There are six chapters in this dissertation thesis.

Chapter I deals with general introduction of subject matters.

Chapter II presents an overview of reviewed literatures in seismology, geology, seismotectonics, seismic hazard and ground response. The major review was carried out in seismic hazard assessment of Asia, India and Nepal along with the site-response in the Kathmandu Valley.

Methods and materials are described in the Chapter III. Probabilistic seismic hazard technique was applied to the comprehensive, magnitude-homogenized earthquake catalogue prepared during this study. In addition to the prepared earthquake catalogue; geological map, geological structures were used in the seismic hazard

assessment. Ground acceleration records of earthquakes, which were recorded in the Kathmandu Valley, were utilized to estimate local site effects.

Probabilistic seismic hazard map of Nepal and response of the Kathmandu valley sediments to earthquake ground motion are the major areas of results of this study, which are presented in Chapter IV,

The major source of seismic hazard in Nepal is the MHT. The soil in the Kathmandu valley responded non-linearly during the Gorkha Earthquake sequence. Such conclusions are described in Chapter V.

The references are presented separately in Chapter VI.

CHAPTER 2
LITERATURE REVIEW

2.1. General

In order to achieve the objectives as mentioned earlier, relevant literatures were reviewed on various aspects. The review was carried out on:

1. Chronological development of hazard assessment
2. Seismic hazard assessment of Asia and Indian subcontinent
3. Seismic response of Kathmandu valley sediments

2.2. Chronological development of seismic hazard assessment

Inclusion of seismic provisions in building codes were first practiced after the 1933 Long Beach, California Earthquake. At the beginning, in the 1940s and 1950s, seismic design provisions in building codes were based on qualitative evaluations of hazard.

A quantitative seismic hazard map based on probabilistic analysis was introduced in Canada after the work of Milne and Davenport (1969). The researchers used extreme value statistics to calculate a gridded map of Peak Ground Acceleration (PGA) having an annual exceedance probability of 0.01 (100 year return period). A related amplitude recurrence method was also developed, based on counting the annual number of exceedance of a specified acceleration at a site.

Cornell (1968) developed a different methodology which was later coded into a FORTRAN algorithm by McGuire (1976). It is widely referred to as the Cornell-McGuire method. In the Cornell-McGuire method, the spatial distribution of earthquakes is described by seismic source zones; an active fault was defined as a linear source, and geologic information and historical seismicity were used to represent the sizes of events and their rates of occurrence at the fault. Areas of diffuse seismicity are represented as area source zones. Because of its ability to incorporate both seismicity and geologic information, the Cornell-McGuire method quickly became popular and was widely used throughout the world. Its application to seismic zoning in Canada has been described by Basham *et al.*, (1982; 1985); Adams *et al.*, (1999); Adams & Halchuk (2003, 2004) and Adams & Atkinson (2003).

Over the period of last 30 years, improved data and knowledge have become available, particularly on the origin, occurrence and effects of earthquakes; accordingly the strong ground motion as a result of earthquakes has been better understood in terms of their generation and propagation. It has facilitated in minimizing the uncertainties in the assessment of seismic hazard.

2.3. Seismic hazard assessment of Asia and Indian sub-continent

2.3.1. Seismic hazard assessment of Asia

Giardini *et al.* (1999) published probabilistic seismic hazard map of Asia (Figure 7) under the Global Seismic Hazard Assessment Program (Figure 7). The map shows seismic hazard in terms of peak horizontal ground acceleration (PGA) at engineering rock site condition. The PGA was calculated for 10% probability of exceedance in 50 years (~500 year return period). This map provides a broader overview of the seismic hazard in Nepal and surrounding regions. According to this map, the PGA varies between 0.4 g and 0.6 g in Nepal.
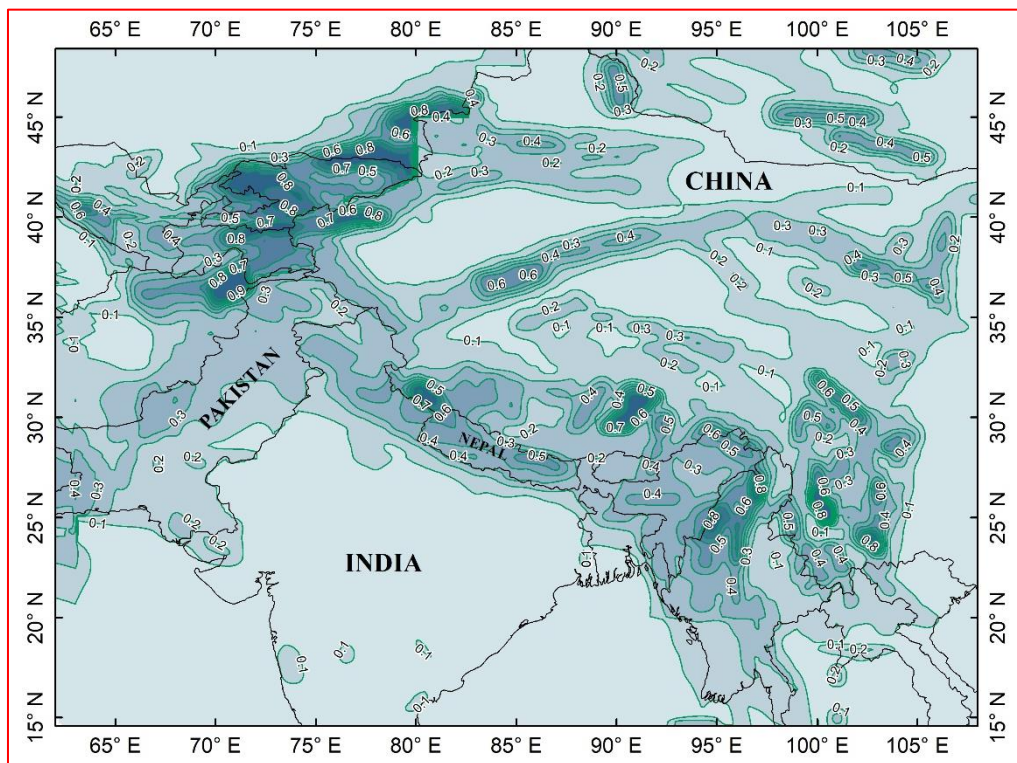
Figure 7: Probabilistic seismic hazard map of Asia by GSHAP (Redrawn using data from http://www.seismo.ethz.ch/static/GSHAP). The PGA values were calculated for engineering rock site condition.

2.3.2. Seismic hazard map of India

(a) Geological Survey of India

The first attempt was made in 1935 to prepare seismic zoning map of India by the Geological Survey of India (GSI) (Khattri, 2006). The map divides the Indian Territory into three zones (Severe, moderate and minor hazard). A new seismic zoning map of India included in IS1893:2002, was published in 1962 by GSI (Khattri, 2006). The map utilizes intensity distribution of past destructive earthquakes as the basis for zoning and therefore represents damages in past destructive earthquakes as high hazard zone. The map was subsequently revised in 1966, 1970, 1984 and 2002 (Khattri, 2006) to incorporate weights of known tectonic features, which still retains the intensities of destructive earthquakes as in the earlier versions. The presently adopted seismic hazard map of India (Figure 8) (IS-1893:2002): Geological Survey of India, (2002) divides India into four zones: Zone II (Intensity VI), Zone III (Intensity VII), Zone IV (Intensity VIII) and Zone V (Intensity IX or larger), which have anticipated peak ground acceleration of 0.1 g, 0.18 g, 0.24 g and 0.36 g. This map is based on the intensity of past destructive earthquakes of the region and therefore does not consider probability.
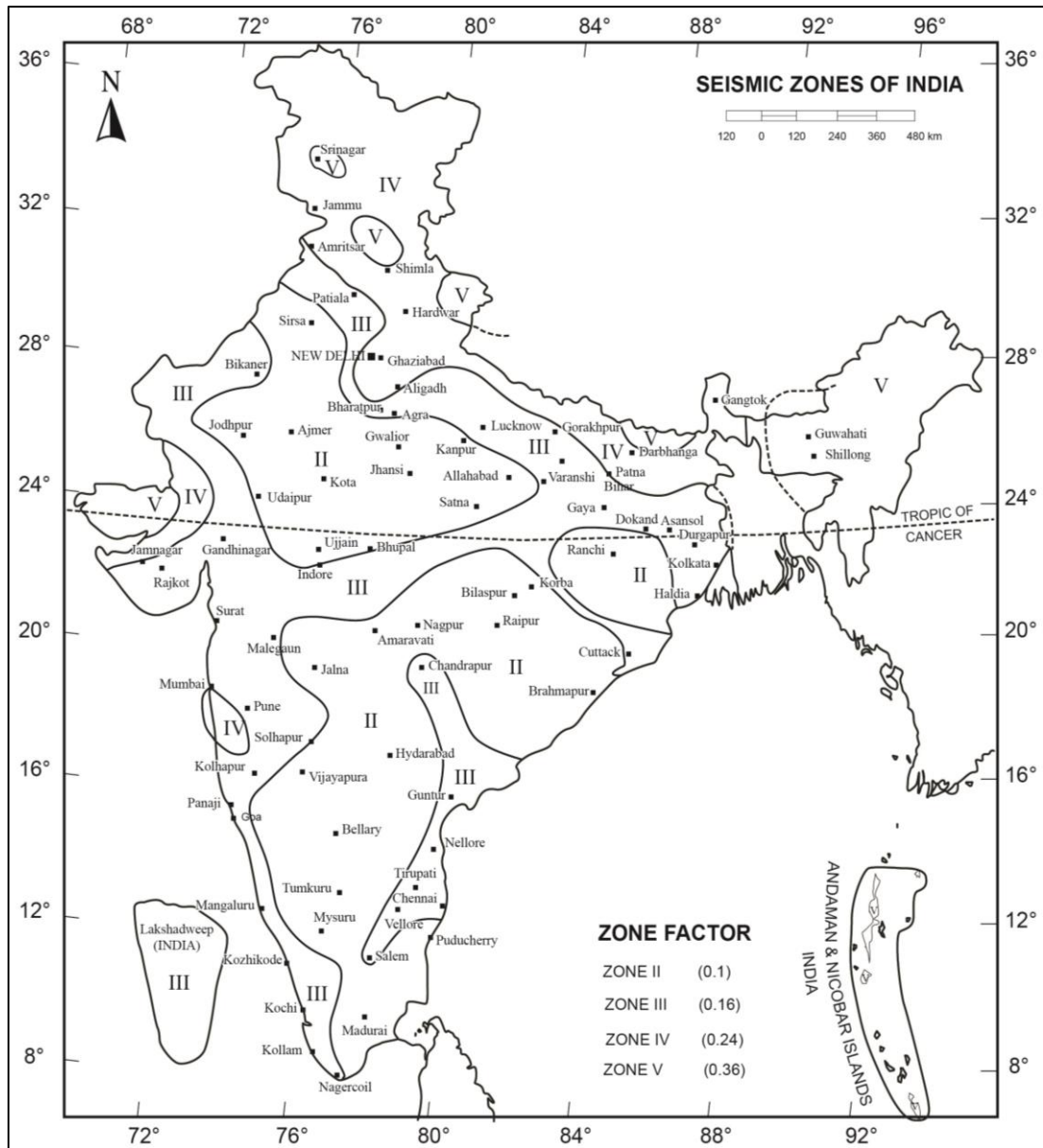
Figure 8: Seismic zoning map of India (modified from IS: 1893 (Part-1)). Nepal falls in a region, which has PGA larger than 0.24 g.

(b) Nath and Thingbaijam (2012)

Nath and Thingbaijam (2012) prepared probabilistic seismic hazard map of India and adjoining regions (Figure 9). The seismic hazard map shows the seismic hazard corresponding to 10% probability of exceedance in 50 years. The maximum hazard is noticed near the Nepal-India border in the west and Indo-Myanmar border region and reaches up to 0.6 g in some regions.
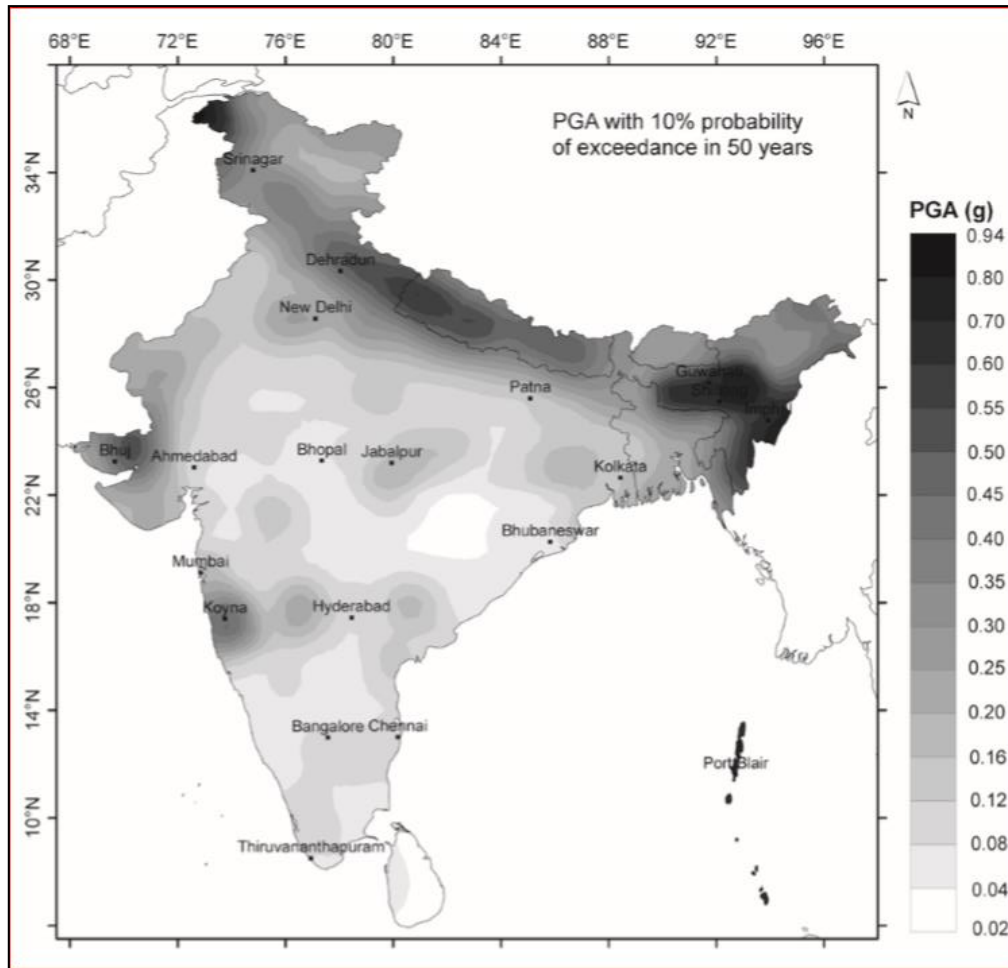
Figure 9: Probabilistic seismic hazard map of India and adjoining region corresponding to 10% probability of exceedance in 50 years at engineering rock site condition. The PGA over Nepal ranges between 0.3 g and 0.5 g (Nath & Thingbaijam, 2012).

(c) National Disaster Management Authority (NDMA), India

A working committee of expert formed by the National Disaster Management Authority, Government of India (NDMA, India 2010) submitted its final report on "Development of Probabilistic Seismic Hazard Map of India" to the Government of Indian 2010. The seismic hazard map (Figure 10) shows the PGA corresponding to Type 'A' site conditions. According to the National Earthquake Hazard Reduction Program (NEHRP), Type 'A' site has shear wave velocity (Vs) larger than 1500 m/s. Type 'A' sites have Vs larger than that at engineering soil sites (760<Vs<1500 m/s. The largest PGA in Nepal is about 0.18 g in the western part of Nepal and the lowest is 0.06 in the southern part. The site classification for seismic site response (NEHRP 1994) is given in Appendix 3.
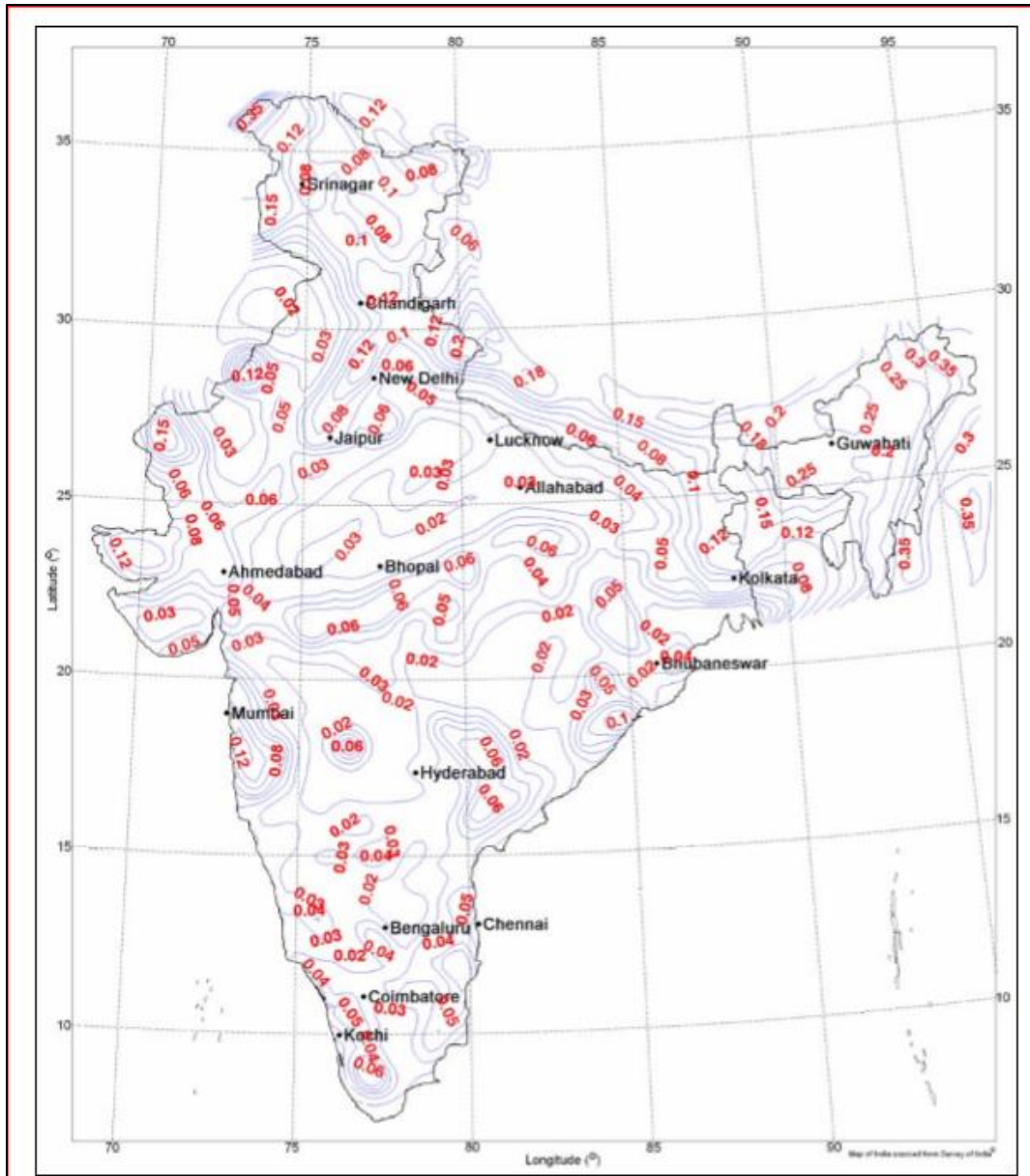
Figure 10: Probabilistic seismic hazard map of India and the adjoining region corresponding to 10% probability of exceedance in 50 years. The PGA was calculated for 'A' type soil class. According to this map the PGA varies between 0.06 g and 0.18 g in Nepal (NDMA, 2010).

2.3.3. Seismic hazard assessments of Nepal

The research on seismic hazard in Nepal has been carried out by several institutions and researchers. Some of the important works in this regard have been reviewed in the following sections.

2.3.3.1. Seismic hazard mapping and risk assessment for the National Building Code, Nepal (1993)

This work on "Seismic hazard mapping and risk assessment" was carried out by Beca Worley International *et al.* (1993)l for the seismic design of buildings in Nepal in 1994 (NBC-105). The map (Figure 11) shows horizontal PGA at rock site for 10% probability of exceedance in 50 years. According to this result, the PGA values vary between 0.26 g and 0.42 g. The maximum PGA (>0.42 g) is estimated in the western part of Nepal.
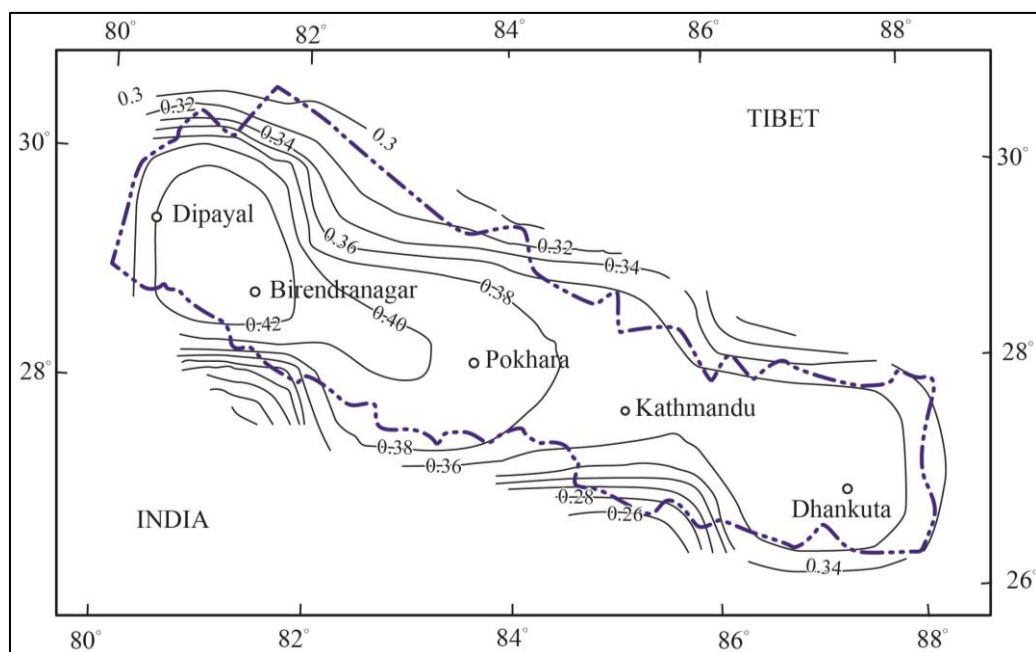
Figure 11: Probabilistic Seismic hazard map (NBC-105) of Nepal corresponding to 10% probability of exceedance in 50 years for an engineering rock site condition. The PGA varies between 0.26 g and 0.42 g across Nepal (Modified from Beca Worley *et al.*, 1993).

2.3.3.1.1. Global seismic hazard program map (1999)

The Global Seismic Hazard Assessment Program (GSHAP) was launched in 1992 by the International Lithosphere Program (ILP). The program was supported by the

International Council of Scientific Unions (ICSU) and was completed in 1999. The GSHAP prepared probabilistic seismic hazard map for different regions of the world. Figure 12 is the probabilistic seismic hazard map (Figure 12) of Nepal reproduced using GSHAP data. The PGA value varies between 0.3 g and 0.5 g in Nepal.
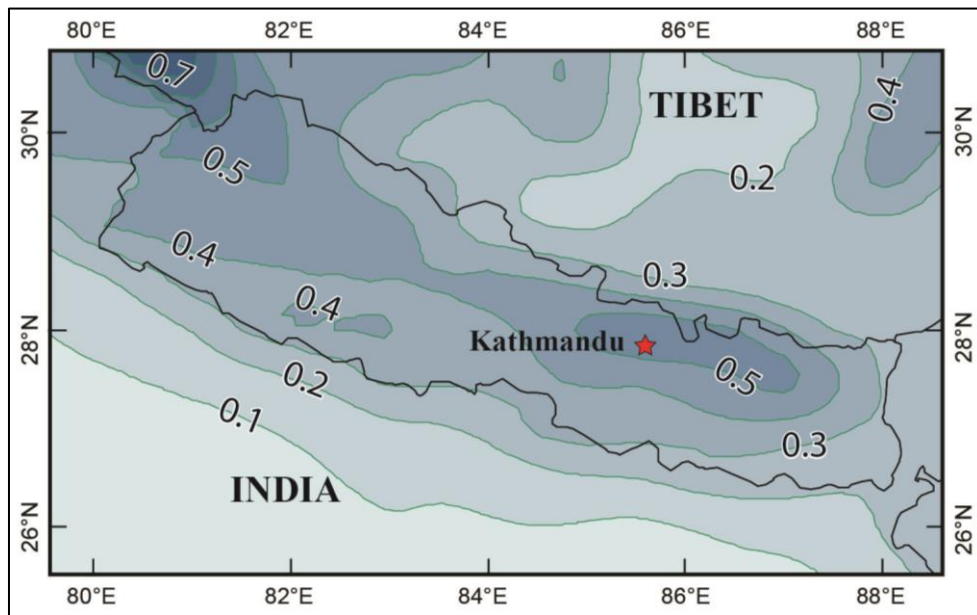
Figure 12: Probabilistic seismic hazard map of Nepal corresponding to 10% probability of exceedance in 50 years at an engineering rock site condition. (Reproduced using data from http://www.seismo.ethz.ch/static/GSHAP).

2.3.3.1.2. Pandey *et al*. (2002)

Pandey *et al.* (2002) prepared seismic hazard map of Nepal (Figure 13). The seismic hazard map depicts a belt of high hazard (PGA>200 gal; 1 gal = 1cm/sec^2) that runs parallel to the Himalaya. The PGA varies between 50 gal and 450 gal (1 gal = 1 cm/sec^2), which was calculated for an engineering rock site condition.
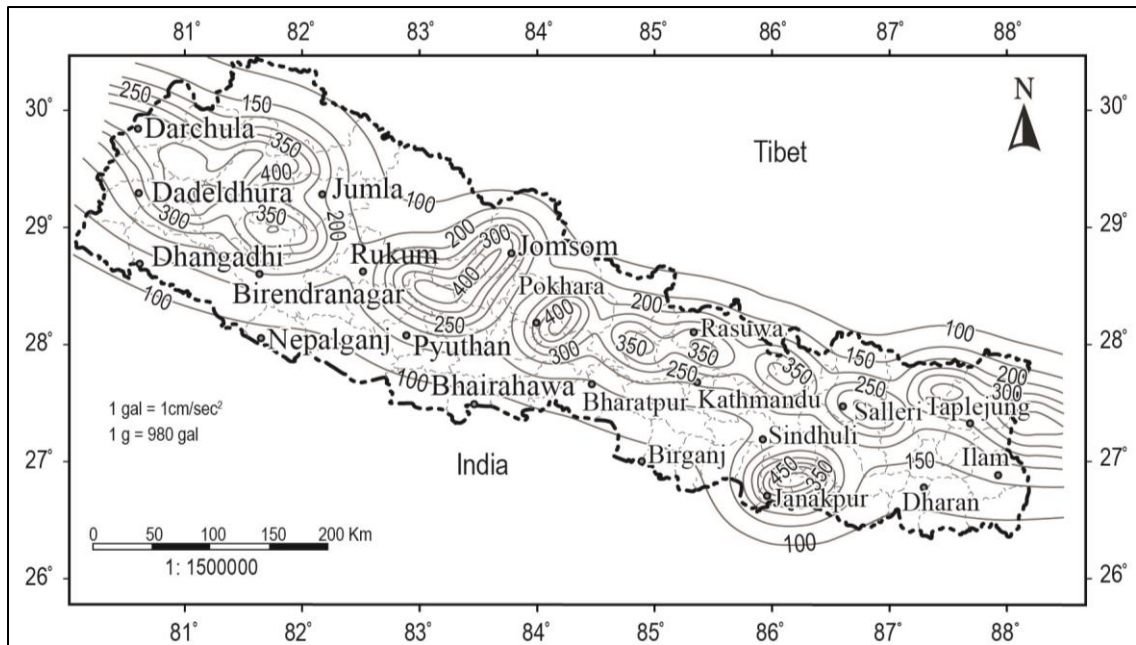
Figure 13: Probabilistic seismic hazard map of Nepal corresponding to 10% probability of exceedance in 50 years for engineering rock site condition (Redrawn from Pandey *et al*., 2002). The PGA varies between 100 and 400 gal

2.3.3.1.3. Thapa & Wang (2013)

Thapa & Wang (2013) prepared seismic hazard map of Nepal using probabilistic seismic hazard analysis technique developed by China Earthquake Administration (CEA), 2005. They estimated horizontal peak ground acceleration corresponding to 63%, 10% and 2% probability of exceedance in 50 years at engineering bedrock, using attenuation relation developed by CEA (2005) for western China. The result shows that the estimated PGA value varies between 0.2 g and 0.57 g (Figure 14).
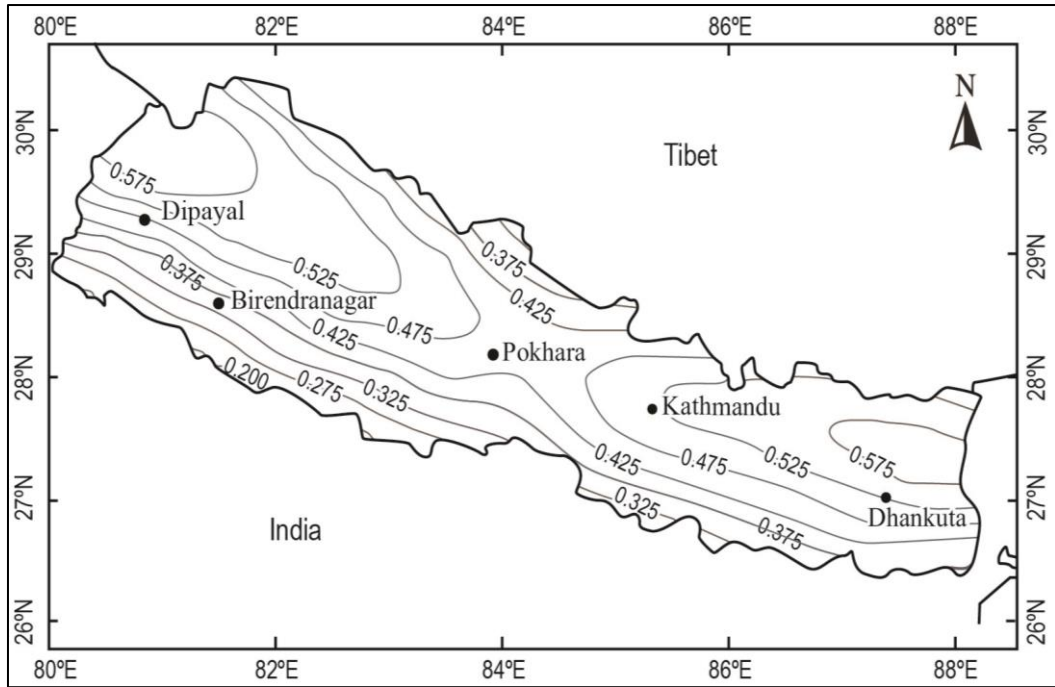
Figure 14: Probabilistic seismic hazard map of Nepal corresponding to 10% probability of exceedance in 50 years for an engineering rock site condition. (Modified from Thapa & Wang, 2013). The PGA varies between 0.2 g and 0.57 g across Nepal.

2.3.3.1.4. Rahman & Bai (2018)

Rahman & Bai (2018) prepared probabilistic seismic hazard map of Nepal using multiple source models. They have estimated maximum PGA of about 0.64 g in the far-western Nepal (Figure 15). In this figure also, the largest PGA is estimated in the western and eastern part of Nepal.

In addition to the earthquake sources used by Thapa & Wang (2013), they used smoothed gridded, linear as well as areal sources.
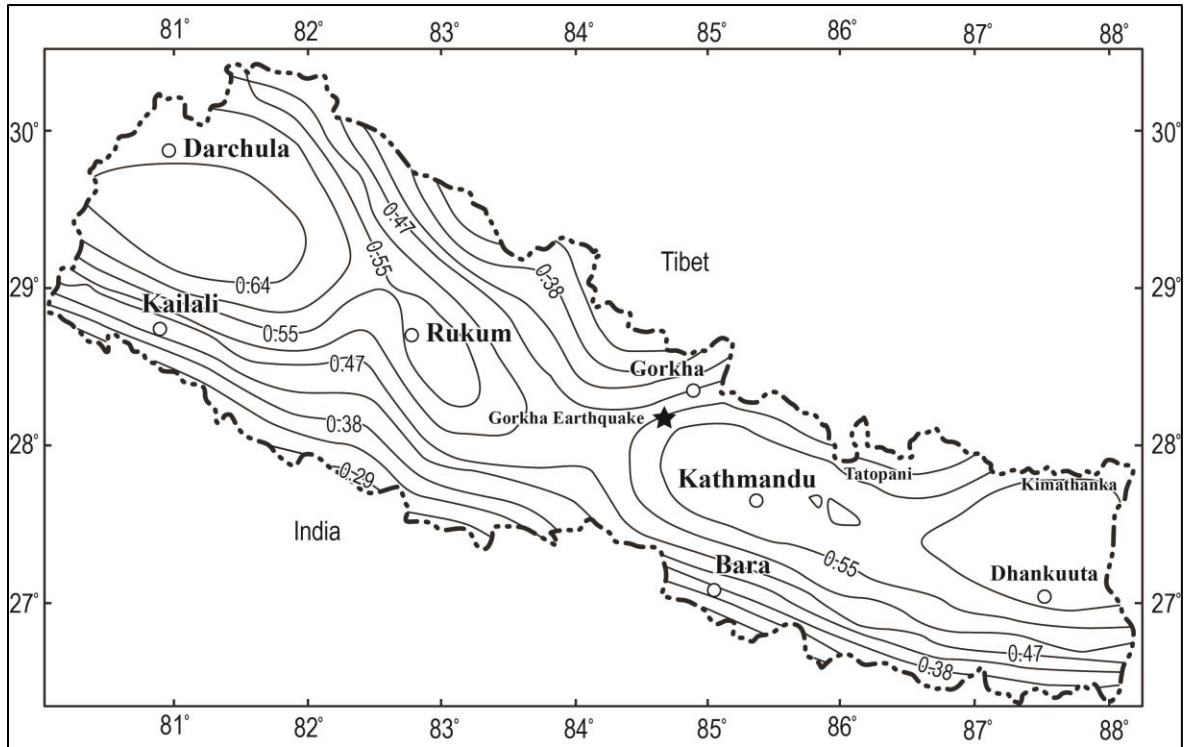
Figure 15: Probabilistic seismic hazard map of Nepal corresponding to 10% probability of exceedance in 50 years (Modified from Rahman & Bai, 2018) for an engineering rock site condition. The PGA varies between 0.29 g and 0.64 g.

2.3.3.1.5. Stevens *et al.* (2018)

Stevens et al. (2018) prepared probabilistic seismic hazard map (Figure 16) of Nepal using the detailed geometry of the Main Himalayan Thrust (MHT). The entire MHT, having maximum potential magnitude as large as (Mw) 9.2, was used as a single source. In addition to MHT, normal faults in South Tibet also were used as potential earthquake sources. Earthquake catalogue, comprising data between 1995 and 2016, was used to find earthquake recurrence parameters. A fixed b-value (1.0) was used for the entire region and a-values were recalculated from the catalogue. The maximum PGA (0.6 g) is estimated in the southern part of Nepal.
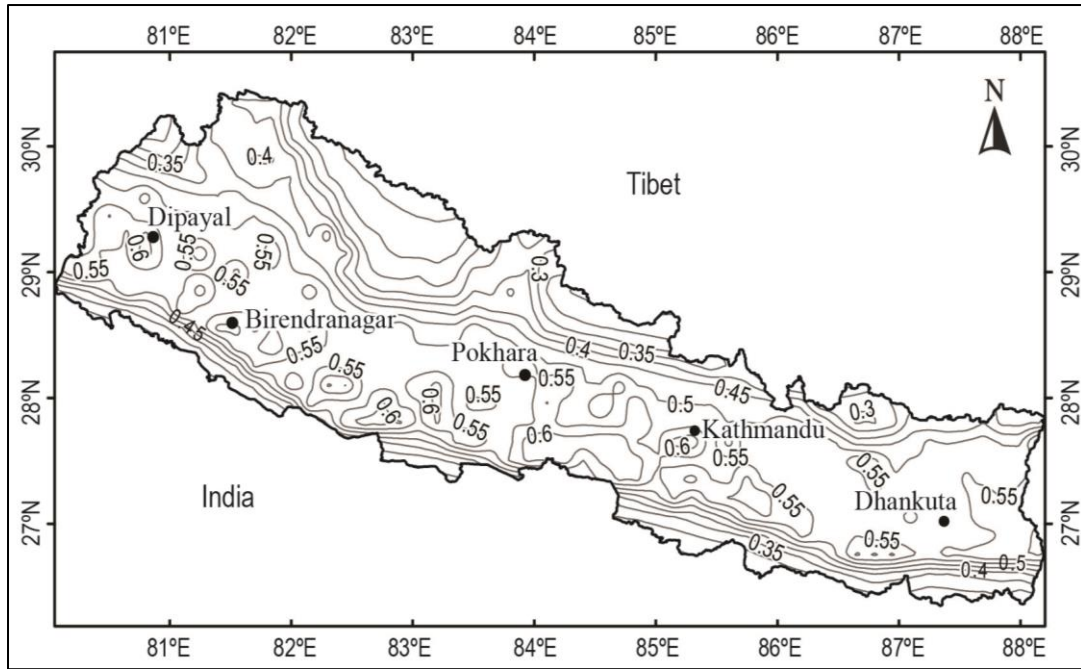
Figure 16: Probabilistic seismic hazard map of Nepal corresponding to 10% probability of exceedance in 50 years (Redrawn from Stevens *et al*., 2018) for an engineering rock site condition. The maximum PGA reaches up to 0.6 g at some places.

2.4. Ground response of the Kathmandu valley sediments

The seismic response of a site is affected by many factors, such as source characteristics, propagation path and local site conditions. Among all these factors, the local site conditions may have significant impact on the seismic site response (Borcherdt & Glassmoyer, 1992).These effects caused by local site condition are well known among the geotechnical engineers and seismologists as site effect. Local site conditions may cause significant amplification of ground motion and concentrated damage during an earthquake (Asimaki & Gazetas, 2004).

The Kathmandu valley is a bowl-shaped depression, filled with fluvio-lacustrine sediments, on top of the Precambrian metamorphic rocks. Due to the vertical variation in lithology and lateral variation in sediment characteristics, seismic waves are influenced in the basin. As a result, the Kathmandu valley experiences varying degree of ground shaking/destruction (e.g. Pandey & Molnar, 1988 and Rajaure *et al*., 2015). The damage pattern of the 1934 (M 8.1) earthquake (Bilham *et al*., 1995), in particular suggests that ground amplification due to fluvio-lacustrine sediments plays a major role in intensifying the ground motion in the basin (Paudyal *et al*., 2013).

The ground response of the valley has been studied by some researchers in the past, which are described below.

2.4.1. Pandey (2000)

Pandey (2000) used relative power spectra of ambient noise recorded at 60 soil sites with reference to that at rock site in the Kathmandu sedimentary basin. He reported that the predominant frequency at 2 Hz was amplified. There are other peaks of amplification in the range between 0.6 and 5 Hz, but the amplification factor varied across the valley. The amplification factor was about 5 to 6 in the lacustrine area, between 2 to 3 in transitional area and between 1 and 2 in fluviatile area.

2.4.2. JICA (2002)

The Japan International Cooperation Agency (JICA) and Ministry of Home Affairs, His Majesty's Government of Nepal, jointly carried out a study entitled "Earthquake disaster mitigation in the Kathmandu Valley, Kingdom of Nepal" in 2002.

Ground condition of the Kathmandu Valley was analyzed and classified to establish ground models. The ground models were used in the investigation of amplification of seismic motion, evaluation of liquefaction and stability of slope. The study team made five boreholes in order to understand essential ground properties such as shear wave velocity, density, N value, groundwater level and mean particle size. One dimensional response analysis was carried out using ground models derived from borehole data. Several layers were identified based on the soil type and shear wave velocity. The amplification factor for the ground models vary between 1.0 and 2.0.

2.4.3. Piya (2004)

Piya (2004) studied the liquefaction hazard in the Kathmandu valley. He used geological information from boreholes and prepared liquefaction susceptibility map for the valley. He found that Kathmandu valley could be susceptible to liquefaction in case a strong earthquake occurs nearby with strong ground shaking in the Kathmandu Valley. The finding was based on the presence of liquefiable soils (sand and silts), high groundwater level and the possibility of potential strong ground motions in the region.

2.4.4. Khanal (2005)

Khanal (2005) carried out preliminary seismic microzonation of the Kathmandu valley using one-dimensional seismic response analysis. Borehole logs of deep tube wells from Kathmandu valley and the strong motion record of the 1999 Chamoli (India) earthquake were used in this study. The investigation shows one to two story buildings are safer considering the input ground motion used.

2.4.5. Bhattarai *et al*. (2011)

Bhattarai *et al.* (2011) reported analysis of acceleration data recorded at DMG and at Kakani (KKN) site (about 20 km in the north of Kathmandu valley on rock). They analyzed two earthquakes one of which occurred at a distance of 25 km (15 July 2010, M_L 3.4 (NSC)), in Nepal, and other occurred over 110 km distance (17 October 2010, M_L 5.7 (NSC)) in South Tibet. The study shows large PGA at a hard rock site located at about 110 km from the accelerometric stations, which they speculate might be caused by topographic amplification at KKN.

2.4.6. Paudyal *et al*. (2012)

Paudyal *et al.* (2012) applied horizontal-to-vertical ratio of Fourier spectra (H/V ratio technique) of ambient noise recorded at soil sites to estimate fundamental frequency at different parts of the Kathmandu Valley. They reported that the valley has fundamental frequencies in the range between 0.48 to 8.9 Hz in the central and northern part of the sedimentary basin. In addition to the fundamental frequency, they reported other peaks between 4 and 6 Hz in the central and northern part of the basin. Preliminary basement topography of the Kathmandu sedimentary basin was estimated, which correlates with the result from gravity survey carried out by Morayabashi and Maruo (1980) and shows thick sediments in the middle part of the valley.

2.4.7. Takai *et al*. (2016)

Takai *et al.* (2016) studied the strong ground motion records of the 2015 Gorkha Earthquake. They observed the vertical ground velocities at the sedimentary sites were the same pulse motions that were observed at the rock site. On the other hand,

the horizontal ground velocities as well as accelerations observed at the sedimentary sites showed long duration with obvious long-period oscillations, caused by the valley response. The records reveal that the horizontal valley response was amplified about 10 times (in the long period) and prolonged oscillations. The predominant period and envelope shape of their oscillations was not consistent, across the soil indicating a complicated basin structure. The horizontal long-period oscillations on the sedimentary sites were strong enough to damage the high-rise buildings with natural periods of 3 to 5 s.

CHAPTER 3

MATERIALS AND METHODS

3.1. Materials

Different related information have been used for the seismic hazard assessment of Nepal and the ground response analysis of the Kathmandu valley. These are briefly described in the following sections.

3.1.1. Maps and images

Various maps and images were used to gather the secondary data required for the seismic hazard analysis. Epicenter distribution map of Nepal by Pandey *et al.*, (1999) (Figure 5) and local earthquakes relocated by Rajaure *et al.*, (2013) (Appendix 4) were used to understand the seismicity pattern of Nepal and adjoining areas. Geological map of Nepal published by the Department of Mines and Geology (1987) (Appendix 5) and active fault map of Nepal (Nakata, 1989) (Appendix 6) were used to gather information on fault line and active fault sources. Google Earth Images also were used to check features such as lineaments and faults (Appendix 7).

3.1.2. Earthquake catalogue

Earthquake catalogues are fundamental inputs in seismic hazard assessment. Catalogues of earthquakes are used to determining magnitude-frequency relation coefficients ('a' and 'b'-values) in the Gutenberg-Richter recurrence relation and the mean annual rate of occurrence of earthquakes, which are basic requirement in seismic hazard calculation. A complete earthquake catalogue, both in magnitude range and time, is therefore an essential component in such studies. An earthquake catalogue normally has a date and time of origin, location (latitude, longitude, and depth), magnitude and uncertainties in the location. The catalogues can be grouped into two types: instrumentally recorded and pre-instrumental earthquakes. Earthquakes, which occurred after 1900 AD are grouped into "Instrumentally recorded", and which occurred before 1900 AD are grouped into "Pre-instrumental".

3.1.2.1. Instrumentally recorded earthquakes

Instrumentally recorded earthquake data were collected from International Seismological Centre, UK (ISC: www.isc.ac.uk), United States Geological Survey (USGS), USA (www.earthquake.usgs.gov), Incorporated Research Institutions in Seismology, USA (www.iris.edu) and Department of Mines and Geology, Nepal (www.seismonepal.gov.np), in a rectangular region between 24° N and 34° N latitude and 75° E and 95° E longitudes. The International Seismological Centre (ISC) has been collecting, reviewing and publishing earthquake catalogue, which contains earthquake data since 1905, however, in the early days; such data was available for strong earthquakes only. The detection threshold of seismic observatories improved afterwards on account of addition of new networks, expansion of existing networks and ever changing technology. Similarly, the USGS has been compiling and publishing earthquake catalogue since 1900. Likewise, the IRIS earthquake catalogue has earthquake data since 1970.

The Department of Mines and Geology, Nepal has been operating a network of short period, vertical component seismic stations since 1995 in collaboration with Departement Analyse Surveillance Environnement (DASE). This network has produced a very important dataset of small earthquakes, particularly in Nepal Himalaya because of the spacing between seismic stations and coverage in the Nepal Himalaya. This catalogue has been used to delineate seismogenic sources and for a comparison of earthquake recurrence parameters with other data sets.

3.1.2.2. Pre-instrumental (historical) earthquakes

Data of large earthquakes is available in historical records in the form of reports of destruction in inscriptions and chronicles. The large destructive earthquakes, which occurred before the arrival of instruments, were collected from literatures. Locations as well as magnitudes of such pre-instrumental earthquakes were estimated from the area of maximum destruction and the intensity of maximum destruction respectively. Therefore, the locations and magnitudes of pre-instrumental earthquakes might have large uncertainties in comparison to instrumentally recorded earthquakes.

The pre-instrumental earthquakes, which occurred before the development of instruments, were collected from Rana (1935), Chitrakar & Pandey (1986), Bilham *et*

al. (1995), Pant (2002), Bilham (2004), Ambrasseys & Douglas (2004) and Szeliga *et al.* (2010).

3.1.3. Strong ground motion data

The Hokkaido University (Japan), in collaboration with the Central Department of Geology, Tribhuvan University, installed four accelerometers (KTP, TVU, PTN, THM) in 2011 on an east-west profile that runs from Kirtipur to Sanothimi in Bhaktapur (Table 1, Figure 17). One of the accelerometer is at a rock site (KTP) and the rest four are on soil (TVU, PTN, and THM). The accelerometers (Mitsuyo JEP-6A3-2 accelerometers) operate on continuous mode, at 100 Hz sampling rate. In addition to these accelerometers two more accelerometers were operating during the earthquake; one at the premises of the Department of Mines and Geology (DMG), Lainchaur and the other at the US recreation center at Kantipath (KATNP). The DMG and USGS accelerometers were manufactured by GEOSIG. Their dynamic range is 2 g and sampling frequency is 200 Hz.

Strong motion (acceleration) data of earthquakes, which occurred on 30 August 2013, South Tibet Earthquake (M 4.9), the 25 April 2015 Gorkha Earthquake (Mw 7.8) and its three strong aftershocks (25 April, 26 April and 12 May 2012) were used in this study. The earthquakes were recorded by five accelerometers operating in the Kathmandu Valley.

Table 1: Location of accelerometers in the Kathmandu Valley.

Site code	Latitude (°N)	Longitude (°E)	Location
KTP (rock)	27.68	85.27	Kirtipur Municipality office, Kirtipur
TVU (soil)	27.68	85.28	Central Department of Geology/Tribhuvan University
PTN (soil)	27.68	85.31	Engineering College, Pulchowk
THM (soil)	27.68	85.37	University Grant Commission office, Sanothimi, Bhaktapur
KATNP (soil)	27.71	85.31	Kantipath, Kathmandu
DMG (soil)	27.73	85.31	Department of Mines and Geology, Lainchaur, Kathmandu

34
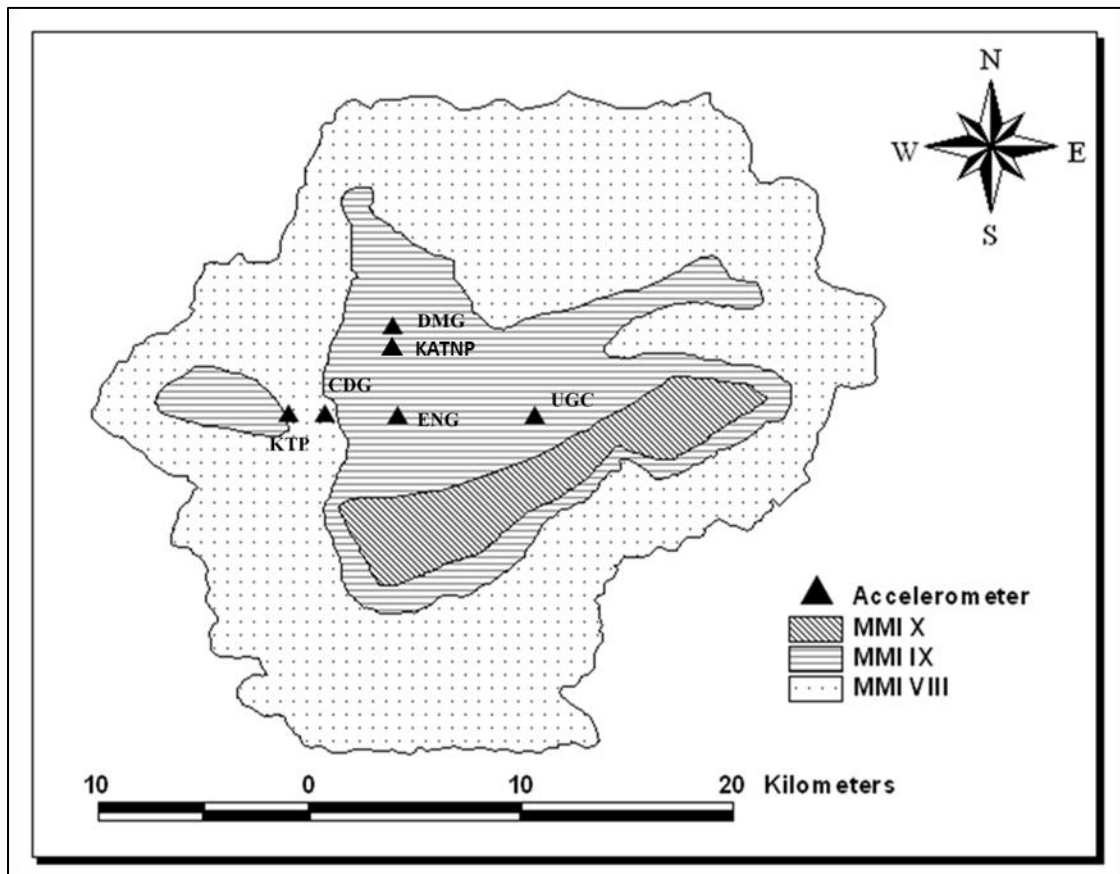
Figure 17: Location of strong motion instruments (accelerometers) operating in the Kathmandu Valley. The shaded polygons represent the intensities observed during the 1934 Bihar-Nepal earthquake (Modified from Roy *et al.*, 1939).

3.1.4. Software

R-CRISIS (Aguilar & Armandeo, 2017) software was used to compute seismic hazard in terms of peak ground acceleration, peak spectral acceleration and uniform hazard seismic response spectra. The R-CRISIS is a new version of CRISIS2015, which is a versatile tool that has been widely used to perform probabilistic seismic hazard assessment (Armando *et al.*, 2017). It is a Windows based software with the capability to perform PSHA using fully probabilistic approach that allows the calculation of results with different characteristics (i.e. exceedance probability plots, set of stochastic events). It is a free software available at http://www.r-crisis.com and has been tested and validated (Armandeo *et al.*, 2017).The software computes seismic hazard by considering earthquake occurrence probabilities, attenuation characteristics and the geographical distribution of earthquakes (Ordaz *et al.*, 2017) using different

source geometry models of earthquakes in order to describe the characteristics of the seismic sources. The available geometry models in R-CRISIS are:

a) Area sources (where area planes and volumes correspond to particular cases) that are modeled as planes by means of a set of vertexes that account for a three-dimensional representation.

b) Line sources that are modeled as polylines with constant or variable depths.

c) Point sources (where grid sources are a particular case).

In addition to this software, some codes were written by myself on FORTRAN77 in order to process data to bring into required formats. ArcGIS, Adobe Illustrator and the Generic Mapping Tools (GMT) were used for drawing maps and figures.

3.2. Methods

3.2.1. Probabilistic seismic hazard analysis

Probabilistic seismic hazard analysis (PSHA) is a methodology based largely on the work by Cornell (1968). Codes for seismic hazard evaluation based on the methods of Cornell (1968) were published by McGuire (1976) and Bender and Perkins (1987).This method estimates the rate of exceedance of some ground motion levels, generally expressed in terms of peak ground acceleration or peak spectral acceleration (McGuire, 2004). It provides a framework in which the uncertainties can be identified, quantified and incorporated to provide a better image of the seismic hazard. The method has four basic steps (Figure 18), which are described below:

Step 1: Identify all earthquake sources capable of producing damaging ground motions.

Step 2: Characterize the distribution of earthquake magnitudes (the rates at which earthquakes of various magnitudes are expected to occur) and he distribution of source-to-site distances associated with potential earthquakes.

Step 3: Predict the resulting distribution of ground motion as a function of earthquake magnitude, distance, etc.

Step 4: Combine uncertainties in earthquake size, location and ground motion intensity, using a calculation known as the total probability.
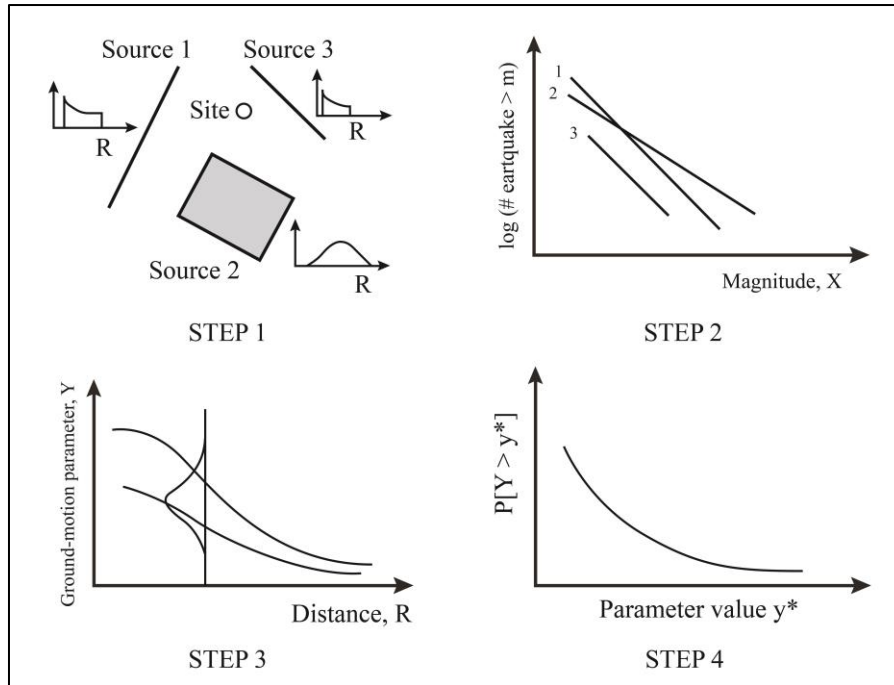
Figure 18: Four steps of probabilistic seismic hazard analysis (Redrawn from Kramer, 2007)

The methodology adopted in the present research is given in the following flow chart (Figure 19).
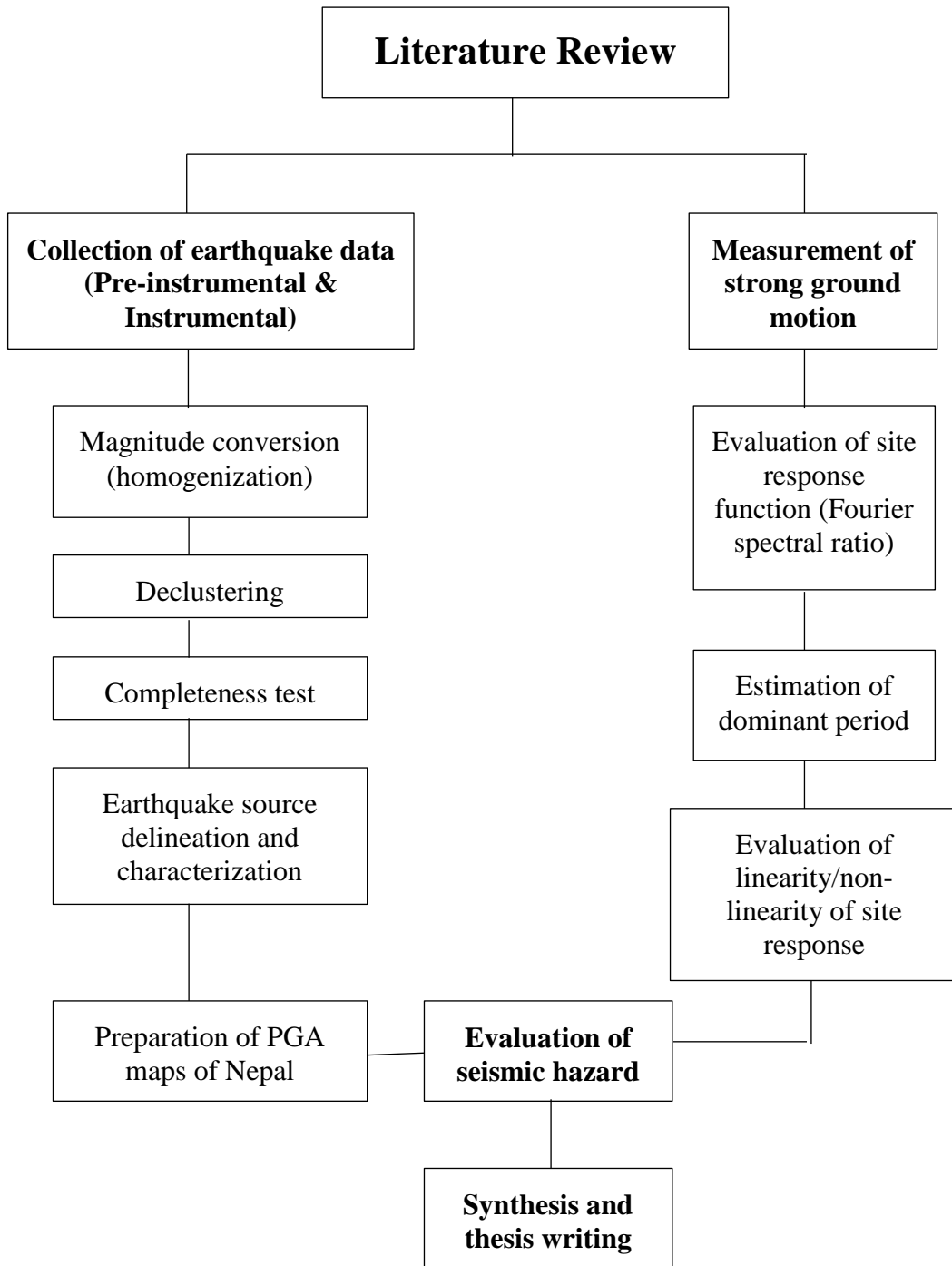
Figure 19: Flow chart of the research work.

3.2.1.1. Data collection and compilation

Data collected from different sources (ISC, USGS, IRIS and literatures) were merged into a single catalogue (Table 2, Figure 20). This catalogue was processed to develop a comprehensive and magnitude-homogenized standard catalogue to be used in the probabilistic seismic hazard analysis.

Table 2: Earthquake catalogues from different sources.

Source	Magnitude		Availability		Number
	Min	Max	From	Up to	
ISC	3	8.2	1901	2017	10882
USGS	3	8	1905	2017	4545
IRIS	3	7.8	1970	2017	9079
ISC-GEM	5	8	1905	2015	699
Pre-instrumental	5.1	8.5	1100		29
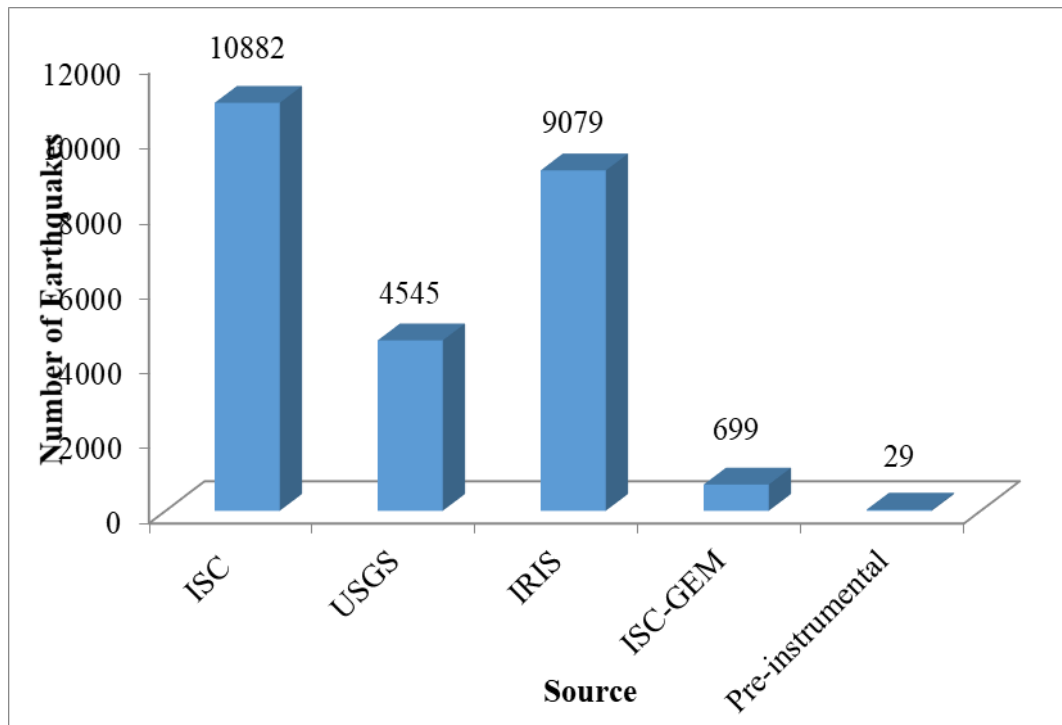
Figure 20: Different earthquake catalogues used to develop standard catalogue for PSHA.

Required data of earthquakes (origin date, time, latitude, longitude, and depth, magnitude, and magnitude type) were collected from different sources, which have published primary earthquake catalogues. Instrumentally recorded Earthquake catalogues are published by several agencies such as ISC (www.isc.ac.uk), USGS (https://earthquake.usgs.gov/), IRIS (https://ds.iris.edu/ds/nodes/dmc/data/types/events/catalogs/), and DMG (www.seismonepal.gov.np).Historical earthquakes, which occurred before the development of instrument were collected from published literatures (e.g. Szeliga *et al.*,2010; Chitrakar & Pandey, 1986; Bilham, 2004, Ambrasseys & Douglas, 2004).

After collection of earthquake catalogues from before mentioned sources, the catalogues were merged into a single catalogue for further processing.

3.2.1.2. Magnitude homogenization

Earthquake magnitude is a number, which is used to characterize the relative size of an earthquake. Magnitude is based on the measurement of the maximum amplitude recorded by instrument (seismograph). There are several defined scales in common use, but the most commonly used are (1) local magnitude (ML), commonly referred to as "Richter scale", (2) surface-wave magnitude (Ms), (3) body-wave magnitude (Mb), and (4) moment magnitude (Mw). Scales ML, Ms and Mb have limited range and applicability and do not satisfactorily measure the size of the largest earthquakes. The moment magnitude (Mw) scale, which is based on the concept of seismic moment, is popular and commonly used to all sizes of earthquakes but is more difficult to compute than the other types of magnitudes. Mw is considered the most scientific and the best compared to other magnitudes because it does not saturate even at large earthquakes (Kanamori, 1977; Kanamori & Hanks, 1979). Therefore, the other types of magnitudes (Mb, Ms and Ml) reported in the catalogue are required to be converted into moment magnitude (Mw). Empirical relations (Equation 1 to 4) derived by Scrodilis (2006) are commonly used to convert other magnitudes into Mw. The relations were established by regression analysis of global data.

Mw =0.67(±0.005) * MS + 2.07(±0.03),   Equation 1

(For shallow earthquakes (depth <70 Km) and Ms between 3.0 and 6.1),

M_w=0.99(±0.02) * M_s + 0.08(±0.13),   Equation 2

(For Ms between 6.2 and 8.2)

M_w=0.813(±0.04) * M_b + 0.367(±0.23),   Equation 3

(For Mb between 3.5 and 5)

Mw = 1.745*M_b - 4.191   Equation 4

Similarly, the local magnitude (ML) reported by the National Seismological Center (NSC) of the Department of Mines and Geology (DMG), Government of Nepal was converted into Mw using Equation 5 (Ader et al., 2012).

(For ML_{DMG} and Mw)

Mw = 0.84* ML_{DMG} + 0.21   Equation 5

3.2.1.3. Declustering

An earthquake catalogue may contain foreshocks and aftershocks. Both foreshocks and aftershocks are dependent earthquakes, which precede and follow strong earthquakes and appear in clusters. The number of foreshocks is, in general, small in comparison to aftershocks.

In probabilistic seismic hazard assessment, independent earthquakes are required, which follow Poisson distribution (Gardner & Knopoff, 1974; Shearar & Stark, 2011; Abrahamson, 2006). Therefore, the identification and removal of dependent earthquakes (foreshocks and aftershocks) is carried out to develop a catalogue of only independent events, which will be consistent with a spatially inhomogeneous, temporally homogeneous Poisson process. The dependent earthquakes can be identified on the basis of their spatio-temporal proximity to other, previous earthquakes. The dependent earthquakes occur at rates higher than the average seismicity rate averaged over long durations.

There are two methods commonly used to decluster an earthquake catalogue, which are 'window' method and 'cluster' method (Van et al., 2012). Gardner and Knopoff (1974) introduced a declustering algorithm (a windowing method) that uses the proximity of earthquakes in space and time as an indicator of clustering. Table 3 shows the time and distance criteria, which is used to identify aftershocks in an earthquake catalogue.

Table 3: Aftershock identification windows (Gardner and Knopoff 1974)

Mw	Distance(km)	Time(days)
2.5	19.5	6
3	22.5	11.5
3.5	26	22
4	30	42
4.5	35	83
5	40	155
5.5	47	290
6	54	510
6.5	61	790
7	70	915
7.5	81	960
8	94	985

The 'cluster' technique (Reasenberg, 1985) identifies aftershocks by associating earthquakes to clusters according to spatial and temporal interaction zones. The algorithm of Reasenberg (1985) assumes an interaction zone that is centered on each earthquake. Earthquakes occurring within the interaction zone of a prior earthquake are considered aftershocks. The zone is dynamically modeled with spatial (R_{fact}) and temporal (τ_{max}) parameters. The length scale R_{fact} is proportional to the source dimension, and the temporal scale τ_{max} is determined using a heterogeneous Poisson process for aftershocks with rate $\lambda(t)$. Given $t>0$, the probability of observing n earthquakes in the time interval $[t, t+\tau]$ is given by:

$$P(\chi([t, t + \tau]) = n) = \frac{e^{-\lambda(t)t}[\lambda(t)\tau]^n}{n!}$$

Equation 6

With $\lambda(t)$ following the Omori law

$$\lambda(t) = k(t + c)^{-P}$$

Equation 7

Where $\aleph$ is the process, which counts the number of aftershocks occurring in the time interval $[t, t+\tau]$, whereas k, c, and p are positive constants representing the Omori law parameters. The waiting time interval, τ_w, required observing the next event with probability, P, in a given sequence of aftershocks is

$$\tau_w = \frac{-t\log(1-P)}{10^{2(M_{max}-m_c-1)/3}}$$

Equation 8

M_{max} and mc in this equation are the largest magnitude in the sequence and completeness magnitude, respectively. The waiting time is constrained as falling between the minimum and the maximum look-ahead times (i.e., $\tau_{min} \leq \tau_w \leq \tau_{max}$).

3.2.1.4. Completeness test

The earthquake catalogue is a combination of instrumental, historic and pre-historic earthquake data. Large events appear in the catalogue since comparatively long time in comparison to smaller events because of either absence of instrument or sparse distribution in the past. The completeness of different magnitudes, in terms of years, is required in order to precisely estimate recurrence parameters of them. The completeness is evaluated visually, using technique proposed by Stepp (1972), which examines the stationary nature of the activity rate. For completeness test, the earthquake data is grouped into different magnitude classes, for example, $4 \leq Mw < 5$,

5≤Mw<6, 6≤Mw<7, 7≤Mw<8 and 8≤Mw<9. The average number of events per year in each magnitude range is calculated separately. If χ_1, χ_2, ... χ_n are the annual rates of events in a magnitude range, then the mean rate of earthquakes is calculated using Equation (9)

$$\chi = \frac{1}{n}\sum_{i=1}^{n} x_i \qquad\qquad \text{Equation 9}$$

Where n is the number of unit time intervals. The variance is given by Equation (10)

$$\sigma_\chi^2 = \frac{\chi}{T} \qquad\qquad \text{Equation 10}$$

Where T is the duration of the sample in years.

This test relies on the statistical property of the Poisson distribution that highlights time intervals during which the recorded earthquake occurrence rate does not change. The test (Figure 21) evaluates the stability of the mean rate of occurrences (χ) of events which fall in a predefined magnitude range in a series of time windows (T). If the rate of occurrence χ is constant, then the standard deviation of the rate (σ_χ) varies as $1/\sqrt{T}$ and χ is not stable if σ_χ deviates from the straight line of the $1/\sqrt{T}$ slope. The length of the time interval for which the standard deviation does not vary from the straight line is the completeness time interval for that particular magnitude class. In general, the standard deviation shows the smaller earthquakes are stable for shorter windows and the large magnitude earthquakes are stable for longer time windows. However, it is true only if the time window is significantly larger than the return period of events. In the figure it breaks for Mw>8.
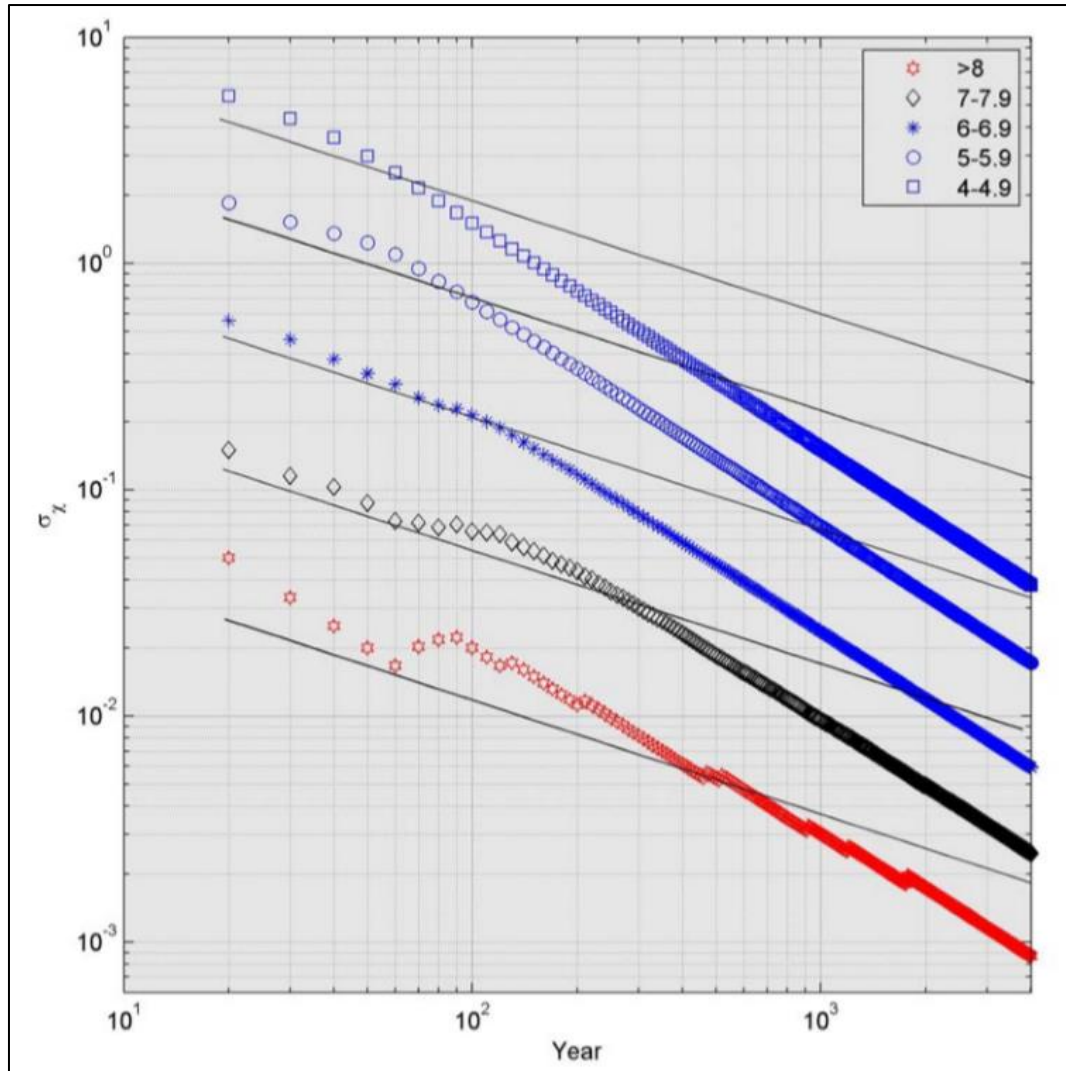
Figure 21: An example of completeness test. The blue dots represent data (λ) and the straight lines represent $1/\sqrt{T}$ (NDMA, 2010).

3.2.1.5. Magnitude of completeness

An earthquake catalogue contains earthquakes, which have magnitudes of all possible ranges. The small earthquakes are not reported completely in comparison to the large ones because the distribution of seismic stations was limited in the early days. In probabilistic seismic hazard analysis, a minimum magnitude, called magnitude of completeness (M_c) is important and, therefore, should be estimated. The catalogue is considered complete for earthquakes having magnitude equal to or larger than Mc and can be used in probabilistic seismic hazard assessment.

The M_c of the catalogue is estimated using assumption of self-similarity (Wiemer & Wyss, 2000). This method provides a fast and reliable estimate of the Mc defining the

point of maximum curvature in non-cumulative frequency-magnitude distribution graph. A plot of cumulative and non-cumulative number of earthquakes is plot (e. g. Figure 22) against respective magnitude class to identify the magnitude of completeness (Mc). The magnitude corresponding to peak on the non-cumulative curve in the plot is the magnitude of completeness (Mc).
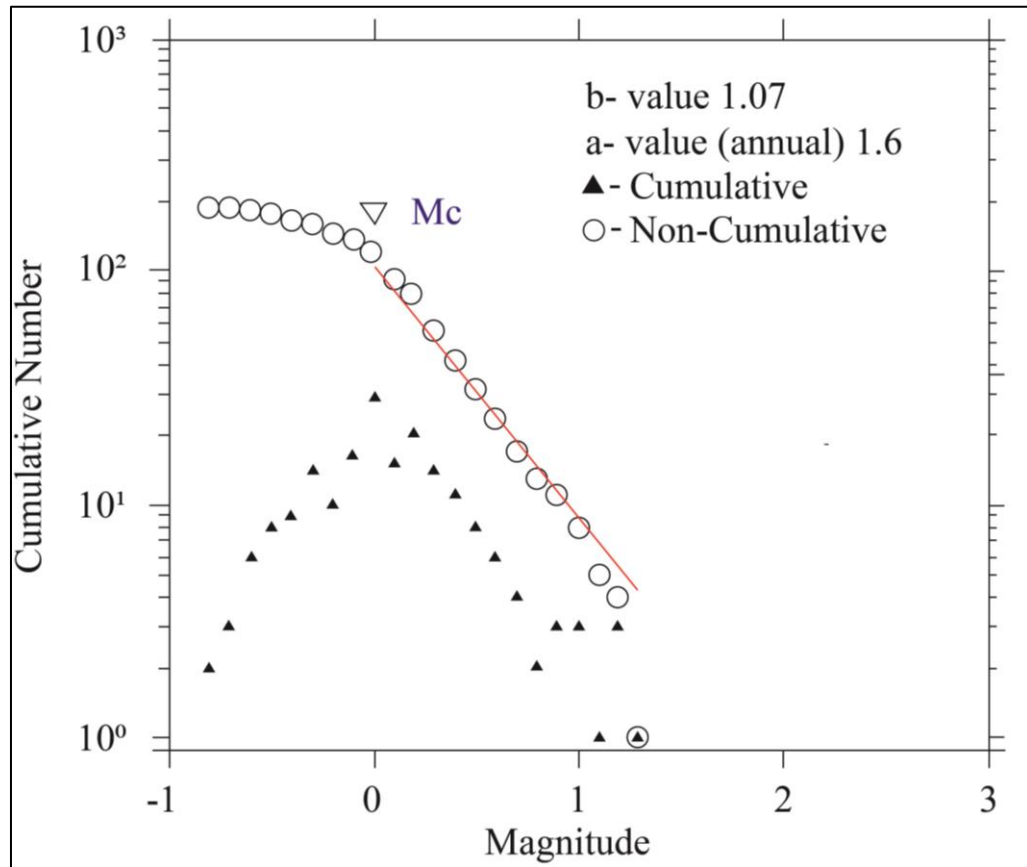
Figure 22: An example of determination of Mc. The curve with triangle corresponds to non-cumulative number of earthquakes and the circle represent the cumulative number. The peak value of the non-cumulative curve is considered to be Mc. (Modified from Romano *et al*., 2015)

3.2.1.6. Identification and characterization of seismogenic sources

(a) Identification of potential sources:

Probabilistic seismic hazard analysis requires identification and delineation of all potential earthquake sources, which are close to the site of interest. Ground motion is calculated using various characteristics (magnitude, distance and recurrence parameters) of the sources and appropriate ground motion prediction model (attenuation relation). Therefore, identification of potential earthquakes sources is very important in any types of seismic hazard assessment. Earthquake sources are

45

identified and delineated using local seismicity pattern, location of historical earthquakes, seismotectonics, geodetic information and geological structures. The potentially strong earthquake sources are geological faults (e. g. Figure 23: source 1 and source 3), which are planar surfaces. If faults are not easily identifiable (as in the less seismically active regions of the eastern United States), then earthquake sources are simply described by areal regions (e. g. Figure 23, source2), where earthquakes may occur at any place (Baker, 2013).
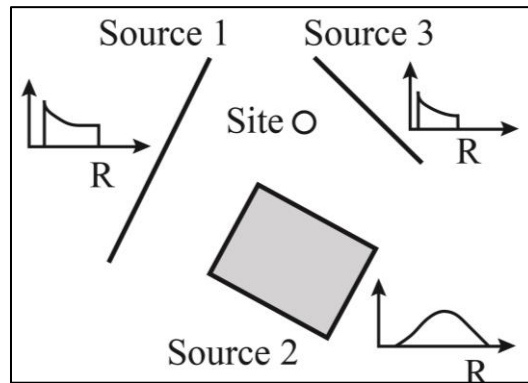
Figure 23: Possible earthquake source models (Modified from Baker, 2013).

(b) Maximum Potential Magnitude:

After identification and delineation of sources, the maximum potential magnitudes of the identified sources are estimated. The maximum potential magnitudes of identified sources are estimated using empirical relations, which are functions of area of sources, length of faults and displacement on faults, or are adopted from the magnitudes of known, historical destructive earthquakes. Empirical relations (Equation 11 through Equation 15) established by Wells & Coppersmith (1994) were used to estimate the maximum potential magnitudes...

$M_w = 4.33 + 0.90 \log A$, $(\sigma M_w = 0.25)$ reverse fault $\hfill$ Equation 11

$M_w = 3.93 + 1.02 \log A$, $(\sigma M_w = 0.25)$ normal fault $\hfill$ Equation 12

$M_w = 5.0 + 1.22 \log L$ $(\sigma M_w = 0.28)$ reverse fault $\hfill$ Equation 13

$M_w = 5.16 + 1.12 \log L$ $(\sigma M_w = 0.28)$ strike slip fault $\hfill$ Equation 14

$M_w = 4.86 + 1.32 \log L$ $(\sigma M_w = 0.34)$ normal fault $\hfill$ Equation 15

In the above relations, M_w is the maximum possible moment magnitude (Mw), A is the area (in km^2) of the source region, L is the length of the fault in km; σM_w is the standard deviation of moment magnitude from the median.

(c) Gutenberg-Richter Relation

Gutenberg & Richter (1944) were the first to study the distribution of earthquake magnitudes, who noted that the number of earthquakes in a region, greater than a given size, generally follows a particular distribution called Gutenberg-Richter relation (Equation 16).

$$\log \lambda_m = a - b * m$$
<div align="right">Equation 16</div>

Where 'λ_m' is the rate of earthquakes with magnitudes greater than 'm', and 'a' and 'b' are constants called 'a-value' and 'b-value' respectively.

Gutenberg–Richter relation is well known empirical relation in seismology which describes the frequency of occurrence of earthquakes as a function of magnitude. In the relation (Equation 16), the factor 'a' (a-value) is the logarithm of the total number of earthquakes with magnitude greater than or equal to 'm'. It is a constant, which depends on many parameters like size of the area, time interval, total number of earthquakes and magnitudes of each earthquake and the value of "b" (Bora *et al.,* 2018). Mathematically speaking, a-value is the log number of earthquakes with magnitude equal to 0 (Allen, 1986) and describes total activity of earthquakes in the region. The a-value depends on the rate of seismicity and the length of observation time.

The factor 'b' (b-value) describes the relative number of large and small earthquakes. It is important because it is used to quantify seismic activity and seismic hazard. The b-value is the slope of the curve (Figure 24) of cumulative number of earthquakes versus magnitude. For active tectonic region its value is about 1 and for volcanic region it is 2.5 (e. g. Throne & Terry, 1995) or higher. A small b-value means strong earthquakes are frequent and vice versa. The b-value depends on tectonics, structural heterogeneity and stress distribution in space (Schorlemmer *et al.*, 2005; Khan & Chakraborty, 2007; Mousavi, 2017a, 2017b). This relationship between earthquake magnitude and frequency of occurrence is found remarkably consistent in worldwide

data, although the values of a-value and b-value may vary from region to region or over time. When b-value is 1.0, for a given frequency of magnitude 4.0 or larger events there will be 10 times as many magnitude 3.0 or larger quakes and 100 times as many magnitude 2.0.

Earthquakes with magnitude larger than or equal to the magnitude of completeness (Mc) are used to derive the Gutenberg-Richter relation, because below Mc, $\log \lambda_m$ cannot behave linearly due to insufficient coverage (e.g. Wiemer & Wyss, 2000).

An example of the law is shown in Figure 24 below.
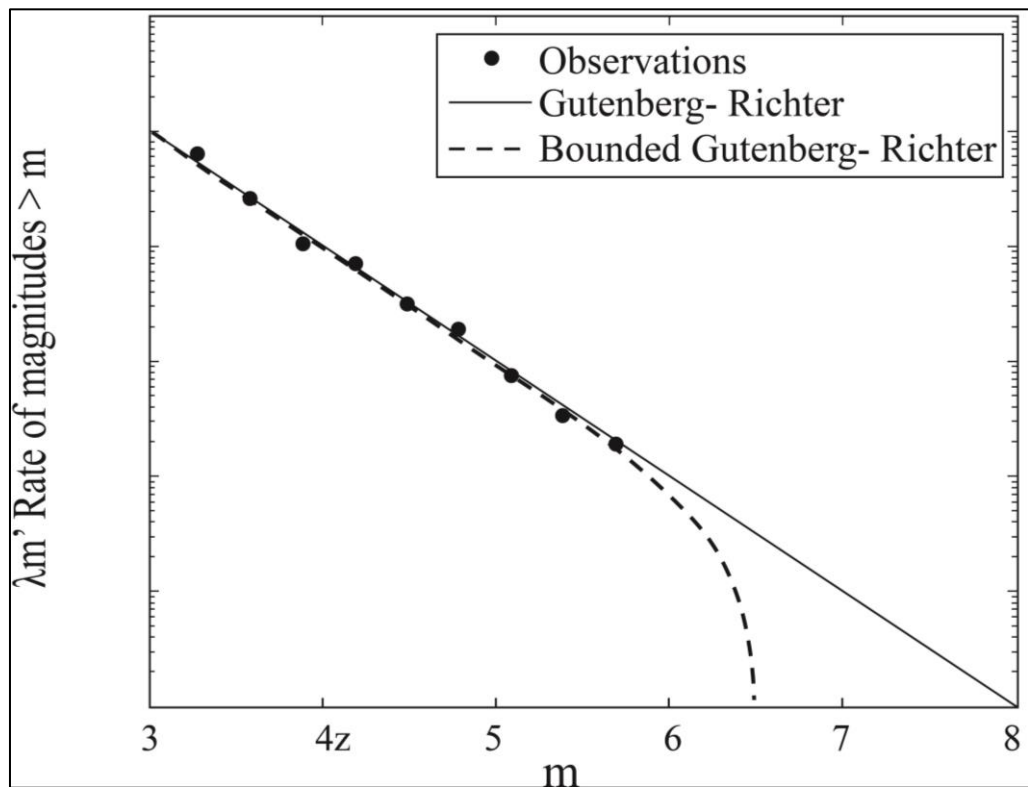
Figure 24: An example of Gutenberg-Richter relation plot. The slope of the curve is the 'b' value in the G-R relation.

The common technique of estimating 'b' value is the least squares fit to the logarithm of the data. This technique leads to an answer that is biased for small data sets and apparent errors that are much smaller than the real ones. The maximum likelihood method (Equation 17) of Aki (1965) is preferred over the least square method to calculate 'b' value, but it requires large data sets. Aki (1965) indicate that a minimum of 2000 earthquakes are required to calculate 'b' to within 0.05 at 98% confidence. Significant problems for 'b' value calculation can be caused by choosing a smaller magnitude of completeness (Mc).

$$b = log_{10}e/(M_{mean} - M_{min})$$ Equation 17

Where 'b' is b-value, M_{mean} is the average magnitude in the catalogue and M_{min} is the minimum magnitude. $Log_{10}e$ equals 0.434 and, therefore, the equation can be rewritten as:

$$b = 0.434/(M_{mean} - M_{min})$$ Equation 18

The equation 16 can be rearranged as

$$\lambda_m = 10^{(a-bm)} = \exp(\alpha - \beta*m_o).$$ Equation 19

Where $\alpha = 2.303*a$ and $\beta = 2.303*b$.

Equation (19) shows that earthquake magnitudes are distributed exponentially. This relation covers earthquakes of infinite ranges i. e. from infinitely small to infinitely large. Very small earthquakes have importance in science but the effect is of little interest in engineering field, therefore, small earthquakes are commonly ignored because they cannot cause damage to structures. The lower threshold magnitude is set to 4.0 or 5.0 in most PSHAs because earthquakes smaller than these seldom cause damage (Kramer, 2007). If earthquakes with magnitude smaller than a lower threshold are ignored, the mean annual rate of exceedance can be written (McGuire & Arabasz, 1990) as:

$$\lambda_m = v\,e^{[-\beta(m-m_0)]}\ m > m_l$$ Equation 20

Where $v = e^{(\alpha-\beta m)}$

The standard Gutenberg-Richter relation can predict non-zero mean rates of exceedance for earthquakes of infinitely large size. But earthquakes of size larger than Mw 10 have not been known so far. An earthquake source has its maximum potential

magnitude and if we know the maximum potential magnitude of the earthquakes source, the mean annual exceedance rate can be estimated using Equation (21) (McGuire & Arabasz, 1990).

$$\lambda m = \nu \frac{e^{[-\beta(m-m_l)]} - e^{[-\beta(m_{max}-m_l)]}}{1 - e^{[-\beta(m_{max}-m_l)]}} m_l \leq m \leq m_{max} \qquad \text{Equation 21}$$

Equation (21) is the bounded or tapered recurrence law, which is graphically shown in Figure 24 for constant mean annual exceedance rate of m_l for different maxium magnitudes. The annual exceedance rate decreases with the increase of maximum magnitude.

(c) Magnitude Characterization:

All the earthquake sources have their own maximum potential magnitude. Earthquakes smaller than magnitude 5 are not considered as strong ones to cause damage, therefore, the probability of intermediate magnitudes above Mw 5 and below the maximum magnitude are calculated (e. g. Figure 25). The cumulative density function (CDF) and probability density function (PDF) for the Guttenberg - Richter relation with upper and lower bounds can be expressed as:

$$FM(m) = P[M < m \backslash m_0 \leq m \leq m_{max} = \frac{1 - \exp[-\beta(m-m_0)]}{1 - \exp[-\beta(m_{max}-m_0)}} \qquad \text{Equation 22}$$

$$f_M(m) = \frac{\beta \exp[-\beta(m-m_0)]}{1 - \exp[-\beta(m_{max}-m_0)}} \qquad \text{Equation 23}$$

Where, F_M (m) and f_M(m) are cumulative density function and probability density function. β is earthquake recurrence parameter and equals to 2.303*b, m is magnitude considered, m_0 is minimum magnitude and m_{max} is maximum potential magnitude for the given source.
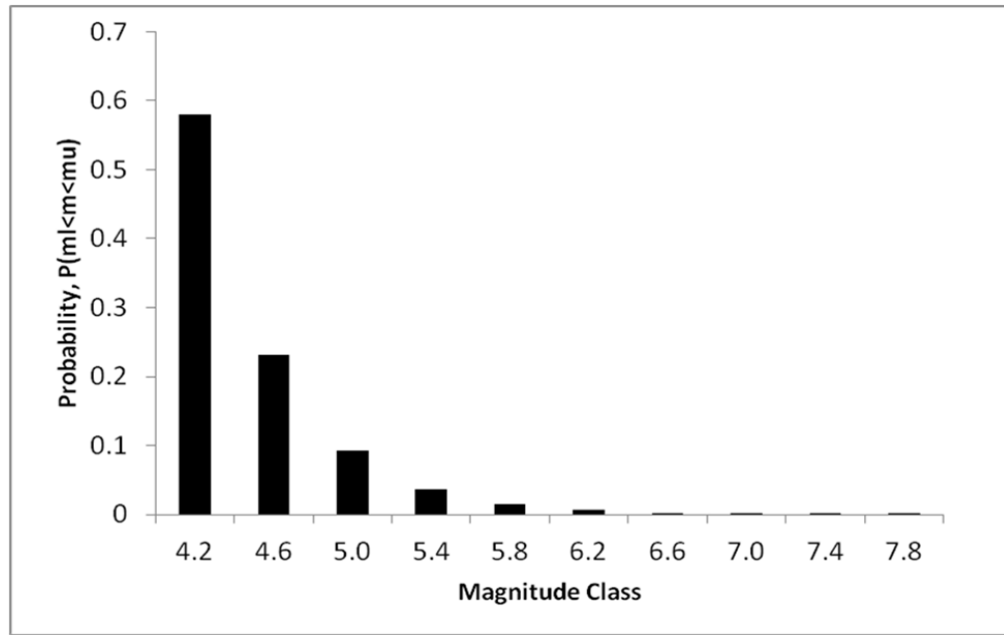
Figure 25: An example of probability density function of intermediate magnitude earthquakes.

(a) Spatial characterization:

Earthquakes are considered equally likely to occur at any location in any earthquake source. The uncertainty in the location of earthquakes is required to be described by appropriate distance parameter. The spatial uncertainty, generally, is described by a probability density function (e. g. Kramer, 2007). To account for this uncertainty, the source is divided into a number of blocks and distance is calculated from the centre of each block to a particular place where seismic hazard is to be carried out. If the source is divided into n*n blocks; there will be n^2 blocks. The calculated distances are divided into equal distance intervals and source-to-site distances falling in each interval is counted and probabilities P(R) is calculated. An example of the probability of 30 distance classes is presented in Figure 26.

Figure 26: An example of probability density function of distance (km) classes.

3.2.1.7. Calculation of ground motion

Earthquake source, its maximum potential magnitude and distance between the source and site are required to calculate ground motion at a particular location. A ground motion predicting relation (called attenuation relation) is used to estimate ground motion using before-mentioned data. The relations are derived after regression analysis of strong motion data recorded at a large number of sites from large set of earthquakes having different distances, magnitudes, depths and mechanisms. Attenuation relations are available for different types of tectonic environments e.g. subduction, stable continental, active shallow crustal etc. An example of attenuation relation is given in Figure 27.

The standard deviation of the predicted parameter like peak ground acceleration and spectral acceleration are calculated in order to account for uncertainty related with scatter of seismic data and randomness in rupture of seismic sources. From the probability distribution of particular ground motion parameter, the probability that this parameter Y exceeds a certain value, y*, for an earthquake of a given magnitude, m, which occurs at a distance, r, is given by Equation 24 and graphically presented in Figure 28:

P[Y>y*/m, r] =1-F_Y (y*)   Equation 24

Where, $F_Y(y)$ is the value of the cumulative distribution function of Y at m and r. The value of $F_Y(y)$ depends on the probability distribution used to represent Y. In general, ground motion parameters are usually assumed to be log normally distributed (the logarithm of the parameter is normally distributed); however, the unbounded characteristics of that distribution can attribute to a nonzero probability to unrealistic values of the ground motion parameters.
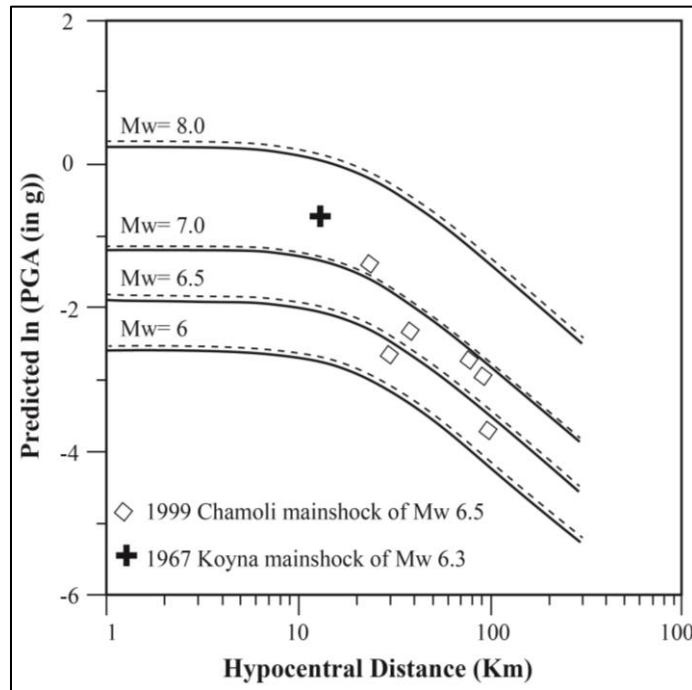
Figure 27: An example of Attenuation curves (modified from Mandal *et al*., 2009).
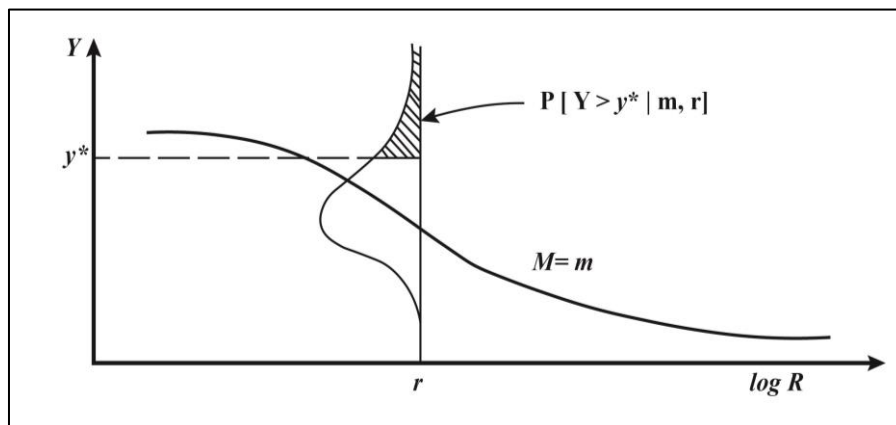
Figure 28: An example of conditional probability of exceeding a particular value of a ground motion parameter for a given magnitude and distance.

53

3.2.1.8. Uncertainties in PSHA

Probabilistic Seismic Hazard Analysis (PSHA) is a method that deals with uncertainty. While there is considerable information on earthquake ground motions and potential future locations of earthquakes, there is also considerable uncertainty in the inputs to the analysis. Therefore, it is important to identify and address these uncertainties in PSHA. Probabilistic Seismic Hazard Analysis (PSHA) aims to quantify these uncertainties, and combine them to produce an explicit description of the distribution of future shaking that may occur at a site (Baker, 2008). The uncertainties can be grouped into epistemic and aleatory uncertainties.

(a) Aleatory uncertainty

Aleatory uncertainty arises from the randomness of the phenomenon and cannot be reduced even we have large additional data or information. Aleatory uncertainties are objective, which can be quantified but cannot be modified with the addition of additional data (Ordaz & Arroyo, 2016):

The followings are the examples of aleatory uncertainties:

- Recurrence relations: The Poisson model assumes that even though we know accurately the recurrence relation we cannot predict where or when the next earthquake will occur or what size it will be.
- Standard deviation of the attenuation relation: No matter how accurately we know the magnitude and distance of a postulated earthquake source, there still will be some uncertainty in predicting the ground motion, which is reflected in the standard deviation.

(b) Epistemic uncertainty

Epistemic uncertainty arises from the lack of knowledge about model and parameter. This type of uncertainty can be reduced using additional data or improved information. In the past it was called statistical or professional uncertainty (McGuire, 2004).Epistemic uncertainty depends on the available information and can be reduced by additional data and therefore varies with time. It is generally subjective, which involves a degree-of-belief in interpretation and probability theory may not apply in this case.

The following are some examples of epistemic uncertainty (Ordaz & Arroyo, 2016):

- What and where are the seismogenic sources?
- Are the sources seismically active at present?
- What are the potential magnitudes of the potential earthquake sources?
- Which attenuation relation best applies to the region of interest?

3.2.1.9. Logic Tree

The probability computation allows us systematic consideration of uncertainties in the values of the parameters in any seismic hazard model (Kramer, 2007). Logic trees are important (Power *et al.*, 1981; Kulkarni *et al.*, 1984; and Coppersmith & Youngs, 1986) in PSHA, which are used to incorporate uncertainties providing a convenient framework for the explicit treatment of model uncertainty (Kramer, 2007).

A reliable and trustworthy probabilistic seismic hazard analysis (PSHA) accounts for the intrinsic variability of the system (aleatory variability) and the limited knowledge of the system itself (epistemic uncertainty). This approach uses alternative models, each of which is assigned a weighting factor, which is interpreted as the relative likelihood of that model being correct. A logic tree consists of a number of nodes, which represent points at which models are specified and the branches represent different models specified at each node. The sum of the probabilities of all branches, which are connected to a given node equals 1. The logic tree (Figure 29) allows incorporation of uncertainty in selection of models for attenuation, magnitude distribution and maximum potential magnitude to be considered in the calculations (Kramer, 2007).
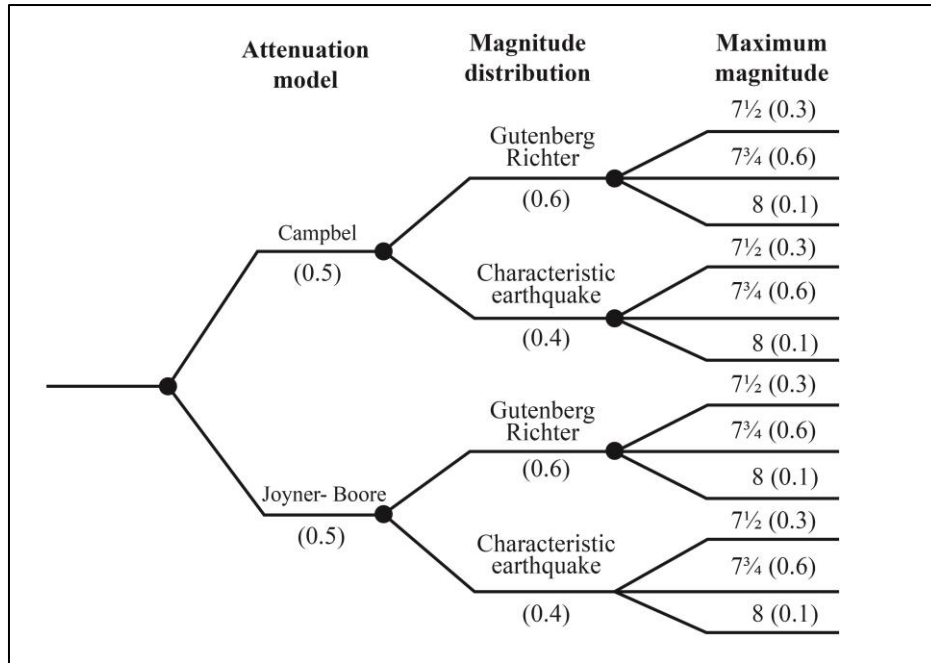
Figure 29: An example of logic tree (Redrawn from Kramer, 2007). It provides a framework in which the uncertainty is treated assigning certain weight.

3.2.1.10. Probability computation

It is the final step in probabilistic seismic hazard analysis. It calculates the total probability of exceedance of specified level of peak ground acceleration. The uncertainties in earthquake size, location and ground motion prediction are combined to obtain the total probability. In general, the magnitude is divided in to 'j' number of intervals for 'i' number of sources and source to site distance is divided into 'k' number of intervals. An attenuation relationship is used to calculate peak ground acceleration in each interval of magnitude and distance. The combined probability of particular ground motion parameter is expressed as mean annual rate of exceedance to that value of ground motion parameter, which is expressed as:

$$\lambda_{y^*} = \sum_{i=1}^{Ns} \sum_{j=1}^{Nm} \sum_{k=1}^{Nr} \nu_i \rho\left[(y > y^*)/m_j, f_k\right] f M_i(m_j) f R_i(r_k) \Delta m \, \Delta r \qquad \text{Equation 25}$$

where, $\lambda_{y}*$ is the annual rate of exceedance of peak ground acceleration y* occurring at source from 1 to number N_S in between magnitudes of total N_M number at source to site distances of ranges from 1 to Nr number. ν_i is the annual rate of exceedance of minimum threshold earthquake (M=4) at source *i* derived using G-R recurrence relationship as represented by Equation (16) in which λ (m=4) = ν, and P[Y>y*/m_j, r_k] is the probability of exceedance of specified peak ground acceleration Y to the value

y* obtained using attenuation relationship for given magnitude m and distance r at each of interval of one to j number and k number respectively. Probability of exceedance of acceleration is calculated using normal distribution function as given by Equation 25. $f_M(m)$ is the function of magnitude probability as given by truncated G-R relationship with upper and lower bound as expressed in Equations (22 and 23). An example of seismic hazard curve (annual probability of exceedance versus PGA) is given in Figure 30.
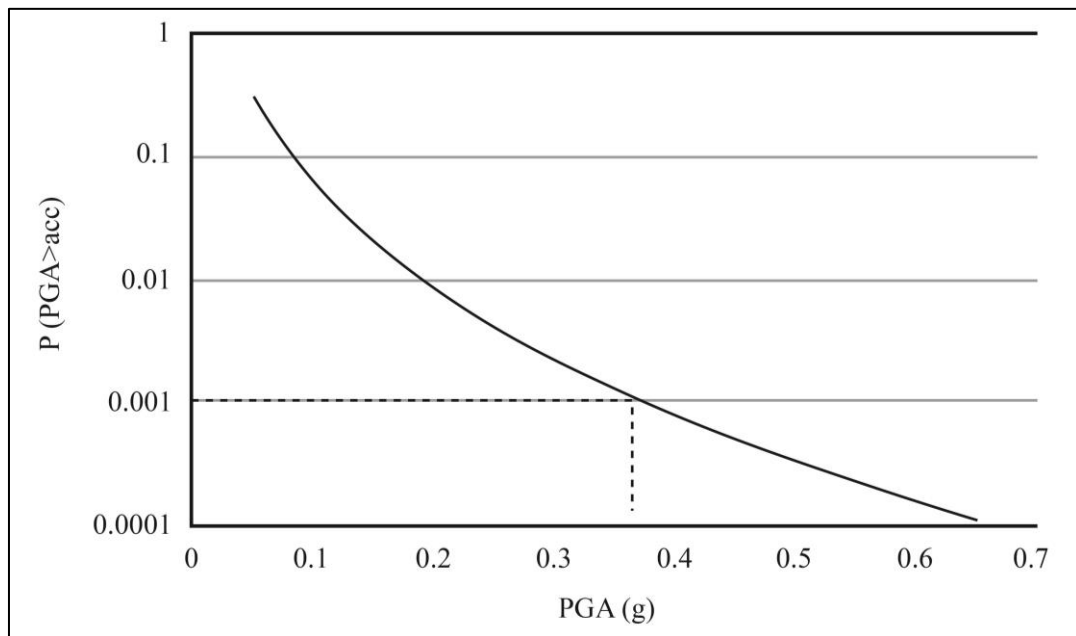
Figure 30: An example of seismic hazard curve. It provides mean annual exceedance rate of PGA for a particular site (Source: Kramer, 2007).

3.2.1.11. Seismic hazard map

To prepare seismic hazard maps, the area of interest is divided into a number of blocks. PGA is calculated for different exceedance rates at each node of the study area. . Finally, the values at the nodes are contoured to produce seismic hazard maps.

3.2.2. Seismic ground response investigation

3.2.2.1. Strong ground motion data recording

Strong motion (acceleration) data recorded on ground is required in this investigation. The records should be free from effects of structures, therefore, should not be from any instrument installed in structures.

3.2.2.2.Determination of PGA in the records

The time series data of strong motion (acceleration) records is baseline corrected and filtered to remove undesirable frequencies. After filtering, the PGA is estimated from the plot of time series data (Figure 31(a)).

3.2.2.3. Fourier transformation

The time series data (Figure 31(a) which come in time-domain are transformed into frequency-domain using Fourier Transformation. The Fourier spectrum (Figure 31(b)) of Fourier amplitude vs. frequency (or period) shows the fundamental period at the site.
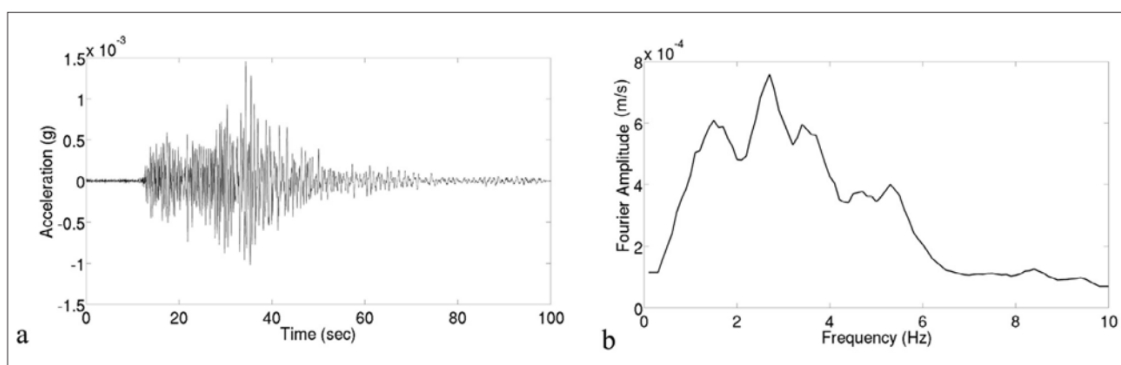
Figure 31:(a) An example of time series (acceleration) data of an earthquake recorded at a site. The PGA is the largest absolute acceleration value on the y-axis. (b) Fourier amplitude spectra of the time series data (a) (source Bohhano *et al.*, 2017).

3.2.2.4. Amplification factor (ratio) calculation

Amplification of ground motion is estimated using strong motion records in frequency domain. Amplification factor is expressed as a ratio of Fourier spectrum (Figure 32) at soil site to that at reference (rock) site.
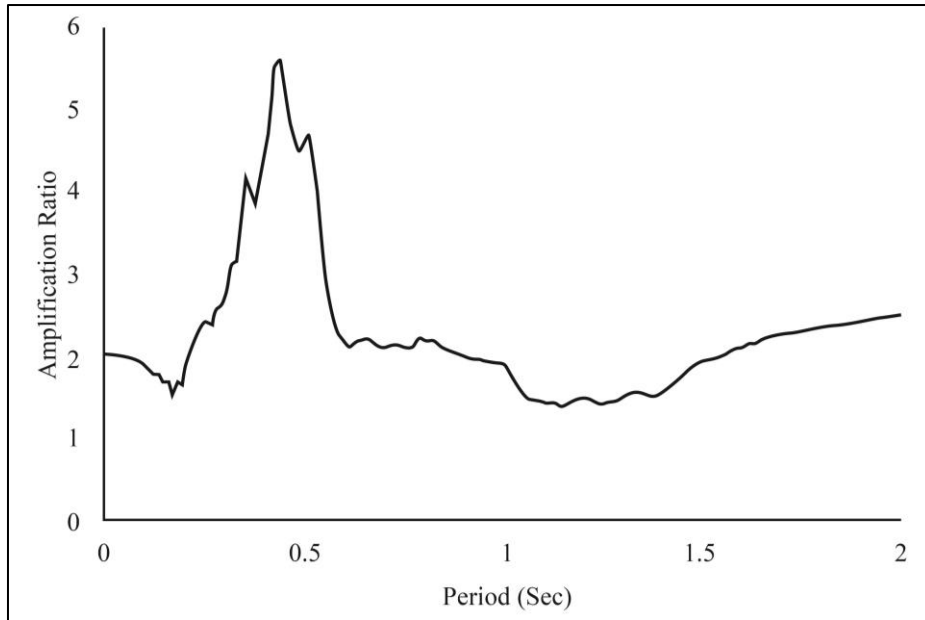
Figure 32: An example of amplification ratio determination. The curve represents ratio of Fourier spectra at soil site to a reference (rock) site.

CHAPTER 4

RESULTS AND DISCUSSIONS

4.1 Data Processing

After collection and compilation of earthquake catalogues collected from different sources (ISC, USGS, IRIS, DMG and published literatures) the catalogue was checked for duplicate events. Duplicate events were removed from the catalogue in order to make catalogue of standard events, which do not have repetition of data in it.

4.2 Magnitude conversion

The merged catalogue had magnitudes presented in terms of moment magnitude (Mw), body wave magnitude (Mb), surface wave magnitude (Ms) and local magnitude (ML). Moment magnitude (Mw) is generally considered the best compared to other magnitudes because it does not saturate even at large earthquakes (Kanamori, 1977; Kanamori & Hanks, 1979). The other types of magnitudes (Mb, Ms and ML) reported in the catalogue were converted into Mw using empirical relations derived by Scrodilis (2006) and a catalogue of magnitude-homogenized earthquakes was prepared. Figure 33 presents the number of earthquakes, after magnitude conversion, in different time intervals. Equations 1, 2, 3, 4 and 5, in Section (§3), were used to convert magnitudes into moment magnitude (Mw). The number of earthquakes increased from 289 to 1000 in 2000 and reached to 1623 in 2017 because of the addition of new networks as well as expansion of existing seismic networks that resulted in the reduction of threshold magnitude of the networks.

The number of earthquakes in different magnitude classes is presented in Figure 34. The number of small earthquakes is naturally larger than that of the strong earthquakes. Earthquake of Mw 4-4.9 are 4323, Mw 5-5.9 are 365, Mw 6-6.9 are 73, Mw 7-7.9 are 33 and Mw>8 are only 6.
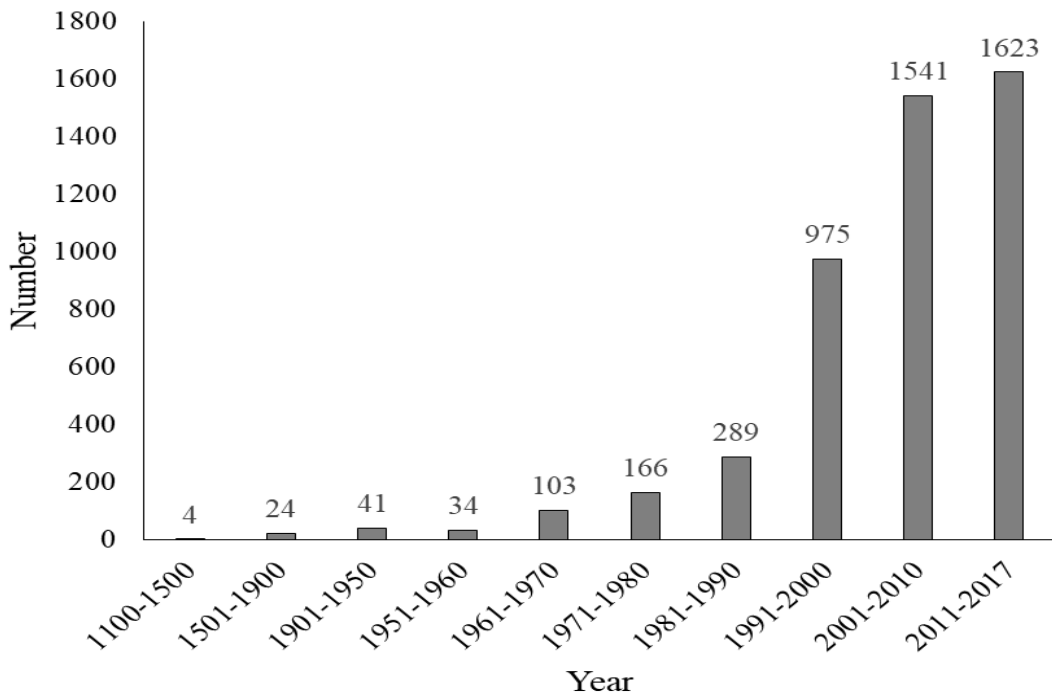
Figure 33: Distribution of earthquakes with magnitude (Mw > 4) in different time intervals after magnitude conversion.
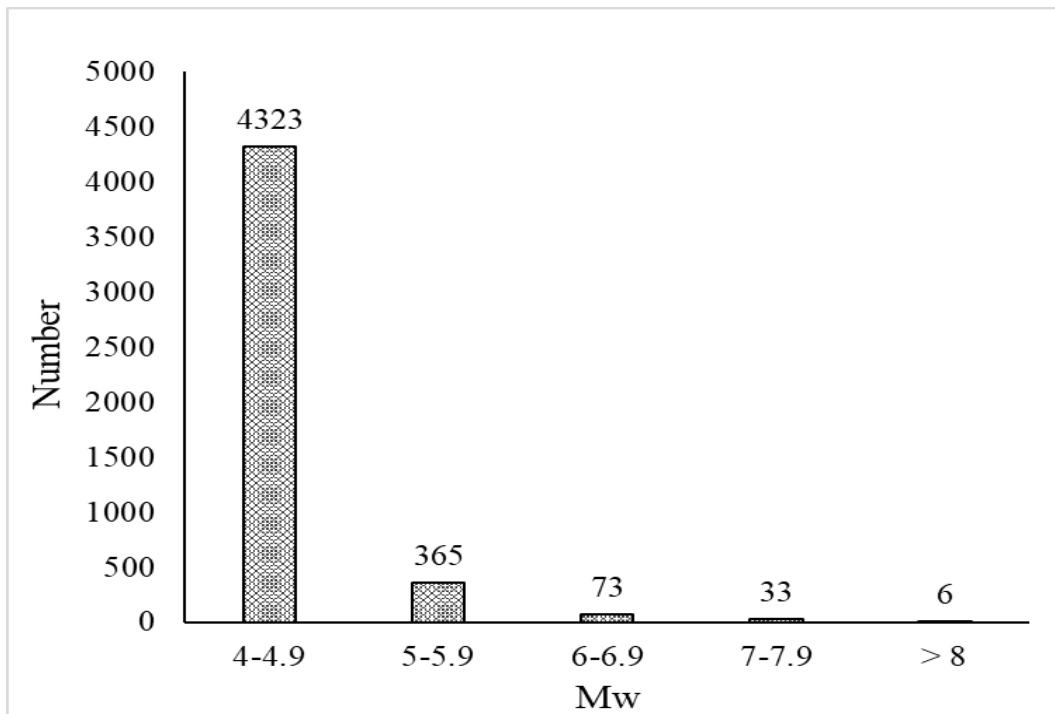
Figure 34: Number of earthquakes in different magnitude classes after magnitude conversion.

4.3 Declustering

The earthquakes contained in the magnitude-homogenized catalogue are graphically presented in Figure 35. The clusters of earthquakes in the figure are mostly aftershocks, which are dependent events. The cluster in the central region of Nepal represents the aftershocks of the 2015 Gorkha Earthquake.
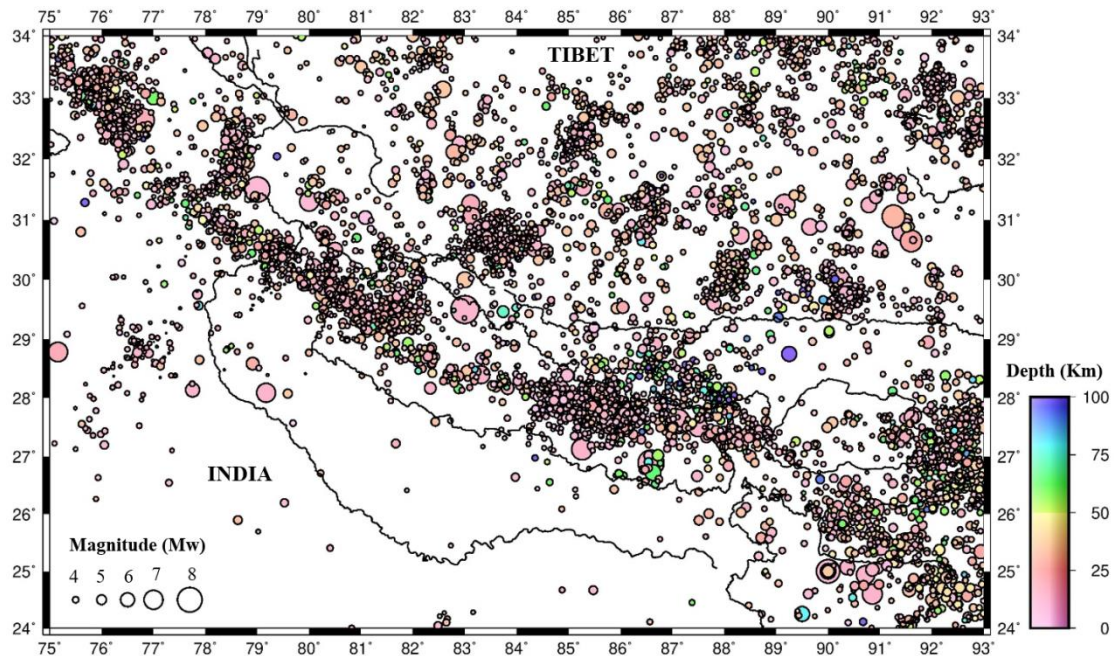
Figure 35: Epicenter distribution of earthquakes in the prepared catalogue. The clusters noticed in the figure are dependent earthquakes. The dense clustering in central Nepal compared to other parts is due to the aftershocks of the 2015 Gorkha Earthquake.

The magnitude-homogenized earthquake catalogue was declustered to identify and remove dependent earthquakes. A FORTRAN program "Cluster 2000" (Equation 6, 7 and 8, §3.2.1.2), was used to decluster the catalogue, which uses 'cluster' technique of Reasenberg, 1985. The program is freely available on https://www.usgs.gov/software/cluster2000.

The distribution of earthquakes, contained in the declustered catalogue, is graphically presented in Figure 36. The dense clusters of earthquakes, which contain dependent earthquakes, present in the earthquake catalogue (Figure 35) disappeared after declustering. An evidence of declustering is shown in Figure 37. The figure shows the cumulative number of earthquakes since 1970 before declustering (green dotted line) and after declustering (blue dotted line). The green line shows sudden rise in the

number of earthquakes at 1999, 2008 and 2015. The increase in number in 2015 belongs to the aftershocks of the 2015 Gorkha Earthquake (Mw 7.8).
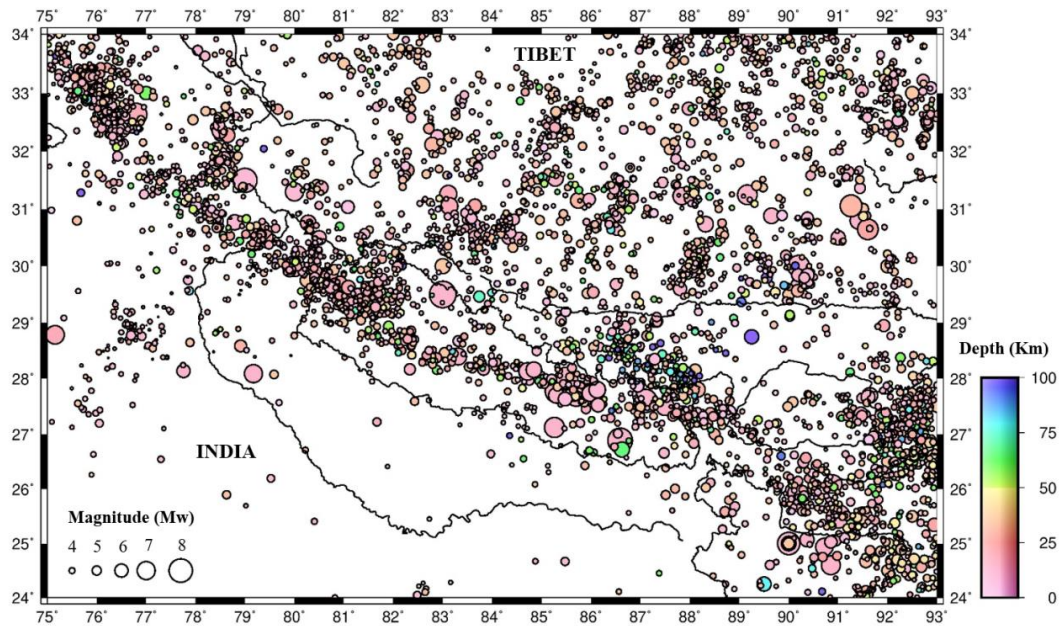
Figure 36: Epicenter distribution of independent events after declustering (free of dependent events) of the catalogue. Note that the clusters (aftershocks) of earthquakes, which appear in Figure 35 disappear, after declustering.
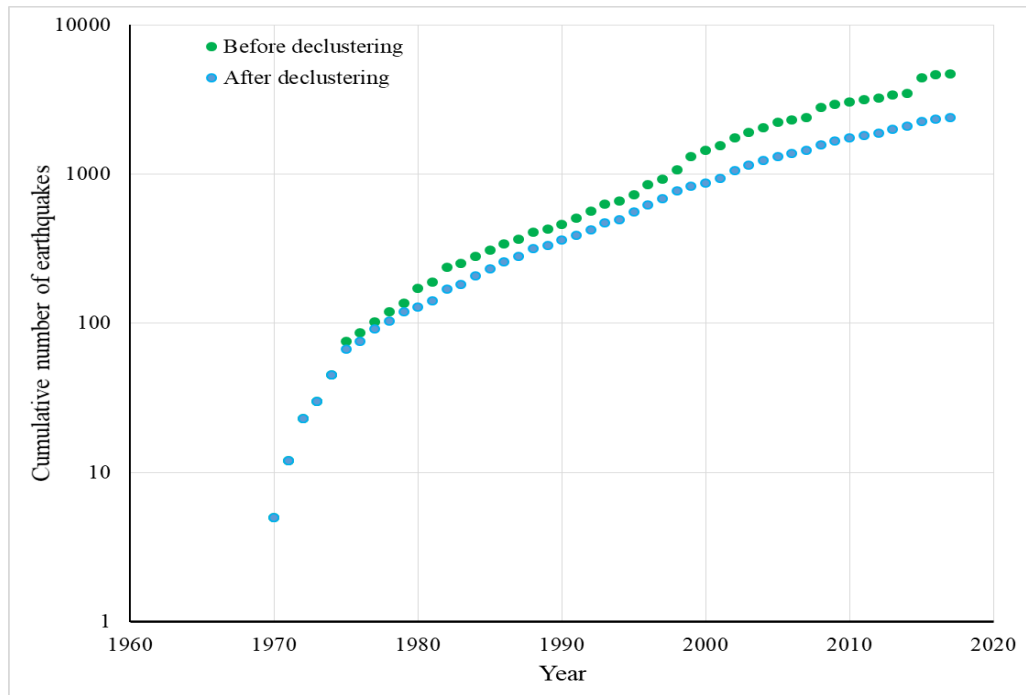
Figure 37: Cumulative number of earthquakes before and after declustering. The curves show the removal of dependent events in 1999, 2008 and 2015, which belong to the aftershocks of 1999 Chamoli Earthquake, 2008 Earthquake and 2015 Gorkha Earthquake in their order.

The magnitude-homogenized earthquake catalogue had 4800 earthquakes (Mw≥4) before the declustering process was applied. After declustering, the number of earthquakes in the catalogue dropped to 2590, whereas 2210 earthquakes were identified as dependent earthquakes (foreshock and aftershock) and removed from the catalogue (Figure 38).
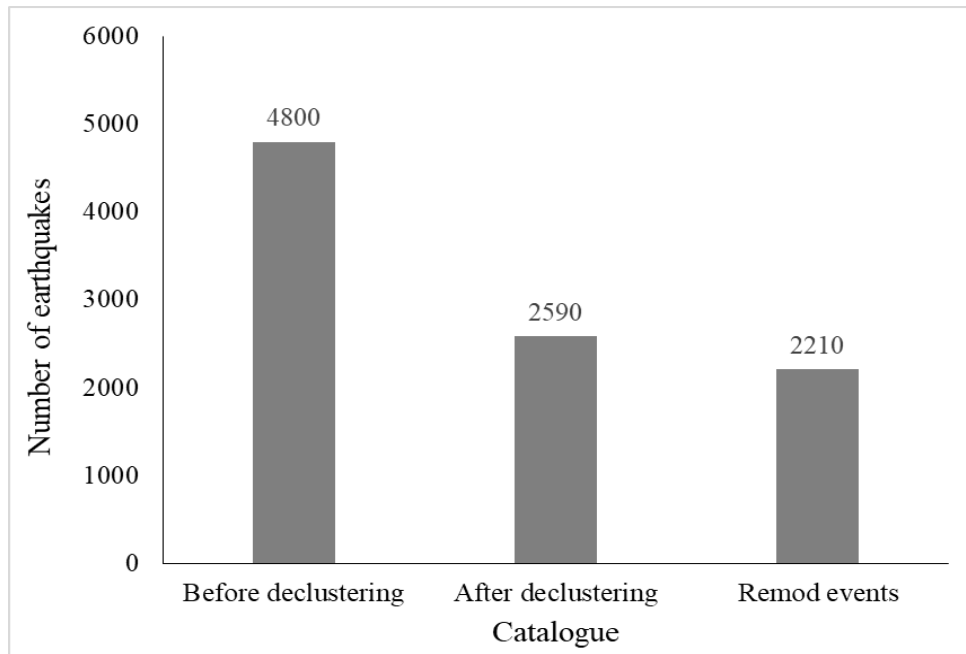
Figure 38: Number of earthquakes before and after applying declustering technique.

4.4. Completeness test

The magnitude-homogenized and declustered catalogue consists of earthquakes of a range of magnitudes, available for different length of time (Figures 39(a) and 39(b)). Both the figures show that small earthquakes (Mw ~4.0) appear in the catalogue very lately (around 1960 AD) in comparison to the large earthquakes (around 1255 AD).
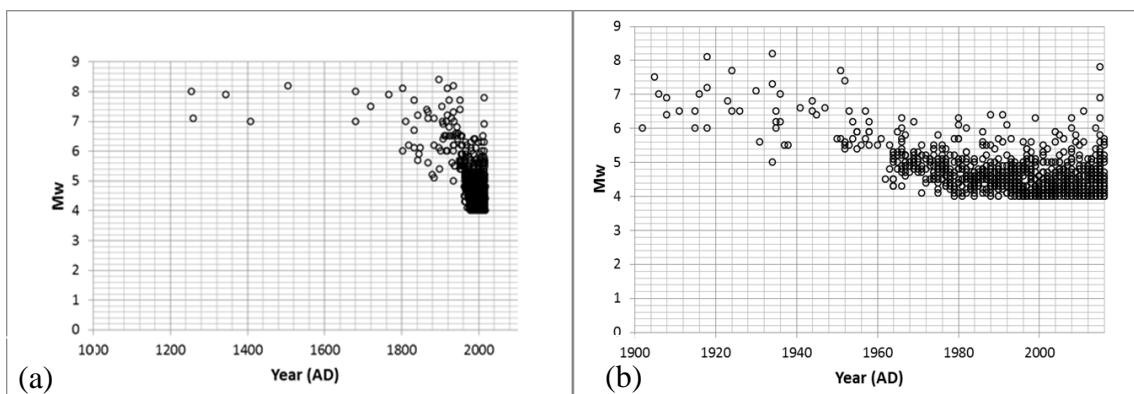
Figure 39: Earthquake magnitude in the catalogue and their reported time. (a) Earthquake data since 1100AD. (b) Earthquake data since 1900 AD.

The complete time interval of each magnitude class was visually determined from the T (time) versus σ (standard deviation of mean of the annual number of earthquakes) plot as shown in Figure 40. In order to estimate the completeness levels of different magnitude classes, the catalog was split into 8 time windows of 100-year length between 1100 (first data entry in the catalogue) and 1900 AD and 11 time windows of 10-year length after 1900 AD. The results of completeness of different magnitude classes for South Tibet and the Himalaya are given in Table 4. The Table 4shows that Mw 4.0 earthquakes are completely reported since last 15 years, Mw 4.5 are reported since last 35 years, Mw 5.0 since last 55 years and so on for both Himalaya and South Tibet.
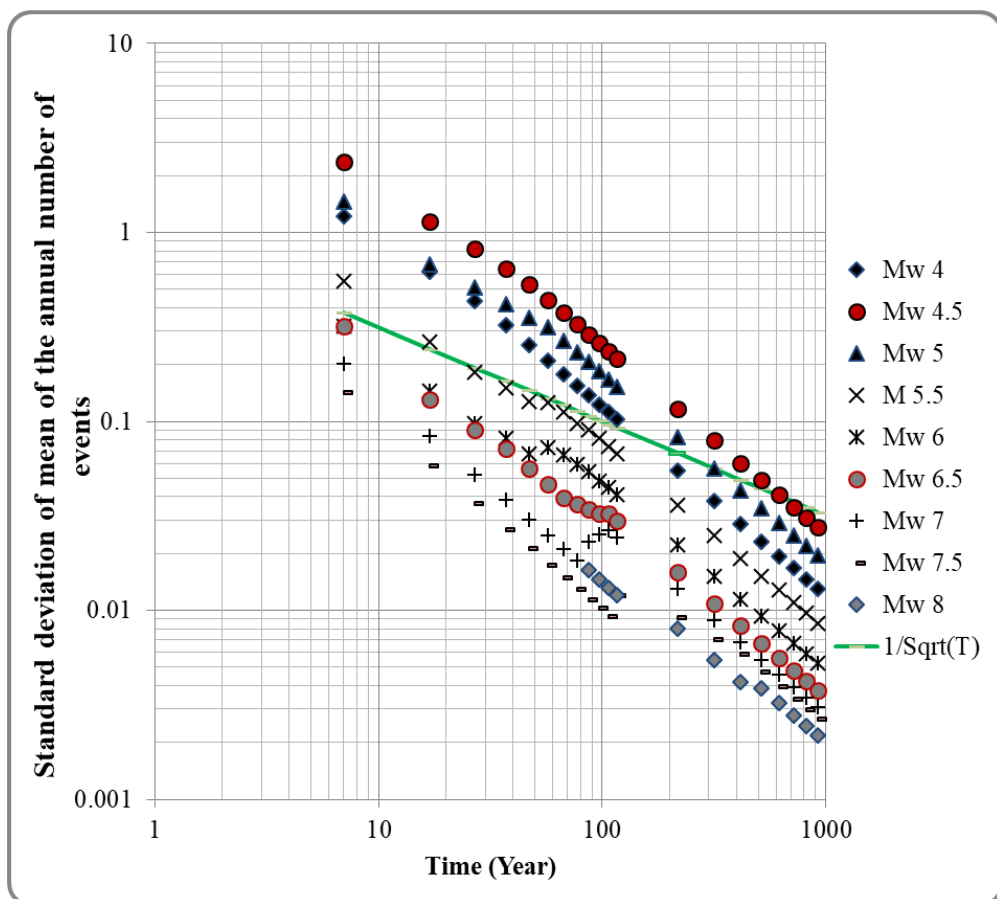
Figure 40: Completeness test of homogenized composite catalogue following Stepp (1972) technique. The small earthquakes are complete for short time whereas the large ones are complete gradually for large time-lengths. The green dots represent 1/√T slope.

Table 4: Completeness of different magnitude classes for South Tibet and the Himalaya.

Mw	Complete Year	
	Himalaya	South Tibet
4	15	15
4.5	35	35
5	55	45
5.5	75	75
6	100	100
6.5	200	200
7	300	300
7.5	400	
>8	900	

4.4. Magnitude of completeness

Magnitude of completeness (Mc) was estimated, visually, using assumption of self-similarity (Wiemer & Wyss, 2000) from the plot (Figure 41) of cumulative and non-cumulative number of earthquakes of different magnitude classes. In the figure, the non-cumulative curve has a peak at Mw 4.3, which is the Mc of the catalogue.
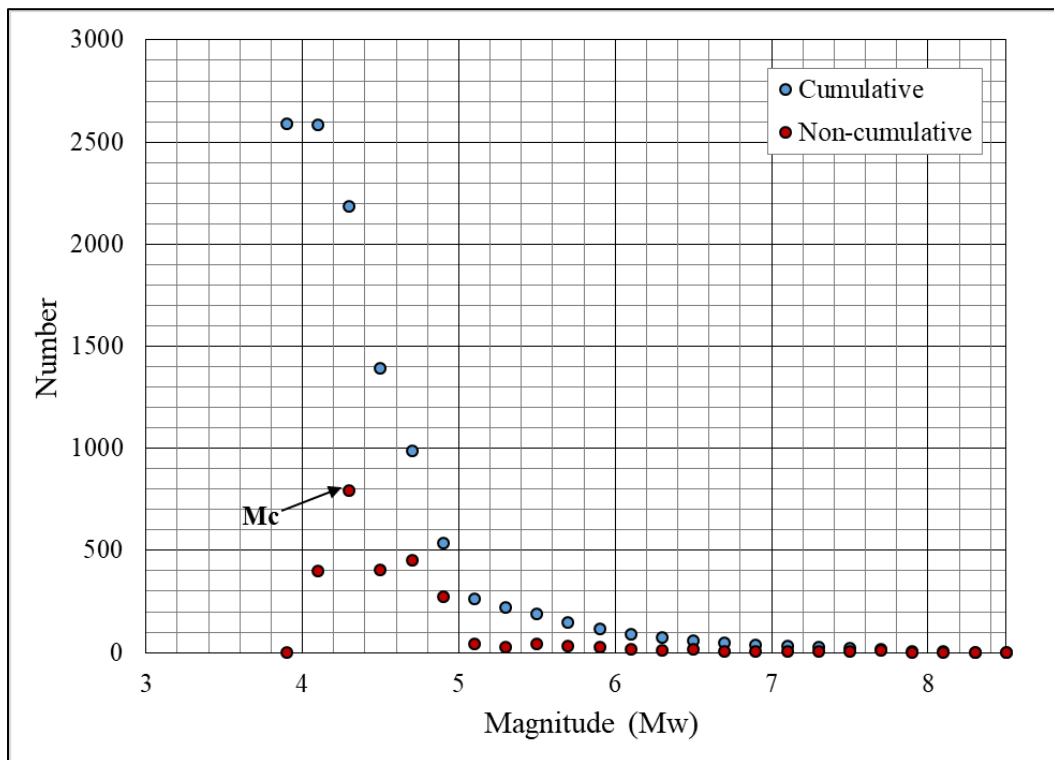
Figure 41: Cumulative and non-cumulative frequency of earthquakes in the declustered catalogue. Mw 4.3 has the highest frequency in the catalogue, which is the magnitude of completeness (Mc).

4.5. Earthquake recurrence (Gutenberg-Richter) relation for the region

In the Nepal Himalaya, the earthquakes in the south of 3500 m elevation contour line, in majority, are found to occur on account of thrusting, whereas those in the north and above 3500 m contour line occur because mostly of normal faulting (Rajaure *et al.*, 2013). To estimate the recurrence parameters of earthquakes, the prepared composite catalogue was split into two sub-regions (Figure 42) following the mechanism of deformation in the region. The recurrence parameters (seismic parameters: a- and b-values were estimated using Least Square (LS) (Equation 16) and Maximum Likelihood (ML) method (Aki, 1965) (Equation 18) independently. The b-value estimated using LS and ML methods agree well. The Gutenberg-Richter equations using LS method are presented graphically in Figure 43 and Figure 44 for Himalaya and South Tibet, respectively. These figures implicate that large earthquakes are more frequent in the Himalaya than in South Tibet. The b-value for the Himalayan region is ~0.95 and South Tibet region is ~1.1, which are very much close to the b-value (~1) observed worldwide for converging zones (e.g. Kramer, 2007).
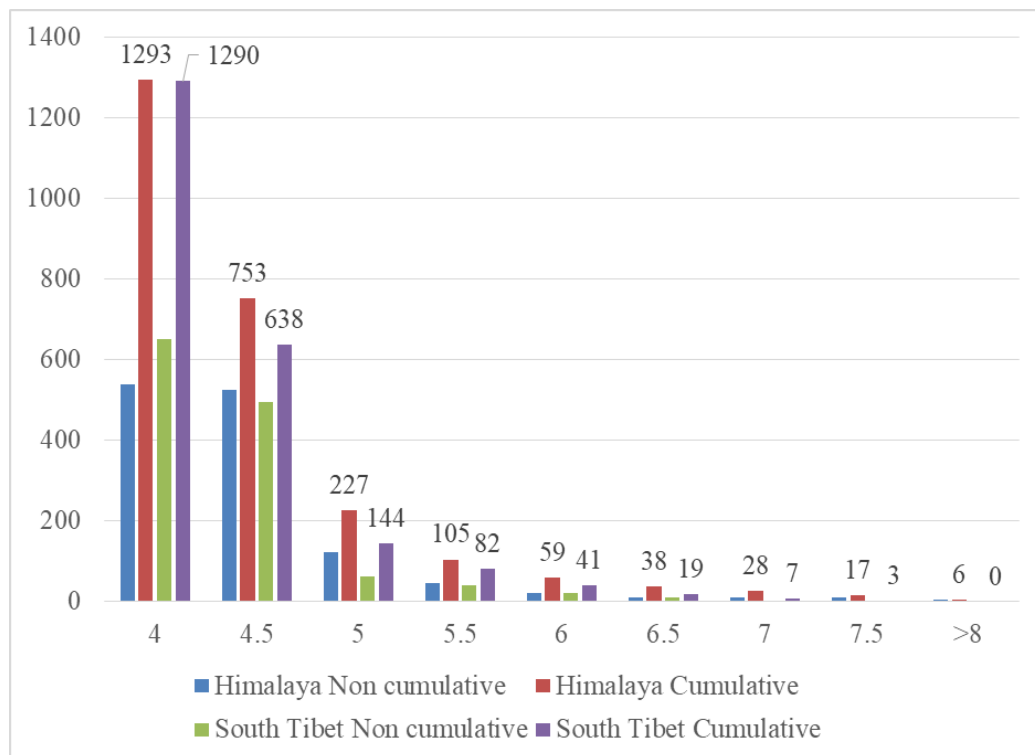
Figure 42: Cumulative and non-cumulative number of earthquakes in South Tibet and the Himalayan region.
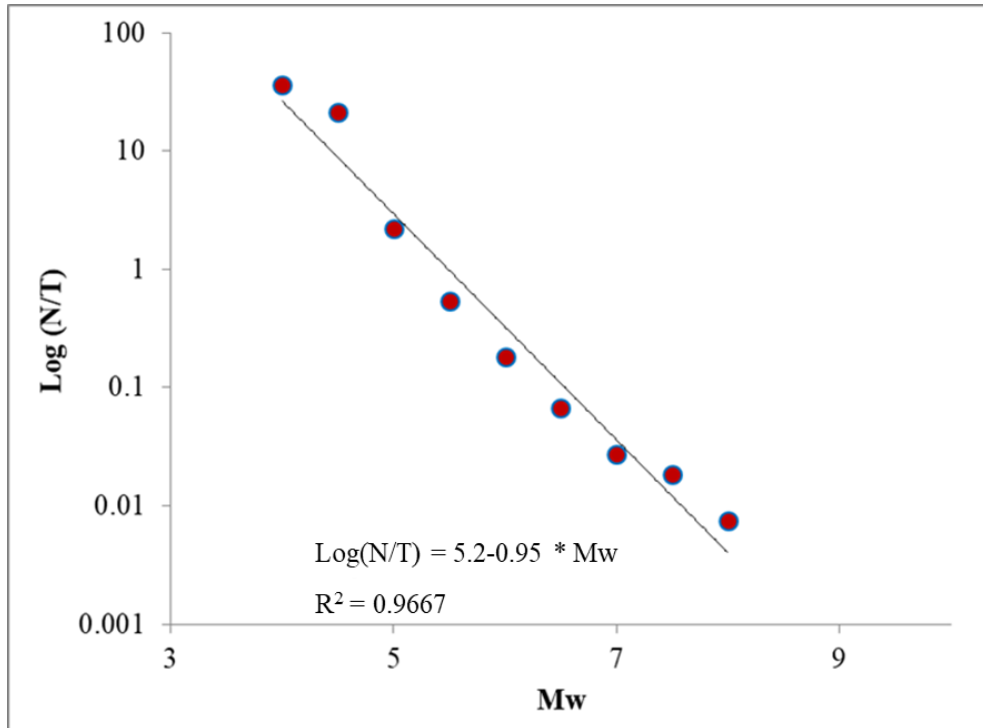
Figure 43: Gutenberg-Richter relation for earthquakes in the Himalaya. The dashed straight line represents the best-fit to data. The b-value for the Himalayan region is about 0.95.
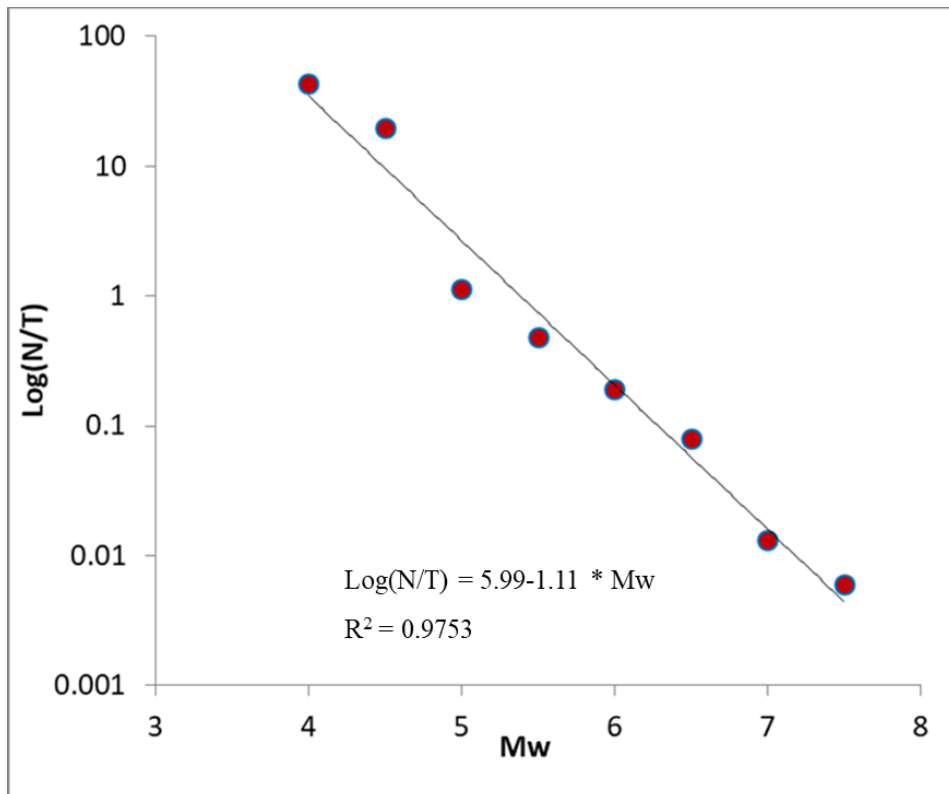
Figure 44: Gutenberg-Richter relation for earthquakes in South Tibet. The dashed straight line represents the best-fit to data. The b-value for the South-Tibet region is about 1.1.

The DMG earthquake data is available since 1995, which contain earthquake data as low as 2.0 M_L in Nepal. The DMG catalogue reports earthquake size in Local Magnitude (M_L). The magnitude was converted into Mw using Equation (5) (Ader *et al.,* 2012). The earthquake recurrence parameters are estimated for earthquakes in the Nepali territory only because the detection threshold decreases outward from Nepal.

The earthquake recurrence parameters estimated applying LS method to the DMG catalogue is presented in Figure 45. The figure depicts that the b-value (~1.0) agrees well with the worldwide observed b-value for such regions (e. g. Kramer, 2007).
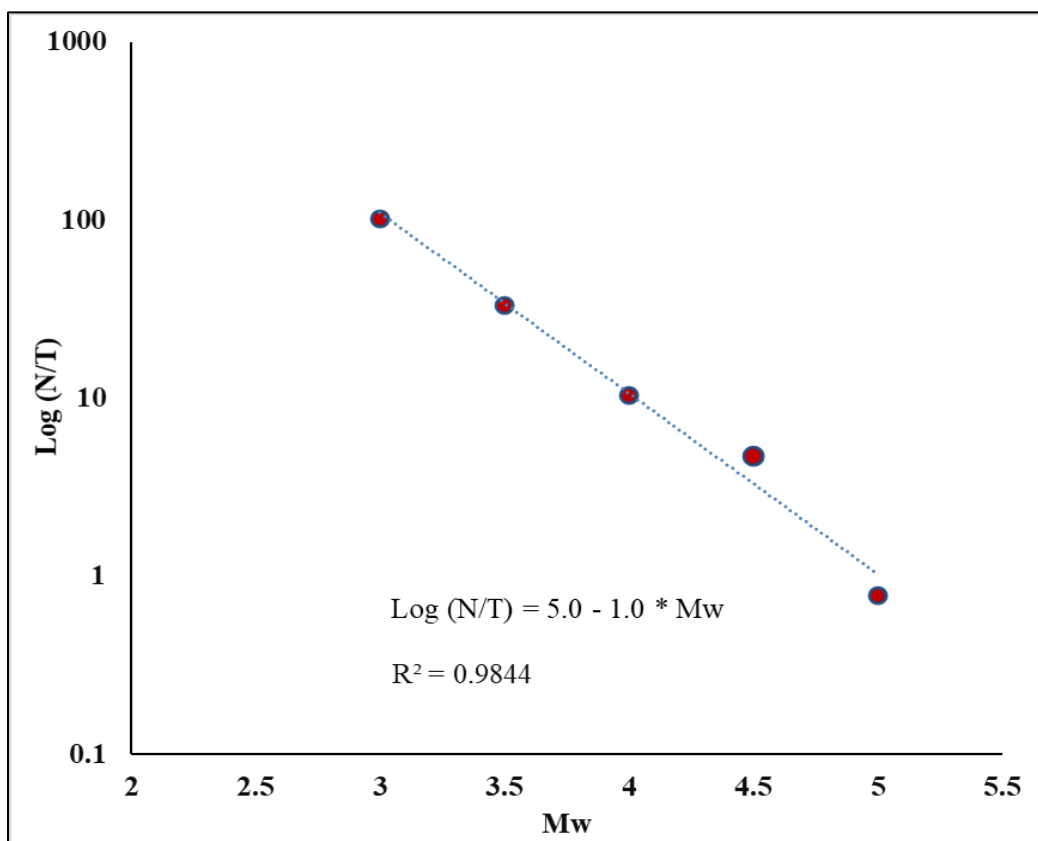
Figure 45: Gutenberg-Richter relation curve for Nepal using DMG catalogue. The b-value is about 1.0 for the Nepal Himalaya.

4.6. Seismic hazard analysis

4.6.1. Seismic source zones

The Main Himalayan Thrust (MHT) is the major source of seismic hazard in Nepal. There are two schools of thoughts regarding the size of rupture of the MHT. One considers earthquakes of maximum magnitude up to 9.0 may occur, similar to the

2004 Indonesia Earthquake (e. g. Bilham &Wallace, 2005; Kumar *et al.*, 2010; Ader *et al.*, 2012; Stevens and Avouac, 2016; Stevens & Avouac, 2017) and the other considers the maximum potential magnitude, possibly, do not exceed Mw 8.5 and the results of paleoseismic investigations are exaggerated (e. g. Valdiya, 1976; Gahalaut and Arora (2014), Gahalaut & Kundu, 2011; Dasgupta *et al.*, 2012; Srivastava *et al.*, 2013; Mugneier *et al.,* 2016; Hubbard *et al.*, 2016). In this study, the second school of thought was considered in seismic source delineation.

Potential earthquake sources were identified and delineated after the analysis of the prepared comprehensive earthquake catalogue, impact of 2015 Gorkha Earthquake, lateral variation in seismicity pattern (Appendix 4) and geological structures (Appendix 8). Similarly, presence of subsurface ridges in north India, tectonics of the region (Appendix 9), and segments proposed by Bilham (2019) (Appendix10) also were considered in the identification and delineation earthquake sources.

There are several linear sources (faults) in the Nepal Himalaya. However, many of them have not been found to be associated with current seismicity (e.g. Pandey *et al.*, 1999; Rajaure *et al.*, 2013) and, therefore, have not been considered in this study. Altogether nine sets of source models (Appendix 11) were identified and delineated. The sources, which are segments of the MHT, are three-dimensional faults. These sources emerge to the surface along the MHT (Depth = 0 km) and deep to a depth of about 20 km in the north (Figure 46). The depth in the north was adopted from the average depth of earthquakes occurring on the seismicity belt (Pandey *et al.,* 1999, Torre *et al.* 2007, Sheehan A. F. 2008 and Rajaure *et al.* 2013).
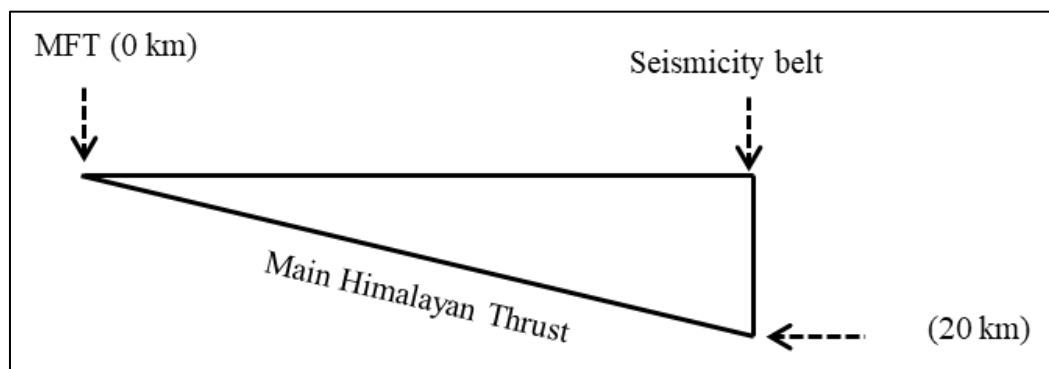
Figure 46: Geometry of earthquake sources along the Himalaya. The sources are three dimensional area planar sources, which are segments of the MHT.

The depth of sources in South Tibet, which have normal faulting mechanism, have a fixed depth of 10 km. This depth has been adopted from the depth of fault plane solutions of earthquakes in the region (e. g. Torre *et al.,* 2007; Sheehan A. F. 2008 and Rajaure *et al.* 2013).Similarly, the depth of earthquakes in the north-east of Nepal, in South Tibet, have been given a fixed depth of 50 km because the depth of foci of earthquakes in this region are greater than 50 km (e. g. Torre *et al.,* 2007; Sheehan *et al.,* 2008; Rajaure *et al.,* 2013). Similarly, the depth of sources in Northern India (in the south of Nepal) is not known well; therefore, the depth was fixed to 35 km that corresponds to the depth of Mohorovicic Discontinuity in continental regions (e. g. Rai *et al.,* 2006, Sheehan *et al.,* 2008; Nabelek *et al.*, 2009).

An example of source delineation (Model 9) based on seismicity is presented in Figure 47.The polygons in Figure 47 are the identified potential earthquake sources in Model 9.
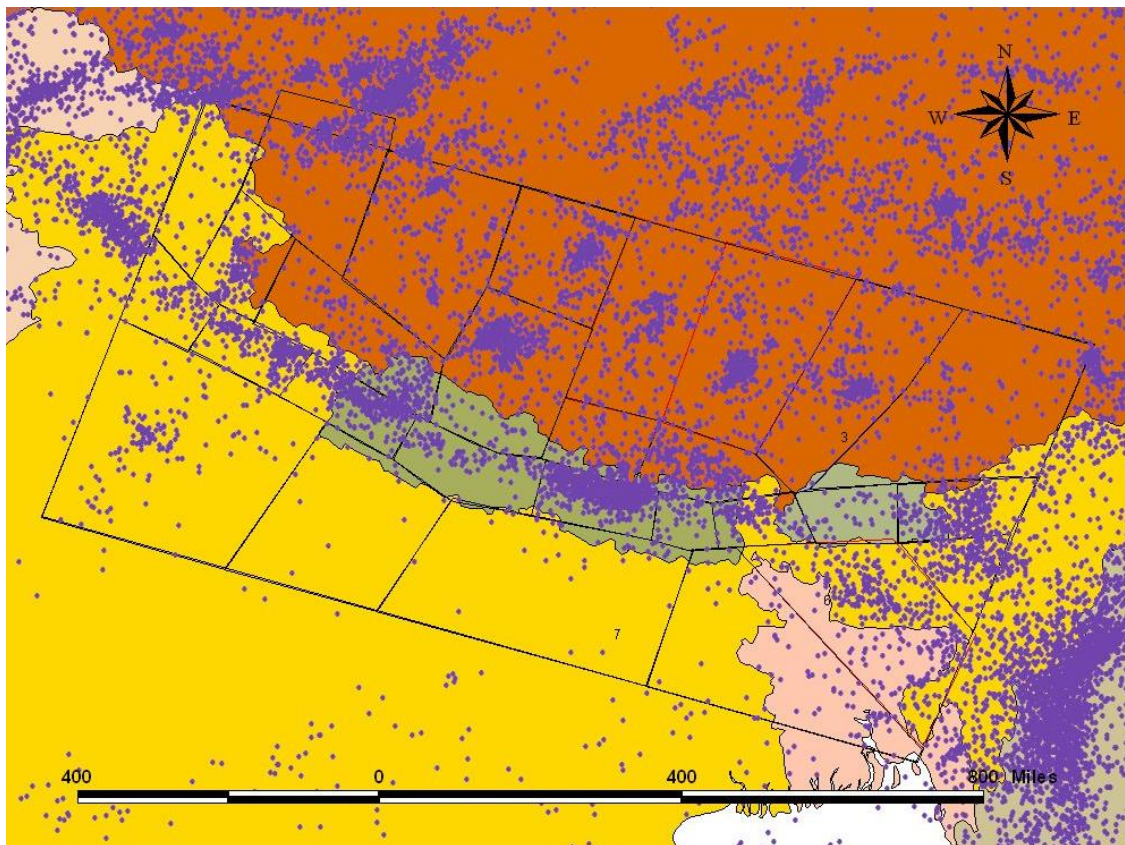
Figure 47: An example of identification and delineation of seismogenic sources (polygons) in and around Nepal based on seismicity pattern (Appendix 11-9).

A test was carried out to check the influence of depth in seismic hazard, keeping source model, attenuation relation and earthquake recurrence parameter same. The

71

variation in seismic hazard with the variation of depth of the sources along the Himalaya (segments of MHT) are presented in Appendix 12. The geometry of the MHT has been found to have small influence on the seismic hazard.

4.6.2. Maximum potential magnitude

The maximum potential magnitudes of earthquake sources along the Himalaya (i.e. MHT) were calculated using empirical relations derived by Wells and Coppersmith (1994). The relations were derived using rupture area, rupture length and displacement and their respective observed magnitudes. The maximum potential magnitude of earthquake sources in South Tibet and north India were fixed because we don't have the history of very large earthquakes in those areas. The summary of the magnitude characterization for different source models is given in Table 5. Details of the magnitude characterization are given in Appendix 13.

Table 5: Summary of magnitude characterization in the study area.

Source model	No. of sources	Min. magnitude	Max. magnitude
1	7	8.0	8.2
2	7	7.5	7.9
3	7	7.5	7.8
4	22	7.5	8.4
5	23	7.5	8.5
6	25	7.5	8.3
7	17	7.5	8.4
8	19	7.5	8.4
9	26	7.5	8.4

Maximum potential magnitude is an important factor in seismic hazard assessment, because overestimation or underestimation might lead to overestimation or underestimation of the results. A test was carried out to check how the seismic hazard varies with different maximum potential magnitudes of sources (Keeping source model (Appendix 11-1), attenuation relation and earthquake recurrence parameters same), the results are presented in Appendix 14 and Table 6.

Table 6: Variation in PGA with variation in maximum potential magnitude (Mw_{max})

Mw_{max}	PGA (g)
6.5	0.35
7	0.4
7.5	0.45
8	0.5
8.5	0.55

4.6.3. Earthquake recurrence parameters of identified sources

Earthquake recurrence parameters of the identified sources were estimated from the prepared catalogue. The b-values were adopted from Figure 43 and Figure 44, which were estimated for the Himalaya and South Tibet respectively, because some of the sources have insufficient data to derive recurrence parameters independently.   The a-values of the identified earthquake sources were recalculated from the data of each source zone using Equation 26 using the 'b-value' from Figure 43 and Figure 44. The earthquake recurrence parameters of the source models are presented in Appendix 15.

$$a = \log\left(\frac{N}{T}\right) + b * Mc \qquad\qquad \text{Equation 26}$$

Where 'a' is the a-value, 'N' is the number of earthquake, 'T' is the time of record in years, 'b' is b-value, and Mc is the magnitude of completeness.

Precise earthquake recurrence parameters are very important in seismic hazard calculation because a small error may result in seismic hazard by manifold. A test was carried out to check the influence of b-value on seismic hazard keeping other parameters same. Different b-values ranging from 0.7 to 1.2 were applied to a common source model and common attenuation relation. The variation in seismic hazard with the variation in b-value is presented in Appendix 16. The largest PGA varies from 0.75 g to 0.25 g respectively for the b-values from 0.7 to 1.2 (Table7).

Table 7: A comparison of largest PGA (10% probability of exceedance in 50 years) in Nepal and Kathmandu valley estimated from different b-values ranging from 0.7 to 1.2. The a-values were recalculated using fixed b-values and the earthquake catalogue. .

b-value	Largest PGA (g)	
	Nepal	KTM Valley
0.7	0.75	0.6
0.8	0.6	0.5
0.9	0.5	0.45
1	0.4	0.35
1.1	0.35	0.3
1.2	0.3	0.25

4.7. Assessment of seismic hazard

Seismic hazard was analyzed comparatively using different datasets, different attenuation relations and different source models. Three datasets, two types of attenuation relations each comprising four attenuation relation for tectonically

different regions and nine source models were used in this assessment, which are described in the following sections.

4.7.1. Different datasets

Different datasets were used to investigate their influence on PGA. Three datasets, which contain earthquakes (i) since 1900 AD (2) since 1100 AD and (3) since 1964AD were, separately, utilized to estimate earthquake recurrence parameters. The first set0, contains instrumentally recorded earthquakes only; the second one contains instrumentally recorded as well as historically reported earthquakes; whereas the third set contains earthquakes since 1964. The third set was used because the detection threshold of earthquakes decreased to magnitude 4 on account of expansion of existing networks and establishment of numerous networks globally. The variation in PGA was studied using a common source model (Appendix 11-1), a common attenuation relation (Atkinson, Silva & Kamai, 2014) and common earthquake recurrence parameters (a- and b-values) derived from above mentioned three sets of data. The variation in PGA are graphically presented in Appendix (17) and summarized in Table 8. The result (Table 8) depicts the influence of the datasets on the result. The dataset containing earthquakes since 1900 results in smaller PGA in comparison to the other two.

Table 8: Maximum PGA (10% probability of exceedance in 50 years) in Nepal and Kathmandu Valley calculated using different catalogues. A common attenuation relation (Atkinson, Silva & Kamai, 2014), a common source model (Model-1, Appendix 11-1) and different a- and b-values were used for this comparative study.

Largest PGA (g)				
Earthquake catalogue				
Region	Since 1900		Since 1100		Since 1964 fixed b-value (0.95) and recalculated a-value
	calculated a- and b-value	fixed b-value (0.95) and recalculated a-value	Calculated a- and b-value	fixed b-value (0.95) and recalculated a-value	
Nepal	0.35	0.5	0.45	0.45	0.55
KTM	0.3	0.3	0.45	0.4	0.4

4.7.2. Different attenuation relations

For calculation of ground motion (PGA), two types of attenuation relations, one for subduction zone (Appendix 18-1) and the other for active-shallow-crustal (reverse) earthquakes (Appendix 18-2) were used. The seismic hazard maps prepared using different attenuation relations are presented in Appendix 19 and Table 9 for a comparison. Atkinson & Boore (2003) relation produces unrealistically very small PGA in comparison to others, therefore, it is not considered in further calculations. On the other hand, the Youngs *et al.* (1997) attenuation model produces the largest PGA (0.75 g).

Table 9: Maximum PGA (10% probability of exceedance in 50 years) in Nepal and Kathmandu Valley calculated using different attenuation relations. The Atkinson & Boore (2003) relation produces extremely low PGA, whereas the Youngs et al. (1997) relation produces the largest PGA. In comparison to the relations for subduction zones, the relations for active-shallow-crustal earthquakes give consistent PGAs.

Attenuation Relation	PGA (g)		Tectonic region
	Maximum	KTM Valley	
Zhao *et al*. (2006)	0.55	0.35	Subduction Zone
Youngs *et al*. (1997)	0.85	0.6	Subduction Zone
BcHydro (2016)	0.45	0.25	Subduction Zone
Atkinson and Boore (2003)	0.18	0.14	Subduction Zone
Arroyo and Singh (2017)	0.28	0.2	Subduction Zone
Abrahamson, Silva and Kamai (2014)	0.55	0.4	Active Shallow Crustal
Boore *et al*. (2014)	0.55	0.4	Active Shallow Crustal
Chiou and Youngs (2014)	0.55	0.35	Active Shallow Crustal
Campbell and Bozorgnia (2014)	0.55	0.35	Active Shallow Crustal

4.7.3. Different source models

Nine source models (Appendix 11-1 to Appendix 11-9) were used to calculate seismic hazard keeping earthquake recurrence parameters and attenuation relation same as in previous tests. . The source models consider three types of ruptures scenario of the MHT. The first type considers entire north-south rupture of MHT, from the boundary between locked part in south (up to the surface exposure of MFT) and the boundary between currently locked part of MHT and aseismically creeping part in the north. This type of rupture (e. g. Appendix 11-1) was considered following the reports of entire N-S rupture (e.g. 1100 (Yule *et al*., 2005), 1255 (Sapkota *et al*., 2013), 1505 (Yule *et al.*, 2006) and 1934 (Sapkota *et al.*, 2013)). In the second type of s, the

northern half (rupture) of the MHT was considered. Such rupture is represented, for example, by Model 2 (Appendix 11-2), which was considered following the rupture of the 2015 Gorkha Earthquake (Mw 7.8) and possibly the 1833 earthquake (Mw 7.6) also ruptured the northern part of MHT. The third type of rupture considers the southern part of the MHT that did not rupture during the 2015 Gorkha Earthquake (Appendix 11-3). Results from these three source models are graphically presented in Appendix 20-1, Appendix 20-2 and Appendix 20-3 respectively and in Table 10. Model 1, 2 and 3 (Appendix 11-1, 11-2 and 11-3) were used for a comparative study only, which were not considered in the final calculations as they do not consider other earthquake sources in the adjoining region.

The seismic hazard maps prepared from above mentioned nine source models are presented in Appendix 20 for a comparison.

Table 10: A comparison of PGA (10% probability of exceedance in 50 years) in Nepal and the Kathmandu Valley, calculated using different source models.. The comparison shows approximately comparable result except for Model 3, which is the southern half rupture scenario of the MHT.

| Source Model | PGA (g) | | Source region |
	Nepal	KTM Valley	
Model-1	0.55	0.4	Himalaya only
Model-2	0.5	0.4	
Model-3	0.7	0.25	
Model-4	0.55	0.4	Himalaya as well as Surrounding
Model-5	0.4	0.4	
Model-6	0.55	0.4	
Model-7	0.45	0.35	
Model-8	0.5	0.3	
Model-9	0.55	0.45	

4.8. Seismic hazard map

Seismic hazard maps have been prepared for five different return periods (approximately 500 year, 1000 year, 2500 year, 5000 year and 10000 year). The seismic hazard maps have been prepared using a logic tree (Figure 48). The logic tree was applied to incorporate uncertainties in earthquake source model, maximum potential magnitude, attenuation relations and ruptures of MHT. Six source models (Appendix 11-4 to Appendix 11-9), two types of attenuation relations (Appendix 18-1 and Appendix 18-2) and three types of rupture scenarios of the MHT (Appendix 11-1,

Appendix 11-2 and Appendix 11-3) were utilized to produce seismic hazard maps. The subduction type attenuation relations (Appendix 18-1) were applied to earthquake sources which fall in the MHT and its adjoining region in the south. The second type of attenuation relations (Appendix 18-2) were applied to sources in South Tibet.

Figure 49 is an example of seismic hazard map prepared by R-CRISIS software. The map corresponds to 10% probability of exceedance in 50 years (approximately 500 year return period). The data calculated by R-CRISIS (latitude, longitude and PGA in three columns), at every 20 km, spacing was used to produce Figure 50 utilizing ArcGIS.
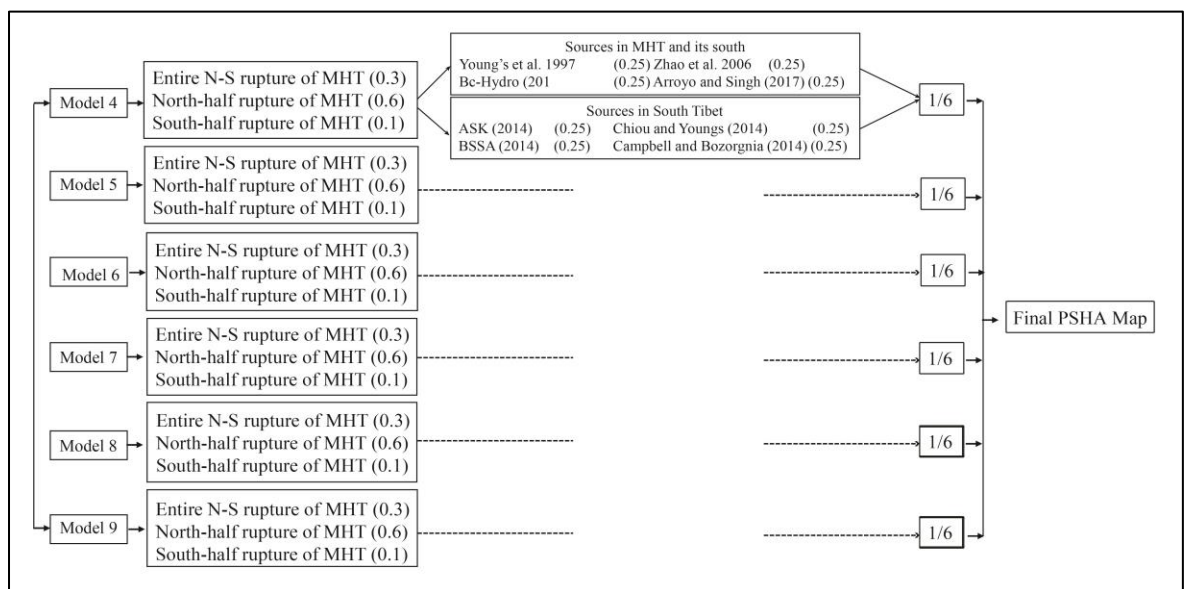
Figure 48: Logic Tree used to prepare final seismic hazard maps.

The peak ground acceleration (PGA) in major towns of different parts of Nepal are presented in Table 11.
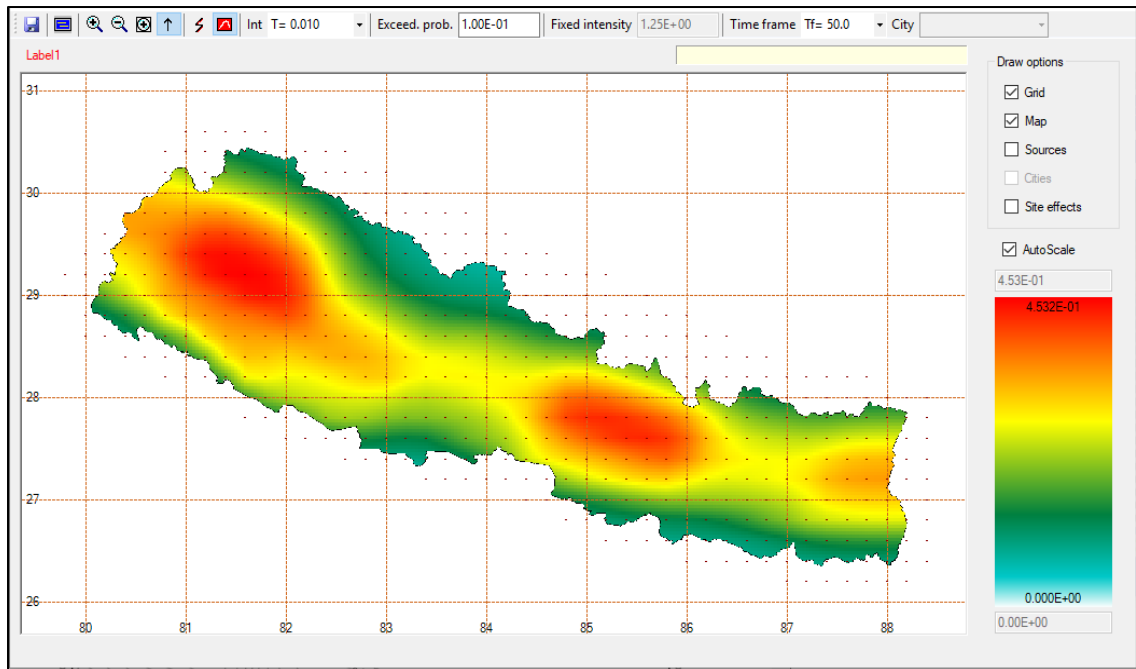
Figure 49: Seismic hazard map (10% probability of exceedance in 50 years) prepared utilizing R-Crisis. The maximum PGA is about 0.45 g in Far-west Nepal.
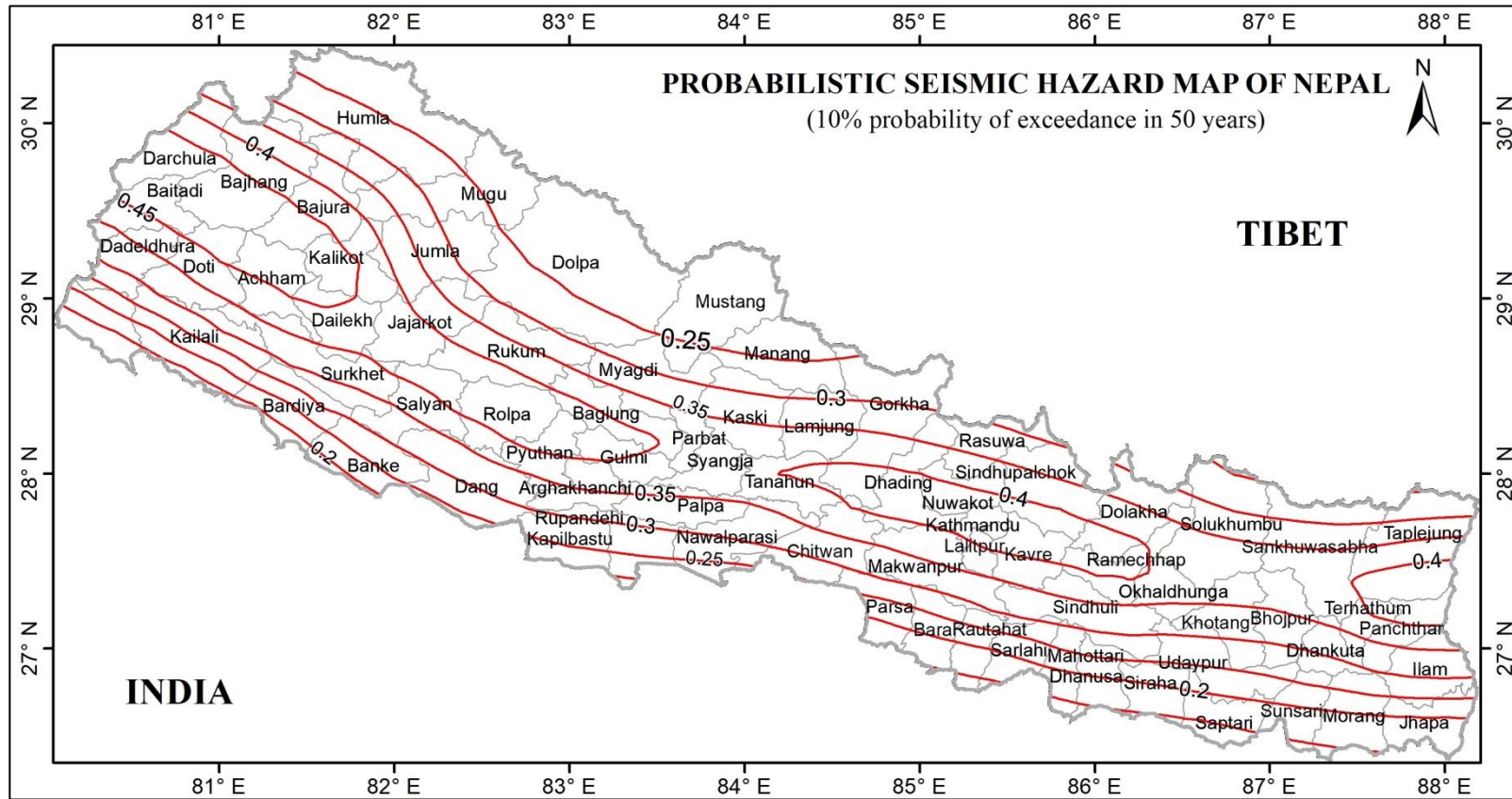
Figure 50: Seismic hazard map of Nepal for 500 year return period (10% probability of exceedance in 50 years) for an engineering rock site condition. The largest PGA (0.45 g) is estimated in the far-west Nepal.

Table 11: PGA estimated for major cities of Nepal. The PGA values correspond to 10% probability of exceedance in 50 years for engineering rock site condition.

Place	Latitude (°E)	Latitude (°N)	PGA (g)
Baglung	83.600	28.266	0.370
Bajhang	81.199	29.550	0.470
Bhairahawa	83.450	27.500	0.230
Biratnagar	87.283	26.467	0.150
Birgunj	84.867	27.017	0.160
Chaurjhari	82.193	28.626	0.420
Dadheldhura	80.567	29.300	0.400
Darchula	80.764	29.872	0.466
Dhankuta	87.340	26.970	0.300
Dipayal	80.930	29.243	0.448
Dunai	82.900	28.933	0.280
Gorkha	84.629	28.000	0.410
Hilsa	81.334	30.151	0.290
Ilam	87.910	26.910	0.330
Janakpur	85.917	26.733	0.160
Jiri	86.229	27.628	0.400
Jomsom	83.730	28.783	0.240
Jumla	82.193	29.274	0.320
Kathmandu	85.317	27.700	0.410
Mahendranagar	80.300	28.967	0.240
Mugu	82.085	29.502	0.330
Nepalgunj	81.617	28.067	0.200
Palpa	83.550	27.866	0.350
Pokhara	83.983	28.217	0.370
Pyuthan	82.853	28.101	0.400
Salyan	82.161	28.375	0.380
Simikot	81.819	29.968	0.270
Surkhet	81.600	28.600	0.360
Taplejung	87.650	27.370	0.410
Tumlingtar	87.193	27.314	0.370

Seismic hazard map corresponding to 10% probability of exceedance in 50 years (500 year return period) is commonly used in building codes. The In addition to the seismic hazard map for a 500 year return period, four additional seismic hazard maps are prepared for 1000 year (Figure 51), 2500 year (Figure 52), 5000 year (Figure 53) and 10000 year (Figure 54) return period.
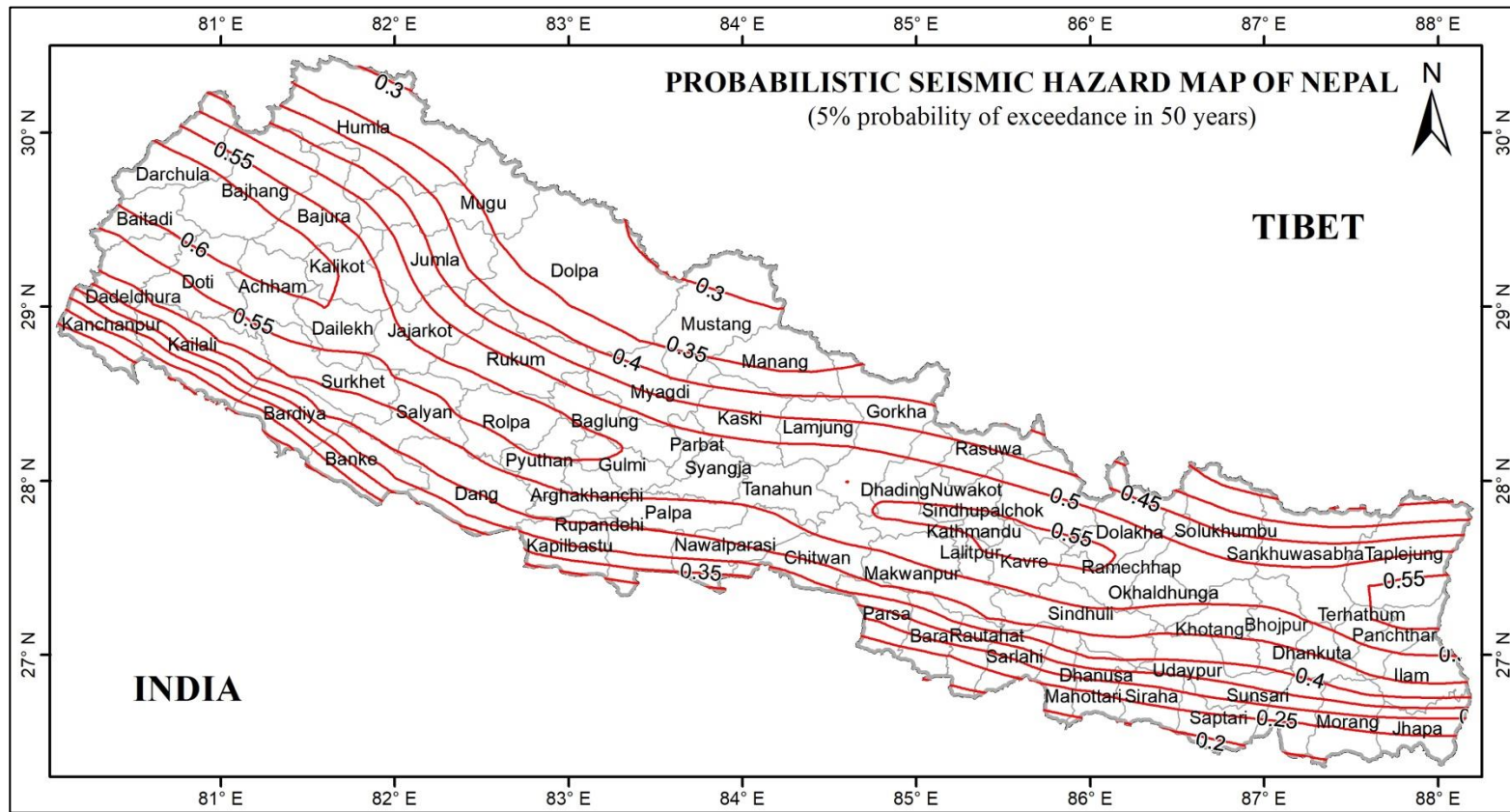
Figure 51: Seismic hazard map of Nepal for 1000 year return period (5% probability of exceedance in 50 years) for an engineering rock site condition. The largest PGA (0.6 g) is estimated in the far-west Nepal.
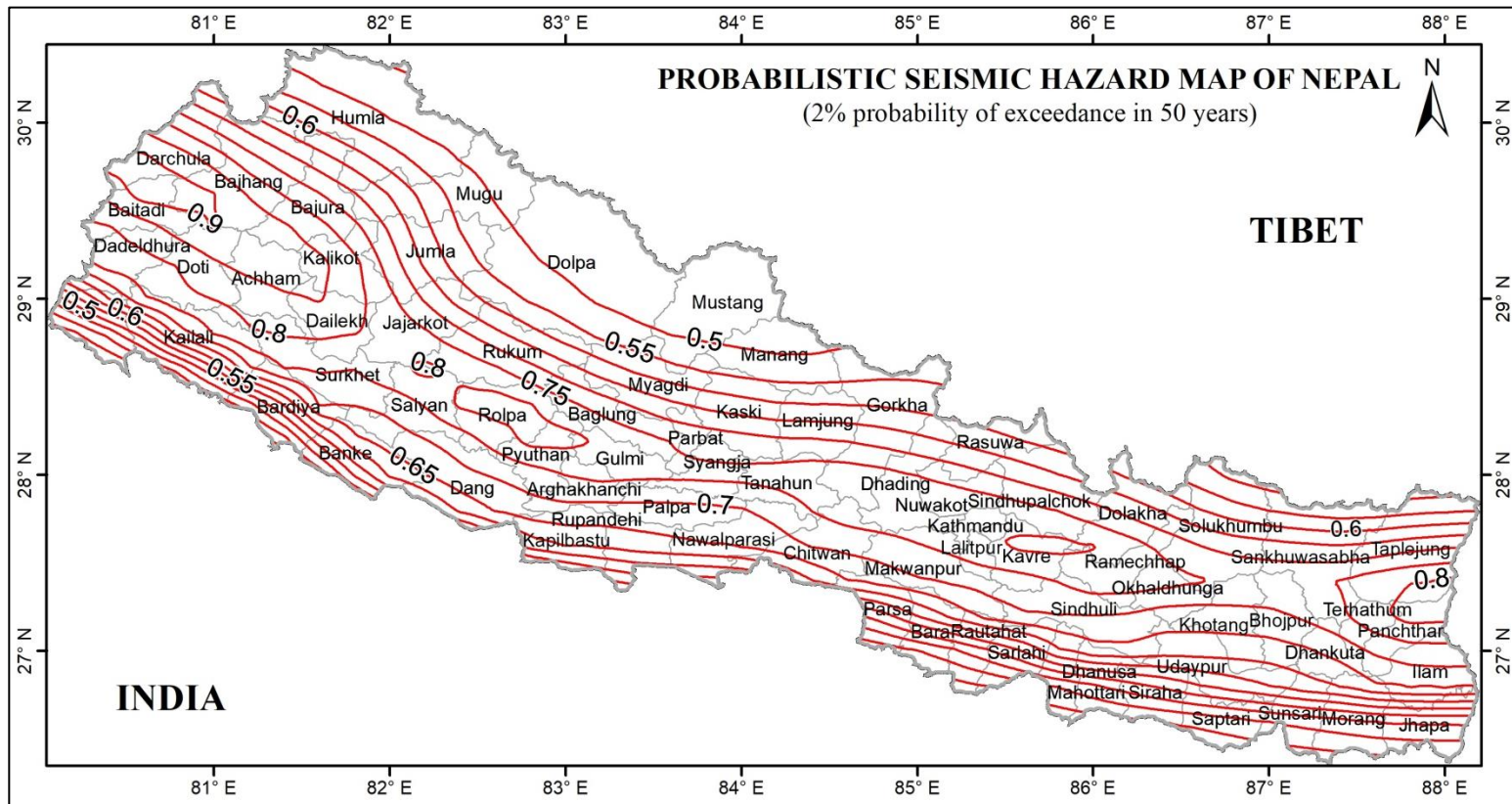
Figure 52: Seismic hazard map of Nepal for 2500 year return period (2% probability of exceedance in 50 years) for an engineering rock site condition. The largest PGA (0.9 g) is estimated in the far-west Nepal.
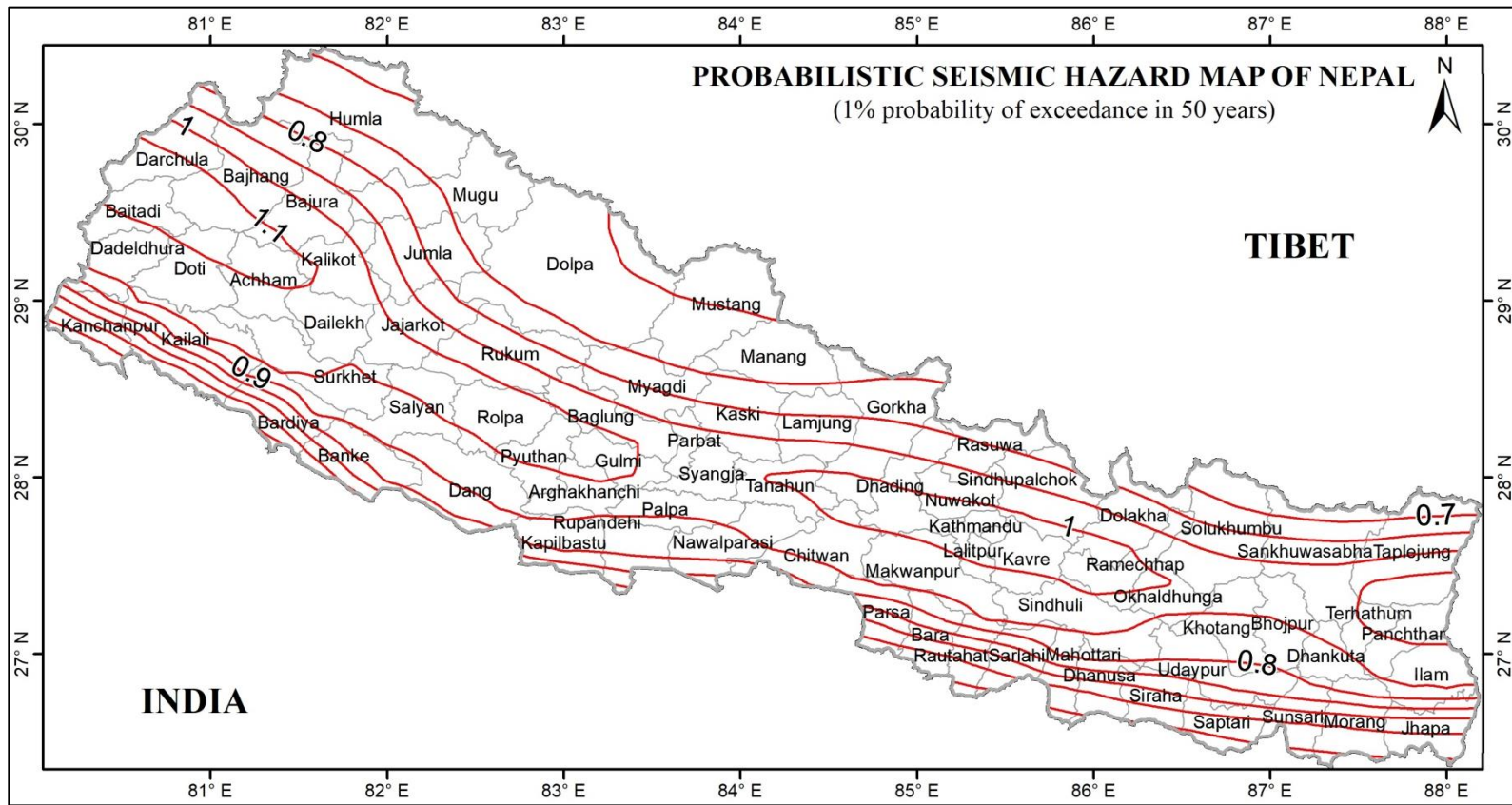
Figure 53: Seismic hazard map of Nepal for 5000 year return period (1% probability of exceedance in 50 years) for an engineering rock site condition. The largest PGA (1.1 g) is estimated in the far-west Nepal.
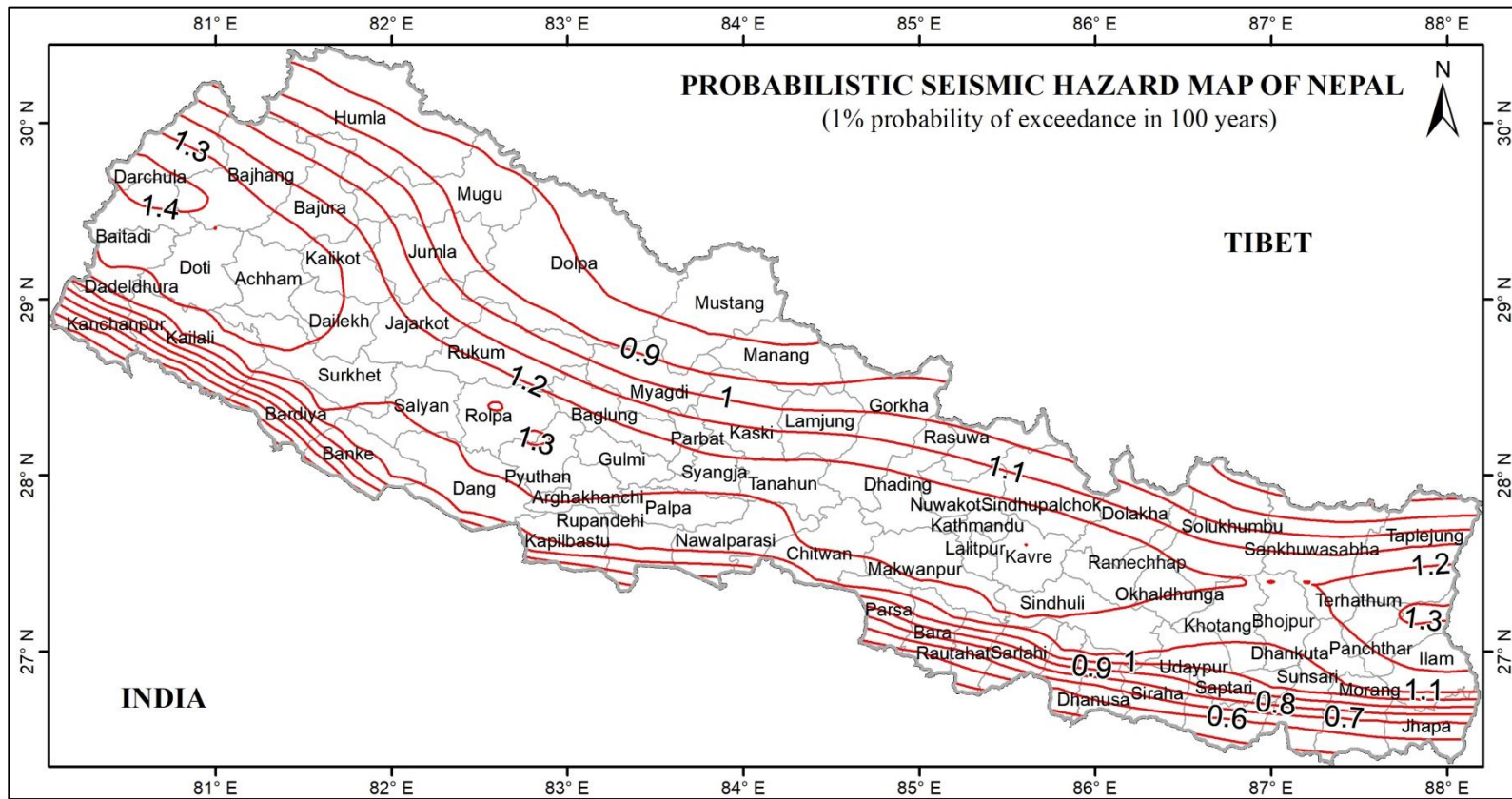
Figure 54: Seismic hazard map of Nepal for 10000 year return period (1 % probability of exceedance in 100 years) for an engineering rock site condition. The largest PGA (1.4 g) is estimated in the far-west Nepal.

4.9. Ground response of the Kathmandu valley sediments

The seismic hazard map presented in Figure 50 is for an engineering rock site, where the shear wave velocity is about 760 m/s or larger. Earthquake ground motions are influenced by local geology and topography. Topographic effect is beyond the scope of this research and an attempt has been made to investigate the response of local geology to seismic ground motion. The required data for ground response analysis is available in Kathmandu valley only.

The response of the Kathmandu Valley sediments to recently recorded earthquakes in the valley is described in the following sections.

4.9.1. 2013 August 30, south Tibet Earthquake

An Mb 4.9 earthquake occurred in South Tibet (Figure 55), which was felt in Kathmandu and its adjoining region. The ground acceleration of the earthquake was recorded by accelerometers at five sites KTP, TVU, PTN, THM and DMG (Figure 56), which was used in this study. Among the five sites, KTP is a rock site, installed in Kirtipur, and the others are soil sites.

Analysis of the ground acceleration record reveals that that the EW component was dominant across the valley except for at PTN. The other stations on sediments recorded PGA much higher than at the rock site (Figure 57).
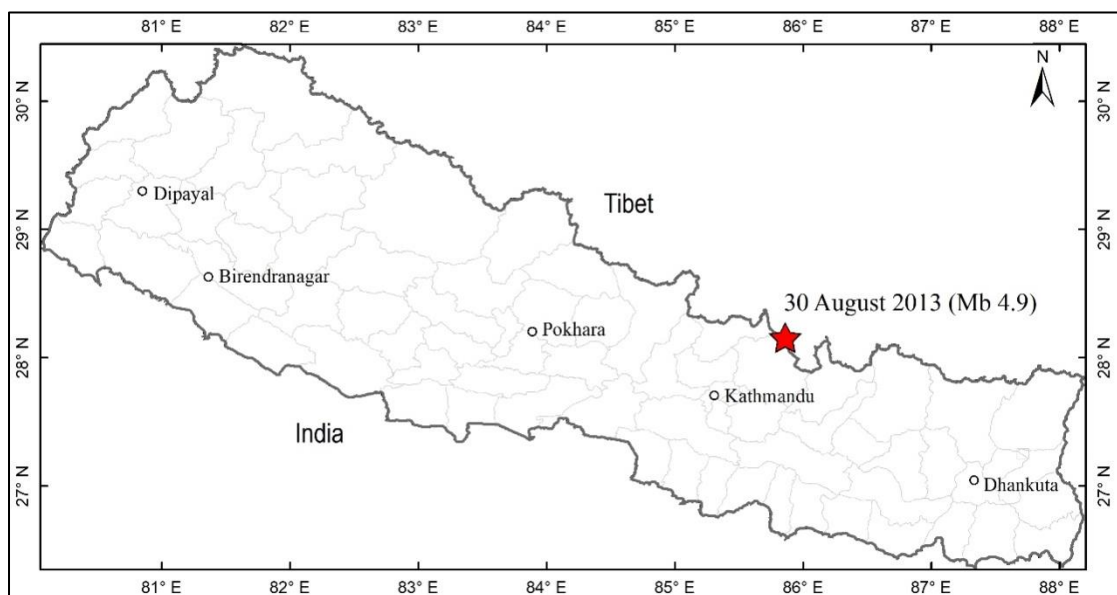
Figure 55: Location of the 2013 August 30 South Tibet Earthquake (Mb 4.9).
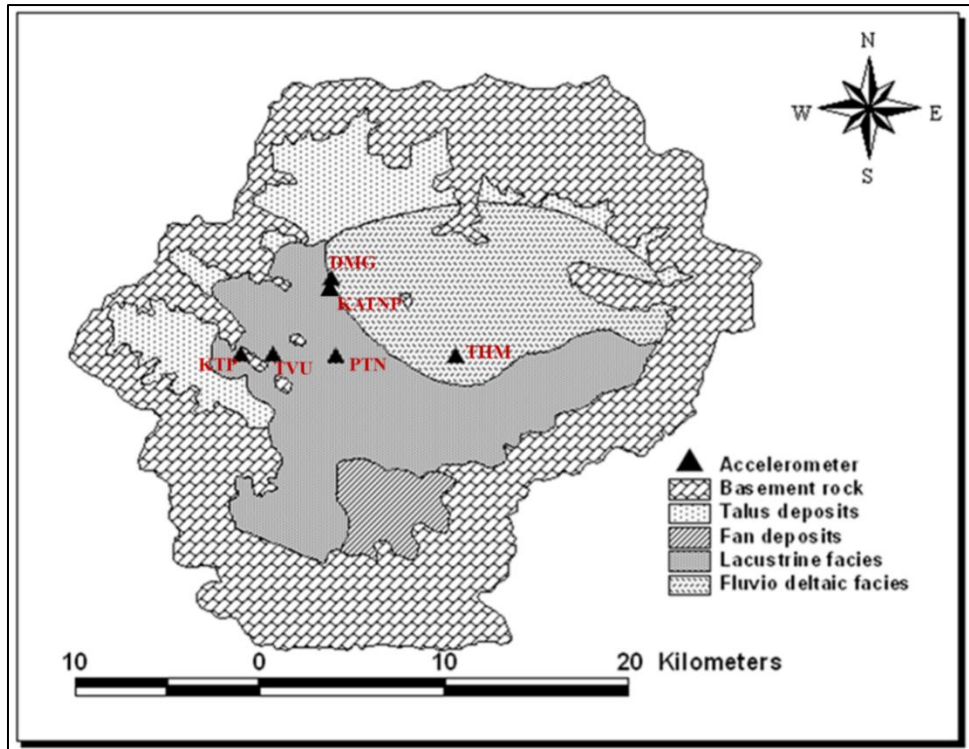
Figure 56: Location of the strong motion stations. KTP is a rock site and others are soil sites. The maximum PGA was recorded at DMG. (KTP: Kirtipur (rock site); TVU: Tribhuvan University, Central Department of Geology; PTN: Pulchowk Engineering Campus; THM: Sanothimi, University Grant Commission; DMG: Department of Mines and Geology; KATNP: Kantipath).
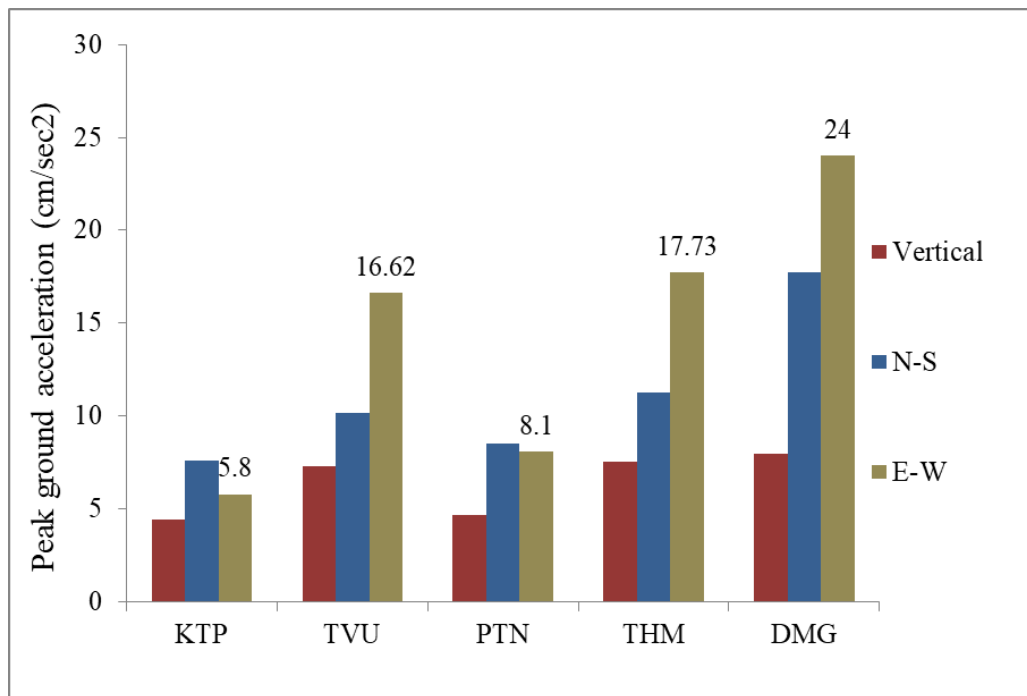
Figure 57: Peak ground acceleration (cm/sec^2) recorded at five sites. DMG, which is a soil site, has recorded the largest PGA.

The site response functions were evaluated as the Fourier spectral ratios of the horizontal components on soil relative to the corresponding component on rock (Figure 58). The functions are remarkably similar in the low frequency range (<0.8 Hz) and reveal strong amplification that is possibly caused by basin effects. By contrast, the high frequency site response shows strong variability across the soil sites, which can be attributed to the underlying stratigraphy of the deeper and shallow soil layers of the valley. The most pronounced differences manifest in the frequency range > 2 Hz, which is consistent with the variability in PGA across the valley.
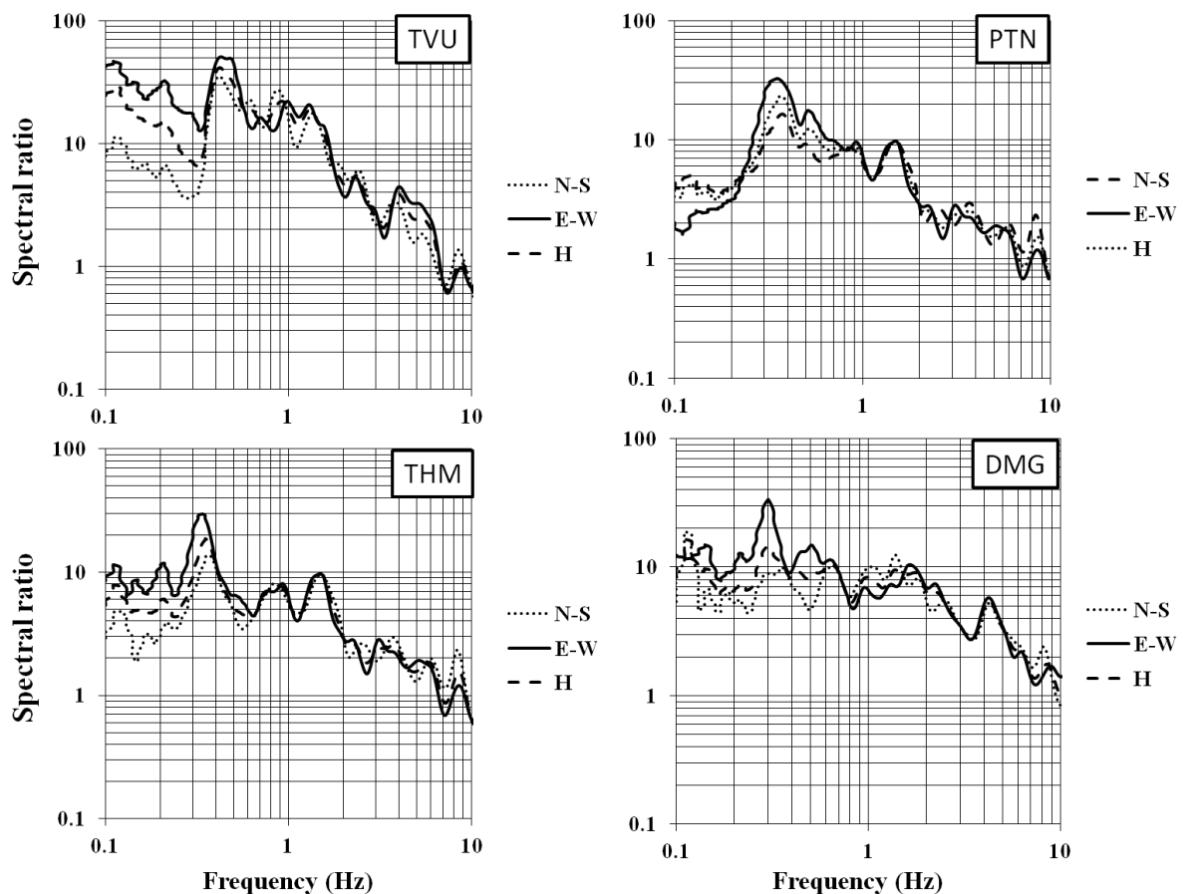
Figure 58: Spectral ratio at four soil sites relative to a rock site (KTP) (Rajaure *et al*., 2014).

4.9.2. April 25, 2015 Gorkha earthquake sequence

The Gorkha Earthquake occurred on 25th April of 2015. It rocked a large area in Nepal as well as the adjoining region in India and China. The Gorkha Earthquake and its three strong aftershocks (Mw >6.5) (Figure 59) were well recorded (Figure 60) by accelerometers deployed in Kathmandu sedimentary basin (Figure 56).

87
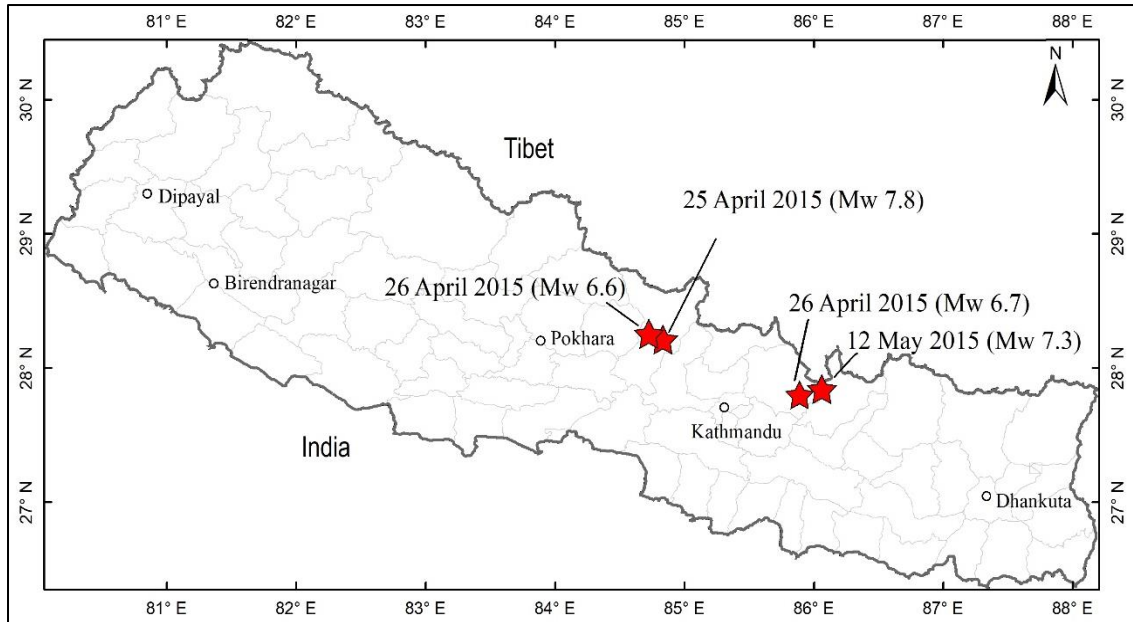
Figure 59: Location of four earthquakes, the strong motion records of which were utilized in this study.

Strong motion (ground acceleration) data (Figure 60) of Gorkha Earthquake and its three strong aftershocks (Figure 59; Table 12) were used to investigate response of the site to seismic ground motion.

Table 12: List of Gorkha Earthquake and its strong aftershocks, which were used in this study.

Date	Mw	Latitude (°N)	Longitude (°E)
25 April 2015	7.8	28.13	84.71
25 April 2015	6.6	28.16	84.84
26 April 2015	6.7	27.73	85.97
12 May 2015	7.3	27.80	86.12

The signals were high passed at 0.1 Hz using fourth order Butterworth filter. This approach produces the maximized spectrum defined as the maximum amplitude of shaking at a given frequency in the horizontal plane, eliminates the need to rotate the component, and produces results similar to the standard averaging methods. Then, soil-to-bedrock amplification ratios of the soil sites relative to the reference (rock site) station for all four events are calculated.

The records depict that, the PGAs were smaller (Table 13, Figure 61) than expected, however the velocity were relatively large (Figure 62).

Figure 63 shows the Fourier spectrum of the data and it's very clear that the high frequencies (> 1.0 Hz) are strongly damped at all the sites. The predominant period of the ground motion at soil sites varies between 3 and 5 s. The rock site (KTP) is dominated by high frequency energy, whereas the soil sites are dominated by low frequency energy (Figures 60 and Figure 63).
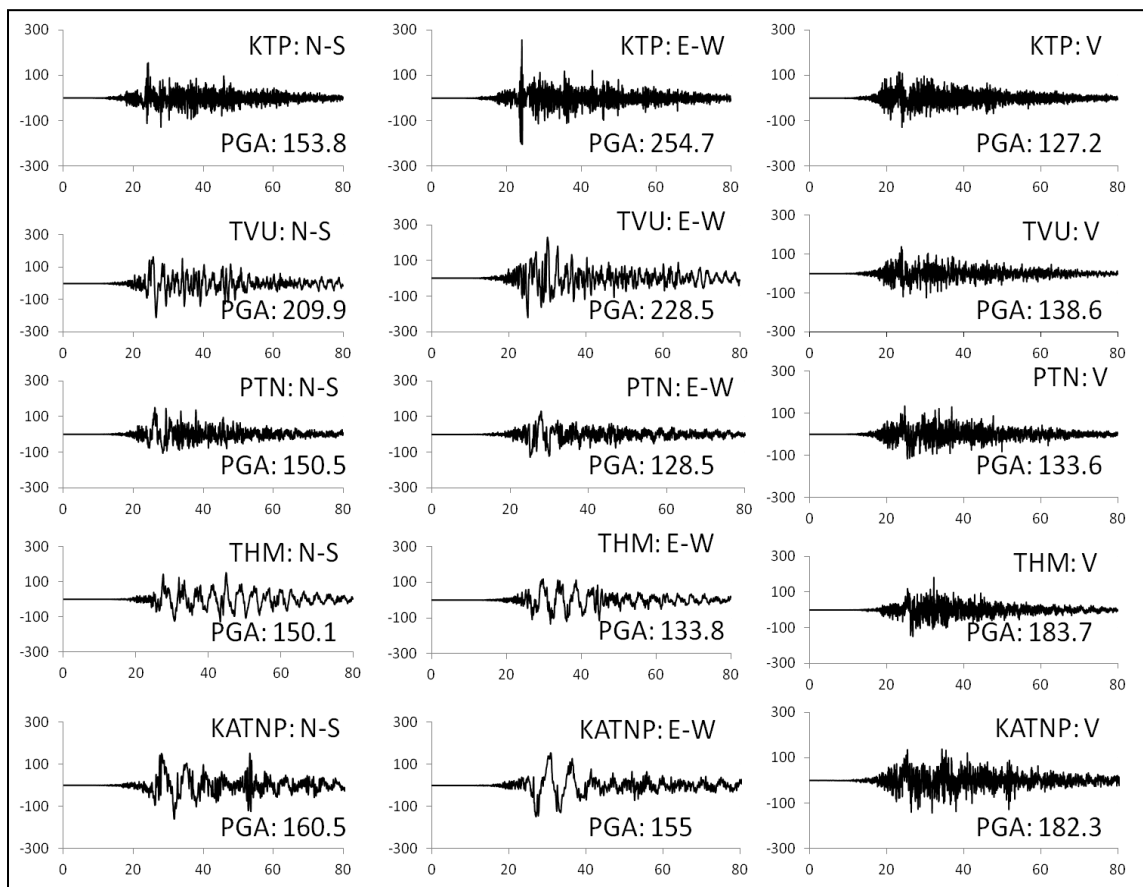
Figure 60: Acceleration time history recorded at five sites. KTP is a rock site and other are soil sites. E-W, N-S and V stand for east-west, north-south and vertical components. The maximum PGA is recorded by KTP (E-W component) (Rajaure *et al.*, 2017).

Peak ground acceleration is a high frequency characteristic of ground motion, which is an important parameter to rigid structures (small story structures). During the Gorkha Earthquake, the high frequencies were damped and therefore majority of the small story structures survived the ground shaking. On the other hand, the peak ground velocity is a low frequency characteristic of ground motion and is an

important parameter to the flexible structures (tall buildings). The damage to tall buildings correlates well with the large peak ground velocity.

Table 13: Peak ground acceleration (cm/sec^2), peak ground velocity (cm/sec) and peak ground displacement of four earthquakes recorded at four sites. The largest PGA (254.7 cm/sec^2) was recorded during the Mw 7.8 earthquake at rock site (KTP).

Earthquake		Acceleration (cm/sec^2)			Velocity (cm/sec)			Displacement (cm)		
		N-S	E-W	V	N-S	E-W	V	N-S	E-W	V
20150425 (7.8)	KTP	153.8	254.7	127.2	33.39	29.74	35.88	35.64	25.5	31.9
	TVU	209.9	228.5	138.6	105.5	79.27	39.75	62.2	44.5	32
	PTN	150.5	128.5	133.6	66	56.69	46.37	65.57	55.68	46
	THM	150.1	133.8	183.7	68.23	77.15	50.84	64.7	68.6	31
20150425 (6.6)	KTP	27.7	36.1	23.8	3.21	3.54	3.28	1.6	1.2	2
	TVU	68	114.7	38.4	16.45	22.43	6.46	6.1	6.7	2.5
	PTN	58	53.3	24	9.57	6.82	4.58	4.6	3	2.8
	THM	40.5	44.1	17.6	9.72	11.31	4.02	5.2	3.8	1.7
20150426 (6.7)	KTP	49.8	42.6	28.1	2.4	2.5	1.96	0.39	0.6	0.4
	TVU	89.2	107.1	50.4	10.78	17.39	5.96	2.9	6.2	1.2
	PTN	58.6	52.2	37.2	6.75	5.9	3.76	2.75	2.43	1
	THM	101.6	70.4	64	13.76	11.81	6.18	5.9	3.3	2.2
20150512 (7.3)	KTP	63.2	67.6	36.7	7.78	4.57	5.47	2.3	2.5	2.48
	TVU	112.5	111	68.1	26.01	22.9	11.16	8.86	9.97	4.1
	PTN	84	62.8	60.1	11.76	12.54	7.11	6.2	5.3	4.9
	THM	85.7	116.2	85.1	18.61	25.08	10.04	10.36	8.94	4.88
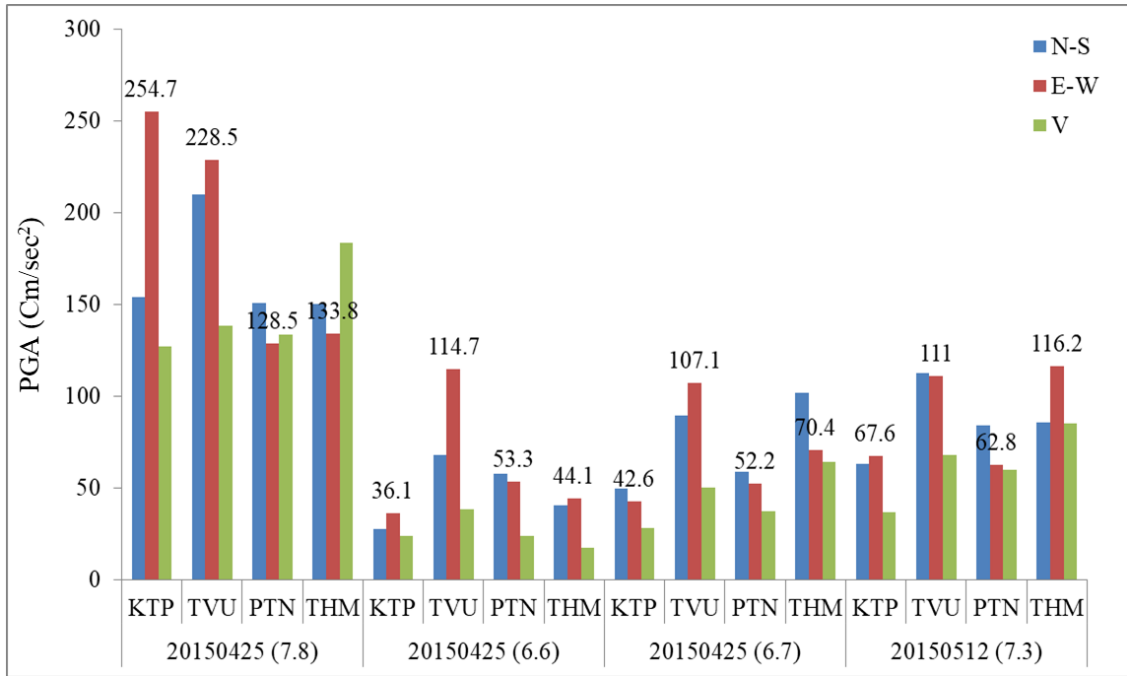
Figure 61: Peak ground acceleration (cm/sec^2) of the Gorkha Earthquake and its strong aftershocks recorded at four sites. Note that the maximum PGA was recorded at rock site (KTP).
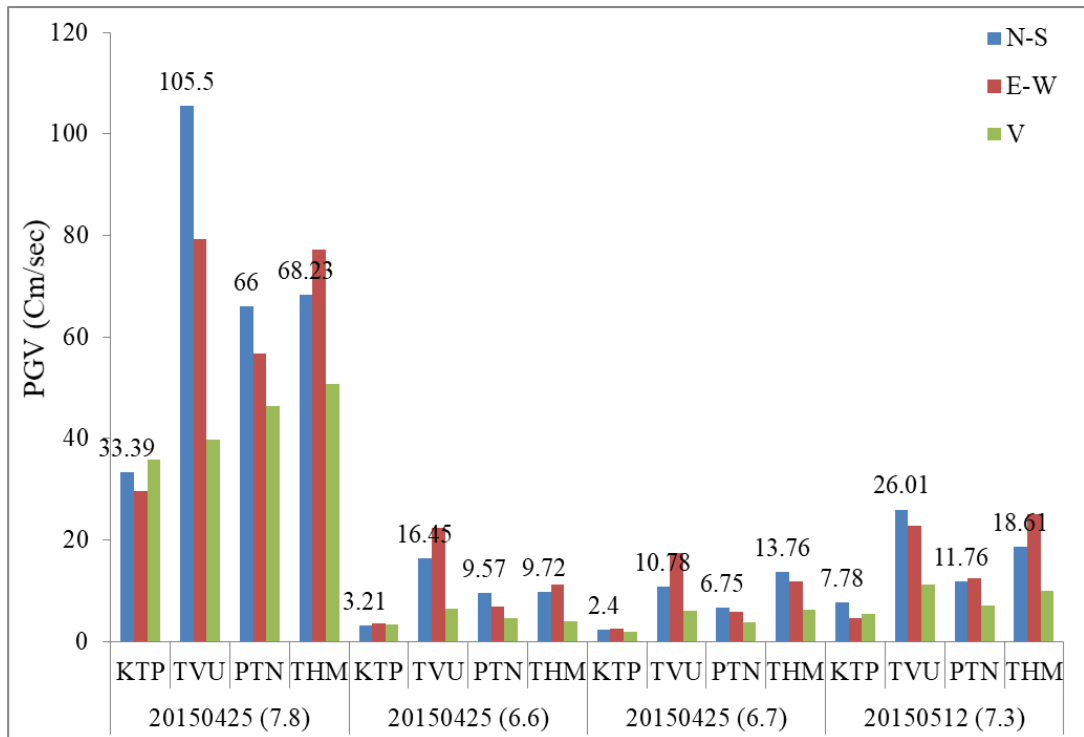
Figure 62: Peak ground velocity (cm/sec) recorded during the earthquakes at four sites. Note that the rock site has recorded the smallest PGV in all cases.
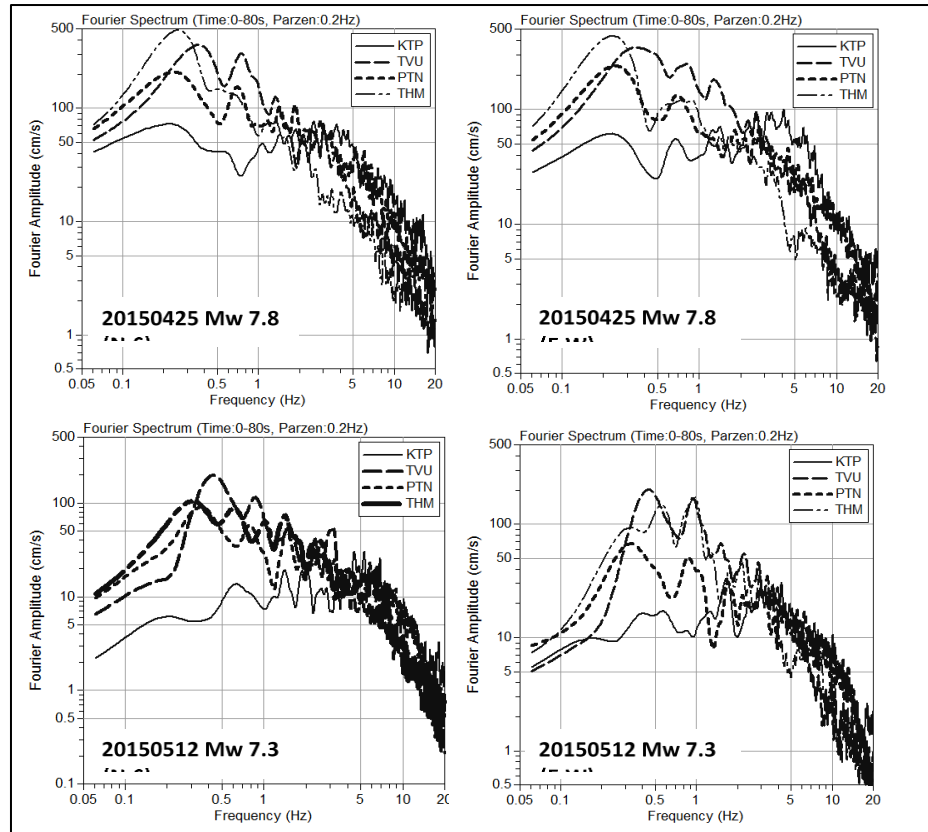
Figure 63: Fourier amplitude spectra of the earthquakes recorded at four sites. In all cases the lowest amplitude corresponds to the rock (KTP) site (Rajaure *et al.*, 2017).

Ratio of Fourier spectrum of ground motion at rock site to that at a soil site was used to investigate the amplification of seismic wave amplitude in Kathmandu valley during the Gorkha Earthquake sequence. In order to check the azimuthal influence of earthquakes, the earthquakes were grouped into two (Figure 64); two earthquakes in the west (Gorkha) and two earthquakes in the east (Dolakha). Figure 64 reveals the features of amplification in the Kathmandu valley during the Gorkha Earthquake sequence. The figures in the left column belong to the Mw 7.8 and Mw 6.6 earthquake which occurred in the west of Kathmandu at about 80 km; and the figures in the right hand column belong to the Mw 7.3 and Mw 6.7 earthquake which occurred in the east of Kathmandu at about 80 km. The results are grouped separately in order to check the azimuthal variation (if any). In the figures, it is clear that the amplification factor, which is a ratio of Fourier spectrum at soil site to that at the rock site (KTP) is smaller for the large earthquakes than the smaller ones. Similarly, the peak of amplification also moved towards high frequency during the smaller earthquakes. It clearly demonstrates that the sedimentary basin responded non-linearly during the earthquake sequence.

92
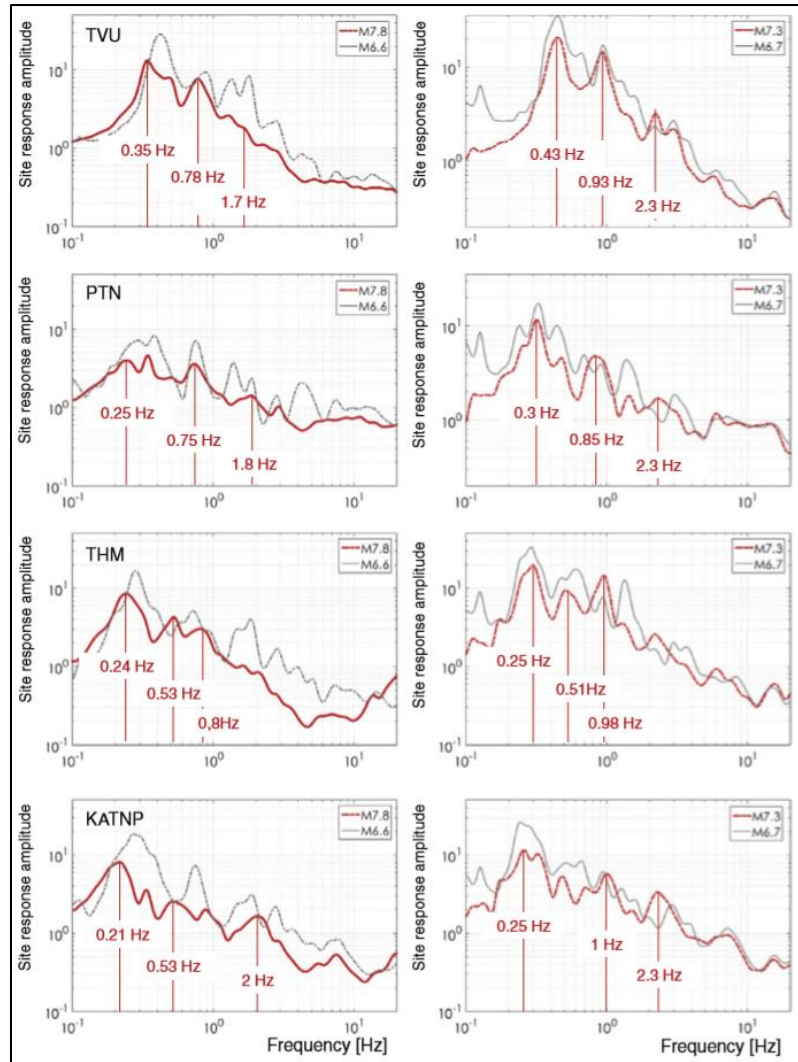
Figure 64: Ground response of the local geology of soil sites relative to rock site (KTP). This figure shows that amplification (ratio) during large magnitude earthquakes were comparatively smaller than during smaller earthquakes (Rajaure *et al.*, 2017).

4.10. Discussions

4.10.1. Seismic hazard in Nepal

Seismic hazard analysis of Nepal has been carried out incorporating the developments in the field of technology, improved knowledge of seismicity, seismotectonics, geodetic results, and impact of 2015 Gorkha Earthquake. Seismic hazard maps for five return periods have been prepared corresponding to 500, 1000, 2500, 5000 and 10000 year return periods.

Multiple source models and multiple attenuation relations are used to evaluate seismic hazard in Nepal. Earthquake sources are considered both in Nepal and in the

93

surrounding areas of the region, which fall up to 250 km from the border of Nepal. The MHT is treated as a segmented source. Logic trees are used to incorporate uncertainties in source models and attenuation relations. Most of the previous works have prepared seismic hazard maps corresponding to 500 year return period, which is commonly used in building codes, therefore, further discussion is made on seismic hazard maps of 500 year return period only

The result (Figure 50) shows a belt of high hazard (PGA >0.3) in the middle part of Nepal parallel to the Himalaya. The maximum hazard (PGA>0.45) g is present in the far-western part of Nepal. The seismic hazard map (Figure 50) was prepared using attenuation relations (Appendix 18-1 and Appendix 18-2) described in 4.7.2. Among the relations, Young's *et al*. (1997) produces considerably large PGA (e. g. Appendix 19-1) in comparison to other relations. When Young's *et al.* (1997) relation is omitted for the subduction zone sources (MHT segments), the largest PGA is about 0.35 g (Appendix 21-2) in far-west and about 0.3 g in the Kathmandu Valley. As a local attenuation model is not available for Nepal and it is not known which specific model from other regions best fits the local attenuation pattern, Youngs *et al.* (1997) attenuation relation is continued to be used and the seismic hazard maps (Figure 50, Figure 51, Figure 52, Figure 53 and Figure 54) are adopted as the final seismic hazard maps corresponding to 500, 1000, 2500, 5000 and 10000 year return period.

A test is carried out to understand the major source of seismic hazard in the urban areas of Nepal. A seismic hazard map was prepared without considering the MHT sources, which shows considerably small PGA (Appendix 21-3) in the urban areas in Nepal. But the sources in the north (South-Tibet) have influence in the northern part reaching about 0.2 g Jomsom area. Evidently, the MHT is a major source of seismic hazard in the urban areas of Nepal.

The prepared seismic hazard map (Figure 50) is in a good agreement with frequently experienced and reported earthquakes in history, which have destroyed the northern part of Nepal many times (e.g. 1833 North Kathmandu Earthquake (Mw 7.6) and 2015 Gorkha Earthquake (Mw 7.8). A comparison of the present result (Figure 50) with the results from three previous works (corresponding to 500 year return period) is presented in (Figure 65).
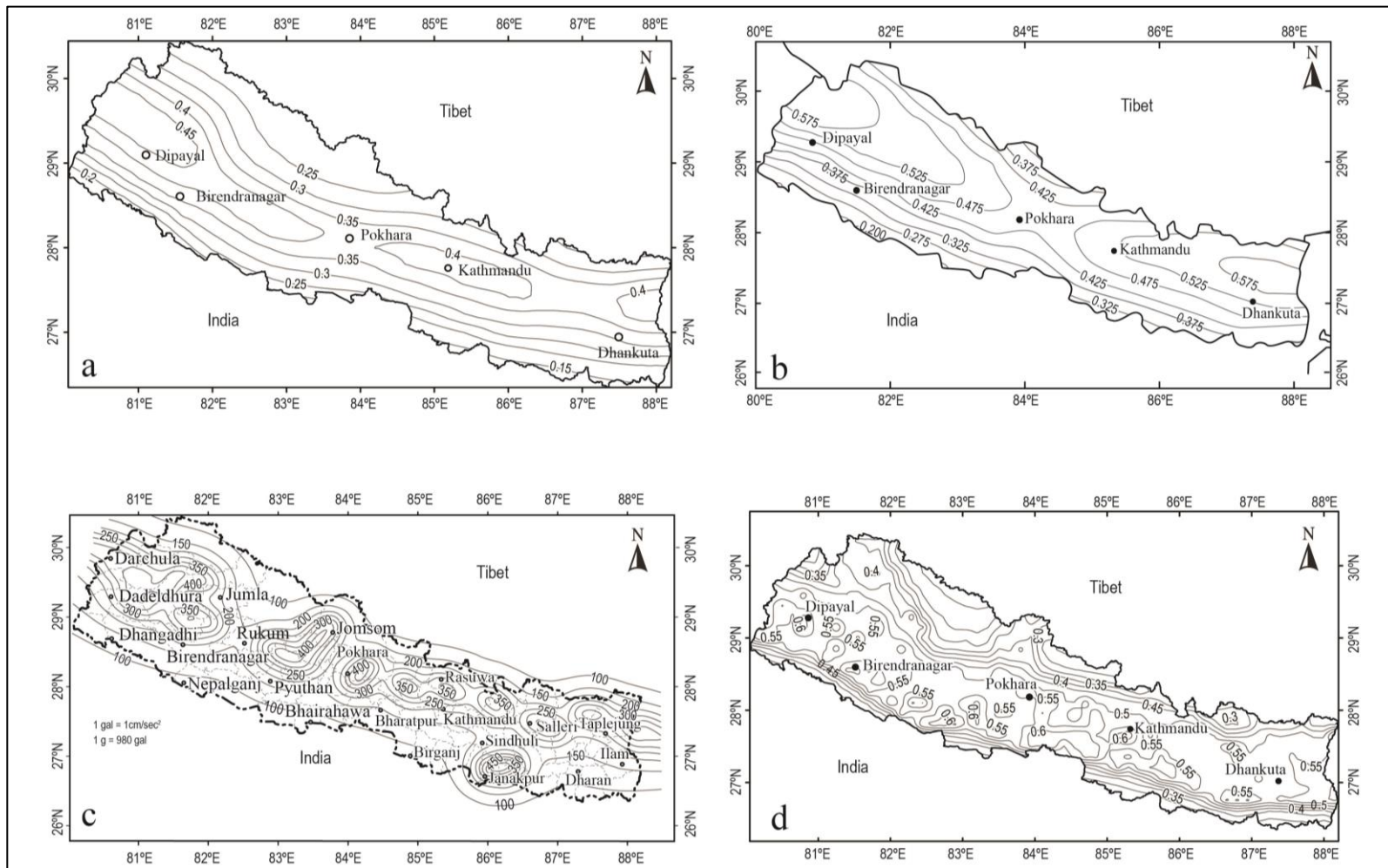
Figure 65: A comparison of the seismic hazard map (a) prepared in this study with other previous works by Thapa and Wang (2013) (b), Pandey *et al*. (2002) (c) and Stevens *et al*. (2018) (d). The depicted PGA corresponds to 10% probability of exceedance in 50 years at engineering rock site condition.

The result from this study (Figure 65(a)) agrees with the results obtained by Pandey *et al.*, (2002) in terms of the high hazard zone in the northern part of Nepal (Figure 65 (c)). The seismic hazard map (Figure 65(a)) was published using area sources and thrust faults as potential earthquake sources. The area sources are segments of the MHT and the thrusts are other geological faults. Young's *et al.* (1997) attenuation relation was used to derive the PGA. The PGA corresponds to 10% probability of exceedance in 50 years at the engineering bedrock. The pattern of large PGA distribution correlates with the pattern noticed in the present result. The PGA in this result varies between 0.1 and 0.4 g.

The seismic hazard map of Nepal (Figure 65 (b)) by Thapa & Wang (2013) shows PGA higher than in this result, which might have resulted from differently estimated earthquake recurrence parameters and the considered earthquake sources, which are not based on the geometry of the MHT. They have estimated b-value that is smaller (0.85) than estimated in this study for the region. They have followed the procedure developed by CEA (2005) to estimate seismic hazard using attenuation relation developed by CEA (2005) for western China. The smaller b-value might be responsible for the large PGA estimated. The large PGA in the north resulted on account of the division of MHT into two sources and possibly the recurrence parameters were estimated using data specific to the sources.

Stevens *et al.* (2018) prepared seismic hazard map of Nepal (Figure 65 (d)) using MHT as a single source with maximum potential magnitude up to Mw 9.0 and other faults in the north and northwest of Nepal. The researchers have used fixed b-value (1.0) in accordance with the worldwide observation of b-value in similar tectonic regions. The b-value (1.0) used by Stevens *et al.* (2018) is not small, however the predicted maximum PGA is relatively large (0.6 g). The large PGA possibly resulted from a very large single earthquake source (MHT). Present study considers segments of MHT, which have smaller maximum potential magnitude (up to 8.5) than considered by Stevens *et al.* (2018) (Mw 9.2). Additionally, Stevens *et al.* (2018) considered entire N-S rupture of the MHT, whereas weighted mean of three types of scenario rupture of MHT are considered in the present study, hence high hazard is estimated in the middle part of Nepal and the southern part has less hazard.

Seismic hazard analysis requires record of earthquakes recorded for long span of time and it should cover complete seismic cycles of large earthquakes. Systematic recording of earthquakes started very lately and therefore such a record does not extend back beyond 1900 AD. Records of the historical earthquakes have uncertainty in terms of their precise size and location. The presently prepared seismic hazard maps are prepared using instrumentally recorded data for the last 120 years and pre-instrumental data (before 1900 AD) which are available since 1100 AD. The earthquake recurrence parameters based on such a limited data were used to evaluate seismic hazard. The pre-instrumental data could have higher uncertainties because of their locations and magnitudes being estimated from the macroseismic data.

Furthermore, well established attenuation relations are not available for the region and Nepal particularly. Therefore, such relations have to be borrowed from other regions, which have similar tectonic environment. In addition to these uncertainties about attenuation relation, the scattering in attenuation relation, maximum potential magnitude of potential earthquake also influence the uncertainties in the result.

4.10.2. Ground response of Kathmandu valley

The results from seismic hazard analysis are calculated at the engineering rock site condition, where the shear wave velocity (Vs) is larger than 760 m/s. However, the ground motions may be influenced by local geology and soft sediments.

Earlier reports on the 1934 Bihar-Nepal Earthquake (Mw 8.2) and 1833 North Kathmandu Earthquake (Mw ~7.6) discuss localized massive destruction in the Kathmandu valley and attribute the massive destruction to local geology of the basin (Pandey and Molnar, 1988).

Present study utilized strong motion records of different earthquakes which occurred in and around Nepal to investigate the effect of local geology on ground shaking. The result depicts that the peak value of amplification increased gradually during the large-to-small earthquakes. The amplification was smaller during strong earthquakes (Mw 7.8 and Mw 7.3) in comparison to other strong aftershocks (Mw 6.6 and Mw 6.7) (Table 12). Apparent azimuthal effect was not noticed from the analysis of

records, two of which occurred in the west of Kathmandu and two in the east. The soft sediments of Kathmandu valley damped the frequencies above 2.5 Hz, which correspond to low rise buildings (up to 4 story), therefore the low rise buildings survived the shaking than was anticipated. Because of the amplification of motion at low frequency (<2.5 Hz) the tall structures were affected considerably. Based on a few observations, it is too early to generalize the observations of Gorkha Earthquake to future strong earthquakes.

CHAPTER 5
CONCLUSIONS AND RECOMMENDATIONS

5.1 Conclusions

Probabilistic seismic hazard maps (Figure 50, Figure, 51, Figure 52, Figure 53 and Figure 54) of Nepal have been prepared. The maps show PGA values for engineering soil site conditions corresponding to 10%, 5%, 2%, 1% probability of exceedance in 50 years and 1% probability of exceedance in 100 years (approximately 500 year, 1000 year, 2500 year, 5000 year and 10000 year return period in their order).

The seismic hazard maps are prepared using two types of attenuation relations (Appendix 18-1 and Appendix 18-2). Among the relations, Young's *et al.* (1997) relation produces the largest PGA (Appendix 19-1) whereas the Atkinson and Boore (2003) relation produces the smallest. When Young's *et al.* (1997) relation is omitted for the subduction zone sources (MHT segments), the largest PGA, corresponding to ~500 year return period, is about 0.35 g in far-west and about 0.3 g in the Kathmandu Valley (Appendix 21-2). Considering the unavailability of a local attenuation model for Nepal, our knowledge on which model best fits the local attenuation model and the PGA recorded during 2015 Gorkha Earthquake, we chose to use Young's *et al.* (1997) attenuation relation also in all calculations.

The seismic hazard maps show the eastern Nepal (Taplejung and Terhathum), central Nepal (Kathmandu, Kavre, Sindhupalchok, Nuwakot, Dhading and Makawanpur) and far western Nepal (Jajarkot, Jumla, Kalikot, Dailekh, Achham, Bajura and Bajhang) have relatively high hazard.

The major conclusions on the seismic hazard analysis of Nepal are as follows.

I.   A comprehensive, magnitude-homogenized earthquake catalogue is prepared from catalogues collected from different sources. The catalogue contains independent earthquakes that are required in probabilistic seismic hazard analysis.

II. Altogether nine earthquake source models are identified and delineated. Out of the nine models, six models are used in the preparation of seismic hazard maps.

III. Peak ground acceleration is estimated at grid of ~20 km spacing. Probabilistic seismic hazard maps of Nepal have been prepared for 500, 1000, 2500, 5000 and 10000 year return periods.

IV. The major source of seismic hazard in Nepal is the Main Himalayan Thrust.

V. The region between MCT and MFT shows relatively high hazard.

VI. The seismic hazard depends more on the maximum potential magnitude and earthquake recurrence parameters than on geometry of MHT.

VII. The peak ground acceleration in major places are as follows. The PGA values correspond to 500 year return period for engineering rock site conditions.

Place	Latitude (°E)	Latitude (°N)	PGA (g)
Baglung	83.600	28.266	0.370
Bajhang	81.199	29.550	0.470
Bhairahawa	83.450	27.500	0.230
Biratnagar	87.283	26.467	0.150
Birgunj	84.867	27.017	0.160
Chaurjhari	82.193	28.626	0.420
Dadheldhura	80.567	29.300	0.400
Darchula	80.764	29.872	0.466
Dhankuta	87.340	26.970	0.300
Dipayal	80.930	29.243	0.448
Dunai	82.900	28.933	0.280
Gorkha	84.629	28.000	0.410
Hilsa	81.334	30.151	0.290
Ilam	87.910	26.910	0.330
Janakpur	85.917	26.733	0.160
Jiri	86.229	27.628	0.400
Jomsom	83.730	28.783	0.240
Jumla	82.193	29.274	0.320
Kathmandu	85.317	27.700	0.410
Mahendranagar	80.300	28.967	0.240
Mugu	82.085	29.502	0.330
Nepalgunj	81.617	28.067	0.200
Palpa	83.550	27.866	0.350
Pokhara	83.983	28.217	0.370
Pyuthan	82.853	28.101	0.400
Salyan	82.161	28.375	0.380
Simikot	81.819	29.968	0.270
Surkhet	81.600	28.600	0.360
Taplejung	87.650	27.370	0.410
Tumlingtar	87.193	27.314	0.370

Ground response of the Kathmandu valley sediments has been investigated utilizing strong motion records of the 2015 Gorkha Earthquake recorded in the Kathmandu sedimentary basin. The major observations on the ground response of the Kathmandu Valley are as follows.

I.   During the Gorkha Earthquake sequence, the PGA at soil sites were damped for frequencies larger than 2.5 Hz and amplified in the lower frequency (<2.5 Hz). Because of this reason, the small story buildings were less affected and the tall structures were affected more.

II.   The amplification factor was smaller during strong earthquake and was larger during smaller earthquakes. This is non-linear effect caused by the properties of soil in the Kathmandu Valley.

III. The results on ground response are based on analysis of records recorded at a few places, therefore, should not to be generalized for other locations.

IV.   These results on ground response are based on strong motion records of a few earthquakes, therefore, should not be generalized for other future strong earthquakes.

5.2 Recommendations

The followings are the main recommendations of this study:

I.   The prepared seismic hazard maps incorporate the experience of the 2015 Gorkha Earthquake and its different characteristics, multiple source models, multiple attenuation relations, different datasets and different earthquake recurrence parameters estimated using different methods. Additionally, three rupture scenarios of the sources from MHT were considered. The PGA values estimated for different part of Nepal in the present study are more realistic. Therefore, these findings should be considered in next revision of the Building code of Nepal

II.   The seismic hazard map and ground response results should be considered in policy making, planning, formulation and revision of building code, design of new infrastructures and retrofitting of existing infrastructures. It will facilitate the risk assessment, insurance policies and many others.

III. Present study reveals that the effect of an earthquake in the Kathmandu valley is not uniform at all places. Therefore, a detailed study is required to completely understand the site characteristics in the Kathmandu sedimentary basin.

IV. The Kathmandu valley sediments amplified low frequencies (<2.5 Hz) and damped high frequencies (> 2.5 Hz) during the 2015 Gorkha Earthquake. A dense network of strong motion instruments should be installed and operated continuously keeping always in mind that strong earthquakes are lessons to improve our understanding and move forward accordingly. Such a network will help in the derivation of local attenuation relation for Nepal that is not available to the date.

V. Ground response of other major cities of Nepal where sediment cover is very thick such as Pokhara, cites at dun valleys and Terai etc, site characteristics is still unknown. Installation and operation of strong motion instruments is necessary for those cities also to better understand the ground response during earthquakes.

CHAPTER 6
SUMMARY

Nepal lies in the central part of the Himalaya which is one of the most seismically active zones in the world. The Himalaya is a converging zone, where the Indian Plate is continuously thrusting under the Eurasian Plate. The Main Himalayan Thrust (MHT) is the detachment surface, which separates these two plates. The Main Central Thrust (MCT), Main Boundary Thrust (MBT) and the Main Frontal Thrust are major thrust systems in Nepal. In addition to these thrust systems, there are several reverse faults in Nepal and normal faults in South Tibet.

Nepal has witnessed several mega-earthquakes and thousands of small earthquakes in the past. The 2015 Gorkha earthquake is one of the latest mega-earthquakes in Nepal, which resulted on account of the slip on the MHT. Large earthquakes (Mw>7.5), which are less frequent, are believed to occur at the depth of the MHT (~20 km). The consequences of occasional large earthquakes have remained very painful to the people, society, economy and the nation as a whole. The more frequent smaller earthquakes may occur off the MHT and could in particular be shallower. These smaller and shallow events being more frequent may impact in the hazard level significantly. The preparation of seismic hazard map and evaluation of site specific ground motion due to earthquake could be the basic steps of earthquake risk reduction. The policy making, planning, formulation/revision of building code, strengthening of existing structures and risk analysis all require the results from the seismic hazard analysis.

A number of attempts have been made to produce seismic hazard maps of Nepal in the past. However, in one hand, those maps prepared by different authors do not agree with each other. On the other hand preparation of a seismic hazard map is a dynamic process and the map evolves through time when there are new data, techniques and better understanding of geology, seismotectonics etc. Therefore, present study was undertaken to develop new seismic hazard maps of Nepal, corresponding to different return periods, using multiple dataset, multiple source models, and multiple attenuation and recurrence relations. Seismic hazard maps of different return periods

have been prepared so that they would be helpful in planning and in the design of different kinds of hydropower projects as well as other development infrastructures

A comprehensive, magnitude-homogenized earthquake catalogue is prepared from earthquake catalogues collected from different sources. The prepared catalogue can serve as an input in further seismic hazard analysis.

Three rupture scenarios of the MHT were used with different weight factors to account for uncertainty in the dimension of rupture, as revealed by 2015 Gorkha Earthquake, possibly the 1833 North Kathmandu Earthquake and other rupture areas revealed by paleoseismic investigations carried out in Nepal. Further, 2015 Gorkha Earthquake and its aftershock area (rupture area) have been used in the present study to prepare the seismic hazard map of Nepal and analyze the ground response of the Kathmandu valley.

In this study, the Probabilistic Seismic Hazard Analysis (PSHA) technique developed by Cornell (1968) and Algermissen *et al.* (1982) was used to evaluate seismic hazard in Nepal. The prepared seismic hazard maps depict seismic hazard expressed in terms of PGA (g) across the country. The maps show a belt of relatively high hazard in the middle part of Nepal that runs parallel to the Himalaya. The belt of high hazard correlates with the location of the MHT, often felt earthquakes and the rupture area of the 2015 Gorkha Earthquake. Relatively high hazard is depicted in the far-western part of Nepal. The hazard strongly drops in the southern part of Nepal (in the south of the MFT) because of the boundary of major source of earthquakes (MHT) ends there. The MHT is the major contributor of seismic hazard in Nepal.

Characteristics of ground motion may be influenced by local geology. Local geology can bring changes in amplitude, duration and frequency content of ground motion. Variable destruction pattern was reported during 1934 Bihar-Nepal Earthquake (Mw 8.2). Strong motion records of earthquakes recorded in the Kathmandu Valley were used to investigate characteristics of the ground motion and amplification in the valley. Local geology of Kathmandu sedimentary basin responded non-linearly to the ground motions during the Gorkha Earthquake and its three strong earthquakes. The amplification was small during strong earthquakes in comparison the smaller

earthquakes. The amplitudes at frequencies larger than 2.5 Hz were strongly damped and those smaller than 2.5 Hz were amplified. Because of damping of high frequencies, the small storied buildings were less affected than was anticipated initially. Similarly, the tall buildings were severely affected because of amplification of frequencies smaller than 2.5 Hz.

The result of seismic hazard analysis is important for a nation like Nepal which is pursuing to accelerate its development works. The result can help in policy making, planning, formulation and revision of building code, design of new infrastructures and strengthening of existing ones. Similarly, it can help in risk assessment, insurance policies and many others. The result of ground response in Kathmandu Valley are based on acceleration data of a very few earthquakes recorded at six locations. The results from these limited number earthquakes, recorded at a few sites should not be generalized for entire Kathmandu Valley.

REFERENCES

Abrahamson, N., & Somerville, P. (1996). Effects of the Hanging Wall and Footwall on Ground Motions Recorded during the Northridge Earthquake. *Bulletin of the Seismological Society of America*, 86.

Abrahamson, N. A. (2006). Seismic hazard assessment: Problems with current practice and future developments. *Proceedings of the First European Conference on Earthquake Engineering and Seismology, Geneva*, 17.

Abrahamson, N. A., Silva, W. J., & Kamai, R. (2014). Update of the AS08 Ground-Motion Prediction Equations Based on the NGA-West2 Data Set, *Earthquake Spectra* (in review).

Abrahamson, N., Gregor, N., & Addo, K. (2016). BC hydro ground motion prediction equations for subduction earthquakes, Earthquake Spectra, 32, no. 1, 23–44.

Adams, J., Weichert, D.H., & Halchuk, S. (1999). Lowering the probability level — Fourth generation seismic hazard results for Canada at the 2% in 50 year probability level. In Proceedings of the 8th Canadian Conference on Earthquake Engineering, 13– 16 June 1999, Vancouver, B.C. *Canadian Association for Earthquake Engineering*. pp. 83–88.

Adams, J., & Atkinson, G.M. (2003). Development of Seismic Hazard Maps for the 2005 National Building Code of Canada. *Canadian Journal of Civil Engineering*, **30**: 255-271.

Adams, J., & Halchuk, S. (2003). Fourth generation seismic hazard maps of Canada: Values for over 650 Canadian localities intended for the 2005 National Building Code of Canada. *Geological Survey of Canada*, Open File, **4459**: 1-155.

Adams, J., & Halchuk, S. (2004). Fourth generation seismic hazard maps for the 2005 National Building Code of Canada. *13th World Conference on Earthquake Engineering*, Vancouver, Canada. Paper 2502 on CD-ROM. 1-6 August 2004, Vancouver.

Ader, T., Avouac, J. P., Bollinger L., Lyon-Caen, H. D., Chanard, K., Galetzka, J., Genrich J., & Sapkota, S. (2011). Convergence rate across the Nepal Himalaya and interseismic coupling on the Main Himalayan Thrust: implications for seismic hazard. *Journal of Geophysical Research*, **117**: B04403, https://doi.org/10.1029/2011JB009071

Ader, T., Avouac, J.P., Liu-Zeng, Lyon-Caen, H., Bollinger, L., Galetzka, J., Thomas, M., Chanard, K., Sapkota, S. N., Rajaure, S., Shrestha, P., Ding, L. and Flouzat, M. (2012) Convergence rate across the Nepal Himalaya and interseismic coupling on the main Himalaya thrust: Implications for seismic hazard. *Journal of Geophysical Research*., v.117 B04403, doi:10. 1029/2011 JB009071.

Aguilar-Meléndez, A., Ordaz, M., De La Puente, J., González, R. S., Rodríguez-Lozoya, H., Ceballos, A., García-Elías, A., Calderón-Ramón, C., Escalante-Martínez, J., Laguna-Camacho, J., & Campos-Rios, A. (2017). Development and Validation of Software CRISIS to Perform Probabilistic Seismic Hazard Assessment with Emphasis on the Recent CRISIS2015.*Computacion y Sistemas*. 21. 10.13053/CyS-21-1-2578.

Aguilar-Meléndez, A., Ordaz, M., De La Puente, J., Beneit, L., Barbat, A., Rodríguez-Lozoya, H., Monterrubio-Velasco, M., Escalante-Martínez, J., & Campos-Rios, A. (2018). Sensitivity Analysis of Seismic Parameters in the Probabilistic Seismic Hazard Assessment (PSHA) for Barcelona Applying the New R-CRISIS.*Computacion y Sistemas*,**22**:1099-1122. doi. 10.13053/CyS-22-4-3084.

Aki, K. (1965). Maximum Likelihood estimate of b in the formula logN = a - bM and its confidence limits. *Bulletin of Earthquake Research Institute*, **43**: 237–239.

Algermissen, S. T., Perkins, D. M., Thenhaus, P. C., Hanson, S. L., & Bender, B. L. (1982). Probabilistic estimates of maximum acceleration and velocity in cork in the contiguous United States. *Open file report 82-1033, U. S. Geological Survey*, Washington, D.C.

Ambraseys, N., & Jackson, D. (2003).A note on early earthquakes in northern India and southern Tibet. *Current Science* (Bangalore).**84:**570-582.

Ambraseys, N., & Douglas, J. (2004).Magnitude calibration of North Indian earthquakes. *Geophysical Journal International*.**159:**165 - 206. 10.1111/j.1365-246X.2004.02323.x.

Arita, K., 1983, Origin of the inverted metamorphism of the Lower Himalayas, Central Nepal. *Tectonophysics*, v. 93, pp. 43-60.

Asimaki, D., & Gazetas, G. (2004).Soil and Topographic Amplification on Canyon Banks and the 1999 Athens Earthquake.*Journal of Earthquake Engineering*, 8: 1-43. 10.1080/13632460409350479.

Atkinson, G. M., & Boore, D. M. (2003).Empirical ground-motion relations for subduction-zone earthquakes and their application to Cascadia and other regions, *Bulletin of Seismological Society of America*, v 93, no. 4, 1703–1729.

Avouac, J. P. (2003). Mountain building, erosion, and the seismic cycle in the Nepal Himalaya. *Advances in Geophysics*, 46:1–80. doi 10.1016/S0065-2687(03)46001-9.

Basham, P. W., Weichert, D. H., Anglin, F. M., & Berry M. J. (1985). New probabilistic strong seismic ground motion maps of Canada. *Bulletin of the Seismological Society of America*, **75:** 563-595.

Bazzurro, P., & Cornell, A. C. (1999).Disaggregation of Seismic Hazard.Bulletin of the *Seismological Society of America*. 89.

Bettinelli, P., Avouac, J. P., Mireille, F., Jouanne, F., Bollinger, L., Wills, P., & Chitrakar, G. R. (2006). Plate motion of India and interseismic strain in the Nepal Himalaya from GPS and DORIS measurements, *Journal of Geodesy*, doi: 10.1007//s00190-006-0030-3.

Bhattarai, M., Gautam, U., Pandey, R., Bollinger, L., Hernandez, B., & Boutin, V. (2011).Capturing first records at the Nepal NSC accelerometric network. *Journal of Nepal Geological Society*, **43** (Special Issue):137-144.

Bilham, R., Bodin, P., & Jackson, M. (1995).Entertaining a great earthquake in western Nepal. *Journal of Nepal Geological Society*, **11 (1)**:73-78.

Bilham, R. (1995). Location and Magnitude of the 1833 Nepal Earthquake and its Relation to the Rupture zones of Contiguous Great Himalayan earthquakes. *Current Science*, **69(2):**155-187.

Bilham, R., Gaur, V. K. &Molnar, P. (2001). Himalayan Seismic Hazard, Science, **293**.

Bilham, R., Larson, K., Freymueller, J., & Idylhim members (1997). GPS measurements of present-day convergence across the Nepal Himalaya, *Nature*, **386:**1-94.

Bilham, R. (2004). Earthquakes in India and the Himalaya: tectonics, geodesy and history. *Annalis of Geophysics*. Version: 1 Meeting on Virtual Astrophysical Jets, **47:**839-858, Dogliani, ITALY, OCT 02-04, 2003, ISSN: 1593-5213, ids: 857QB

Bilham, R., & Ambraseys, N. (2004). Apparent Himalayan slip deficit from the summation of seismic moments for Himalayan earthquakes, *Current Science*, 1500-2000.

Bilham, R., & Wallace, K. (2005). Future Mw 8 earthquake in Himalaya: implication for the 26 December, 2004 M=9 earthquake on eastern margin. *Geological Survey of India, India Special Publication,* No. 85, pp.1-14.

Bilham, R. (2019). Himalayan earthquakes: a review of historical seismicity and early 21st century slip potential. *Geological Society, London, Special Publications*. SP483.16. 10.1144/SP483.16.

Bodenhausen, J.W. A., & Egeler, C. G. (1971). On the geology of the upper Kali Gandaki Valley, Nepalese Himalayas, I: *Akademic van Wetenschappen Proceedings*, **74:**526-538.

Boore, D. M., Stewart, J. P., Seyhan, E., & Atkinson, G. M. (2014). NGA-West2 Equations for Predicting Response Spectral Accelerations for Shallow Crustal Earthquakes, *Earthquake Spectra* (in review).

Bora, D. K., Borah, K., Mahanta, R., & Borgohain, J. (2018). Seismic b-values and its correlation with Seismic Moment and Bouguer Gravity Anomaly over Indo-

Burma ranges of northeast India: Tectonic Implications. *Tectonophysics*.728. 10.1016/j.tecto.2018.01.001.

Borcherdt, R. D. (1992). Simplified site classes and empirical amplification factors for site-dependent code provisions. NCEER, SEAOC, BSSC workshop on site response during earthquakes and seismic code provisions, *University of Southern California, Los Angeles, California*, Nov. 1992.

Bordet, P., Colchen, M., Krummenacher, D., Le Fort, P., Mouterde, R., & Remy, M. (1971).Recherches Ge´ologiques dans l'Himalaya du Ne´pal, Re´gion de la Thakkhola. Centre *National de la Recherche Scientifique*, **86:**1–279.

Campbell, K. W., & Bozorgnia, Y. (2014). NGA-West2 Campbell-Bozorgnia Ground Motion Model for the Horizontal Components of PGA, PGV, and 5%-Damped Elastic Pseudo-Acceleration Response Spectra for Periods Ranging from 0.01 to 10 sec, *Earthquake Spectra* (in review).

Cattin, R. & Avouac, J.P. (2000).Modeling mountain building and the seismic cycle in the Himalaya of Nepal. *Journal of Geophysical Research* , **105:**13,389-13,407.

Chen, W.P., Nabelek, J. L., Fitch, T.J., & Molnar P. (1981). An intermediate depth earthquake beneath Tibet: Source characteristics of the event of September 14, 1976. *Journal of Geophysical Research*, **86:**2863-2876.

Chen, W.P., & Molnar, P. (1983).Focal Depths of Intracontinental and Intraplate Earthquakes and Their Implications for the Thermal and Mechanical Properties of the Lithosphere. *Journal of Geophysical Research*, **88:**4183-4214. 10.1029/JB088iB05p04183.

Chen, W.P., & Zhou, Y. (2004) Earthquakes beneath the Himalayas and Tibet: Evidence for strong lithospheric mantle, *Science*, **304:**1949–1952.

China Earthquake Administration (CEA) (2005).Training Material on Seismic Hazard Analysis for Engineering Sites (GB17741-2005). (in Chinese).

Chiou, B-S.J., & Youngs, R. R. (2014). Update of the Chiou and Youngs NGA Ground Motion Model for Average Horizontal Component of Peak Ground Motion and Response Spectra, *Earthquake Spectra* (in review).

Chitrakar, G. R., & Pandey, M. R. (1986).Historical earthquakes of Nepal. *Bulletin of the Nepal Geological Society*, **4:**7-8.

Colchen, M., Le Fort, P., & Peˆcher, A. (1981). Geological map of Annapurna-Manaslu-Ganesh Himalaya of Nepal, 1:200,000. Washington, D.C.: *American Geophysical Union*.

Colchen, M., Le Fort, P., & Peˆcher A. (1986). Recherches geˊologiques dans l'Himalaya du Neˊpal: Annapurna Manaslu-Ganesh Himal (p. 136). Paris: *Editions du Centre National de la Recherche Scientifique*.

Cornell, C.A. (1968). Engineering seismic risk analysis, *Bulletin of the Seismological Society of America*, **58:**1583-1606.

Coward, M. P., David, C. R., Khan, A., Windley, B. F., Broughton, R. D., Luff, I. W., Petterson, M. G., & Pudsey, C. J. ((1986). Collision tectonics in the NW Himalayas. Geological Society, London, Special Publications. 19. 10.1144/GSL.SP.1986.019.01.11.

Dewey, J., & Bird, J. M. (1970).Mountain Belts and the New Global Tectonics. *Journal of Geophysical Research*, **75:**2625-2647. 10.1029/JB075i014p02625.

Dhital, M. R. (2015). *Geology of the Nepal Himalaya: Regional perspective of the classic collided orogen*. 10.1007/978-3-319-02496-7.

DMG (Department of Mines and Geology) (1987). Geological map of central Nepal in 1:250000 scale.

Earthquake catalogue (1995-2008), Department of Mines and Geology, Kathmandu, Nepal.

Earthquake catalogue (2017) https://www.usgs.gov/faqs

Gahalaut, V. K., & Kundu, B. (2012).Possible influence of subducting ridges on the Himalayan arc and on the ruptures of great and major Himalayan earthquakes.*Gondwana Research*. **21:**1080-1088. 10.1016/j.gr.2011.07.021.

Gansser, A. (1964), *Geology of the Himalayas*: Interscience Publishers, John Wiley and Sons, London, 289 p.

Gardner, J. K., & Knopoff, L. (1974). Values for foreshocks and aftershocks in real and simulated earthquake sequences, *Bulletin of the Seismological Society of America*, **72(5):** 1663-1676.

Giardini, D., Grunthal, G., Shedlock, K. M., & Zhang, P. (1999). The GSHAP Global Seismic Hazard Map*, Annali Di Geofisica*, **42(6).**

Gutenberg, B., and Richter, C.F. (1954).Frequency of earthquakes in California. *Bulletin of the Seismological Society of America*, **34(4):**185-188.

Hagen T. (1968). Report on the geological survey of Nepal. Geology of the Thakkhola.*DenkschrSchweiznaturforsch. Ges.*,**86(2):**1-159.

Hanks, T.C., & Kanamori, H. (1979). A moment magnitude scale, *Journal of Geophysical Research*, **84(5):**2348-2350, 9B0059, doi:10.1029/JB084iB05p02348.

Hashimoto, S., Ohta, Y. & Akiba, C. (Editors), 1973 .Geology of the Nepal Himalayas.*Saikon Publishing Co., Tokyo*, 286pp.

International Seismological Centre (2017), *On-line Bulletin, https://doi.org/10.31905/D808B830*

IS: 1893 (Part-1), Indian Standard criteria for Earthquake Resistant Design of Structures (Fifth Revision), *Bureau of Indian Standards*, New Delhi, 2002.

Jackson, M., & Bilham, R. (1994). Constraints on Himalayan deformation inferred from vertical velocity fields in Nepal and Tibet, *Journal of Geophysical Research*, **99(B7):**13897-13912.

Jouanne, F., Mugnier, J., Pandey, M., Gamond, J., Le Fort, P., Serrurier, L., Vigny, C., & Avouac, J. P. (1999). Oblique Convergence in the Himalayas of Western Nepal Deduced from Preliminary Results of GPS Measurements. *Geophysical Research Letters*, **26(13):** 1933–1936.

Jouanne, F., Mugnier, J., Gamond, J., Le Fort, P., Pandey, M.R., Bollinger, L., Flouzat, M., & Avouac, J. P. (2004). Current shortening across the Himalayas of Nepal.*Geophysical Journal International*, 157: 1–14.

Kanamori, H. (1977). The energy release in great earthquakes.*Journal of Geophysical Research*, **82:**2981–2987.

Kanamori H. (1983). Magnitude scale and quantification of earthquakes.*Tectonophysics,* **93:**185-199.

Kayal, J. (2001).Microearthquake activity in some parts of the Himalaya and the tectonic model.*Tectonophysics*.**339:**331-351. 10.1016/S0040-1951(01)00129-9.

Khanal, R.P. (2005).*Preliminary Seismic Microzonation of Kathmandu Valley, Nepal Using One Dimensional Seismic Response Analysis* [Unpublished Master of Since dissertation].Enschede, the Netherlands, International Institute for Geo-information Science and Earth Observation (ITC).

Khattri, K. N., & Tyagi, A. K. (1983). Seismicity pattern in the Himalayan plate boundary and identification of areas of high seismic potential. *Tectonophysics*, **96**: 281-297.

Khattri, K.N. (1987). Great earthquakes, seismicity gaps and potential for earthquake disaster along the Himalaya Plate boundary, *Tectonophysics*, **138:**79-92.

Kramer, S.L., (2007). Geotechnical Earthquake Engineering, *Pearson Education*, 653 p.

Kumar, S., Wesnousky, S. G., Rockwell, T. K., Bridges, R. W., Thakur V. C., & Jayangondaperumal, R. (2006). Paleoseismic evidences of great surface rupture earthquakes along the Indian Himalaya. Journal Geophysical Research, v.111 B03304, doi: 10.1029/ 2004JB003309.

Larson, K. R., Bürgmann, R. B., & Freymueller, J. T. (1999).Kinematics of the India-Eurasia collision zone from GPS measurements. *Journal of Geophysical Research*, **104:**1077–1093.

Lave´, J., & Avouac, J. P. (2000).Active folding of fluvial terraces across the Siwaliks Hills, Himalayas of central Nepal. *Journal of Geophysical Research,***105:**5735–5770.

Lave´, J., & Avouac, J. P. (2001). Fluvial incision and tectonic uplift across the Himalayas of Central Nepal. *Journal of Geophysical Research,***106:**26561–26592.

Lave, J., Yule, D., Sapkota, S. N., Basant, K., Madden, C., Attal, M., & Pandey, R. (2005). Evidence for a great medieval earthquake (~1100A.D.) in the central Himalayas, Nepal. Science, 307:1302–1305.

Le Fort, P. (1975). Himalayas: The collided range: Present knowledge of the continental arc. *American Journal of Science*, **275(A):** 1–44.

Mandal, P., Kumar, N., Satyamurthy, C., & Raju, I. P. (2009). Ground-motion Attenuation Relation from Strong-motion Records of the 2001 Mw 7.7 Bhuj Earthquake Sequence (2001–2006), Gujarat, India. *Pure and Applied Geophysics*, **166:**451-469. 10.1007/s00024-009-0444-y.

McGuire, R. K. (1976). FORTRAN computer program for seismic risk analysis.*U.S. Geological Survey Open-file Report*, 76-67.

McGuire, R. K. (1977). Seismic design spectra and mapping procedures using hazard analysis based directly on oscillator response. *Journal of Earthquake Engineering and Structural Dynamics*, **5:**211-234.

McGuire, R. K. (2004). Seismic Hazards and Risk Analysis.*Earthquake Engineering Research Institute,* Oakland.

Milne, W. G., & Davenport, A. G. (1969).Distribution of earthquake risk in Canada. Bulletin of the Seismological Society of America, **59(2):**729–754.

Mugnier, J. L., Huyghe, P., Leturmy, P., & Jouanne, F. (2003). Episodicity and rates of thrust sheet motion in Himalaya (Western Nepal), in Thrust Tectonics and Hydrocarbon Systems, ed. Mc Clay, AAPG Mem., **82:**1–24. *SPI Publisher Services*, Ashland, VA.

Nakata, T. (1989).Active faults of the Himalaya of India and Nepal. *Geological Soceity of America*, special paper, **232 :**243–264.

Nath, S., & Thingbaijam, K. K. S. (2012).Probabilistic Seismic Hazard Assessment of India. *Seismological Research Letters*, **83:** 135-149. 10.1785/gssrl.83.1.135.

National Disaster Management Authority (NDMA), Government of India (2010).Development of Seismic Hazard Map of India, Final report.

Nepal National Building Code (NBC 105) (1994). Seismic Design of Buildings, Department of Urban Development and Building Construction, Government of Nepal.

Ordaz, M., & Arroyo, D. (2016).On uncertainties in PSHA.*Earthquake Spectra*.10.1193/052015EQS075M.

Ordaz M.,& Salgado-Gálvez M. A. (2017). R-CRISIS Validation and Verification Document. *Technical Report*. Mexico City, Mexico.

Pandey, M. R., & Molnar, P. (1988).The distribution of Intensity of the Bihar Nepal earthquake of 15 January 1934 and bounds on the extent of the rupture. *Journal of Nepal Geological Society*. Nepal Geol. Soc, **5:**22-44.

Pandey, M. R., and M. Nicolas (1991). The aftershock sequence of the Udayapur (Nepal) earthquake of august 20, 1988, Journal of Nepal Geological Society, 7, 19-29.

Pandey, M. R., Tandukar, R. L. P., Lave, J. P., & Massot, J. P. (1995). Interseismic Strain Accumulation on the Himalayan Crustal Ramp, Nepal. *Geophysical Research Letters*, **22(7):**751-754.

Pandey, M. R., Tandukar, R. P., Avouac, J. P., Vergne, J. & Heritier, T. (1999).Seismotectonics of the Nepal Himalaya from a local seismic network. *Journal of Asian Earth Sciences*, **17:**703-712.

Pandey, M. R. (2000). Ground Response of Kathmandu Valley on the basis of microtremors.*12WCEE 2000 (12thWorld Conference on Earthquake Engineering)*, **2106:**1-6.

Pandey, M. R., Chitrakar, G. R., Kafle, B., Sapkota, S. N., Rajaure, S., & Gautam, U. P. (2002).Seismic Hazard Map of Nepal. *National Seismological Centre*, Kathmandu Nepal.

Pant, M. R. (2002). A step toward a historical seismicity of Nepal, in Adarsa, edited, pp. 29-60, Odisha, India.

Paudyal, Y. R., Yatabe, R., Bhandary, N., & Dahal, R. (2012). A study of local amplification effect of soil layers on ground motion in the Kathmandu Valley

using microtremor analysis. *Earthquake Engineering and Engineering Vibration*, **11(2):**257–268.

Paudyal, Y., Yatabe, R., Bhandary, N., & Dahal, R. (2013). Basement topography of the Kathmandu Basin using microtremor observation. *Journal of Asian Earth Sciences*.**62:**627–637. 10.1016/j.jseaes.2012.11.011.

Piya, B. K., (2004). *Generation of Geological Database for Liquefaction Hazard Assessment in Kathmandu Valley* (Unpublished of Master of Science dissertation).*Enschede, the Netherlands, International Institute for Geo-information Science and Earth Observation* (ITC).

Powell, C. McA., & Conaghan, P. (1973).Plate tectonics and the Himalaya. *Earth and Planetary Science Letters*, **20:**1-12. 10.1016/0012-821X(73)90134-9.

Rahman, M. M., and Bai, L. (2018).Probabilistic seismic hazard assessment of Nepal using multiple seismic source models. *Earth Planetary Physics*, **2(4):** 327–341. http://doi.org/10.26464/epp2018030

Rajaure, S., Sapkota, S.N., Adhikari, L.B., Koirala, B., Bhattarai, M., Tiwari, D.R., Gautam, U., Shrestha, P., Maske, S., Avouac, J.P., Bollinger, L., & Pandey, M. R. (2013). Double difference relocation of local earthquakes in the Nepal Himalaya, *Journal of Nepal Geological Society*, **46:**133-142.

Rajaure, S., Koirala, B., Pandey, R., Timsina, C., Jha, M., Bhattarai, M., Dhital, M., Paudel, L., & Bijukchhen, S. (2014). Ground response of the Kathmandu Sedimentary Basin with reference to 30 August 2013 South-Tibet Earthquake. *Journal of Nepal Geological Society*, *47*(1), 23-34. https://doi.org/10.3126/jngs.v47i1.23101

Rajaure, S., Dhital, M., & Paudel, L. (2015).The 2015 Gorkha Earthquake and response of the Kathmandu Valley sediments. *Journal of Nepal Geological Society*, *49*(1), 1-5. https://doi.org/10.3126/jngs.v49i1.23136

Rajaure, S., Asimaki, D., Thompson, E., Hough, S., Martin, S., Ampuero, J. P., Dhital, M., Inbal, A., Takai, N., Shigefuji, M., Bijukchhen, S., Ichiyanagi, M., Sasatani, T., & Paudel, L. (2017).Characterizing the Kathmandu Valley sediment response through strong motion recordings of the 2015 Gorkha

Earthquake sequence. *Tectonophysics.*, 714. 146-157. 10.1016/j.tecto.2016.09.030.

Rajaure, S., & Paudel, L. (2018).A comprehensive earthquake catalogue for Nepal and its adjoining region. *Journal of Nepal Geological Society.* 56. 65-72. 10.3126/jngs.v56i1.22747.

Rana, B. S. (1935). *Nepalko Maha Bhukampa* (The Great Earthquake of Nepal).

Reasenberg, P. (1985). CLUSTER2000, JGR, **90:**5479-5495.

Reasenberg, P. (1985). Second-order moment of central California seismicity, 1969-82, J. Geophys. Res., 90, 5479– 5495. 3, 4, 5, 7, 8, 10, 11, 12, 18

Romano, M. A., Peruzza, L., Priolo, E., Garbin, M., Picotti, V. L., Guido, F., & Ponza, A. (2015). Preliminary imaging of active faults in the Montello-Collalto area (Southeastern Alps, Italy) by a high-sensitivity seismometric network.

Roy, S. C., Dunn J. A., Auden J. A., & Ghosh A. M. N. (1939).The Bihar-Nepal earthquake of 1934.*Memoir of Geological Survey of India* 73:391

Sakai, H. (1983). Geology of the Tansen Group of the Lesser Himalaya in Nepal.*Memoirs of the Faculty of Science, Kyūsyū University. Series D, Geology*, **25(1):**27-74.

Sakai, H., Fuji, R., Kuwahara, Y., Upreti, B. N., & Shrestha S. D. (2001). Core drilling of the basin-fill sediments in the Kathmandu Valley for palaeoclimatic study: Preliminary results. *Journal of Nepal Geological Society.* 25. 9-18.

Sapkota, S., Bollinger, R., Klinger, Y., Tapponnier, P., Gaudemer, Y., & Tiwari, D. R. (2013). Primary surface ruptures of the great Himalayan earthquakes in 1934 and 1255. *Nature Geoscience.***6:**152-. 10.1038/ngeo1720.

Scordilis, E.M. (2006). Empirical global relations converting MS and mb to moment magnitude. *Journal of Seismology*, **10:**225–236.

Shearer, P. M., & Stark, P. B. (2011). Global risk of big earthquakes has not recently increased. *Proceedings of the National Academy of Sciences*, **109:**717–721.

Sheehan, A. F., Torre, T. de la, Monsalve, G., Schulte Pelkum, V., Bilham, R., Blume, F., Bendick, R., Wu, F., Pandey M. R., Sapkota, S., &Rajaure, S. (2007).Earthquakes and Crustal Structure of the Himalaya from the Himalayan-Nepal-Tibet seismic experiment (HIMNT).*Journal of Nepal Geological Society*, sp. v., p. 8

Srivastava, H. N., Bansal, B. K., & Verma, M. (2013). Largest earthquake in Himalaya: An appraisal. *Journal of the Geological Society of India*. 82. 10.1007/s12594-013-0117-4.

Stein, S., Geller, R., & Liu, M. (2013). Reply to comment by Arthur Frankel on "Why Earthquake Hazard Maps Often Fail and What to do About It". *Tectonophysics*. 592. 207–209. 10.1016/j.tecto.2013.01.024.

Stepp, J. C., (1972). Analysis of completeness of earthquake sample in the Puget Sound area and its effect on statistical estimates of earthquake hazard. *National Oceanic and Atmospheric Administration Environmental Research Laboratories*, Boulder Colorado, 80302.

Stevens, V. L., & J. P. Avouac (2015). Interseismic coupling on the main Himalayan thrust, *Geophysical Research Letters,* 42, no. 14, 2015GL064845, 5828–5837.

Stevens, V. L., & J. P. Avouac (2016). Millenary Mw > 9:0 earthquakes required by geodetic strain in the Himalaya, *Geophysical Research Letters ,* 43, no. 3, 2015GL067336, 1118–1123.

Stevens, V. L., & J. P. Avouac (2017).Determination of M_{max} from background seismicity and moment conservation. *Bulletin of the Seismological Society of America*, 107, no. 6, 2578.

Stevens, V. L., Shrestha, S. N., & Maharjan, D. K. (2018).Probabilistic Seismic Hazard Assessment of Nepal.*Bulletin of the Seismological Society of America*, **108(6)**3488-3510.https://doi.org/10.1785/0120180022

Stöcklin, J., & Bhattarai, K.D. (1977). In: Himalaya Report Geology of Kathmandu Area and Central Mahabharat Range Nepal. *Department of Mines and Geology Kathmandu, Nepal*, 86p.

Stöcklin, J. (1980). Geology of Nepal and its regional frame. *Journal of the Geological Society of London.***137:**1– 34.

Szeliga, W., Hough, S., Martin, S., & Bilham, R. (2010). Intensity, Magnitude, Location, and Attenuation in India for Felt Earthquakes since 1762.*The Bulletin of the Seismological Society of America*. 100. 10.1785/0120080329.

Takai, N., Shigefuji, M., Rajaure, S., Bijukchhen, S., Ichiyanagi, M., Dhital, M., & Sasatani, T. (2016). Strong ground motion in the Kathmandu Valley during the 2015 Gorkha, Nepal, Earthquake. *Earth, Planets and Space*, **68.**10.1186/s40623-016-0383-7.

Thapa, D. R., & Wang, G. (2013). Probabilistic Seismic Hazard analysis in Nepal, *Earthquake Engineering and Engineering Vibration*, **12(4):** 577-586.

Torre, T., Monsalve, G., Sheehan, A. F., Sapkota, S., & Wu, F. (2007). Earthquake processes of the Himalayan collision zone in eastern Nepal and the southern Tibetan Plateau. *Geophysical Journal International*. 171. 718-738. 10.1111/j.1365-246X.2007.03537.x.

Upreti, B.N. (1999). An overview of the stratigraphy and tectonics of the Nepal Himalaya. *Journal of Asian Earth Sciences*, **17:**577– 606.

Van Stiphout, T., J. Zhuang, J., Marsan, D. (2012). Seismicity declustering, Community Online Resource for Statistical Seismicity Analysis, doi:10.5078/corssa52382934. Available at http://www.corssa.org.

Wells, D. L., & Coppersmith, K. J. (1994). New Empirical relationships among magnitude, rupture length, rupture width, rupture area and surface displacement, *Bulletin of the Seismological Society of America*, **84(4):**974-1002.

Wiemer S., & Wyss, M. (2000). Minimum Magnitude of completeness in Earthquake Catalogs: Examples from Alaska, the Western United States, and Japan. *Bulletin of the Seismological Society of America*, **90(4):**859–869.

Wikipedia 2019: https://en.wikipedia.org/wiki/Disaster#cite_note-ifrc-1, retrieved on 27 May, 2019.
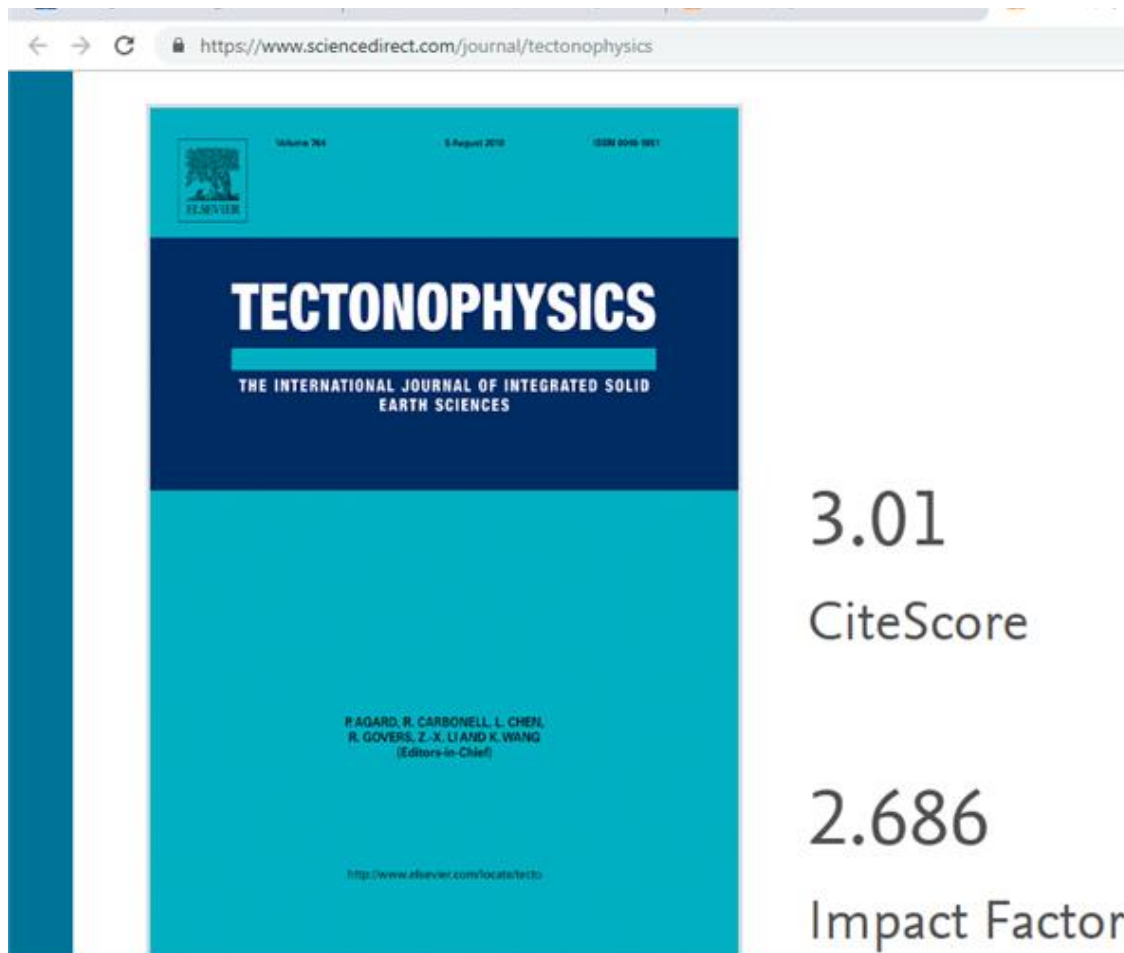
Yoshida, M., & Igarashi, Y. (1984).Neogene to Quaternary Lacustrine sediments in the Kathmandu Valley, Nepal. *Journal of Nepal Geological Society*, **4:**73-100.

Youngs, R. R., Chiyou, S., Silva, W. J., & Humphrey, J.R. (1997). Strong ground motion attenuation relationships for subduction zone earthquakes, *Seismological Research Letters*, **68(1):**59-73.

Yule, D., Dawson, S., Lave, J., Sapkota, S. N., Tiwari, D. R. (2006). Possible evidence for surface rupture of the Main Frontal Thrust during the great 1505 Himalayan earthquake, far-western Nepal.EOS, *Trans. American Geophysical Union Fall Meeting*.

Yule, D., Lavé, J., Sapkota, S.N., Tiwari, D., Kafle, B., Pandey, M. R., Dawson, S., Madden, C., & Attal, M., (2006): Large Surface Ruptures of the Main Frontal Thrust in East-central and Western Nepal: Evidence for an Unprecedented Type of Himalayan Earthquake.? Abstract Volume*, International Workshop on Seismology, Seismotectonics and Seismic Hazard in the Himalayan Region*, **28-29:**13-14.

Zhao, L. S., & Helmberger, D. (1991). Broadband modeling along a regional shield path, Harvard recording of the Saguenay earthquake. *Geophysical Journal International*, **105:**301 -312. 10.1111/j.1365-246X.1991.tb06715.x.

Zhao, X., Jianjing, Z., Asano, A., Ohno, Y., Taishi, O., Takahashi, T., Ogawa, H., Kojiro, I., Hong, T., Paul, S., Yasuhiro, F. (2006). Attenuation relations of strong ground motion in Japan using site classification based on predominant period. *Bulletin of the Seismological Society of America*. 96. 898-913.

Zhu, L., & Helmberger, D. (1996).Advancement in source estimation techniques using broadband regional seismograms. *Bulletin of Seismic Society of America*, 86p.1

APPENDIX 1

LIST OF PUBLICATIONS RELATED TO PHD RESEARCH

Appendix 1.1. International Journal with impact factor (Impact factor 2017/2018=2.686; 5-Year Impact Factor: 3.200)

Rajaure S., D. Asimaki, E. M. Thompson, S. Hough, S. Martin, J.P. Ampuero, A. Inbal, M. Dhital, L. Paudel (2017). "Characterizing the Kathmandu Valley sediment response through strong motion recordings of the 2015 Gorkha Earthquake sequence", Tectonophysics, 714-715, pp. 146-157.doi: 10.1016/j.tecto.2016.09.030.

Characterizing the Kathmandu Valley sediment response through strong motion recordings of the 2015 Gorkha earthquake sequence

S. Rajaure[a], D. Asimaki[b,*], E.M. Thompson[c], S. Hough[d], S. Martin[e], J.P. Ampuero[b], M.R. Dhital[f], A. Inbal[b], N. Takai[g], M. Shigefuji[g], S. Bijukchhen[g], M. Ichiyanagi[g], T. Sasatani[g], L. Paudel[f]

[a]Department of Mines and Geology, Lainchaur, Kathmandu, Nepal
[b]California Institute of Technology, Pasadena, CA, USA
[c]U.S. Geological Survey, Golden, CO, USA
[d]U.S. Geological Survey, Pasadena, CA, USA
[e]Earth Observatory of Singapore, Nanyang Technological University, Singapore
[f]Tribhuvan University, Kathmandu, Nepal
[g]Hokkaido University, Sapporo, Japan

ARTICLE INFO

ABSTRACT

We analyze strong motion records and high-rate GPS measurements of the M 7.8 Gorkha mainshock, M 7.3 Dolakha, and two moderate aftershock events recorded at four stations on the Kathmandu basin sediments, and one on rock-outcrop. Recordings on soil from all four events show systematic amplification relative to the rock site at multiple frequencies in the 0.1–2.5 Hz frequency range, and de-amplification of higher frequencies ($>$2.5–10 Hz). The soil-to-rock amplification ratios for the M 7.8 and M 7.3 events have lower amplitude and frequency peaks relative to the ratios of the two moderate events, effects that could be suggestive of nonlinear site response. Further, comparisons to ground motion prediction equations show that 1) both soil and rock mainshock recordings were severely depleted of high frequencies, and 2) the depletion at high frequencies is not present in the aftershocks. These observations indicate that the high frequency deamplification is additionally related to characteristics of the source that are not captured by simplified ground motion prediction equations, and allude to seismic hazard analysis models being revised – possibly by treating isolated high frequency radiation sources separately from long period components to capture large magnitude near-source events such as the 2015 Gorkha mainshock.

© 2016 Elsevier B.V. All rights reserved.

1. Introduction

The Kathmandu Valley in central Nepal hosts several rapidly developing urban areas, including the capital city of Kathmandu, Patan, and Bhaktapur. With a population of 2.5 million people, and a 4 percent growth per year, the Kathmandu Valley is one of the fastest-growing metropolitan areas in South Asia (Muzzini and Aparicio, 2013). It is also the first region in Nepal to face the unprecedented challenges of rapid urbanization on a metropolitan scale alongside the exposure of its growing population and infrastructure to natural hazards such as landslides, floods and earthquakes (Yadav et al., 2004).

The Kathmandu Valley has experienced numerous large earthquakes in the last 1500 years (Pandey and Molnar, 1988; Martin and Szeliga, 2010). Prior to the Gorkha earthquake, the most

recent large event, the Great Nepal-Bihar Earthquake of 1934, with an estimated magnitude of M 8.1–8.4 (Chen and Molnar, 1977; Chitrakar and Pandey, 1986; Bilham et al., 2001; Sapkota et al., 2013; Bollinger et al., 2014) caused 8500 fatalities, and destroyed 20% and damaged 40% of the valley's building stock, including one quarter of the buildings in Kathmandu and many of the temples in Bhaktapur (e.g. Pandey and Molnar, 1988). Within the basin, estimated intensities correlated qualitatively to the thickness of the basin sediments, suggesting that site effects played a major role in modifying the ground motion within Kathmandu (Dixit et al., 1998). A number of studies have concluded that the 1934 earthquake damage was accentuated by ground motion amplification and liquefaction in the fluvio-lacustrine sediments of the southern Kathmandu Valley (Rana, 1935; Chitrakar and Pandey, 1986; Pandey and Molnar, 1988; Bilham et al., 2001; Paudyal et al., 2013).

While the importance of site response in Kathmandu Valley has long been clear, strong motion data have been scarce (Rajaure et al., 2014), and the detailed nature of site effects has thus remained

---

* Corresponding author.
E-mail address: domniki@caltech.edu (D. Asimaki).

poorly understood. To date, site response studies have relied almost exclusively on ambient noise (microtremor) data (Pandey, 2000; Paudyal et al., 2012a,b). Data from the 2015 Gorkha earthquake sequence provide a unique opportunity to better understand site effects on multiple spatial and frequency scales, for strong as well as weak motions. In this paper we analyze ground motions from the 25 April 2015 Gorkha mainshock (M 7.8), the 12 May Dolakha aftershock (M 7.3), and two moderate aftershocks recorded by four strong motion stations on unconsolidated sediments and one on reference (rock) site conditions. The strong motion data are complemented at long periods by two high-rate GPS stations, one on sediments in the Kathmandu Valley, and one on rock at the town of Kakani, 25 km north-west of Kathmandu. The stations are depicted in Fig. 1, over-laid on the intensity map by Martin et al. (2015), and their code names and locations are listed in Table 1.

2. Geology of the Kathmandu Valley

The intermontane Kathmandu Valley is a tectonic basin located in a region of central Nepal known as the Midlands (Dhital, 2015). It is surrounded by the Higher Himalayan and Tethyan Himalayan rocks. The basement rock of the Kathmandu Valley, known as the Kathmandu Nappe (Hagen, 1951), was formed by thrusting along the Mahabharat or Main Central Thrust (MCT). According to Stöcklin (1980), the nappe is composed of two rock types, the Proterozoic Bhimphedi and Paleozoic Phulchoki. The Kathmandu basin lies on the nappe within the so-called Great Mahabharat Synform (Dhital, 2015), the core of which was occupied by a lake from the Pliocene to Pleistocene (Yoshida and Igarashi, 1984).

The basin is currently filled with a thick sequence of fluvio-lacustrine sediments, which range in age from 2.5 Ma to about 20 ka (Sakai et al., 2001; Moribayashi and Maruo, 1980). The depth of lake bed sediments remains in question, with maximum depth estimates ranging from 250 m (Paudyal et al., 2012b) to 500–600 m (Moribayashi and Maruo, 1980). The semi-consolidated sediments consist primarily of muds, silts, sandy silts, fine to coarse sands and gravel to pebbly conglomerates (Katel et al., 1996), and their depositional environment can be traced back to the delta plain, the delta front and the prodelta environments (Sakai et al., 2006, 2001). These geologic processes have led to a complex basement geometry and a strongly heterogeneous basin stratigraphy, which together suggest that the ground shaking within the Kathmandu basin could be affected by complex, three-dimensional site effects.

3. Strong ground motions

Following the September 18, 2011 M 6.9 Sikkim Earthquake (also known as the 2011 Himalayan earthquake) in the Kathmandu Valley, Hokkaido University, Japan (Takai et al., 2015) installed four Mitsutoyo JEP-6A3-2 accelerometers in collaboration with the Central Department of Geology (CDG) at Tribhuvan University (TU). The strong motion stations have a 100 Hz sampling rate and operate continuously. One station, KTP, was installed at the Kirtipur Municipality Office, located on a rock outcrop 'island' near the west-most basin edge; the other three, TVU, PTN and THM, were installed on soft sediments along an east-west linear array across the valley (Fig. 1). In addition to the above instruments, the U.S. Geological Survey (USGS) installed one (GeoSIG NetQuakes) accelerometer (KATNP) on the Kathmandu Valley sediments (Dixit et al., 2015); the station began operation in April 2011, but had ceased transmission in near real-time in 2013 due to an unreliable Internet connection. Recordings of the Gorkha mainshock were nonetheless obtained and retrieved manually from the ring buffer several days later. Lastly, the Department of Mines and Geology operated a strong motion instrument in central Kathmandu (Bhattarai et. al, 2015). The instrument is part

of the National Seismological Centre of Department of Mines and Geology (NSC-DMG), was installed in 2011 and was funded by a technical cooperative agreement between the Departement Analyse Surveillance de l'Environnement (DASE), the Commissariat Energie Atomique (CEA), the Government of France, the Department of Mines and Geology in Nepal, and the Government of Nepal that was established in 1978. All these instruments recorded the 2015 sequence (Dixit et al., 2015; Bhattarai et. al, 2015; Takai et al., 2016). Data from the USGS permanent strong motion instrument were made available to the international community within nine days; the mainshock data recorded by the four station array installed by Hokkaido and Tribhuvan Universities are also available (Takai et al., 2016), while the aftershocks recorded by the same array will be made available in the near future.

The 25 April 2015 M 7.8 Gorkha and the 12 May 2015 M 7.3 Dolakha earthquakes, as well as several aftershocks of the Gorkha sequence, including the 26 April 2015 M 6.7 and the 25 April 2015 M 6.6 events, were recorded by the stations listed in Table 1. The epicenters of the M 7.8 mainshock and the M 6.6 aftershock were located approximately 80 km NW of the Kathmandu Valley, while the epicenters of the M 7.3 and M 6.7 aftershocks were located approximately 80 km northeast of the valley (Fig. 1). Peak ground accelerations of the M 7.8 and M 7.3 acceleration recordings are indicated on Fig. 2. The reference station, KTP, recorded the maximum horizontal ground acceleration during the M 7.8 mainshock (0.25 g in the EW direction); the east-most station of the array, THM, which was also the closest to the Dolakha epicenter, recorded the maximum horizontal acceleration during the M 7.3 aftershock (0.17 g in the EW direction).

The most striking characteristics of the ground motions at the four soil sites that can be seen in Fig. 2 are 1) the presence of reverberating long-period waves that are not present at KTP, and 2) the lack of high-frequency energy, which is especially pronounced in the M 7.8 event. The Fourier amplitude spectra of the horizontal ground motion components (vector summation of NS and EW components) during the M 7.8 mainshock (Fig. 3) show that the motions on soil are systematically amplified (up to an order of magnitude in the vicinity of 0.2 Hz) relative to the rock shaking over a wide range of frequencies (approximately 0.1–2.5 Hz), and de-amplified by approximately a factor of two for frequencies higher than 3 Hz. This effect is less pronounced in the case of the M 7.3 event: the cross-over from long period amplification to high frequency de-amplification of both horizontal and vertical components occurs at higher frequencies (4 Hz vs. 3 Hz for the H-component, and 8 Hz vs. 7 Hz for the V-component in Fig. 3); and also, the strong motion records on sediments are not as severely depleted of high frequencies relative to KTP as in the case of the mainshock.

The waveforms in Fig. 2 and the magnitude-dependent contrast between the amplitude of high frequency components on soil relative to rock (Fig. 3) are consistent with the effects of nonlinear site response, which refers to the strain-dependent stiffness reduction and damping increase due to soil yielding that causes amplitude reduction and shift of the frequency content similar to that of the mainshock records in Fig. 3 (Dixit et al., 2015). This effect is also observed, but to a less extent, for the M 7.3 aftershock, although as we will show in Section 5 it primarily manifests as reduction in amplitude that could be explained by increase in the material damping alone. Still, whether the reduction in amplitude and shift in frequency content is indeed a manifestation of nonlinear site response, and if so, what the relative role of nonlinearity was in shaping the mainshock strong motion frequency content relative to phenomena such as source radiation, rupture directivity and 3D basin effects is unclear, and is currently the subject of ongoing research.

We next compare the rotation independent response spectral acceleration RotD50 (Boore, 2010) of the M 7.8 mainshock and M 7.3, M 6.7 and M 6.6 aftershocks to response spectra predicted using
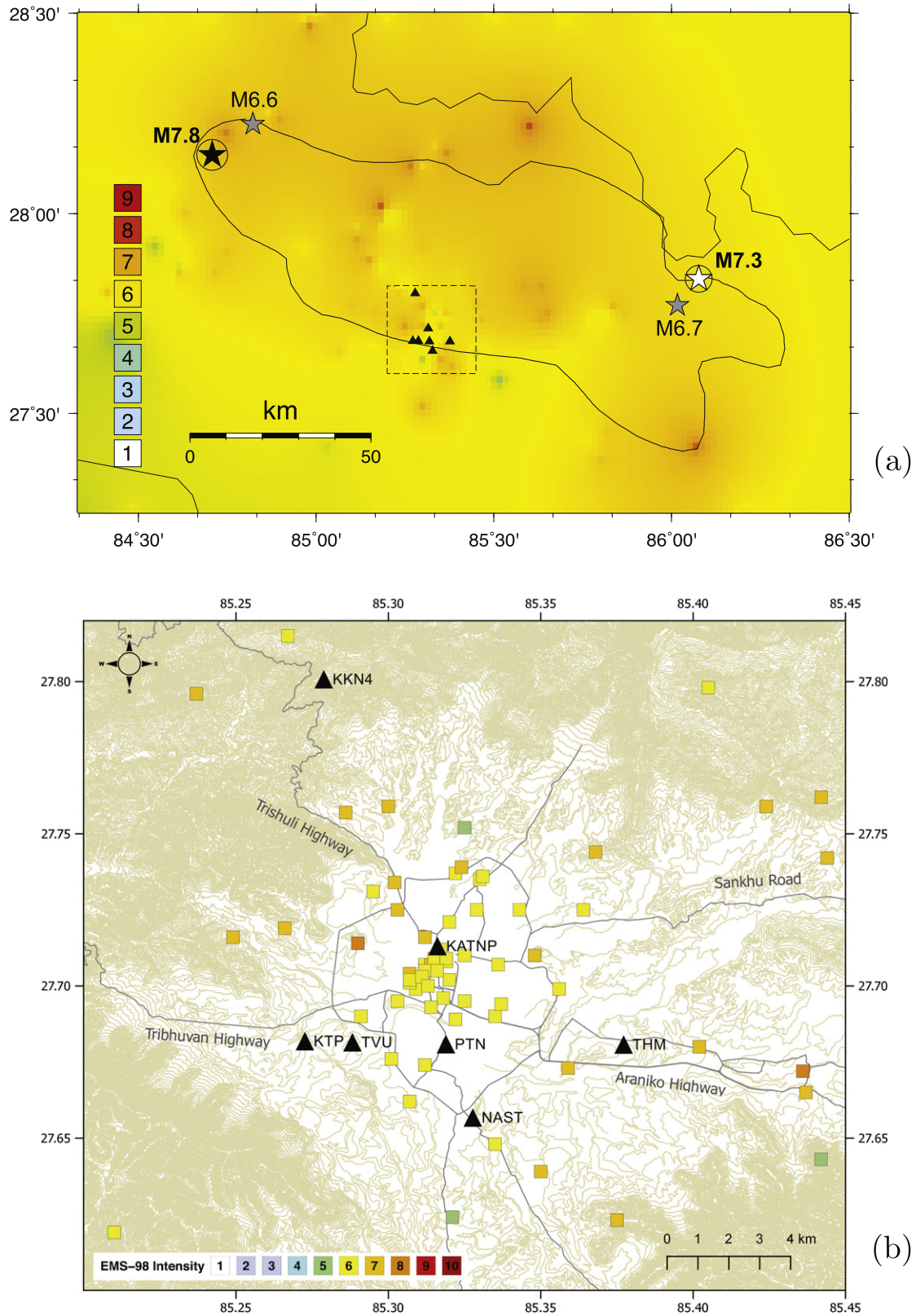
Fig. 1. (a) Intensity assignments from Martin et al. (2015). The assignments in the vicinity of the mainshock were smoothed with a Laplacian operator using a tension factor of 1.0, which produces a harmonic surface with no maxima or minima except for control points; the surface projection of the mainshock is given along with the epicenters of the mainshock and the large aftershocks. Epicenter locations from McNamara et al. (2016); (b) inset from (a) showing individual intensity assignments in the Kathmandu Valley, the locations of the 5 strong motion instruments, and the two high-rate GPS stations discussed in this study. The Nepal Survey Department topographic contour data used as basemap are freely available at https://data.hdx.rwlabs.org/dataset/nepal-contour-lines-cod.

Table 1
Strong motion (SM) and GPS stations used in this study.

Site code	Lat (N)	Long (E)	Instrument	Location
KTP (rock)	27.68182	85.27261	SM	Kirtipur Municipality Office
TVU (soil)	27.68145	85.28821	SM	Central Department of Geology
PTN (soil)	27.68082	85.31897	SM	Engineering College, Pulchowk
THM (soil)	27.68072	85.3772	SM	University Grant Commission Office, Bhaktapur
KATNP (soil)	27.71307	85.3161	SM	Kantipath
KKN4 (rock)	27.80075	85.278802	GPS	Kakani
NAST (soil)	27.65672	85.327726	GPS	Khumaltar

the Abrahamson et al. (2016) (also known as BC Hydro) and Boore et al. (2014) ground motion prediction equation (GMPEs) (Fig. 4). Although the Boore et al. (2014) equations (known by and frequently referred to by the acronym BSSA14) were developed primarily with ground motions from the Western United States (WUS), we can see in Fig. 4 that it provides a reasonable analog for Nepal as both are active crustal regions. Note that no GMPE is perfectly applicable for this event; subduction zone GMPEs are primarily developed from data in ocean-continent or ocean-ocean subduction zones (Atkinson, 2003; Petersen et al., 2015; Kanno et al., 2006; Ghofrani and Atkinson, 2013). The primary difference between BC Hydo and BSSA14 is that the latter predicts greater amplitudes at long period motions, which are reflective of the surface waves generated in deep sedimentary basins such as Los Angeles and Kathmandu. For these comparisons, we have computed the Joyner-Boore distance (R_{JB}) (Joyner and Boore, 1981) from the Hayes et al. (2015) finite fault models for the M 7.8 and M 7.3 events and used the epicentral distance for the M 6.7 and M 6.6 for R_{JB}. For the time-averaged shear wave velocity of the top 30 m, we have assumed $V_{S30} = 200$ m/s for the soil sites (JICA, 2002), and $V_{S30} = 760$ m/s for the reference station (KTP).

Comparison of the mainshock recordings at all stations to BCHydro and BSSA14 confirms that the ground motions were severely depleted of high-frequency energy (i.e. at periods less than approximately 1 s) relative to the GMPE predicted levels, up to an order of magnitude for the strong motion records on sediments. While this high-frequency anomaly of the mainshock is more pronounced in the records on sediments, it is also observed at the reference site (KTP), suggesting that the depletion of high frequencies is at least attributed to some extent to the characteristics of the mainshock source (Ampuero et al., 2016). Additional evidence that the M 7.8 mainshock produced less high-frequency energy than usual is that the corresponding frequency components of the aftershocks are generally in closer agreement with the GMPEs (Fig. 4). On the other hand, the long period components of the aftershock records (<0.5 Hz or >2 s) on sediments (stations KATNP, THM, and TVU), which reflect the constructive interference of vertically reverberating long period body waves and surface waves generated at the basin edges, are significantly larger than the GMPE predicted values. This discrepancy suggests a potential shortcoming in the parameterization of WUS GMPEs to capture the complex physics of long period ground motions in deep sedimentary basins, which in this case are only captured through correlations with V_{S30}. The basin-depth parameter in BSSA14 ($z_{1.0}$, the depth at which $V_S = 1.0$ km is exceeded) was not used in these comparisons because we do not have a 3D velocity model from which to estimate this parameter. Thus, it is possible that the comparison at long periods could be improved with better constraints on the basin shape.

4. Effects of the source characteristics

Sokolov and Chernov (1998) showed that the severity of earthquake damage (expressed as macroseismic intensity) is not only a function of amplitude and duration, but also of the ground motion

frequency content. Additionally, they concluded smaller intensities are more closely associated with high-frequency amplitudes while the larger intensities are associated with longer period ground motion amplitudes. The high-frequency energy in an earthquake may not be uniformly distributed throughout the rupture, which can affect the frequency content of the ground motions, thereby affecting damage patterns (Meng et al., 2011). The effects of spatial patterns of the source frequency content generally cannot be accounted for in ground motion prediction equations because they are based on distances defined relative to the complete rupture area. Avouac et al. (2015) and Ampuero et al. (2016) showed that the high frequency energy was predominantly released approximately 34 km from the strong motion array along the downdip edge of the rupture (Avouac et al., 2015; Ampuero et al., 2016).

To fully consider the extent to which this difference can explain the depletion of high frequency energy in Kathmandu, one must compare the recorded ground motions to GMPEs developed using the distance to high frequency radiation sources rather than R_{JB}. Such relationships are unavailable and additionally would require that the high frequency radiation distribution is a systematic and predictable phenomenon. The lack of such relationships notwithstanding, Ampuero et al. (2016) recently compared the mainshock ground motions to the BSSA14 predictions, and found remarkable agreement between the recorded high frequencies and the BSSA14 GMPE with distance $=34$ km instead of $R_{JB} = 0$ km. Longer period characteristics of the strong motion records on the other hand, such as the amplification observed in the period range 3–5 s, were better captured by BSSA14 with $R_{JB} = 0$ km. Ampuero et al. (2016) thus suggest that the mainshock source characteristic of concentrated high frequency radiation sources at the down-dip edge of the rupture is at least partially responsible for the strongly attenuated high frequencies of the mainshock strong motions. In the following sections we explore the extent to which ground motions might have been controlled by linear and nonlinear site effects.

5. Observations of site effects in Kathmandu Valley

To investigate the role that site effects played in shaping the amplitude and frequency content of the recorded ground motions in the valley, we computed the soil-to-rock amplification ratio of the soil sites relative to the reference station for all four events (Fig. 5). We first high passed the ground motion records above 0.1 Hz using a fourth order Butterworth filter. We treated the horizontal components as a complex signal according to Tumarkin and Archuleta (1994), and calculated the sum of the spectral amplitude value corresponding to two symmetric frequencies. This approach produces the maximized spectrum (Shoja-Taheri and Bolt, 1977) defined as the maximum amplitude of shaking at a given frequency in the horizontal plane, eliminates the need to rotate the components, and produces results similar to standard averaging methods (Steidl et al., 1995). The site amplification factors were smoothed using the Konno and Ohmachi (1998) logarithmic filter (with smoothing parameter b = 40). The instrument response of the triaxial accelerometers
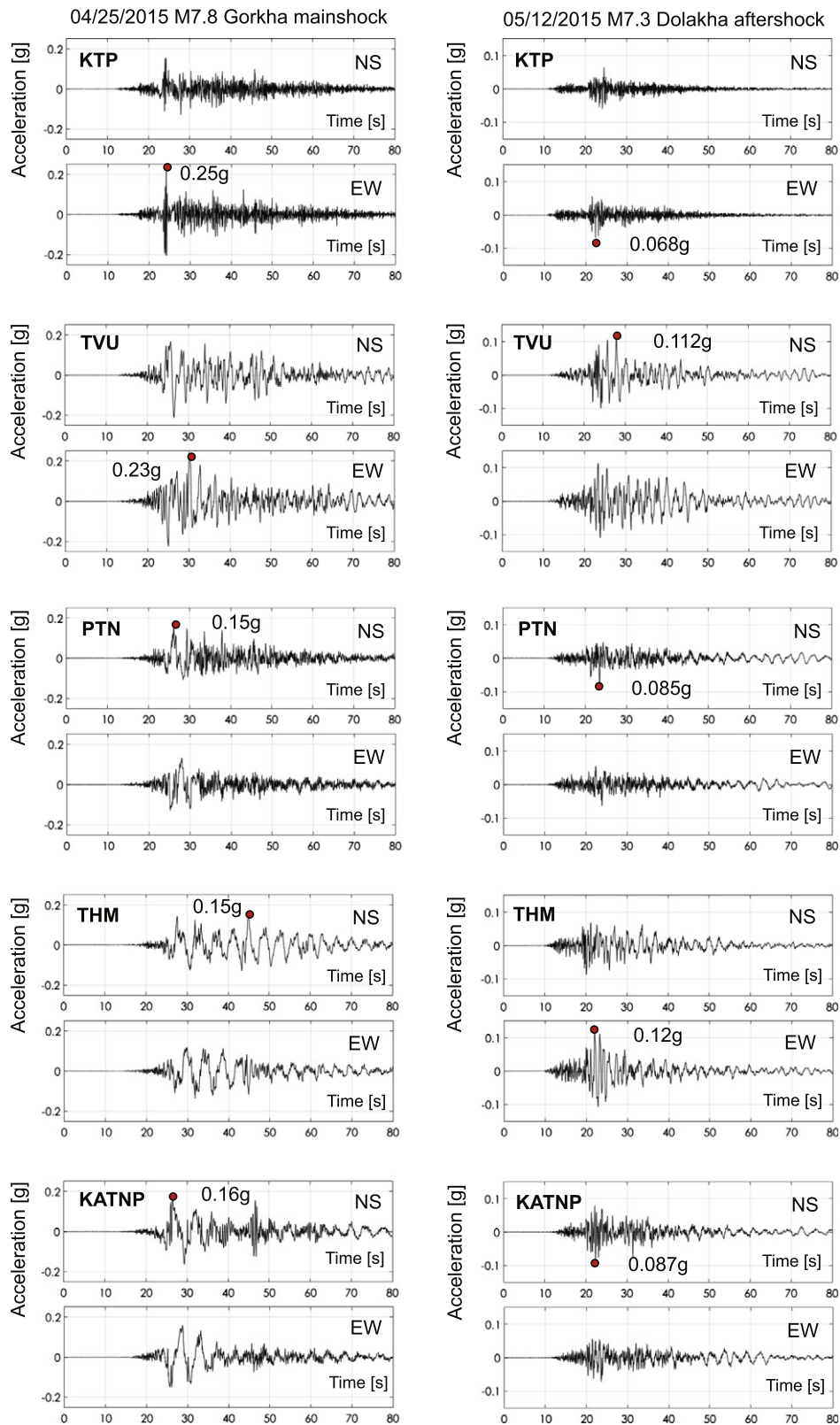
Fig. 2. NS and EW components of the 04/25/2015 M 7.8 Gorkha and the 05/12/2015 M 7.3 Dolakha earthquakes recorded at the five strong motion stations.

(Mitsutoyo Co. Ltd.), comprising a highly damped moving coil and a natural frequency of 3 Hz, was shown to have minimal effects on the acceleration ground motions in the frequency range (>0.1 Hz) of interest of this study, and was thus not removed from the strong motion time-series presented here.

As can be seen in Fig. 5, the ground motion amplification and deamplification pattern at all stations is very similar, a fact that we already observed by comparing the Fourier amplitude spectra in (Fig. 3); regardless of the strong motion intensity, the basin sediments systematically amplify the low frequency ground motion
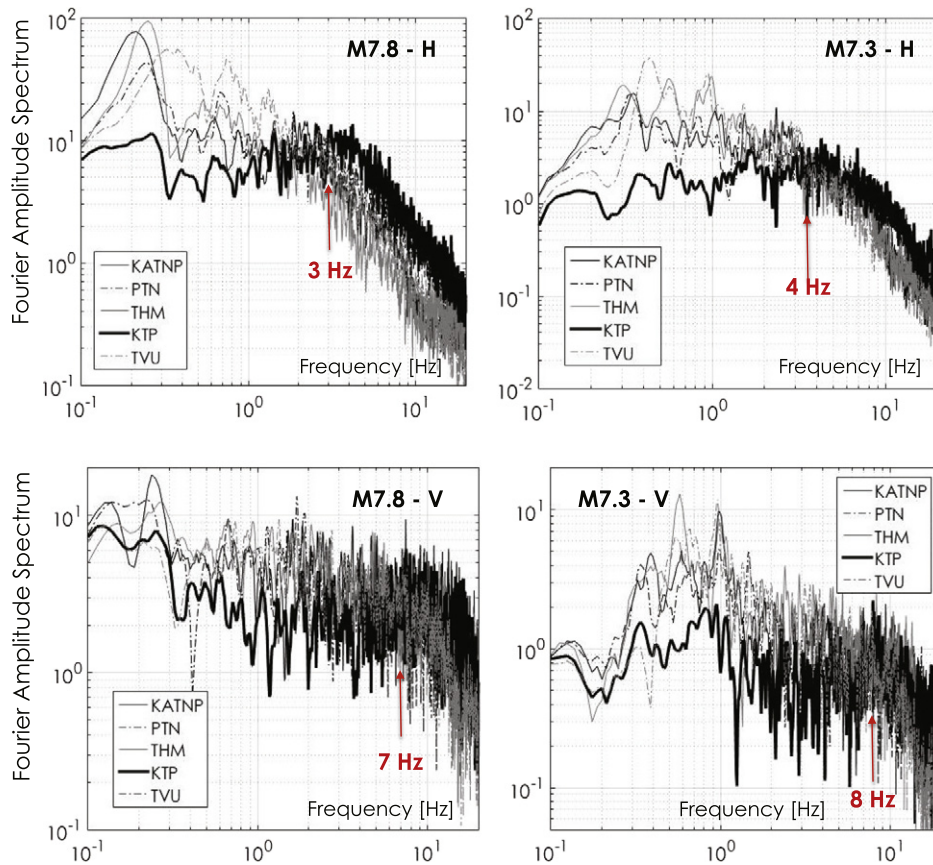
Fig. 3. Fourier spectra of the horizontal and vertical components of the M 7.8 and M 7.3 events, depicting the frequency (denoted with red arrows) at which the high frequency content of the rock outcrop strong motion surpasses that of all four soil sites.

components (approximately less than 2.5 Hz) and deamplify higher frequency components.

We next observe that the site response is characterized by three or more prominent peaks at approximately the same frequency range across all stations, which strongly suggests that all four stations (and by extension the basin sediments) are dominated by common amplification mechanisms. Additionally, the site response of the M 7.8 event is shifted to lower frequencies and has lower amplitude than the response to the M 7.3, M 6.6 and M 6.7 events. This result could be seen as evidence that the site response during the mainshock was nonlinear (Dixit et al., 2015), although verification and validation of the hypothesis are still pending.

Nonlinear response is the alteration of site response by the yielding of the near-surface sediments, due to motions strong enough to induce strains beyond the elastic range of soil deformation (Joyner and Chen, 1975; Seed and Idriss, 1970). Pervasive nonlinear response of sediments, not associated with liquefaction, has been observed during a number of large earthquakes (e.g. Field et al. (1997), Bonilla et al. (2011)). This phenomenon has been shown to strongly correlate with the level of ground motion (Beresnev, 2002; Borcherdt, 1994; Hartzell, 1998; Su et al., 1998) and local soil conditions (Beresnev and Wen, 1996; Frankel et al., 2002; Hartzell, 1998; Tsuda et al., 2006), and in terms of ground motion amplitude, typically is manifested beyond an acceleration amplitude threshold of 0.1–0.2 g (Beresnev and Wen, 1996; Wu et al., 2009; Kaklamanos et al., 2013). Given the very low stiffness of the near-surface unconsolidated sediments in Kathmandu (V_{S30} = 180–250 m/s according to JICA (2002)) and the maximum horizontal ground acceleration of 0.25 g recorded at KTP during the mainshock, the possibility of nonlinear effects shaping the strong motion records is highly likely.

Still, studies on the nonlinear soil properties of the Kathmandu black, unconsolidated clay are unavailable, at least to the knowledge of the authors, and thus our 'proof of nonlinear site response' is at this point founded on phenomenology. We also mention that deamplification is observed in the M 7.3 aftershock data as well, yet only in the form of amplitude reduction – namely without significant shift of the frequency peaks. This observation is still consistent with nonlinear site response, yet a lot less prominent than in the mainshock case, and mostly manifesting as increase in intrinsic attenuation and not strong reduction in material stiffness. Again, the effects of strain amplitude on the stiffness and material damping changes of the soil in Kathmandu remain an area that calls for extensive field and laboratory testing studies.

Our observed spectral ratios characterize the site response within Kathmandu Valley for both strong and weak ground motions. As discussed above (also shown in Dixit et al. (2015) and Hashash et al. (2015) who studied the ground motions recorded at KATNP using single station techniques), these results strongly suggest that the valley sediments responded nonlinearly to the M 7.8 mainshock and M 7.3 aftershock. Note that the PGA of the rock (KTP) aftershock record was approximately 0.07 g, namely within the rock PGA range (0.05 g–0.1 g) where the onset of soil nonlinearity is generally expected. Thus, this is potentially a very important recording for studies of the boundary between linear and nonlinear soil behavior.

Furthermore, the prominent manifestation of nonlinear effects (amplitude reduction and frequency shift) that we observe over a very wide frequency range, including the low frequency modes (0.2–0.4 Hz) that cannot be explained by near-surface soil yielding in the context of a one-dimensional soil model, reflect the complex three-dimensional geometry and stratigraphy of the Kathmandu
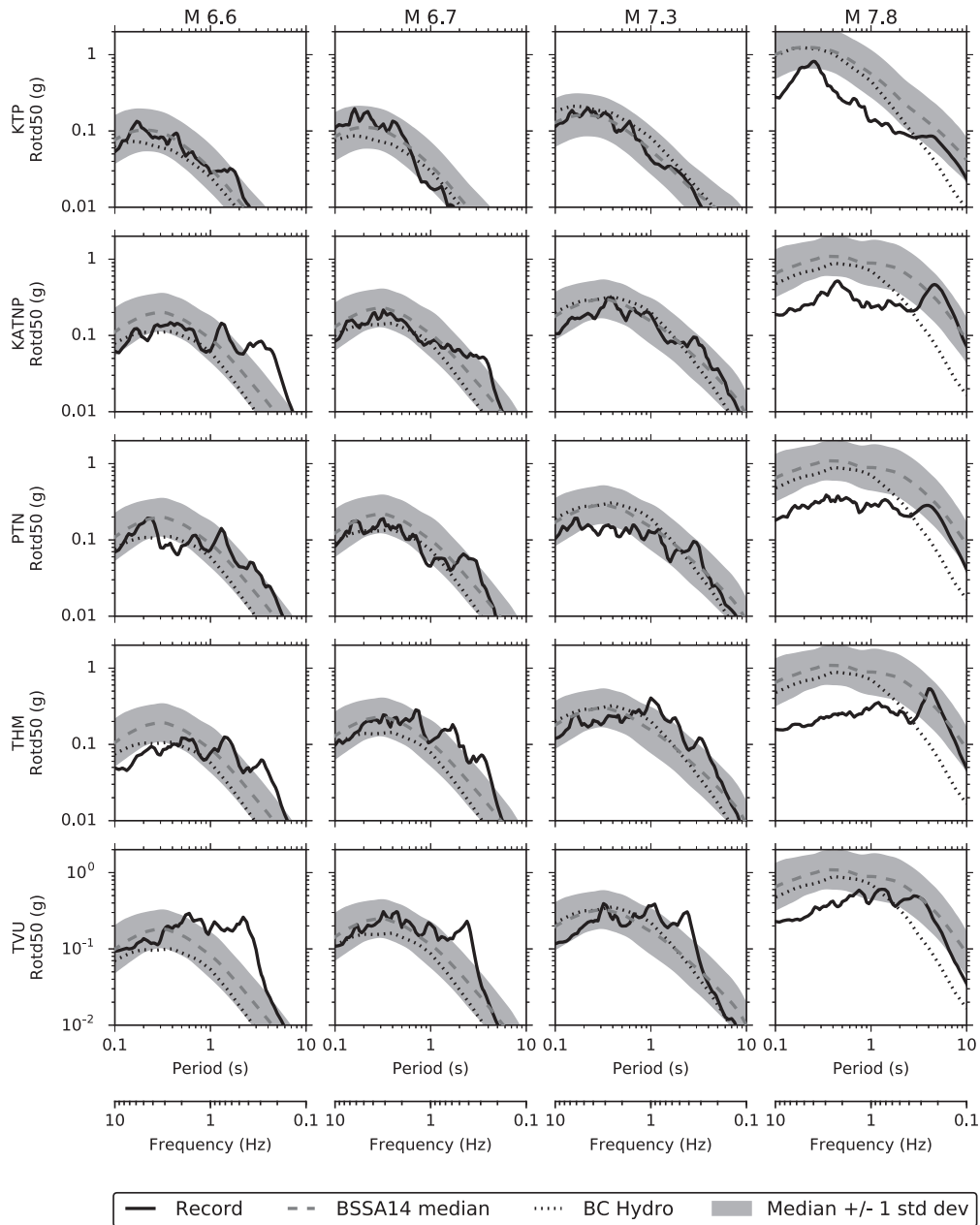
Fig. 4. Orientation independent response spectral acceleration (RodD50) of the four events compared to the BC Hydro (Abrahamson et al., 2016) and BSSA14 GMPEs (Boore et al., 2014) with $R_{JB} = 0$, $V_{S30} = 760$ m/s for KTP, and 200 m/s for the soil sites (JICA, 2002). Note that we provide the ±1 standard deviation confidence interval for BSSA14 as an indication of the uncertainty associated with GMPE predictions.

basin, namely the geologic features of the same length-scale as the wavelength of the low period deamplified frequency components. While an in-depth understanding of site response would thus require three-dimensional numerical modeling and detailed geologic profiles of the valley structure that are not yet available, previous studies have provided some information about Kathmandu Valley structure. We next use these results to develop a preliminary interpretation of the observed site response.

6. Relationship between site effects and basin structure

Paudyal et al. (2012a) estimated that the thickness of the uppermost basin sediments is between 10 and 15 m, combining microtremor inversion with five shear wave velocity profiles (JICA, 2002). The resonant modes of these profiles were shown by Hashash et al. (2015) to coincide with the high frequency peaks in the

site responses depicted in Fig. 5. Furthermore, the fact that these frequencies (>2–3 Hz) are de-amplified regardless of the event suggests that these layers have high inelastic attenuation (low quality factor, Q), and are susceptible to nonlinear site response. In a subsequent study, Paudyal et al. (2012b) used the first mode (peak) of the microtremor measurements to estimate the depth of the valley basement. Their study showed that the central part of the Kathmandu City lies over the main ancient lake of Kathmandu basin, and revealed numerous shallower depressions outside the main ancient lake that are separated/connected by buried ridges.

The one-dimensional (1D) expected fundamental weak-motion resonance mode of the valley depends on the thickness of the sediments. Assuming $V_{S30} = 200$ m/s and a quadratic increase in stiffness with confining pressure with no intermediate sharp contrasts between surface and basement rock, the fundamental mode of the soil column at the deepest location of the basin ranges between
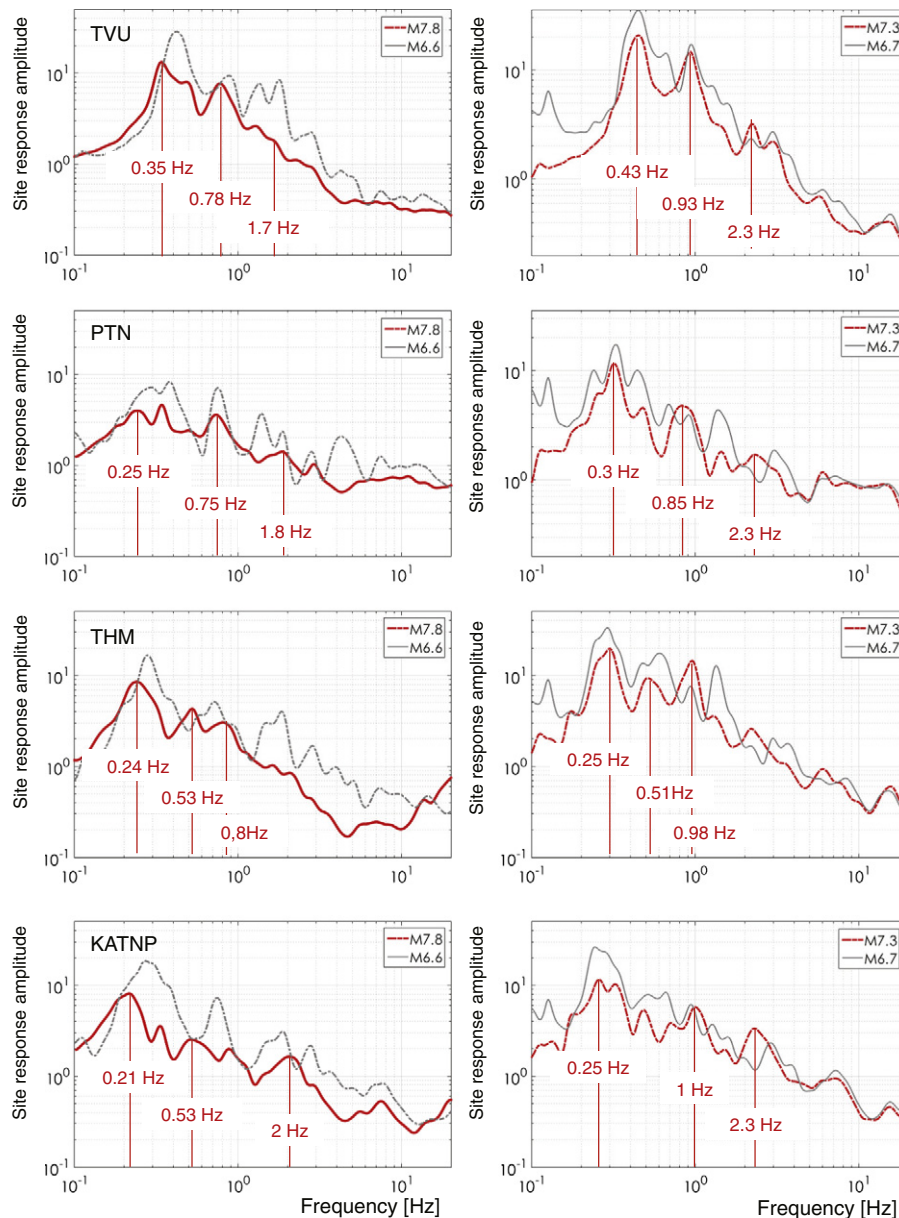
Fig. 5. Site response at the stations on soil relative to KTP. The systematic shift of the site response peaks to lower frequencies during the stronger events, as well as the reduction in amplitude are clear manifestations of nonlinear response. At each site, nonlinearity is observed at several frequencies (red vertical lines).

1.5 and 3 s (or 0.33 and 0.67 Hz) for a range of maximum thickness 250–500 m. While the latter is close to the lowest frequency peak observed in our study (Fig. 5), the range of predicted fundamental mode frequencies reflects the uncertainty regarding the detailed structure of the Kathmandu Valley, which has been previously gleaned from indirect approaches such as microtremor studies. For example, Paudyal et al. (2012a, b) observed a lowest amplification frequency of 0.48–0.58 Hz at 172 sites throughout Kathmandu Valley using horizontal-to-vertical (H/V) spectral ratios of microtremor data. Their results are consistent with the above range of predicted values, but given uncertainties associated with microtremor analysis (Steidl et al., 1995), do not provide a strong constraint on either valley depth or average V_s; for example, some of the weaker aftershocks depicted in Fig. 5 show fundamental resonant modes lower than the values measured by Paudyal and co-workers, which likely reflects the lower resolution of microtremors compared to strong motion records in the low frequency range.

Furthermore, the predicted frequencies of 1D site response do not take into account two- and three-dimensional wave propagation effects. While the Kathmandu Valley is shallow, with a depth/width ratio (d/w) on the order of 0.1, and the predominant frequency of converted surface waves should theoretically be close to the predicted 1D (quarter-wavelength) frequency (Bard and Bouchon, 1985; Harmsen and Harding, 1981), one expects the lower modal frequencies to be strongly affected by body-to-surface wave mode conversion at the basin edges and lateral reverberations of the surface waves across the valley. We can qualitatively identify these effects by studying the filtered waveforms of the strong motion records and two high-rate GPS records (Avouac et al., 2015) of the mainshock in Fig. 6. The strong motion and GPS records at reference sites KTP and KKN4 contain a singular long period pulse in each of the frequency ranges 0–0.2 Hz (Fig. 6 (a)) and 0.2–1 Hz (Fig. 6 (b)). In contrast, the waveforms on the sediments are much more complex, particularly near the basin edges (TVU and PTN) where vertically
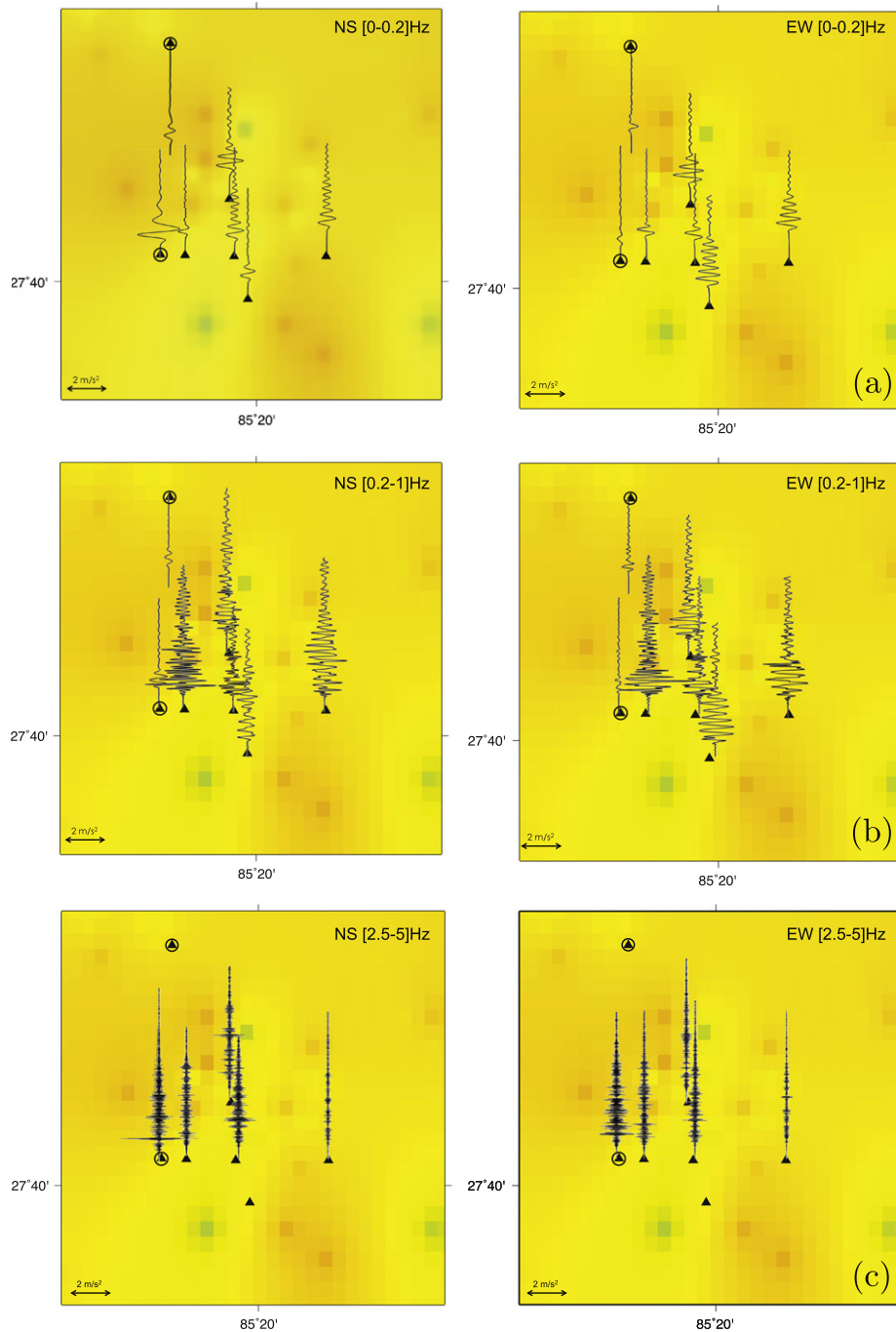
Fig. 6. Horizontal strong motion acceleration components and GPS double differentiated data of the M 7.8 mainshock event, passband filtered in the frequency ranges (a) 0–0.2 Hz and (b) 0.2–1 Hz to highlight the long period amplification and duration elongation on soil relative to the reference sites; and in the frequency range (c) 2.5–5 Hz, to illustrate the attenuation of high frequencies within the basin. Intensity maps from Martin et al. (2015). Circled station locations denote reference site conditions. Note that the intensity scale is given in Fig. 1.

propagating, reverberating shear waves constructively interfere with horizontally propagating surface waves generated by diffraction and amplified by focusing at the basin edges (Toshinawa and Ohmachi, 1992; Furumura and Hayakawa, 2007). By contrast, filtered strong motion data on soil in the 2.5–5.0 Hz frequency range are heavily attenuated relative to the reference site records, which is suggestive of nonlinear site response of the basin sediments (Fig. 6 (c)) (high rate GPS data had a poor signal-to-noise ratio beyond 1 Hz and have thus been omitted from Fig. 6 (c)). We also observe that during the mainshock, the high frequencies attenuate from west to east,

namely in the direction of the rupture propagation, which could be suggestive of a very low quality factor (Q) in the near-surface sedimentary layers; still, the mainshock data are not directly comparable to the smaller events due to the extent and location of the rupture zone, and thus this observation is speculative and subject to further investigation and validation. Lastly, we note that the low frequency spectral components computed from the acceleration strong motion records compare exceptionally well to the corresponding spectral amplitudes computed from the two high-rate GPS records on sediments (NAST) and reference (KKN4) site conditions (Fig. 7), as well
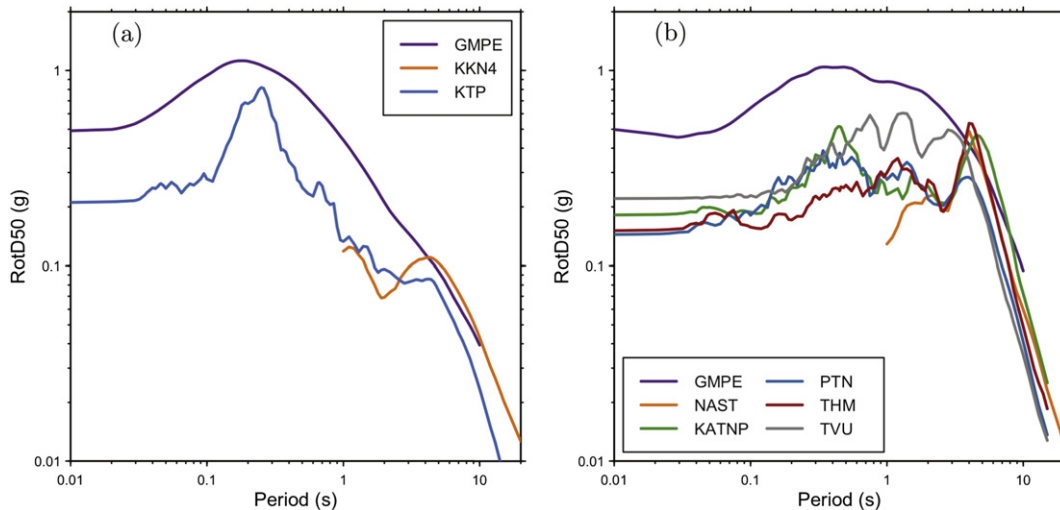
Fig. 7. Comparison of the orientation independent response spectral acceleration (RodD50) of the mainshock (M 7.8) strong motion and high rate GPS records to the BSSA14 GMPE (Boore et al., 2014) for $R_{JB} = 0$, using (a) V$_{S30}$ = 760 m/s for the reference sites; and (b) V$_{S30}$ = 200 m/s for the soil sites (JICA, 2002). The comparison between strong motion, high rate GPS data and the BSSA14 GMPE at long periods (>4 s) is remarkable.

as to the BSSA14 GMPE in the same frequency range (<0.25 Hz or >4 s in terms of periods). This comparison suggests that in absence of strong motion records, high rate GPS measurements can be a reliable source to quantify long-period basin amplification effects.

Despite the strong amplification effects in the low frequency range induced by the deep sedimentary deposits of the basin, the frequency characteristics of the ubiquitous 1–2 story buildings in Kathmandu coincide with the frequency range strongly deamplified by a complex interaction between source effects, anelastic attenuation and nonlinear site response (>3 Hz). The latter fortuitous coincidence is also supported on average by macroseismic data shown in Fig. 1 (b), which reveal generally lower intensities in central Kathmandu Valley compared to adjacent foothills (Martin et al., 2015). Still, the lack of stations and thus records in the zones of the lowest intensities makes it hard to concretely support this point, at least in absence of simulated nonlinear 3D ground motions.

7. Conclusions

We have analyzed strong motion records of the M 7.8 Gorkha mainshock, M 7.3 Dolakha, and two moderate aftershock events recorded at four strong motion stations on soil in the Kathmandu basin, and one station on reference (rock) conditions. The M 7.8 ground motions at the four soil sites are characterized by large amplitude low frequency (<0.5 Hz) waves and severely attenuated high frequencies relative to the reference station records. Comparison of the observations to ground motion prediction equations reveal that the high frequency anomaly was characteristic of the M 7.8 shaking on both soil and rock, suggesting that it was in part an effect of the source characteristics of the mainshock. Site effects also appear to have played a dominant role in shaping the amplitude and frequency content of ground shaking on soil. Strong motions on soil for all four events show systematic amplification relative to the rock site in the low frequency range (0.1–2.5 Hz), and de-amplification of higher frequencies (>2.5 Hz). At the same time, the soil-to-rock amplification ratio for the mainshock and M 7.3 aftershock have lower amplitude compared to two (M 6.6 and M 6.7) moderate events, which could be potentially explained by the fact that site response during the stronger events was nonlinear.

Several questions are unresolved pertaining to the role, severity and spatial extend of nonlinear soil response in shaping the observed high frequency content of the mainshock strong motions.

The paucity of data such as the scarcity and sparsity of velocity profiles in the basin, the uncertainties related to the geometry of the sediment-basement rock interface, and the inelastic and nonlinear soil behavior of the Kathmandu unconsolidated near-surface sediments (namely the relative role of intrinsic attenuation, Q, and sediment strain-dependent stiffness as presented for example in Langston et al. (2003) and Chong and Ni (2009)) – have hindered so far the resolution of these questions.

For example, while some of the observed site amplification characteristics can be explained using a one-dimensional viscoelastic site response model to fully understand the complexity of waveforms and the amplitude and frequency shift in our mainshock observations relative to the weaker ground motions, one would need to conduct nonlinear numerical analyses of a detailed three-dimensional model of the basin. On the other hand, the strong motion time series alone presented in this work has played an important role in motivating several ongoing studies that seek to shed light to the above questions. These studies range from site characterization of the Kathmandu sediments, to nonlinear soil testing, to numerical investigation of the mainshock rupture including inelastic crustal wave propagation and nonlinear site effects. The ultimate goal of these ongoing studies is to develop region-specific, physics-based reliable GMPEs, which in turn will yield improved building codes for the Kathmandu basin and the country of Nepal at large.

descriptive purposes only and does not imply endorsement by the U.S. Government.

References

Abrahamson, N., Gregor, N., Addo, K., 2016. EBC hydro ground motion prediction equations for subduction earthquakes. Earthq. Spectra 32 (1), 23–44.

Ampuero, J.P., Hough, S., Meng, L., Thompson, E.M., Zhang, A., Martin, S.S., Asimaki, D., Inbal, A., 2016. Damage limited by the distribution of high-frequency radiation in the 2015 Gorkha, Nepal, earthquake. Earth Planet. Sci. Lett. (in review).

Atkinson, G.M., 2003. Empirical ground-motion relations for subduction-zone earthquakes and their application to cascadia and other regions. Bull. Seismol. Soc. Am. 93 (4), 1703–1729.

Avouac, J.P., Meng, L., Wei, S., Wang, T., Ampuero, J.P., 2015. Lower edge of locked Main Himalayan thrust unzipped by the 2015 Gorkha earthquake. Nat. Geosci. 1752-0894.

Bard, P.Y., Bouchon, M., 1985. The two-dimensional resonance of sediment-filled valleys. Bull. Seismol. Soc. Am. 75 (2), 519–541.

Beresnev, I.A., 2002. Nonlinearity at California generic soil sites from modeling recent strong-motion data. Bull. Seismol. Soc. Am. 92 (2), 863–870.

Beresnev, I.A., Wen, K.L., 1996. Nonlinear soil response–a reality? Bull. Seismol. Soc. Am. 86 (6), 1964–1978.

Bhattarai, M., Adhikari, L.B., Gautam, U., Laurendeau, A., Labonne, C., Hoste-Colomer, R., Sebe, O., Hernandez, B., 2015. Overview of the large April 25th Gorkha, Nepal, earthquake from an accelerometric perspective. Seismol. Res. Lett. 86 (6). http://dx.doi.org/10.1785/0220150140.

Bilham, R., Gaur, V.K., Molnar, P., 2001. Himalayan seismic hazard. Science 293 (5534), 1442–1444.

Bollinger, L., Sapkota, S.N., Tapponnier, P., Klinger, Y., Rizza, M., Van Der Woerd, J., Tiwari, D., Pandey, R., Bitri, A., Bes de Berc, S., 2014. Estimating the return times of great Himalayan earthquakes in eastern Nepal: evidence from the Patu and Bardibas strands of the main frontal thrust. J. Geophys. Res. Solid Earth 119 (9), 7123–7163.

Bonilla, L.F., Tsuda, K., Pulido, N., Régnier, J., Laurendeau, A., 2011. Nonlinear site response evidence of K-NET and KiK-net records from the 2011 off the Pacific coast of Tohoku earthquake. Earth Planets Space 63 (7), 785–789.

Boore, D.M., 2010. Orientation-independent, nongeometric-mean measures of seismic intensity from two horizontal components of motion. Bull. Seismol. Soc. Am. 100 (4), 1830–1835.

Boore, D.M., Stewart, J.P., Seyhan, E., Atkinson, G.M., 2014. NGA-west2 equations for predicting PGA, PGV, and 5% damped PSA for shallow crustal earthquakes. Earthquake Spectra 30 (3), 1057–1085.

Borcherdt, R.D., 1994. Estimates of site-dependent response spectra for design (methodology and justification). Earthquake spectra 10 (4), 617–653.

Chen, W.P., Molnar, P., 1977. Seismic moments of major earthquakes and the average rate of slip in Central Asia. Journal of Geophysical Research 82 (20), 2945–2969.

Chitrakar, G., Pandey, M.R., 1986. Historical earthquakes of Nepal. Bull Geol. Soc. Nepal 4, 7–8.

Chong, J.J., Ni, S.D., 2009. Near surface velocity and Qs structure of the Quaternary sediment in Bohai Basin. China, Earthquake Science, 22, 451–458.

Dhital, M.R., 2015. Geology of the Nepal Himalaya: Regional Perspective of the Classic Collided Orogen. Springer., pp. 498p.

Dixit, A., Dwelly-Samant, L., Nakarmi, M., Pradhanang, S., Tucker, B., 1998. The Kathmandu Valley Earthquake Management Plan. National Society for Earthquake Technology, Tech. rep..

Dixit, A., Ringler, A., Sumy, D., Cochran, E., Hough, S., Martin, S., Gibbons, S., Luetgert, J., Galetzka, J., Shrestha, S., Rajaure, S., McNamara, D., 2015. Strong motion recordings of the M 7.8 Gorkha, Nepal, earthquake sequence from low-cost. Quake Catcher Network accelerometers, Seismological Research Letters, 86 (6), 1533–1539.

Field, E.H., Johnson, P.A., Beresnev, I.A., Zeng, Y., 1997. Nonlinear ground-motion amplification by sediments during the 1994 Northridge earthquake. Nature 390 (6660), 599–602.

Frankel, A.D., Petersen, M.D., Mueller, C.S., Haller, K.M., Wheeler, R.L., Leyendecker, E., Wesson, R.L., Harmsen, S.C., Cramer, C.H., Perkins, D.M., et al. 2002. Documentation for the 2002 Update of the National Seismic Hazard Maps. US Department of the Interior, US Geological Survey.

Furumura, T., Hayakawa, T., 2007. Anomalous propagation of long-period ground motions recorded in Tokyo during the 23 October 2004 M 6.6 Niigata-ken Chuetsu, Japan, earthquake. Bulletin of the Seismological Society of America 97 (3), 863–880.

Ghofrani, H., Atkinson, G.M., 2013. Ground-motion prediction equations for interface earthquakes of M7 to M9 based on empirical data from Japan. Bulletin of Earthquake Engineering 12 (2), 549–571.

Hagen, T., 1951. Preliminary Note on the Geological Structure of Central Nepal, Tech. Rep 133–134. Verhandlungen der Schweizerischen Naturforschenden Gesellschaft, Luzern.

Harmsen, S., Harding, S., 1981. Surface motion over a sedimentary valley for incident plane P and SV waves. Bulletin of the Seismological Society of America 71 (3), 655–670.

Hartzell, S., 1998. Variability in nonlinear sediment response during the 1994 Northridge, California earthquake. Bulletin of the Seismological Society of America 88 (6), 1426–1437.

Hashash, Y.M., Tiwari, B., Moss, R.E.S., Asimaki, D., Clahan, K.B., Kieffer, D.S., Dreger, D.S., Macdonald, A., Madugo, C.M., Mason, H.B., Pehlivan, M., Rayamajhi, D., Acharya, I., Adhikari, B., 2015. Geotechnical field reconnaissance: Gorkha (Nepal) earthquake of April 25 2015 and related shaking sequence. GEER Association Technical Report No GEER-040, v1.1 1.

Hayes, G.P., Briggs, R.W., Barnhart, W.D., Yeck, W.L., McNamara, D.E., Wald, D.J., Nealy, J.L., Benz, H.M., Gold, R.D., Jaiswal, K.S., Marano, K., Earle, P.S., Hearne, M.G., Smoczyk, G.M., Wald, L.A., Samsonov, S.V., 2015. Rapid characterization of the 2015 Mw 7.8 Gorkha, Nepal, earthquake sequence and its seismotectonic context. Seismological Research Letters 86, 1557–1567.

JICA, 2002. . The Study on Earthquake Disaster Mitigation in the Kathmandu Valley, Tech. RepJapan International Cooperation Agency and the Ministry of Home Affairs of Nepal.

Joyner, W.B., Chen, A.T., 1975. Calculation of nonlinear ground response in earthquakes. Bulletin of the Seismological Society of America 65 (5), 1315–1336.

Joyner, W.B., Boore, D.M., 1981. Peak horizontal acceleration and velocity from strong–motion records including records from the 1979 Imperial Valley, California, earthquake. Bulletin of the Seismological Society of America 71 (6), 2011–2038.

Kaklamanos, J., Bradley, B.A., Thompson, E.M., Baise, L.G., 2013. Critical parameters affecting bias and variability in site-response analyses using KiK-net downhole array data. Bulletin of the Seismological Society of America 103 (3), 1733–1749.

Kanno, T., Narita, A., Morikawa, N., Fujiwara, H., Fukushima, Y., 2006. A new attenuation relation for strong ground motion in Japan based on recorded data. Bulletin of the Seismological Society of America 96 (3), 879–897.

Katel, T., Upreti, B., Pokharel, G., 1996. Engineering properties of fine grained soils of Kathmandu Valley Nepal. Journal of Nepal Geological Society 13, 121–138.

Konno, K., Ohmachi, T., 1998. Ground-motion characteristics estimated from spectral ratio between horizontal and vertical components of microtremor. Bulletin of the Seismological Society of America 88 (1), 228–241.

Langston, C.A., 2003. Local earthquake wave propagation through Mississippi embayment sediments, part II: influence of local site velocity structure on Qp-Qs determination. Bulletin of the Seismological Society of America 93, 2685–2702.

Martin, A., Szeliga, W., 2010. A catalog of felt intensity data for 570 earthquakes in India from 1636 to 2009. Bulletin of the Seismological Society of America 100, 562–569. doi:10.0120080328.

Martin, S.S., Hough, S.E., Hung, C., 2015. Ground motions from the 2015 M 7.8 Gorkha, Nepal, earthquake constrained by a detailed assessment of macroseismic data. Seismological Research Letters 86 (6).

McNamara, D.E., W., Yeck, W., Barnhart, V., Schulte-Pelkum, E., Bergman, L.B., Adhikari, A., Dixit, S., Hough, H., Benz, P., Earle, 2015. Source Modeling of the 2015 Mw 7.8 Nepal (Gorkha) Earthquake sequence: Implications for Geodynamics and Earthquake Hazards. Tectonophysics. http://dx.doi.org/10.1016/j.tecto.2016.08.004.

Meng, L., Inbal, A., Ampuero, J.-P., 2011. A window into the complexity of the dynamic rupture of the 2011 M 9 Tohoku-oki earthquake. Geophysical Research Letters 38, 7.

Moribayashi, S., Maruo, Y., 1980. Basement topography of the Kathmandu Valley, Nepal - an application of gravitational methods to the survey of a tectonic basin in the Himalayas. Journal of the Japan Society of Engineering Geology 21 (2), 80–87.

Muzzini, E., Aparicio, G., 2013. Urban Growth and Spatial Transition in Nepal: An Initial Assessment. World Bank Publications.

Takai, N., Sawada, K., Shigefuji, M., Bijukchhen, S.M., Ichiyanagi, M., Sasatani, T., Dhakal, Y.P., Rajaure, S., Dhital, M., 2015. Shallow underground structure of strong ground motion observation sites in the Kathmandu Valley. In: Adhikari, D.P. (Ed.), Geosciences in Sustainable Development: Challenges and Opportunities. Nepal Geological Society., pp. 50.

Pandey, M., Molnar, P., 1988. The distribution of intensity of the Bihar-Nepal earthquake of 15 January 1934 and bounds on the extent of the rupture zone. Journal of Nepal Geological Society 5 (1), 22–44.

Pandey, M.R., 2000. Ground response of Kathmandu Valley on the basis of microtremors. 12th World Conference on Earthquake Engineering (12 WCEE). 1206.

Paudyal, Y.R., Bhandary, N., Yatabe, R., 2012a. Seismic microzonation of densely populated area of Kathmandu Valley of Nepal using microtremor observations. Journal of Earthquake Engineering 16 (8), 1208–1229.

Paudyal, Y.R., Yatabe, R., Bhandary, N., Dahal, R., 2012b. A study of local amplification effect of soil layers on ground motion in the Kathmandu Valley using microtremor analysis. Earthquake Engineering and Engineering Vibration 11 (2), 257–268.

Paudyal, Y.R., Yatabe, R., Bhandary, N.P., Dahal, R.K., 2013. Basement topography of the Kathmandu Basin using microtremor observations. Journal of Asian Earth Sciences 62, 627–637.

Petersen, M.D., Moschetti, M.P., Powers, P.M., Mueller, C.S., Haller, K.M., Frankel, A.D., Zeng, Y., Rezaeian, S., Harmsen, S.C., Boyd, O.S., Field, N., Chen, R., Rukstales, K.S., Luco, N., Wheeler, R.L., Williams, R.A., Olsen, A.H., 2015. The 2014 United States National Seismic Hazard Model. Earthquake Spectra 31 (S1), S1–S30.

Rajaure, S., Koirala, B., Pandey, R., Timsina, C., Jha, M., Bhattara, M., Dhital, M.R., Paudel, L.P., Bijukchhen, S., 2014. Ground response of the Kathmandu sedimentary basin with reference to 30 August 2013 South-Tibet earthquake. Journal of Nepal Geological Society 47, 23–34.

Rana, B., 1935. Nepal Ko Maha Bhukampa. (Great Earthquake of Nepal), Nepal (in Nepali).

Sakai, H., Sakai, H., Yahagi, W., Fujii, R., Hayashi, T., Upreti, B.N., 2006. Pleistocene rapid uplift of the Himalayan frontal ranges recorded in the Kathmandu and Siwalik Basins. Palaeogeography, Palaeoclimatology, Palaeoecology 241 (1), 16–27.

Sakai, T., Gajurel, A.P., Tabata, H., Upreti, B.N., 2001. Small-amplitude lake-level fluctuations recorded in aggrading deltaic deposits of the upper Pleistocene Thimi and Gokarna formations, Kathmandu Valley Nepal. J Nepal Geol Soc 25 (special issue), 43–52.

Sapkota, S., Bollinger, L., Klinger, Y., Tapponnier, P., Gaudemer, Y., Tiwari, D., 2013. Primary surface ruptures of the great Himalayan earthquakes in 1934 and 1255. Nature Geoscience 6 (1), 71–76.

Seed, H.B., Idriss, I.M., 1970. Soil Moduli and Damping Factors for Dynamic Response Analyses, Earthquake Engineering Research Center, Report No. EERC 70-10 University of California. Berkeley, California.

Shoja-Taheri, J., Bolt, B.A., 1977. A generalized strong-motion accelerogram based on spectral maximization from two horizontal components. Bulletin of the Seismological Society of America 67, 863–876.

Sokolov, V.Y., Chernov, Y.K., 1998. On the correlation of seismic intensity with Fourier amplitude spectra. Earthquake spectra 14 (4), 679–694.

Steidl, J.H., Bonilla, L.F., Tumarkin, A.G., 1995. Seismic hazard in the San Fernando basin, Los Angeles, CA: a site effects study using weak-motion and strong-motion data. Proc. of the 5th International Conference on Seismic Zonation, Nice France 1149–1156.

Stöcklin, J., 1980. Geology of Nepal and its regional frame: thirty-third William Smith lecture. Journal of the Geological Society 137 (1), 1–34.

Su, F., Anderson, J.G., Zeng, Y., 1998. Study of weak and strong ground motion including nonlinearity from the Northridge, California earthquake sequence. Bulletin of the Seismological Society of America 88 (6), 1411–1425.

Takai, N., Shigefuji, M., Rajaure, S., Bijukchhen, S., Ichiyanagi, M., Dhital, M.R., Sasatani, T., 2016. Strong ground motion in the Kathmandu Valley during the 2015 Gorkha, Nepal, earthquake, earth, planets and space, available online. http://dx.doi.org/10.1186/s40623-016-0383-7.

Toshinawa, T., Ohmachi, T., 1992. Love-wave propagation in a three-dimensional sedimentary basin. Bulletin of the Seismological Society of America 82 (4), 1661–1677.

Tsuda, K., Steidl, J., Archuleta, R., Assimaki, D., 2006. Site-response estimation for the 2003 Miyagi-Oki earthquake sequence considering nonlinear site response. Bulletin of the Seismological Society of America 96 (4A), 1474–1482.

Tumarkin, A.G., Archuleta, R.J., 1994. Empirical ground-motion prediction, Annali di Geofisica. (Special Issue: Proceedings of the International School on Earthquake Source Mechanics) 32 (1), 1691–1720.

Wu, C., Peng, Z., Ben-Zion, Y., 2009. Non-linearity and temporal changes of fault zone site response associated with strong ground motion. Geophysical Journal International 176 (1), 265–278.

Yadav, R.R., Park, W.-K., Singh, J., Dubey, B., 2004. Do the western Himalayas defy global warming? Geophysical Research Letters 31 (17). http://dx.doi.org/10.1029/2004GL020201.

Yoshida, M., Igarashi, Y., 1984. Neogene to Quaternary lacustrine sediments in the Kathmandu Valley Nepal. Journal of Nepal Geological Society 4 (Special issue), 73–100.

Appendix 1.2. Indexed Journal

1. Rajaure, S., Koirala, B., Pandey, R., Timsina, C., Jha, M., Bhattarai, M., Dhital, M., Paudel, L., & Bijukchhen, S. (2014). Ground response of the Kathmandu Sedimentary Basin with reference to 30 August 2013 South-Tibet Earthquake. *Journal of Nepal Geological Society*, *47*(1), 23-34. https://doi.org/10.3126/jngs.v47i1.23101

Ground response of the Kathmandu Sedimentary Basin with reference to 30 August 2013 South-Tibet Earthquake

S. Rajaure[1, *], B. Koirala[1], R. Pandey[1], C. Timsina[1], M. Jha[1], M. Bhattarai[1], M. R. Dhital[2], L. P. Paudel[2], S. Bijukchhen[3]

[1]Department of Mines and Geology, Lainchaur, Kathmandu, Nepal
[2]Central Department of Geology, Tribhuvan University, Kirtipur, Kathmandu, Nepal
[3]Hokkaido University, Sapporo, Japan
***Corresponding author: srajaure@gmail.com**

ABSTRACT

Ground acceleration of the 30 August 2013 (M4.9), South Tibet Earthquake has been recorded by five accelerometers deployed in the Kathmandu Valley. Analysis of the ground acceleration record reveals that that the EW component was dominant across the valley, and with the exception of one, all stations on sediments recorded PGA much higher than the station on rock. The site response functions, evaluated as the Fourier spectral ratios of the horizontal components on soil relative to the corresponding component on rock, are remarkably similar in the low frequency range (<0.8 Hz) and reveal strong amplification that likely corresponds to basin effects. By contrast, the high frequency site response shows strong variability across the soil sites, likely attributed to the underlying stratigraphy of the shallow soil layers of the valley. The most pronounced differences manifest in the frequency range >2Hz, which is consistent with the variability in PGA across the valley. Because of the small intensity of this event, the empirical site response recorded can be, approximately, considered linear. As such, this study establishes a reference for future studies on nonlinear site response, which is likely to be triggered during future stronger earthquakes.

Key Words: Peak ground acceleration, Fourier amplitude spectra, ground response, spectral ratio

INTRODUCTION

The Kathmandu valley is an intermontane tectonic basin in the Lesser Himalaya of central Nepal. The valley hosts Kathmandu, the capital city of Nepal, as well as two other major cities, Patan and Bhaktapur, and many newly developing urban areas. The population of the Kathmandu Valley is rapidly increasing than ever before.

The valley has experienced varying degree of ground shaking/destruction in the past earthquakes (Pandey and Molnar 1988). The damage pattern of the 1934 (M 8.1) earthquake (Bilham et. al. 1995), in particular suggests that ground amplification due to fluvio-lacustrine sediments plays a major role in intensifying the ground motion in the basin (Paudyal et. al. 2013).

The valley has been reportedly destroyed many times in the past by historical earthquakes (e. g. Chitrakar and Pandey 1986). Most recently, Kathmandu Valley was heavily damaged by the 1934 Bihar-Nepal Earthquake (e.g., Pandey and Molnar 1988; Rana 1935 and NSET 2011). Rana (1935) compiled an extensive report on the destruction as well as casualties caused by the 1934 earthquake. Pandey and Molnar (1988) and Paudyal et. al. (2013) conclude that the variation in the destruction pattern in the Kathmandu Valley was possibly a consequence of variable ground response-Se of the Kathmandu Valley sediments, which resulted in amplification of seismic wave amplitudes. The estimated intensity distribution of the 1934 great earthquake (Fig. 1) varies from IX to X MMI (Pandey and Molnar 1988, NSET 2011) within different unconsolidated sedimentary deposits in the Kathmandu Valley.

Study of seismic ground response using ground acceleration data for different parts of the valley has not been previously possible in Kathmandu Valley because of lack of accelerometers in the Valley. In this paper we present results on seismic ground response of the Kathmandu Valley Sediments using instrumentally recorded data of the 30th August 2013, South Tibet Earthquake (M4.9) at five sites in the Valley (Fig 1).
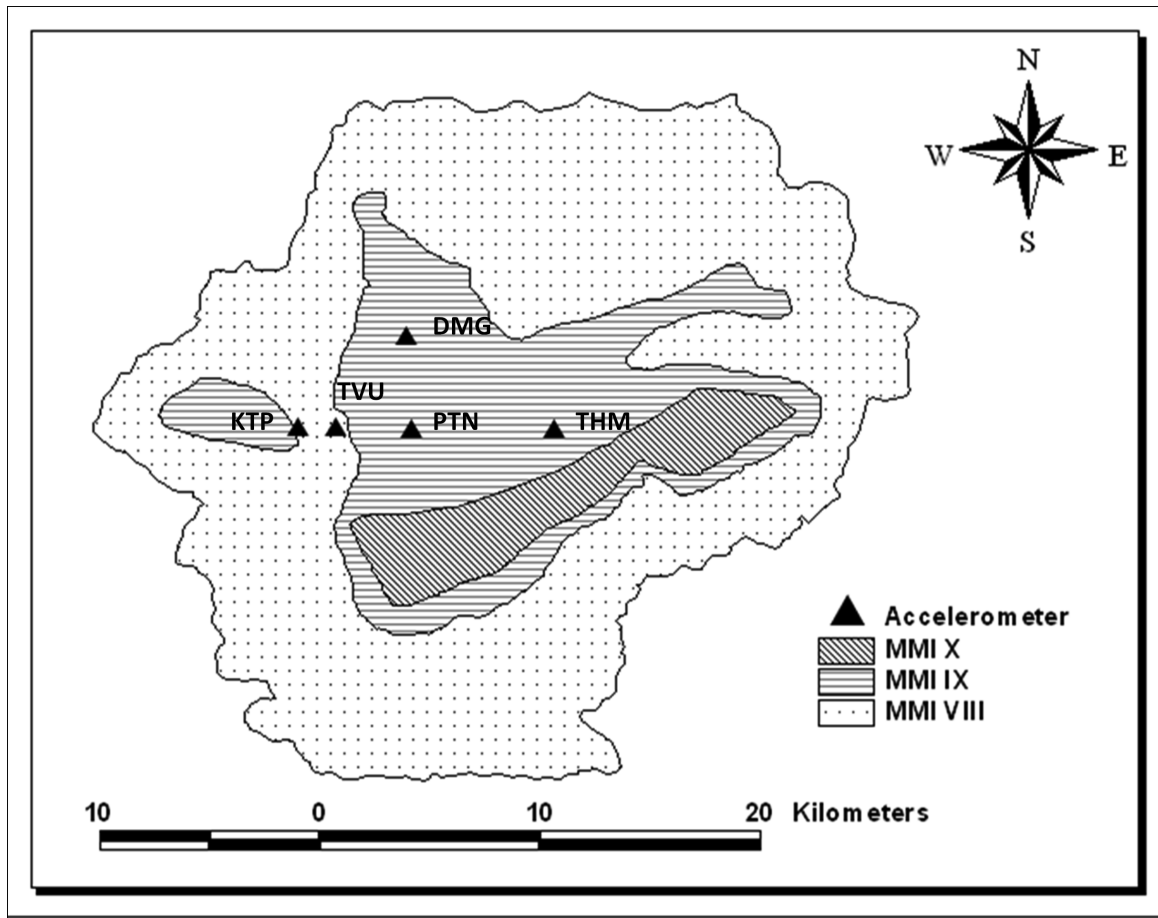
Fig. 1: Intensity distribution of the 1934 Bihar-Nepal Earthquake in the Kathmandu Valley (modified after NSET, 2011). The triangle shows the location of presently installed accelerometers in the Kathmandu valley.

GEOLOGICAL SETTING

The Kathmandu valley is located in the Lesser Himalaya (Fig. 2). The basin falls in the Midland zone of the Lesser Himalaya, and is bounded by the Mahabharat Lekh in the south and the Shivapuri Lekh in the north. The basement of the Kathmandu basin is a huge nappe (Kathmandu nappe) formed by thrusting along Mahabharat Thrust (MT), probably the southward extension of the Main Central Thrust (MCT). It is made up of the Precambrian Bhimphedi Group and Paleozoic Phulchoki Group (Stöcklin 1980).

The Kathmandu basin-fill sediments unconformably lie on the Kathmandu Complex rocks (Fig. 3). The sediments range in age from 2.5 Ma to about 20 kyr with a total thickness of about 600 m at the central part of the basin. The sediments are divided into seven formations on the basis of their sedimentary facies (Sakai 2001). The lowermost and oldest unit is the Tarbhir Formation. It is mainly composed of boulders and cobbles. The Lukondol Formation is a mud-dominant sequence of marginal lacustrine facies. In the southern part of the valley, The Lukondol Formation is overlain by the Itaiti Formation. The Itaiti Formation is a cliff-forming gravel dominant sequence. In the central part of the valley, the Lukondol Formation is overlain by the Kalimati Formation,

dominantly carbonaceous laminated clay. In the northern part of the valley, The Kalimati Formation is overlain by the Gokarna and Thimi Formation. Both the formation are made up of fluvio-lacustrine sandy sediments. The Patan Formation rests on the top of the basin sediments. It is also made up of the fluvio-lacustrine sandy facies.

SEISMICITY

The Kathmandu Valley has witnessed a number of destructive earthquakes in the past (e.g., Chitrakar and Pandey 1986; Bilham et. al. 1995; Bilham and Ambraseys 2004). The destruction caused by the 1934 Bihar-Nepal Earthquake (M 8.1) and 1988 Udayapur earthquake (M6.5) are still in the living memory of Nepali people.

The National Seismological Centre (NSC) of Department of Mines and Geology (DMG) has been operating a network of seismic stations designed to study micro-earthquakes in Nepal. The network began operation in 1995 and has collected a large volume of data. Pandey et. al. (1995) and Pandey et. al. (1999) have studied the seismicity distribution in Nepal using data from the network of the Department of Mines and Geology.

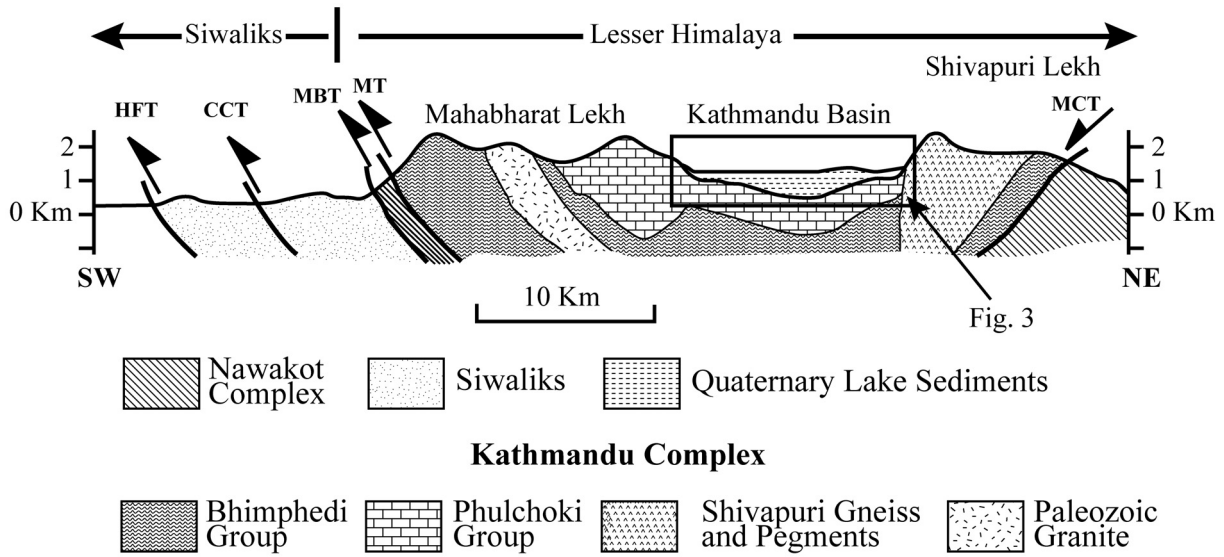**Fig. 2. Schematic geological cross-section across the Kathmandu valley in central Nepal Himalaya (Modified after Sakai et al. 2002). MCT: Main Central Thrust, MT: Mahabharat Thrust, MBT: Main Boundary Thrust, CCT: Central Churia Thrust, MFT: Main Frontal Thrust.**
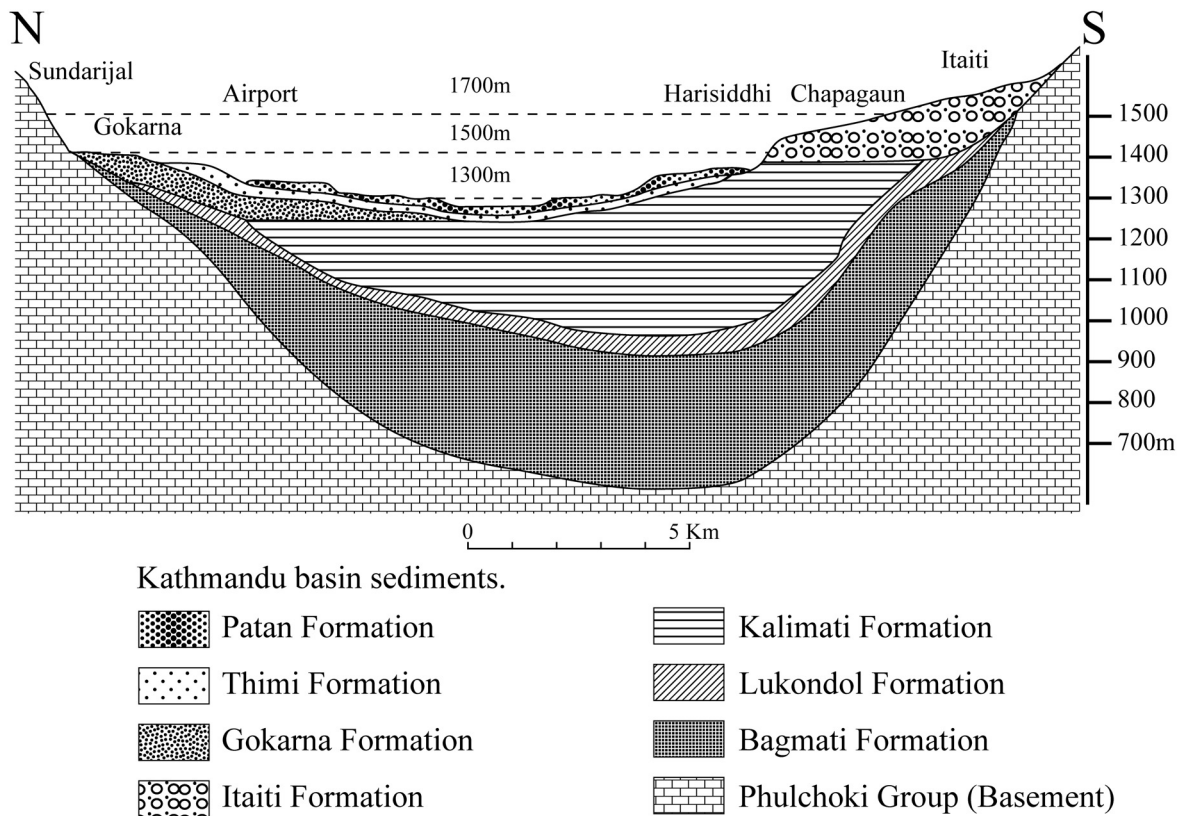
Fig. 3: Schematic geological cross-section of the basin-fill sediments of the Kathmandu sedimentary basin (Modified after Sakai 2001).

Rajaure et. al. (2013) relocated the seismicity of Nepal applying the double-difference relocation technique (Waldhauser and Ellsworth 2000) to local earthquakes recorded by seismic network of the Department of Mines and Geology (DMG). The result of Double Difference Relocation is presented in Fig. 4. The figure shows a continuous belt of microseismic activity all along the Nepal Himalaya, which constrains and better delineates the seismicity belt reported earlier by Pandey et. al. (1995) and Pandey et. al. (1999). The microseismic activity is intense in far-west Nepal and far-east Nepal (Fig. 4). This belt is simple and narrow in the east of 82°E (Pandey et. al. 1999 and Rajaure et. al. 2013); however it is complicated and is separated into two sub-parallel belts between 82°E and 80°E. Majority of the local earthquakes along the seismicity belt are shallow focus earthquakes with depth ranging between 0 and 25 km.
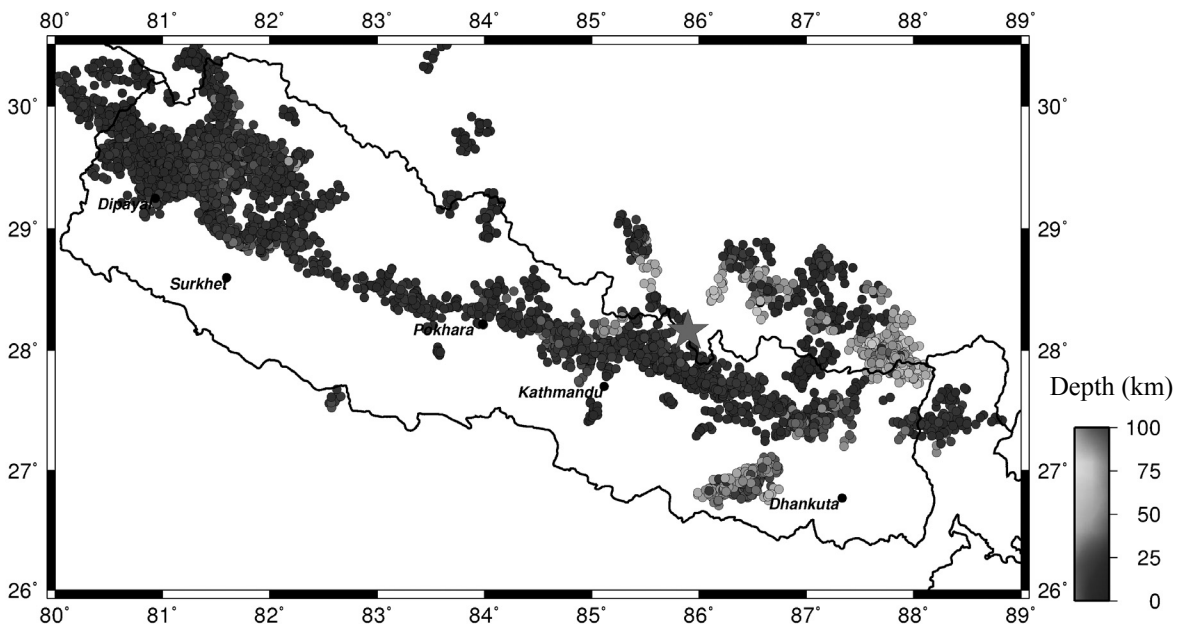
Fig. 4: Epicenter distribution (1995-2004, Ml>2.0) in Nepal (modified from Rajaure et. al. 2013). The epicenters are scaled to depth. The red star stands for the 30 August 2013, South Tibet earthquake.

PREVIOUS STUDIES

Pandey (2000) studied the seismic response of the Kathmandu valley sediments using microtremor data recorded at 60 sites in the valley and implemented a quantitative assessment of site amplification using horizontal relative spectra of microtremor to a reference site. In his study, he found that the predominant amplification peak is around 2 Hz, whereas the relative peak amplification factor is about 12 to 15.

Bhattarai et. al. (2011) reported analysis of accelerometric data recorded at DMG and at Kakani (KKN) site (about 20 km in the north of Kathmandu Valley on rock). They analyzed two earthquakes one of which occurred at a distance of 25 km (15 July 2010, M_L 3.4 (NSC)), in Nepal, and other occurred over 110 km distance (17 October 2010, M_L 5.7 (NSC)) in South Tibet. The study shows large peak ground acceleration (PGA) at a hard rock site located at about 110 km from the epicenter which they speculate might be caused by topographic amplification at KKN.

Paudyal et. al. (2012) carried out seismic microzonation of the Kathmandu Valley using microtremor data recorded in the Kathmandu valley. They applied horizontal-to-vertical spectral ratio technique to estimate the predominant period at the sites. They mentioned that the sites over thick sedimentary deposit, in the central part of the valley, are characterized by amplifications at long period. The authors point out that their results raise concerns due to the continuing construction of new multi-storied buildings in this part of the valley, since the natural periods of these structures is likely to be close to the fundamental period at sites of observation.

DATA

The National Seismological Centre (NSC) of the Department of Mines and Geology (DMG), in collaboration with Departement Analyse Surveillance Environnement (DASE), France, has installed 8 accelerometers in Nepal to study attenuation pattern of seismic wave amplitudes. One of the eight accelerometer owned by DMG has been installed in the premises of DMG at Lainchaur. Similarly, to study the seismic ground response of the Kathmandu Valley sediments, the Central Department of Geology (CDG) of the Tribhuvan University, in collaboration with the Hokkaido University,

Japan installed four accelerometers (KTP, TVU, PTN, THM (Fig. 5, Table 1)) in different parts of the Kathmandu Valley along an E-W profile. The accelerometer installed by DMG is GeoSIG type (sampling rate 200 sps), operated on triggered mode, and the other accelerometers installed by the TVU comprise Mitsutoyo JEP-6A3-2 accelerometers (sampling rate 100 sps) operated on continuous mode.

We have used ground acceleration data of the 30 August 2013, South Tibet Earthquake recorded by all five accelerometers installed in the Kathmandu Valley (Table 1, Fig 5). This earthquake (Mb 4.9) occurred at 28.16^{o}N latitude, 85.89^{o}E longitude (Fig. 4), at a depth of 54.6 km (USGS) at 17:48:42.98 (UTC time, USGS). The earthquake occurred approximately 76 km in North-East direction from the Kathmandu Valley, which was felt in all parts of the Valley.

A fault plane solution for this earthquake is not available; however we presume a normal fault mechanism for this earthquake based on fault plane solution of past earthquakes in the area (Sheehan 2008; Torre et. al. 2007; Rajaure et. al. 2013).

Ground acceleration data recorded by five accelerometers was cut at 17:47:41 UTC to produce a record length of about 90 seconds. 'Seismo Signal' software (Earthquake Engineering Software Solutions) was used for necessary processing of the data to determine ground motion amplitude parameters. The data was band pass filtered between 0.1 and 25 Hz using a Butterworth filter. DIAMANT, a Matlab tool (Hernandez, et. al., 2011), was used to compute spectral ratio relative to the rock site (KTP) as a reference.

Table 1: Location (coordinates) of accelerometers (Fig. 5) used in this study

| Site code	Latitude N)	Longitude (E)	Location
KTP (rock)	27.68182	85.27261	Kirtipur Municipality office
TVU (soil)	27.68145	85.28821	Central Department of Geology/TU
PTN (soil)	27.68082	85.31897	Engineering College, Pulchowk
THM (soil)	27.68072	85.3772	University Grant Commission Office, Bhaktapur
DMG (soil)	27.71881	85.31678	Department of Mines and Geology, Lainchaur
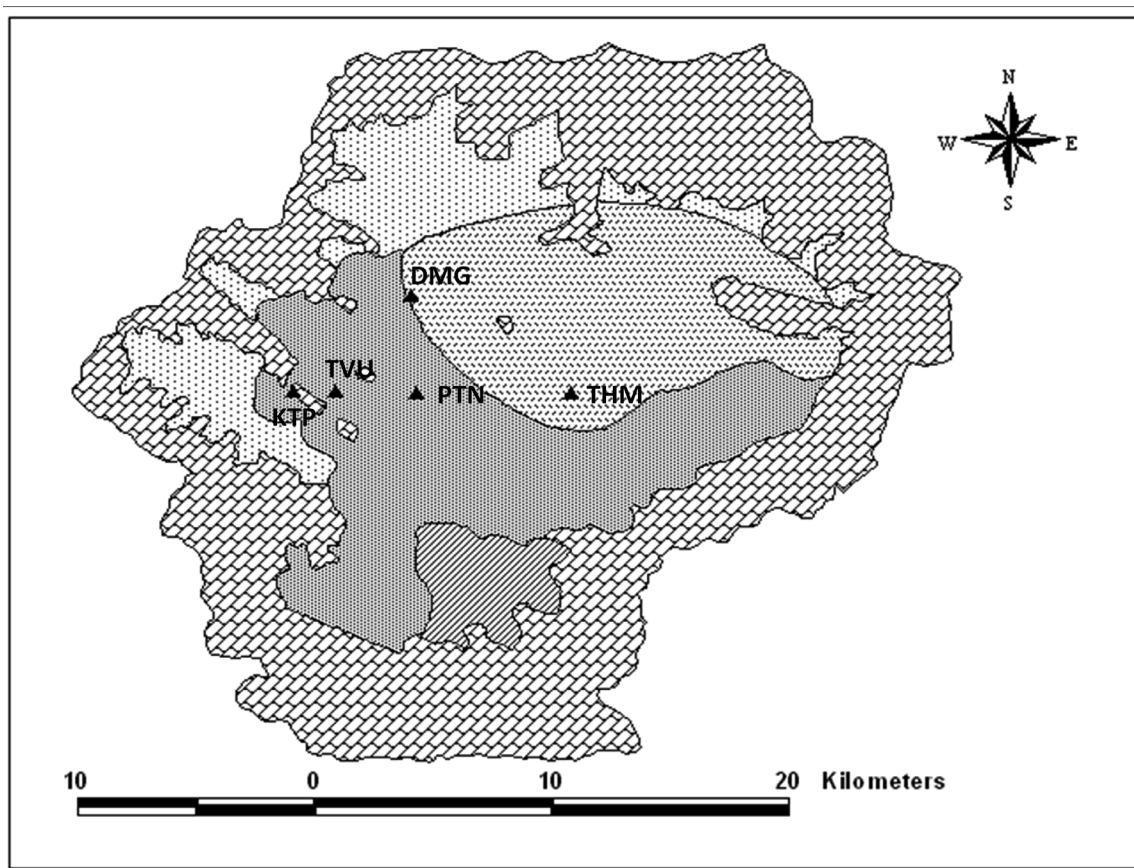
Fig. 5: Geology of the Kathmandu Valley (modified from Sakai and Kuwahara 2002) with the location of five accelerometers (black triangles).

RESULTS

Peak ground acceleration is one of the most common parameters used in engineering applications. The records of the ground acceleration history are presented in Fig. 6 through Fig. 8 recorded by three components (E-W, N-S and V) at KTP, TVU, PTN, THM and DMG sites respectively. The maximum PGA (24 gal) is recorded by the E-W component at the DMG site (Fig. 6), which is a soil site. Similarly, the rock site (KTP) has recorded the smallest PGA (6 gal) on the corresponding E-W component (Fig. 8). The PGA recorded by the E-W component at TVU and THM sites are comparable (Table 2, Fig. 6, 7 and 8).
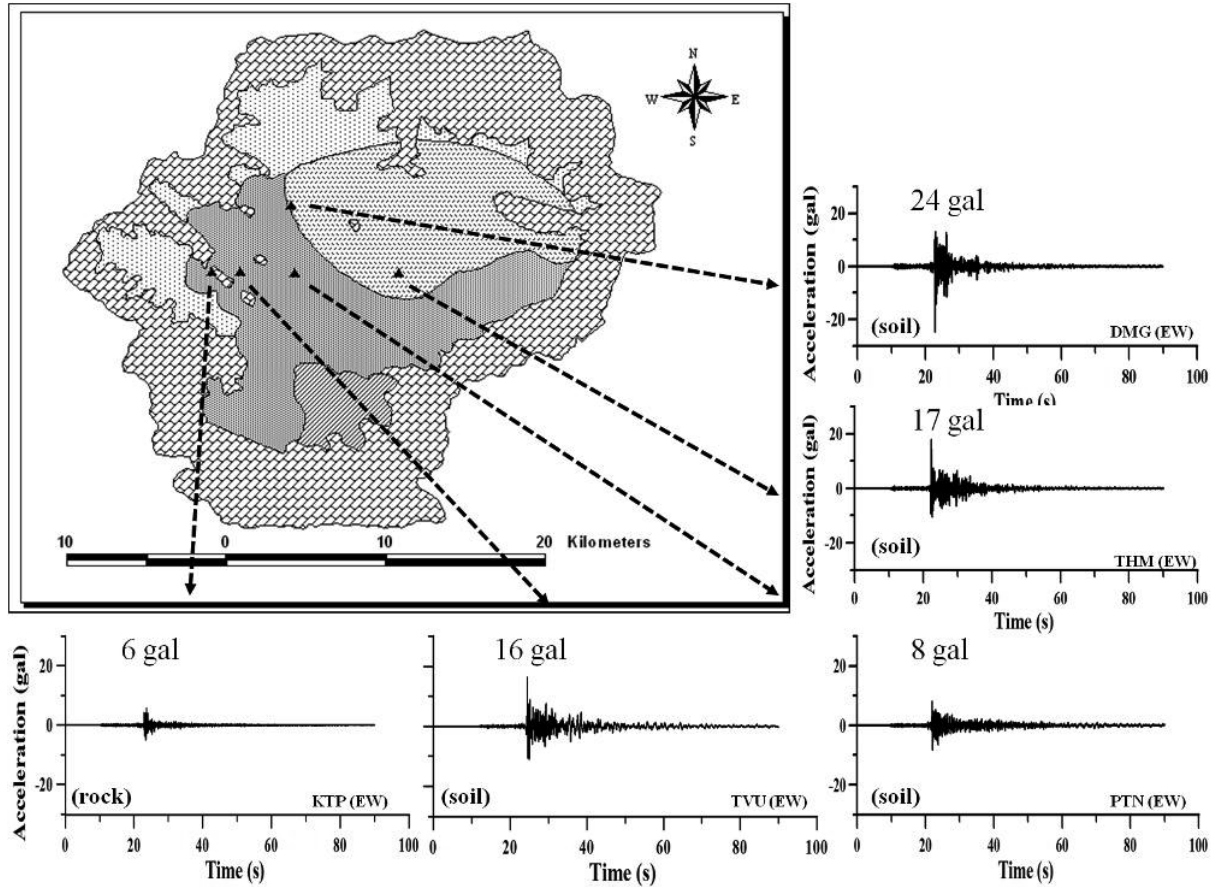
Fig. 6: Ground acceleration history recorded by east-west component at the five sites. Note the duration as well as the amplitudes, at soil sites, are larger in comparison to the rock site (KTP) site.

Despite being a soil site, the PTN site (Pulchowk Campus, Lalitpur) shows comparatively smaller PGA than at other soil sites (TVU, THM and DMG). Smaller PGA at PTN site than expected implicates either bedrock is at shallow depth under the area or the thickness of clay layers is small in comparison to at other soil sites.

Table 2: Peak ground accelerations observed at five sites

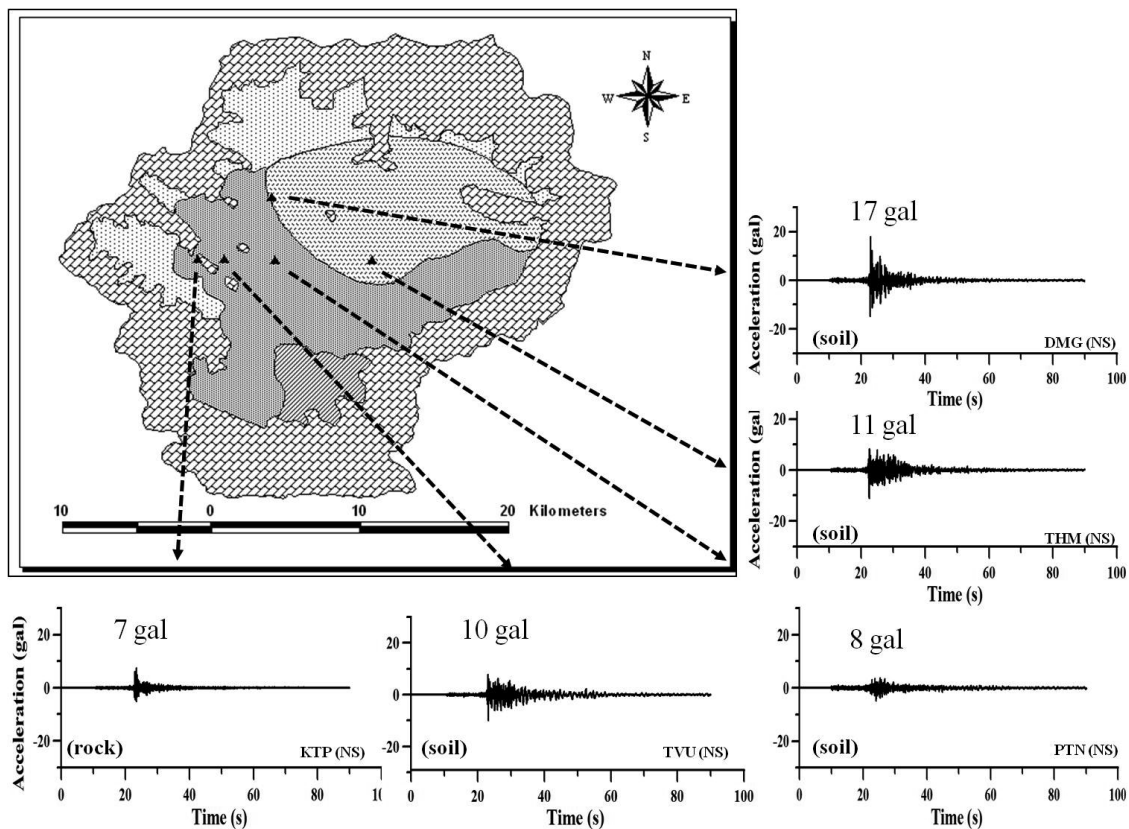| Site	Peak ground acceleration (gal, 1 gal = 1 cm/sec^2) recorded by accelerometers		
	Vertical	North-South	East-West
KTP (rock)	7	7	6
TVU (soil)	7	10	16
PTN (soil)	5	8	8
THM (soil)	7	11	17
DMG (soil)	8	17	24

Fig. 7: Ground acceleration history recorded by north-south component at the five sites. Note the duration as well as the amplitudes, at soil sites, are larger in comparison to the rock site (KTP) site.
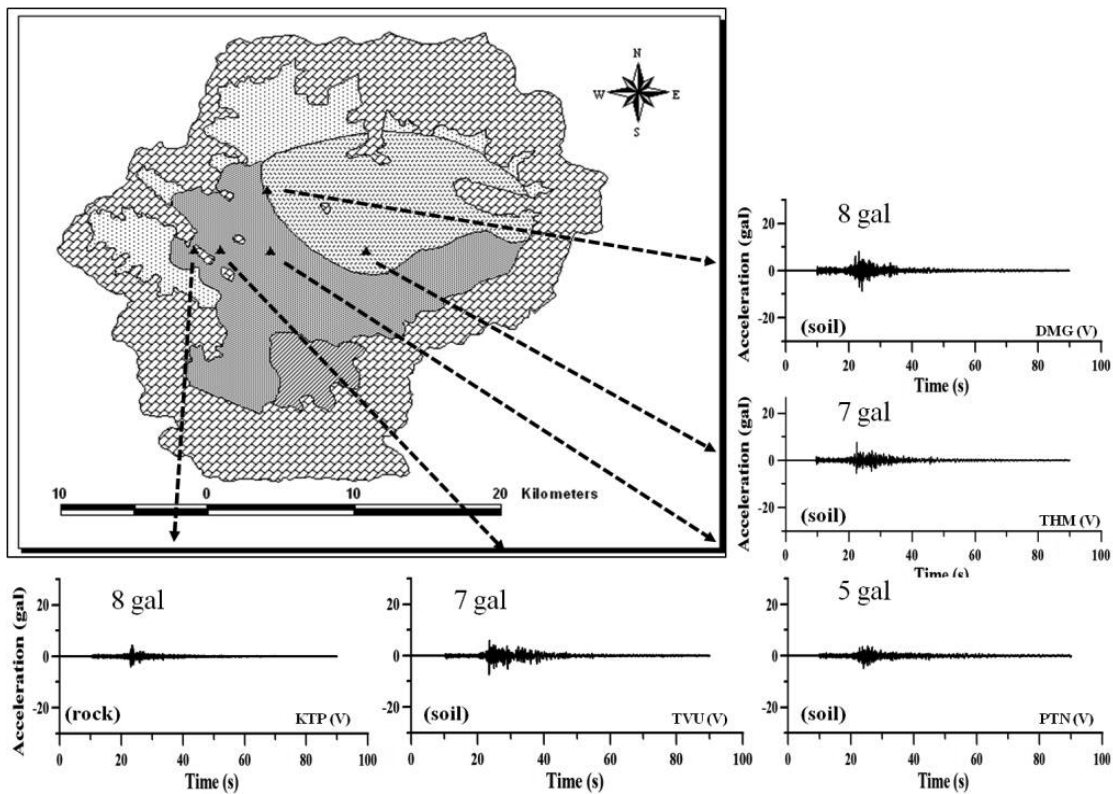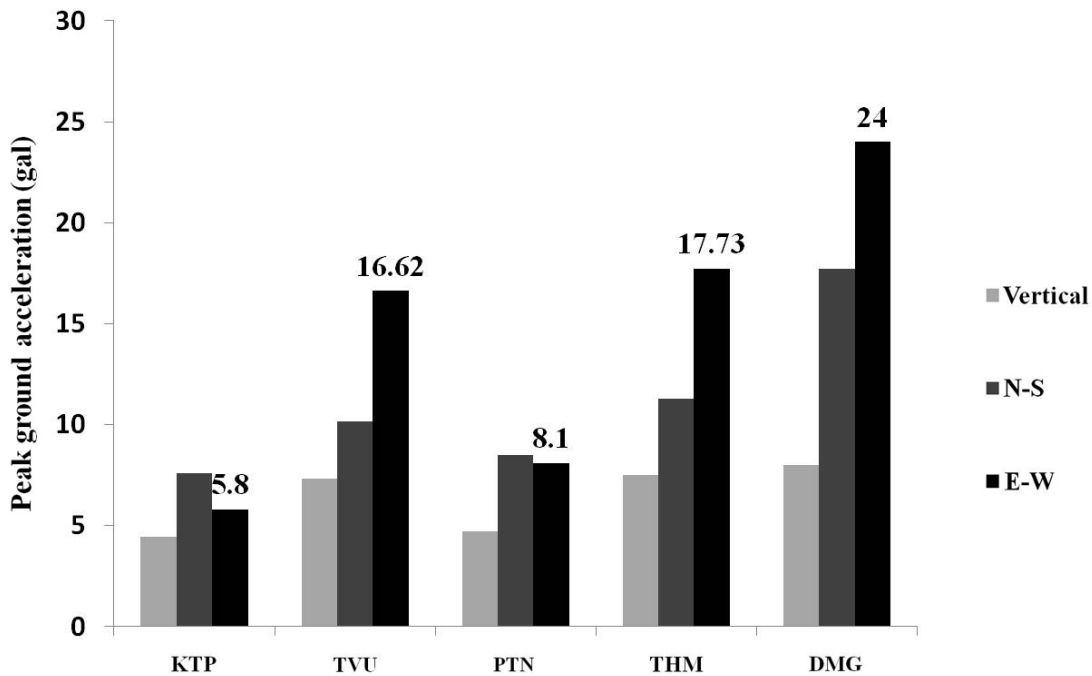

Fig. 8: Ground acceleration history recorded by vertical component at the five sites.

Fig. 9: Peak ground acceleration (PGA)s observed by three components (E-W, N-S and V) of accelerometers at the five sites (KTP is a rock site and others are soil sites.)

The Fourier amplitude spectra of the ground acceleration history (for E-W and N-S components) are presented in Fig. 10. Three soil sites (TVU, THM and DMG) show large peaks of Fourier amplitudes distributed at frequencies between 2 Hz and 5 Hz. The N-S component at the rock site (KTP) reveals a peak at a frequency larger than 5 Hz; however, the E-W component shows two peaks at less than 5 Hz. The Fourier amplitudes at the rock site are smaller, in the case of all components, than that at the rock sites. Three soil sites, namely TVU, THM and DMG show, more or less, similar characteristics, whereas PTN shows difference.

Spectral ratios at a soil site relative to a reference site, especially a rock site, are used to investigate site effect of the subsurface geology to seismic motion. In this study, spectral ratios are calculated assuming the PGA at the rock site (KTP) represents the PGA at bedrock beneath the sedimentary deposit in the Kathmandu Valley. The spectral ratios are calculated at four soil sites (TVU, PTN, THM and DMG) relative to the reference (rock) site (KTP). The spectral ratio (Fig. 11) shows peaks (amplitude 30 to 50) at 0.3 to 0.5 Hz at the low frequency range. Similarly there is another peak (amplitude 10 to 20) at 1.5 Hz of the record.

DISCUSSION AND IMPLICATIONS

It is well known that the Kathmandu Valley experienced substantial damage from the 1934 Bihar-Nepal earthquake. This earthquake killed about 4,296 people (Pandey and Molnar 1988) in the Kathmandu Valley only. It was reported that the destruction pattern was not same in the valley (Rana 1935; Pandey and Molnar 1988). As per the earthquake intensity map redrawn by NSET (2011), the KTP (rock) site falls in Modified Mercalli Intensity (MMI) Zone VIII and the other sites, which overlie thick sediments, fall in MMI zone IX. Such a variation is attributed to the amplification of seismic wave amplitude in areas underlain by soft sediments.

In this study also, we observed variations in the levels of ground acceleration (PGA) as recorded by accelerometers at different places in the valley. The largest ground acceleration (24 gal) is recorded by the east-west (E-W) component of the accelerometer installed in the Department of Mines and Geology (DMG), which is a soil site. Similarly the smallest acceleration (6 gal) on the horizontal components is recorded by the E-W component at the reference (KTP, rock site).
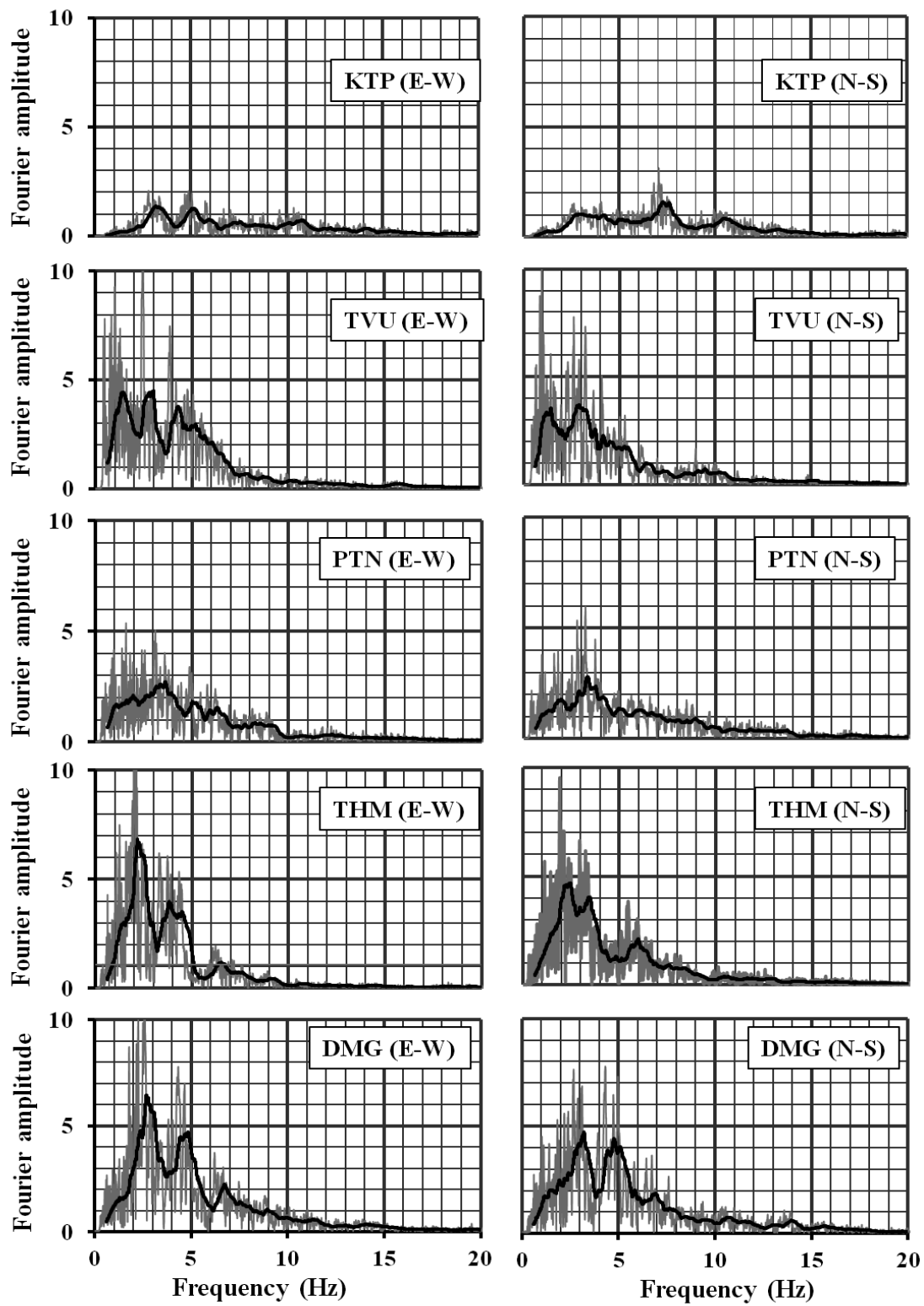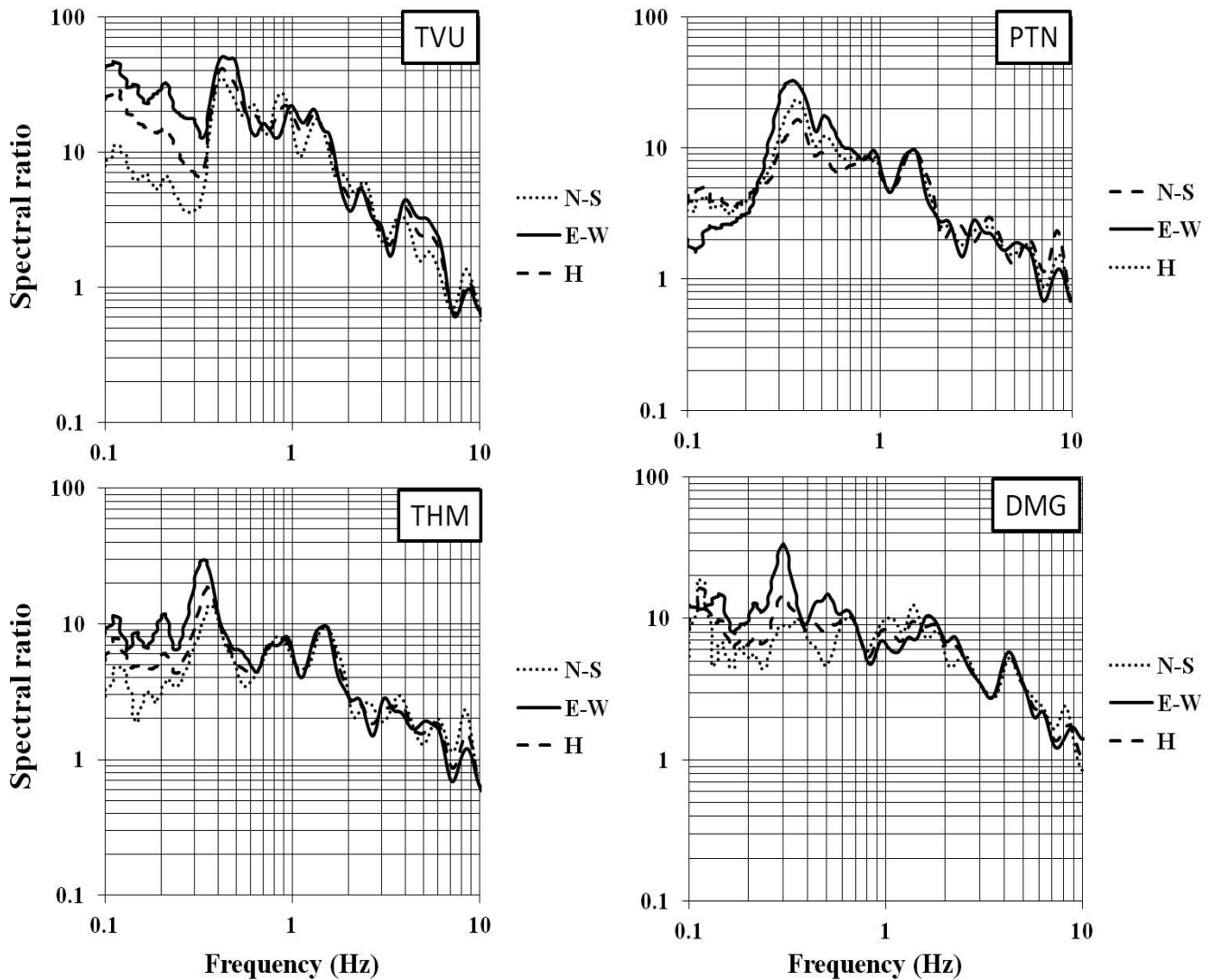
Fig. 10: Fourier amplitude (cm/sec) spectra of ground acceleration data recorded by two components (E-W and N-S) of accelerometers at the five sites.

Fig. 11: Spectral ratios calculated at the four soil sites (CDG, ENG, UGC, and DMG) with reference to the rock site (KTP). N-S, E-W and, H stand for north-south, east-west and mean of the horizontals components respectively).

The peak ground accelerations (16 gal) recorded by the E-W component (Fig. 7) at the TVU (soil site), which is merely a few hundred meters from the KTP (rock site, Fig. 6), and that recorded by the E-W component (17 gal) at the THM (soil site), Sanothimi, Bhaktapur (Fig. 9) are almost equal. The large difference in PGA observed between KTP (6 gal) and TVU (16 gal) implicates geology is very different at these two sites despite they are very close. It can be inferred that the TVU, a soil site, possibly overlies thick succession of clay. The accelerometer installed in the Pulchowk Campus, Institute of Engineering, Lalitpur shows surprisingly smaller value of PGA in comparison to other soil sites (DMG, THM, and TVU). The smaller PGA and Fourier amplitude at PTN implicates that possibly rock is present at shallow depth beneath the site.

The spectral ratio (Fig. 11) shows large amplitude at 0.3 to 0.5 Hz at the four soil sites (TVU, PTN, THM and DMG) relative to the reference rock site (KTP). The peaks at 0.3 to 0.5 Hz possibly represent the response of the basin, whereas that at 1.5 Hz could be the one dimensional response of soil column. Additionally, there are peaks at higher frequencies (>1.5 Hz), which are different for each site. The peaks at higher frequencies, which are different at the sites, are likely to be the response of shallow sedimentary layers, implying that there is strong spatial variability of soil properties across the valley. The peaks at 0.3, 0.5 and 1.5 Hz correspond to buildings of approximately 33, 20 and 6 stories respectively, which in turn reveals the vulnerability of these structures to future events.

The four soil sites that cover a large fraction of the valley surface show remarkable similarity (in low frequency range) in terms of site amplification except in the very high frequency range, and are dominated by long period amplification effects due to resonance of the basin. This similarity doesn't contradict the PGA differences observed at the soil sites, because the PGA is a high frequency characteristic of ground motion–

namely, the sites that only differ in the very near surface in terms of geology and have site amplification very similar in longer periods, like THM, PTN and DMG, can still have very different PGAs, especially since this event is very small magnitude, and thus very rich in high frequencies.

CONCLUSIONS

The analysis of the ground acceleration data, recorded by five accelerometers in the Kathmandu Valley, reveals the response of the sediments of Kathmandu Valley to seismic motion. The observed PGA is not the same at all the soil sites, with the maximum value at DMG and the least at PTN. In the low frequency range, all sites show similar characteristic in terms of amplification, however at high frequencies, the pattern is different. Such variation at high frequency range, possibly, arises from the response of shallow sedimentary layers which, possibly, varies from place to place.

The Kathmandu Valley has witnessed rapid urbanization in the last two decades. The population in the Valley is increasing very rapidly because of various reasons prevailing in the country. It is very important to plan, in time, in order to minimize the possible loss of lives and property from unpredictable future earthquakes than rescuing afterwards. This study is a small attempt to assess the response of the Kathmandu Valley sediments to seismic ground motion in which ground acceleration data of an earthquake that occurred at 76 km distance from the valley and recorded by five accelerometers in the valley is used. To get a better represented picture of the ground response of the sedimentary deposit over the whole area in the Kathmandu Valley, it is important to install and operate a dense network of accelerometers, homogeneously distributed and closely spaced, in the Kathmandu Valley. The long term operation of such a network would help to record earthquakes from a range of magnitudes, mechanisms, distances and azimuths so that ground response of the valley sediments could be better estimated and constrained. Findings of such a study will be fundamental input in the seismic hazard assessment, building code revision and seismic vulnerability assessment of the valley, which would help to adopt appropriate countermeasures to minimize the loss of lives and property from future destructive earthquakes.

The result presented in this article is as observed for the mentioned earthquake which occurred in South-Tibet and should not be generalized in all cases because magnitude, source-site distance, directivity of fault rupture, mechanism of the fault rupture and azimuth of the causative fault plane to the source also play a role in the ground response.

ACKNOWLEDGEMENTS

REFERENCES

Bhattarai M., Gautam U., Pandey R., Bollinger L., Hernandez B., and Boutin V., 2011, Capturing first records at the Nepal NSC accelerometric network. Journal of Nepal Geological Society, v. 43 (Special Issue), pp. 137-144.

Bilham, R., 1995, Location and Magnitude of the 1833 Nepal Earthquake and its Relation to the Rupture zones of Contiguous Great Himalayan earthquakes. Current Science, v. 69(2), pp. 155-187.

Bilham, R., Ambraseys, N., 2004, Apparent Himalayan slip deficit from the summation of seismic moments for Himalayan earthquakes. Current Science, pp. 1500-2000.

Chitrakar, G. R. and Pandey, M. R., 1986, Historical Earthquakes of Nepal. Journal of Nepal Geological Society, v. 4, No. 1, pp. 7-8.

Hernandez, B., Bollinger L., and Boutin, V., 2011, DIAMANT. Traitement des donneìes acceìleìromeìtriques et calcul d'indicateur de nocivité sismique. Guide d'utilisation. CEA/ DIF/DASE/LDG/2011/DO, pp. 1-34.

Nakamura Y (1989), "A method for dynamic characteristics estimation of subsurface using microtremor on the ground surface," Quarterly Report of the Railway Technical Research Institute, 30 (1):25-33.

NSET, 2011, Earthquake intensity map of 1934 Earthquake in Kathmandu Valley.

Pandey M. R. and Molnar P., 1988, The distribution of intensity of the Bihar-Nepal Earthquake of 15 January 1934 and bounds on the extent of the rupture zone. Journal of Nepal Geological Society, v., 5, No., 1, pp 22-44.

Pandey M. R., 2000, Ground Response of Kathmandu Valley based on microtremors, 12WCEE, 2000 (unpublished)

Pandey, M. R., Tandukar, R. L. P., Lave, J. P., Massot, J. P., 1995, Interseismic Strain Accumulation on the Himalayan Crustal Ramp, Nepal. Geophysical Research Letters, v. 22, No. 7, pp. 751-754.

Pandey, M. R., Tandukar, R. P., Avouac, J. P., Vergne, J., Heritier, T., 1999, Seismotectonics of the Nepal Himalaya from a local seismic network. Journal of Asian Earth Sciences v. 17, pp. 703-712.

Paudyal, Y. R. et. al., 2012, Seismic Microzonation of Densely Populated Area of Kathmandu Valley of Nepal using Microtremor Observations. Journal of Earthquake Engineering, 16:8, 1208-1229.

Rajaure, S., Sapkota, S. N., Adhikari, L. B., Koirala, B., Bhattarai, M., Tiwari, D. R., Gautam, U., Shrestha, P., Maske, S., Avouac, J. P., Bollinger, L., and Pandey M. R., 2013, Double difference relocation of local earthquakes in the Nepal Himalaya. Journal of Nepal Geological Society, v. 46, pp. 133-142.

Rana, Maj. Gen. Brahma Shamsher J. B., 1035, Nepalko Mahabhukampa (The Great Earthquake of Nepal), Published in the Kathmandu by the author, second edition.

Sakai, H., 2001, Stratigraphic division and sedimentary facies of the Kathmandu Basin sediments. Journal of Nepal Geological Society, v. 25 (Sp. Issue), pp.19-32.

Sakai, H., Fujii, R., and Kuwahara, Y., 2002, Changes in the depositional system of the Paleo-Kathmandu Lake caused by uplift of the Nepal Lesser Himalayas. Journal of Asian Earth Sciences, v. 20, pp. 267–276.

Sheehan, A. F., Torre, Thomas de la, Monsalve, G., Schulte-Pelkum, vera, Bilham, R., Blume, F., Bendick, R., Wu, F., Pandey M. R., Sapkota, S., Rajaure, 2007, Earthquakes and Crustal Structure of the Himalaya from the Himalayan-Nepal-Tibet seismic experiment (HIMNT). Journal of Nepal Geological Society, sp. v., p. 8.

Stöcklin, J., 1980, Geology of Nepal and its regional frame:Geological Society [London] Journal, v. 137, pp. 1–34.

Torre, T. L. de la., Monsalve, G., Sheehan, A. F., Sapkota, S., and Wu, F., 2007, Earthquake processes of the Himalayan collision zone in eastern Nepal and the southern Tibetan Plateau, Geophys. J. Int. (2007), v. 171, pp 718–738.

Waldhauser, F. and Ellsworth, W. L., 2000, A Double-Difference Earthquake Location Algorithm: Method and Application to the Northern Hayward Fault, California. Bulletin of Seismological Society of America, v. 90, no. 6, pp. 1353-1368.

2. Rajaure, S., Dhital, M., & Paudel, L. (2015). The 2015 Gorkha Earthquake and response of the Kathmandu Valley sediments. *Journal of Nepal Geological Society*, *49*(1), 1-5. https://doi.org/10.3126/jngs.v49i1.23136

The 2015 Gorkha Earthquake and response of the Kathmandu Valley sediments

*Sudhir Rajaure[1], Megh Raj Dhital[2], Lalu Prasad Paudel[2]
[1]Department of Mines and Geology, Nepal
[2]Central Department of Geology, Tribhuvan University, Nepal
*Email: srajaure@gmail.com

ABSTRACT

The Gorkha Earthquake occurred on the gently dipping part of the Main Himalayan Thrust (MHT), close to the Main Central Thrust (MCT). This earthquake possibly occurred in the source zone of the 1833 Nepal Earthquake (Mw 7.6), which occurred after 182 years. The region between the 1905 Kangra Earthquake and 1934 Bihar-Nepal Earthquake has not produced any great earthquake since the last 500 years and still remains a potential site for great earthquake(s) in future. The Kathmandu Valley witnessed moderate ground acceleration and comparatively large velocity as recorded at Kantipath during the Mw 7.8, Gorkha Earthquake. The analysis of the records show that high frequencies were damped and low frequencies were dominant over the sedimentary basin, which can be attributed to the response of the sediments underneath. Because of damping of high frequencies, the engineered, low storey buildings were less damaged and resisted the ground shaking comparatively well. However, on the other hand, the historical monument 'Dharahara' collapsed completely and the high rise apartment buildings suffered more because of the dominance of low frequencies.

Keywords: Peak ground acceleration, predominant period, high frequency, low frequency and damping

INTRODUCTION

The Himalayan Range is an active collisional orogen, which is about 2400 km long. It falls in the boundary between the Indian Tectonic Plate and the Eurasian Tectonic Plate. The Indian Tectonic Plate is moving towards north at an average velocity of about 4 cm a year relative to Eurasia (e.g. Bettinelli et al. 2006). Approximately half of this convergence is absorbed across the Himalaya in straining the crust and resulting in the accumulation of elastic stress in the region. The accumulated elastic stress is released in the form of earthquakes, when the elastic stress exceeds the strength of surrounding rock. Large earthquakes occur less frequently but are capable to cause unimaginable loss of lives and property. It is a cyclic process, because after the release of accumulated energy by large earthquakes, accumulation of energy starts again for next large earthquake right after. Small earthquakes occur frequently but do not contribute much to release the stored elastic energy; therefore large earthquakes are inevitable to release the energy in time and again.

In the last century, the Himalaya hosted four destructive earthquakes, which are the 1897 Shillong Earthquake (Mw 8.1), 1905 Kangra Earthquake (Mw 7.8), 1934 Bihar-Nepal Earthquake (Mw 8.1) and 1950 Assam Earthquake (Mw 8.5) (Ambraseys and Douglas 2004, Seeber and Armbruster 1981, Khattri 1987, Molnar 1990, Molnar and Pandey 1989, Hough and Bilham 2008, Yeats and Lillie 1991, Yeats et al. 1992). The region between the 1934 Bihar-Nepal Earthquake (Mw 8.1) and the 1905 Kangra Earthquake (Mw 7.8) has been reported

not to have produced any great earthquake since the last five hundred years. This stretch of the Himalaya has been termed as seismic gap (Khattri 1987, 1992, Bilham et al. 1995), which is suspected as the site of next great destructive earthquake in the region in future. It should be noted that any earthquake source region has a maximum magnitude potential, which depends on the size (area and length) of the source zone but there is probability of smaller (Mw <8.0) earthquakes (e. g. Kramer 2008) and therefore smaller earthquakes may also occur.

Nepal occupies about one-third arc length of the Himalaya. It falls in a seismically high hazard zone (e. g. Thapa and Wang 2013), which has been reported to have experienced many destructive earthquakes in its written history. Since 1255, the Kathmandu Valley has been reported to have experienced five major destructive earthquakes in 1225, 1408, 1681, 1833 and 1934. The magnitudes of these earthquakes are estimated to be more than 7.5 (Chitrakar and Pandey 1986, Bilham et al. 1995, Pandey et al. 1995, Hough and Bilham 2008). Among these, the 1934 Mw 8.1 Bihar-Nepal earthquake is the most destructive one, which claimed more than 10,700 lives in Nepal and adjoining part of India. This earthquake had a maximum intensity of MMI X in the Kathmandu Valley, which destroyed about 19% and damaged about 38% of the buildings in the valley (Pandey and Molnar 1988, Rana 1935). The 18 September 2011 earthquake has been felt in six countries, i.e. Bangladesh, Bhutan, China, India, Pakistan and Nepal, causing the death toll of more than 100 people in the region (Thapa and Wang 2013). The last great earthquake of 1934 is still in the

living memory of elder people. This earthquake claimed about 4296 (e. g. Pandey and Molnar 1988) lives in Kathmandu Valley only. Documented records of destruction reveal that the Kathmandu Valley has experienced many destructive earthquakes in the past (e.g. Chitrakar and Pandey 1984).

Similar reports of past destructive earthquakes from the western part of Nepal are not available. An Mw 8.5 earthquake reportedly destroyed the western part of Nepal along with the adjoining part of south Tibet and north India (Bilham et. al. 2004). Thus, the region in western Nepal, between Gorkha and Dehradoon of India was anticipated to host great earthquake(s). In contrary to the anticipation, the Gorkha Earthquake (Mw 7.8) occurred in the region, which is believed to have hosted the 1833 Nepal Earthquake (~Mw 7.6, Bilham). Thus, this earthquake can be considered as a repeat of the 1833 (Mw 7.6) Nepal Earthquake. The rupture of the the earthquake did not propagate towards west and the energy stored in that region, which is known as a 'seismic gap', is not released, therefore the threat of great earthquake(s) in the west of Gorkha remains unchanged.

Previous Works

The response of the Kathmandu Valley was first studied by Pandey (2004). He used relative power spectra of ambient noise recorded at 60 soil sites with reference to that recorded at rock site in the Kathmandu Valley. He reported that the amplified predominant frequency is at 2 Hz and the amplification factor ranges between 12 and 15. Similarly there are other peaks of amplification in the frequency range between 0.6 and 5 Hz, but the amplification factor varies across the valley. The amplification factor is about 5 to 6 in the lacustrine area, between 2 to 3 in transitional area and between 1 and 2 in fluviatile area.

Paudyal et al. (2012) applied horizontal-to-vertical ratio of Fourier spectra (H/V ratio technique) of ambient noise recorded at soil sites to estimate fundamental frequency at different parts of the Kathmandu Valley. They reported that the valley has fundamental frequencies in the range between 0.6 to 8.9 Hz in the central and northern part of the sedimentary basin. In addition to the fundamental frequency, they report other peaks between 4 and 6 Hz in the central and northern part of the sedimentary basin.

Rajaure et al. (2014) investigated the response of the Kathmandu Valley sediments using ground acceleration data recorded in the Kathmandu Valley. It is the first investigation of its kind in the Kathmandu Sedimentary basin, which used acceleration data recorded at four soil sites and one rock site. They used the ground acceleration data of the 30 August 2013, South-Tibet Earthquake (M4.9) recorded at five sites in the Kathmandu valley. They evaluated the site response function as ratio of Fourier amplitude spectrum at soil site with reference to that at a rock site. The response of the soil sites are found remarkably similar in the low frequency domain (<0.8 Hz), whereas variation in response can be noticed above 0.8 Hz. The prominent variation exists at frequencies larger than 2 Hz,

which is in consistence with the variation of PGA across the valley implying the shallow depth geology is inhomogeneous. The earthquake was a smaller one and the variation of PGA across the valley has been interpreted as the response of shallow sedimentary layers, which possibly varies laterally across the valley.

Gorkha Earthquake

The Kathmandu Valley and other northern districts between Gorkha (in the west) and Dolakha (in the east) were violently shaken by the 12 April 2015 Gorkha (Mw 7.8, USGS) Earthquake. This is the largest earthquake after the 1934 Bihar-Nepal Earthquake to hit Nepal. The earthquake occurred at 06:11:46 (UTC) in the morning and according to the National Seismological Centre (NSC) of Department of Mines and Geology (DMG), the earthquake occurred at 28.24° N latitude and 84.75° E longitude with focal depth at 15 km. The Seismic network of the Department of Mines and Geology has recorded the earthquake and its aftershocks very well. The distribution of aftershocks (source: www.seismonepal.gov.np) and the fault plane solutions (source: www.isc.ac.uk) depict that the Gorkha Earthquake (Mw 7.8) and the 26 April aftershock (Mw 6.9) occurred on east-west trending, low angle thrust fault (Fig. 1).

This Gorkha earthquake and its aftershocks have caused massive destruction in the region between Gorkha and Dolakha. The epicenter of this earthquake falls in the western part of Gorkha District, at a distance of about 80 km from the Kathmandu Valley. This earthquake was followed by a number of aftershocks in which three aftershocks were strong ones. The first aftershock of Mw 6.5 occurred on 25 April, which is close to the the main shock. The second aftershock (Mw 6.9) occurred on 26 of April in Dolakha District at about 80 km in the north-east direction from the Kathmandu Valley and the strongest aftershock (Mw 7.3) occurred on 12 May at about 80 KM in the north-east from the Kathmandu Valley. Based on the distribution of aftershocks (Fig. 1) the Gorkha Earthquake ruptured an area of about 150 km in the east-west direction and 40 km in the north-south direction. The Gorkha Earthquake and its aftershocks have claimed more than 8500 lives officially.

Ground Motion Parameters

Peak ground acceleration is a high frequency characteristic of ground motion. The observed accelerations during the Gorkha Earthquake are smaller than what was expected and therefore the intensity of this earthquake is comparatively low. The epicentral intensity of this earthquake is about VIII and the intensities in the Kathmandu Valley are only about VI to VII. The peak ground acceleration (PGA) recorded at Kantipath (USGS site) is about 182.5 cm/sec^2 (Fig. 2a) on the vertical component and on the horizontals it's even smaller. However, on the other hand, the velocity is comparatively large (Fig. 2b). Velocity is a low frequency characteristic of the ground motion and is an important parameter for flexible type structures (tall buildings).
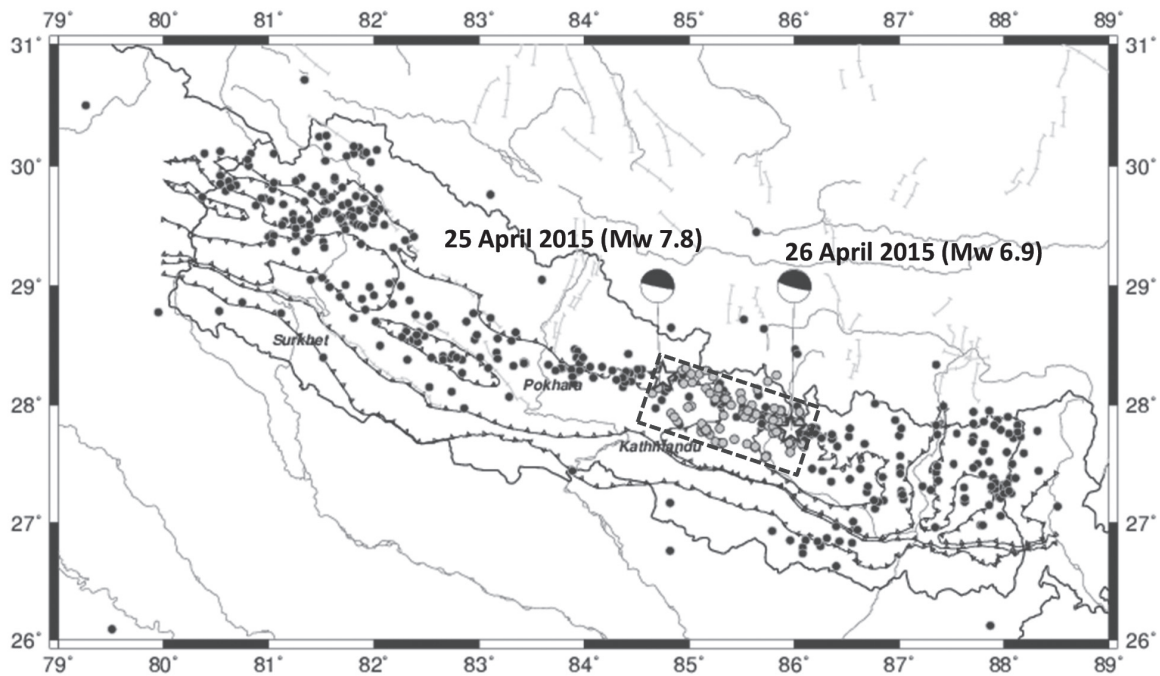
Fig. 1: The Gorkha earthquake (white star at the left), its strong aftershock (Mw 6.9) at the right (white star) and the aftershocks (grey solid circles) which occurred by 30th of April. The black circles are the ML>4.0 earthquakes released by the National Seismological Centre of Department of Mines and Geology (1994-2014). The black dashed rectangle is the inferred rupture area of the Gorkha Earthquake. Fault plane solutions are from the International Seismological Centre (UK).
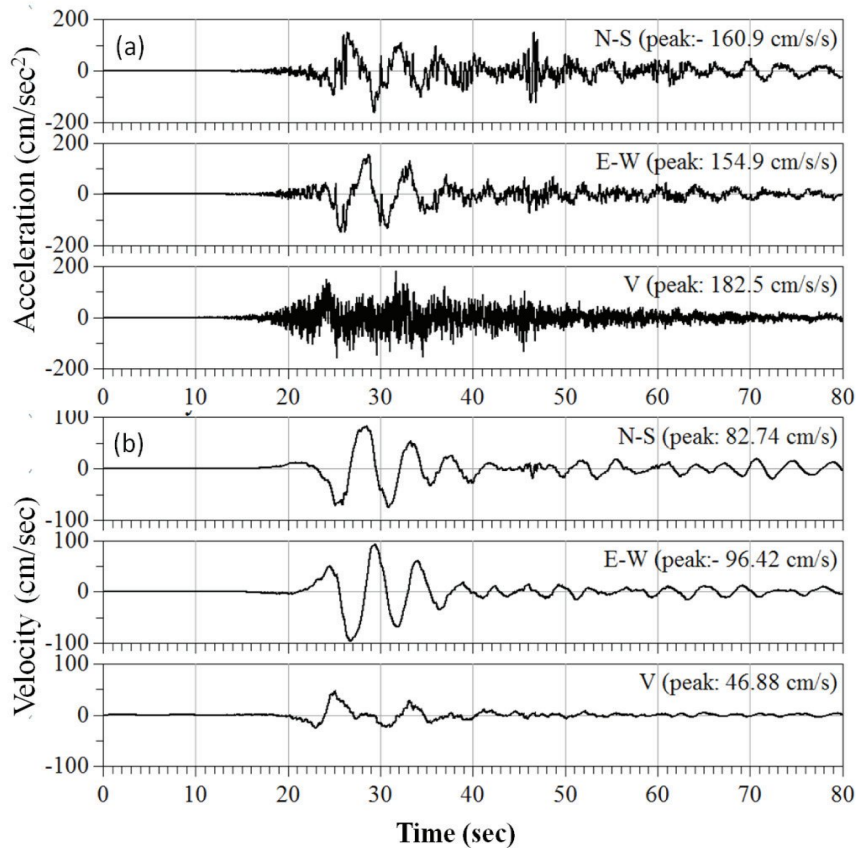
Fig. 2: Ground acceleration (a) and velocity (b) recorded at Kantipath. The maximum peak ground acceleration is observed on the vertical component, whereas the maximum peak ground velocity is observed on the east-west component.

A Fourier amplitude spectrum depicts how the amplitudes are distributed with frequencies (or period) in the ground motion. Fig. 3(a) depicts the distribution of amplitudes with frequency at the Kantipath site and reveals that the high frequencies were damped and low frequencies were dominant. The predominant frequency of the ground motion at Kantipath is about 0.2 Hz. In addition to the peak at 0.2 Hz, two more peaks are noticed at 0.6 Hz and 1.25 Hz in the spectra (Fig. 3a).

Fig. 3: Fourier amplitude spectra of the ground motion at the Kantipath site (a) and H/V ratio of the ground motion (b). The predominant frequency of the ground motion is about 0.2 Hz.

The ratio of Fourier spectrum of horizontal component to that of the vertical component (known as H/V ratio) at a soil site is commonly used to estimate the fundamental frequency of the ground. This technique is commonly used to estimate fundamental frequency of soil site using ambient ground noise. In this study, the H/V ratio technique is applied to earthquake data recorded at the Kantipath site. Here, the H/V ratio is calculated using the following formula.

$$\text{H/V ratio} = \sqrt{\frac{F_{NS}^2 + F_{EW}^2}{F_{Vertical}}}$$

Where, F_{NS}, F_{EW} and F_V stand for the Fourier amplitude of north-south, east-west and vertical components of the ground motion, at the corresponding frequencies, respectively.

The H/V ratio of the earthquake data recorded at Kantipath is presented in Fig. 3(b). The figure shows that the fundamental frequency of the ground is about 0.2 Hz (5 Sec). The fundamental frequency of the ground closely correlates with the predominant frequency of the ground motion.

DISCUSSION AND CONCLUSIONS

Great earthquake was anticipated in the region, west of Gorkha District based on historical records of earthquakes and paleoseismic investigation in the region. However, the Gorkha Earthquake occurred in the region which is believed to have produced the 1833, Nepal Earthquake. Therefore, the threat of great earthquake in the west of Gorkha remains unchanged.

The Gorkha Earthquake occurred on a gently dipping part of the Main Himalayan Thrust beneath the Gorkha District. It ruptured an area of about 150 km in the east-west direction and 40 km in north south direction. The rupture of the earthquake did not propagate towards west of the epicenter, possibly, because a major transverse structure exists close to the epicenter as can be noticed in the result by Pandey et al. (1999) and Rajaure et al. (2013), where the NW-SE, trending seismicity belt is offset.

The Kathmandu Valley is underlain by thick succession of sedimentary layers. During the Gorkha Earthquake, the recorded peak ground acceleration was smaller than expected, however the velocity was relatively large. Peak ground acceleration is a high frequency characteristic of ground motion, which is an important parameter to rigid structures (small storey structures). During the Gorkha Earthquake, high frequencies were damped and therefore majority of the small storey structures survived the ground shaking. On the other hand, the peak ground velocity is a low frequency characteristic of ground motion and is an important parameter to the flexible structures (tall buildings). The damage to tall buildings correlates well with the large peak ground velocity.
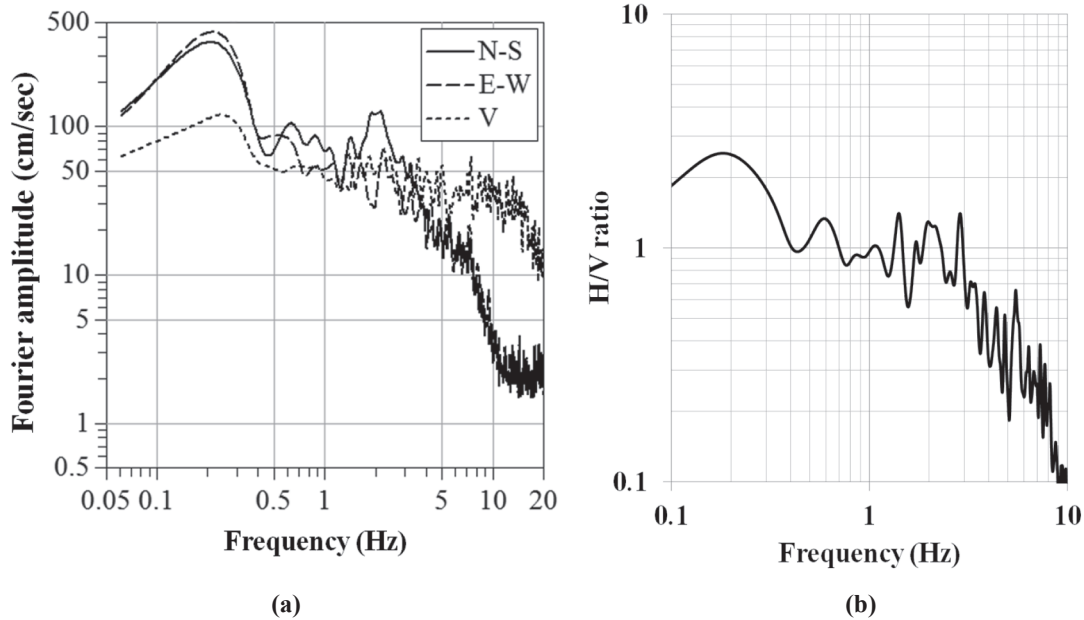
The fundamental frequency of the Kantipath site is about 0.2 Hz. Similarly, there are two other peaks at 0.5 Hz and 1.5

Hz, respectively. The peak at 0.2 Hz, observed in this study, is not noticed in the report of Paudyal et. al. 2012. The peaks at 0.2 Hz and 0.5 Hz possibly represent the basin response, whereas the peak at 1.5 Hz represents the response of shallow sedimentary layer. Multiple resonant frequencies at the site implicate the possibility of resonance at different frequencies

The results presented here correspond to the Kantipath site, which is a soil site and is in the middle part of the Kathmandu Valley. The geology of the Kathmandu Valley is highly variable and its response could be, different at different places accordingly. A thorough investigation of ground response in the Kathmandu Valley would be very helpful to revise building code, strengthen existing structures of historical values and would pave a way for land use planning in the Kathmandu Valley.
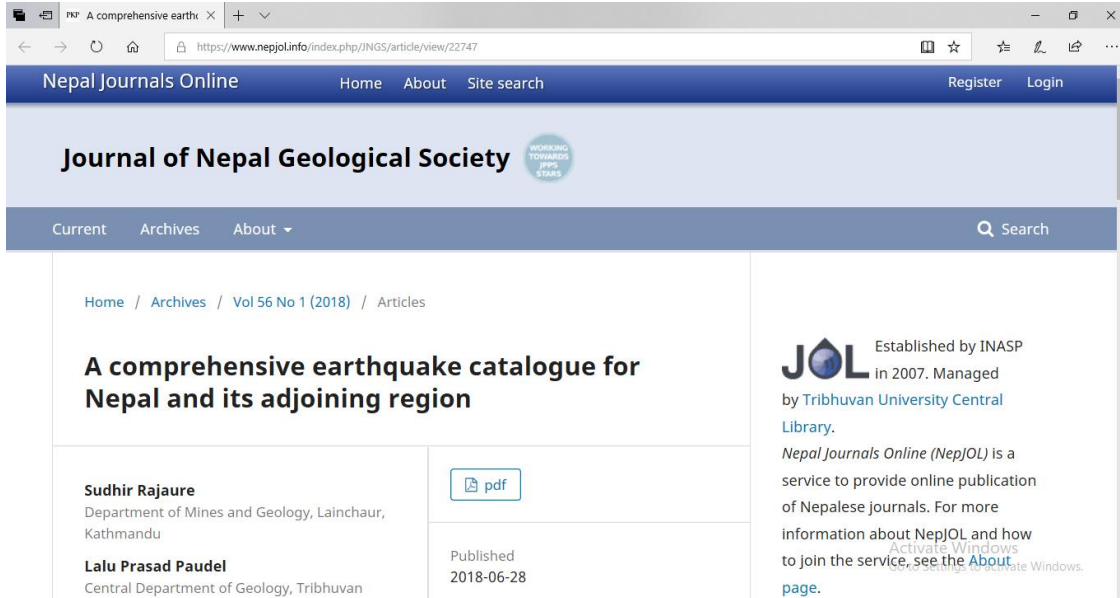
ACKNOWLEDGEMENTS

REFERENCES

Ambraseys, N. N. and Douglas, J., 2004, Magnitude calibration of north Indian earthquakes. Geophys. Jour. Int., v. 159, pp.165–206. doi:10.1111/j.1365-246X.2004.02323.x.

Bettinelli, P., Avouac, J. P., Mireille, F., Jouanne, F., Bollinger, L., Wills, P. and Chitrakar, G. R., 2006, Plate motion of India and interseismic strain in the Nepal Himalaya from GPS and DORIS measurements. Journal of Geodesy. doi: 10.1007//s00190-006-0030-3.

Bilham, R., 2004, Earthquakes in India and the Himalaya: tectonics, geodesy and history. Ann. Geophys., v. 47 pp. 839–858. doi:10.4401/ag-3338.

Bilham, R., 1995, Location and Magnitude of the 1833 Nepal Earthquake and its Relation to the Rupture zones of Contiguous Great Himalayan earthquakes. Current Science, v. 69(2), pp. 155–187.

Bilham, R., Bodin, P. and Jackson, M. 1995, Entertaining a great earthquake in western Nepal; Jour. Nepal Geol. Soc., v. 11(1), pp. 73–78.

Bilham, R., Gaur, V. K. and Molnar, P., 2001, Himalayan Seismic Hazard, Science, v. 293.

Chitrakar, G. R. and Pandey, M. R., 1986, Historical earthquakes of Nepal. Jour. Nepal Geol. Soc., v. 4(1), pp. 7–8.

Department of Mines and Geology (DMG), Seismic data, 1995-2014 (www.seismonepal.gov.np), Kathmandu, Nepal.

Hough, S. E. and Bilham, R., 2008, Site Response of the Ganges Basin Inferred from Re-evaluated Macroseismic Observations from the 1897 Shillong 1905 Kangra and 1934 Nepal Earthquakes. Jour. Earth System and Sci., v. 117, pp. 773–782.

International Seismological Centre. Focal mechanism data, http://www.isc.ac.uk, Internatl. Seis. Cent., Thatcham, United Kingdom.

Khattri, K. N., 1987, Great earthquakes, seismicity gaps and potential for earthquake disaster along the Himalaya Plate boundary. Tectonophysics, v. 138, pp. 79–92.

Khattri, K. N., 1992, Seismic Hazard in Indian Region. Current Sci., v. 62, pp. 109–116.

Kramer, S. L., 2008, *Geotechnical Earthquake Engineering*. Pearson Education, 653 p.

Pandey, M. R. and Molnar, P., 1988, The distribution of intensity of the Bihar-Nepal Earthquake of the 15 January 1934 and bounds on the extent of the rupture zone. Jour. Nepal Geol. Soc., v. 5(1), pp. 22–44.

Pandey, M. R., Tandukar, R. P., Avouac, J. P., Vergne, J. and Heritier, T., 1999, Seismotectonics of the Nepal Himalaya from a local seismic network. Jour. Asian Earth Sci., v. 17, pp. 703–712.

Pandey, M. R., 2000, Ground Response of Kathmandu Valley on the basis of microtremors. 12WCEE, 2000 (unpublished).

Paudyal, Y. R., Bhandary, N. P. and Yatabe, R. 2012, Seismic Microzonation of Densely Populated Area of Kathmandu Valley of Nepal using Microtremor Observations. Journal of Earthquake Engineering, v. 16(8), pp. 1208–1229.

Rajaure, S., Koirala, B., Pandey, R., Timsina, C., Jha, M., Bhattarai, M., Dhital, M. R., Paudel, L. P. and Bijukchhen, 2014, Ground response of the Kathmandu Sedimentary Basin with reference to 30 August 2013 South-Tibet Earthquake. Jour. Nepal Geol. Soc., v. 47, pp. 23–44.

Rajaure, S., Sapkota, S. N., Adhikari, L. B., Koirala, B., Bhattarai, M., Tiwari, D. R., Gautam, U., Shrestha, P., Maske, S., Avouac, J. P., Bollinger, L., and Pandey M. R., 2013, Double difference relocation of local earthquakes in the Nepal Himalaya. Jour. Nepal Geol. Soc., v. 46, pp. 133–142.

Thapa, R. and Wang, G., 2013, Probabilistic seismic hazard analysis in Nepal. Earthquake Eng. and Eng. Vibration, v. 12(4), pp. 577–586.

Molnar, P., 1990, A review of the Seismicity and the Rates of active underthrusting and te deformatation at the Himalaya.

Jour. Himalayan Geol., v. 1, pp. 131–154.

Molnar, P., and Pandey, M. R., 1989, Rupture zones of great earthquakes in the Himalayan Region. Proc. Indian Acad. Sci. (Earth Plan. Sci.), v. 98, pp. 61–70.

Yeats, R. S. and Lillie, R. J., 1991, Contemporary tectonics of the Himalayan frontal fault system: folds blind thrusts and the 1905 Kangra earthquake. Jour. Stru. Geol., v. 13, pp. 215–225.

Yeats, R. S., Nakata, T., Farah, A., Fort, M., Mirza, M. A., Pandey, M. R. and Stein, R. S., 1992, The Himalayan Frontal Fault Sytem. Annales Tectonicae, v. 6, (Sp. Issue) pp. 85–98.

3. Rajaure, S., & Paudel, L. (2018). A comprehensive earthquake catalogue for Nepal and its adjoining region. *Journal of Nepal Geological Society*, *56*(1), 65-72. https://doi.org/10.3126/jngs.v56i1.22747

A comprehensive earthquake catalogue for Nepal and its adjoining region

*Sudhir Rajaure[1] and Lalu Prasad Paudel[2]

[1]Department of Mines and Geology, Lainchaur, Kathmandu, Nepal
[2]Central Department of Geology, Tribhuvan University, Kirtipur, Kathmandu, Nepal
*Corresponding author: srajaure@gmail.com

ABSTRACT

We have prepared a comprehensive earthquake catalogue for Nepal and its adjoining region. The catalogue contains magnitude - homogenized independent earthquakes of magnitude (Mw) between 4.0 and 8.5, which occurred between 1100 AD and 2018 AD. The catalogue contains date, time, latitude, longitude, depth, and magnitude of earthquakes, which are required in the study of seismic activity, tectonics and seismic hazard. Primary earthquake catalogues were collected from the International Seismological Centre (ISC, 2015), United States Geological Survey (USGS), which contain instrumentally recorded earthquake data and date back to 1900 AD. These primary catalogues of instrumentally recorded earthquakes were supplemented by historical earthquakes reported in published literatures, which occurred before 1900 AD. The collected primary catalogues were compiled and processed to develop a comprehensive catalogue. The developed comprehensive catalogue is expected to serve as a basic database for the study of seismic activity and seismic hazard in Nepal and its adjacent area.

INTRODUCTION

Earthquake catalogues provide us basic earthquake information such as the time of earthquake occurrence, their hypocenter locations (latitude, longitude and depth), and magnitudes. The catalogues are often complemented by additional information like damage or other effects. Earthquake catalogues are important in the studies of seismotectonics, seismicity, earthquake physics and hazard analysis (Woessner and Wiemer, 2005). The earlier instrumental records (before 1960) usually had low resolution in time and amplitude, which were manually analyzed. The present instruments and their records are different; the high-resolution digital records are analyzed either interactively or fully automated with the help of an expert.

To understand the seismic activity, seismotectonics and seismic hazard of a region, a complete and magnitude-homogenized catalogue of independent earthquakes is required. The catalogue should contain historical, as well as instrumentally recorded data of earthquakes. Such a catalogue provides us the most direct information of the seismic activity of the region considered.

In Nepal, earthquake catalogues have been prepared specifically for previous studies on seismic hazard assessment by various institutions and researchers (e. g., GSHAP, NBC-105, Pandey et al., 2002; Thapa and Wang, 2013. Ojha et al. (2013) published a catalogue for Nepal for the period between 1255 AD and 2012 AD. These works have compiled data which were available by the time of their completion and do not agree with each other in terms of time of coverage.

This work has been undertaken to develop a composite and comprehensive catalogue of independent earthquakes collecting primary earthquake catalogues from various sources and literatures published till 2017.

METHODOLOGY

Data collection

Primary earthquake catalogues are fundamental inputs in the development of a comprehensive catalogue. Two types of primary catalogues were collected in this study: instrumentally recorded catalogues reported by various seismological agencies and historical catalogues reported in published literatures. Collected catalogues contain date, origin time, latitude, longitude, depth, magnitude and magnitude type of selected earthquakes, the locations of which fall in a rectangular region between 25º N and 32º N latitude and 78º E and 92º E longitudes.

Catalogues of instrumentally recorded earthquakes were collected from the International Seismological Centre (ISC) and the United States Geological Survey (USGS), which date back to 1901 AD (Fig. 1, Table 1). The ISC catalogue contains 5426 earthquakes of magnitude range between 1.2 and 8.2 since 1901 AD (Table 1, Fig. 1). Similarly, the USGS catalogue contains 2056 earthquakes of magnitude range between 3 and 8 since 1908 AD (Table 1, Fig. 1).

Catalogues of the historical (pre-instrumental) earthquakes were collected from published literatures (e. g., Bilham et al., 2004; Ambrasseys and Douglas, 2004; Chitrakar and Pandey,

Table 1: Earthquake data collected from different sources.

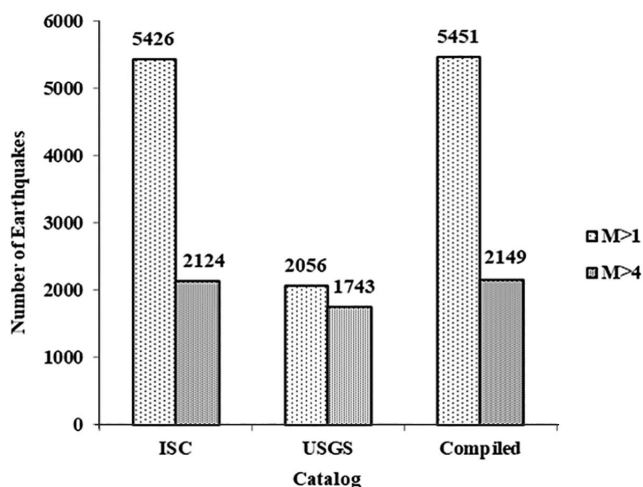| S. N.	Source	From	To	Minimum magnitude	Maximum magnitude	Number	After compilation
1	USGS	1908	2017	3	8	2056	5451
2	ISC	1901	2017	1.2	8.2	5426	

1986; Lave et al., 2005; Szeliga et al., 2010). Data of historical earthquakes is available for strong earthquakes only which reportedly caused considerable destruction in the past. The location and magnitude of historical earthquakes were calculated using empirical relations and macroseismic data of earthquakes (e. g. destruction pattern, liquefaction pattern, and result of paleoseismic investigations). The location and magnitude of historical earthquakes are typically estimated from the intensity of ground shaking and its geographical distribution. Therefore, the location and magnitude of historical earthquakes, typically, might have large uncertainties in comparison to those of instrumentally recorded earthquakes.

The collected primary catalogues were merged into a composite catalogue. The composite catalogue was checked for duplicate events and such duplicate events were removed from the catalogue. The total number of earthquakes in the composite catalogue is 5451 for the magnitude range between 1.2 and 8.2.

Magnitude conversion

The composite earthquake catalogue contains earthquakes collected from different sources (Table 1, Fig. 1), which have reported different types of magnitudes (e. g., moment magnitude (Mw), body wave magnitude (Mb), surface wave magnitude (Ms) and local magnitude (Ml)). Moment magnitude is generally considered the best overall estimate of an earthquake size and does not saturate even at large earthquakes (Kanamori, 1977; Hanks and Kanamori, 1979), therefore it is preferred in the study of seismic activity, seismotectonics and seismic hazard.

In order to develop a comprehensive catalog of consistent magnitude, the other type of magnitudes (Mb, Ms and Ml) were converted into moment magnitude (Mw) using the empirical relations (Equation (1), Equation (2) and Equation 3) from Scrodilis (2006). The number of Mw > 4.0 earthquakes increased after magnitude conversion, which is demonstrated by Fig. 1 and Fig. 7. Other characteristics of the catalogue are presented in Fig. 2 and Fig. 3.

Fig. 2: Number of earthquakes for different magnitude class after magnitude conversion

Fig. 1: Earthquake data collected and compiled in this study. The instrumentally recorded (ISC and USGs) and historical earthquakes were merged into the 'Composite' catalogue.
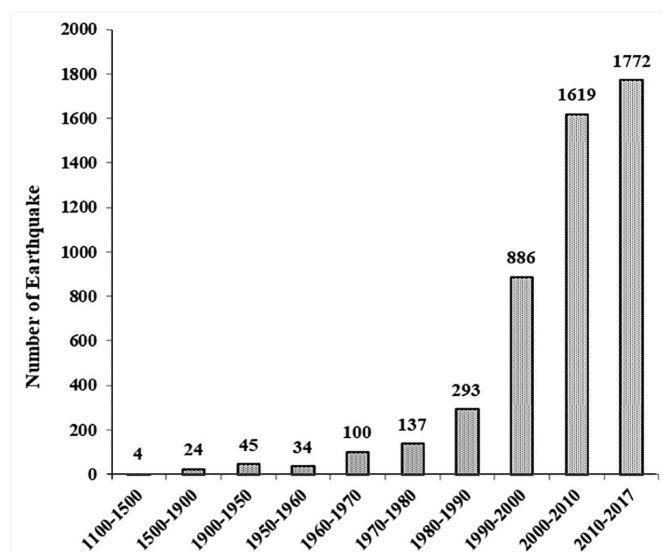
Fig. 3: Number of earthquakes (Mw > 4) for different time intervals (after magnitude conversion)

$$Mw = 0.67(\pm0.005) * MS + 2.07(\pm0.03) \qquad \text{Eq. (1)}$$

(For shallow earthquakes (depth <70 Km) and Ms between 3.0 and 6.1),

$$MW = 0.99(\pm0.02) * MS + 0.08(\pm0.13) \qquad \text{Eq. (2)}$$
(for Ms between 6.2 and 8.2)

$$MW = 0.85(\pm0.04) * mb + 1.03(\pm0.23) \qquad \text{Eq. (3)}$$
(for Mb between 3.5 and 6.2)

Declustering

An earthquake catalogue may contain fore-shocks and aftershocks in addition to mainshocks. A large size earthquake is generally followed by a large number of aftershocks and sometimes it is preceded by foreshocks. The foreshocks and aftershocks are dependent events to the mainshock (Fig. 4). In the study of seismotectonics, seismic activity and probabilistic seismic hazard assessment, a catalogue of independent earthquakes is required which follow the Poisson distribution (e. g., Gardner and Knopoff, 1974; Shearar and Stark, 2011; Abrahamson, 2006).

We used "Cluster 2000" code (USGS) to identify and remove dependent events in the catalogue following Gardner and Knopoff (1974) method. The code is freely available on website of the USGS (#CLUSTER). The code uses spatio-temporal window with reference to the mainshock to identify and remove the dependent events. The seismicity after declustering is presented in Fig. 5. The magnitude of completeness in the declustered catalogue is Mw 4 (Fig. 6).

Completeness Test

The developed catalogue contains earthquakes of a range of magnitudes, which are not available for the entire span of time (1100 AD to 2017 AD). Large events are reported for longer time but the small earthquakes are reported for short time (Fig. 8).

To assess completeness of different magnitude classes, we followed the Stepp (1972) technique. The technique divides an earthquake catalogue into (T) time intervals and the magnitude range into (n) magnitude classes. This test relies on the statistical property of the Poisson distribution that highlights time intervals during which the recorded earthquake occurrence rate does not change. The test evaluates the stability of the mean rate of occurrences (λ) of events which fall in a predefined magnitude range in a series of time windows (T). If the rate of occurrence λ is constant, then the standard deviation of the rate (σ) varies as $1/(T)^{0.5}$ and λ is not stable if σ deviates from the straight line of the $1/(T)^{0.5}$ slope. The length of the time interval for which the standard deviation does not vary from the straight line is the time interval of completeness for that particular magnitude class. The complete time interval of each magnitude class is visually determined from the plots.
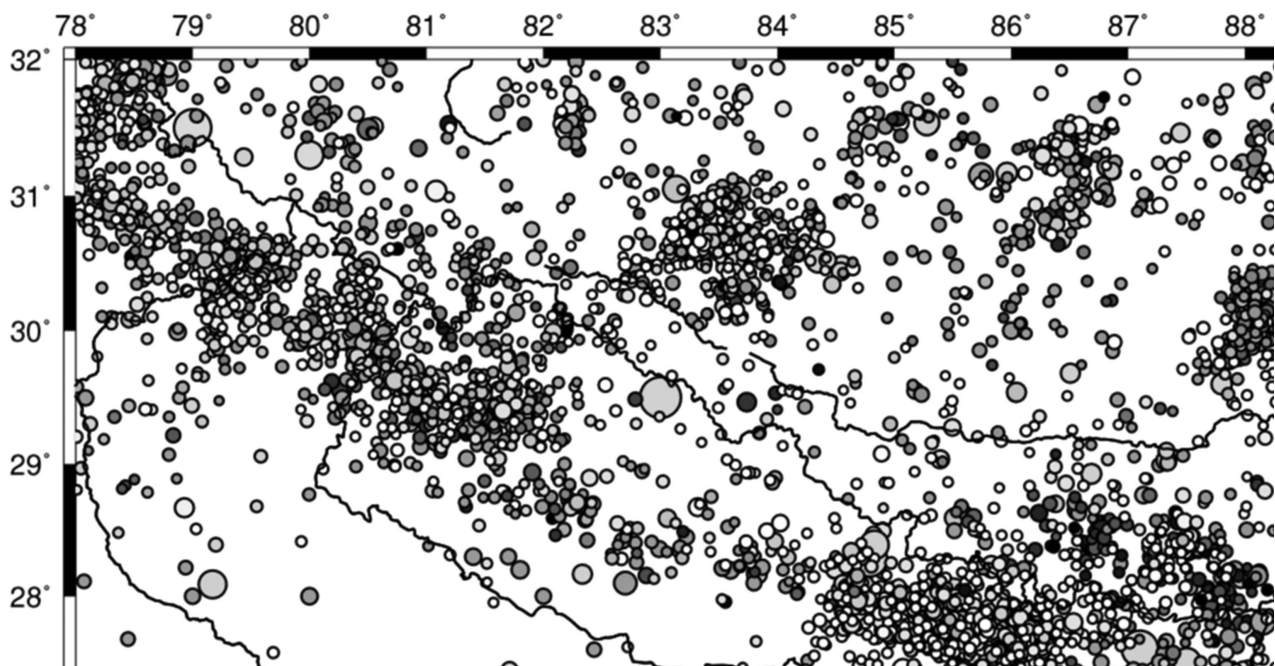
Fig. 4: Epicenter distribution before declustering the composite catalogue. The clusters noticed in the figure are dependent events. The dense cluster in Central Nepal represents the aftershocks of the 2015 Gorkha Earthquake. The scale stands for depth (km).
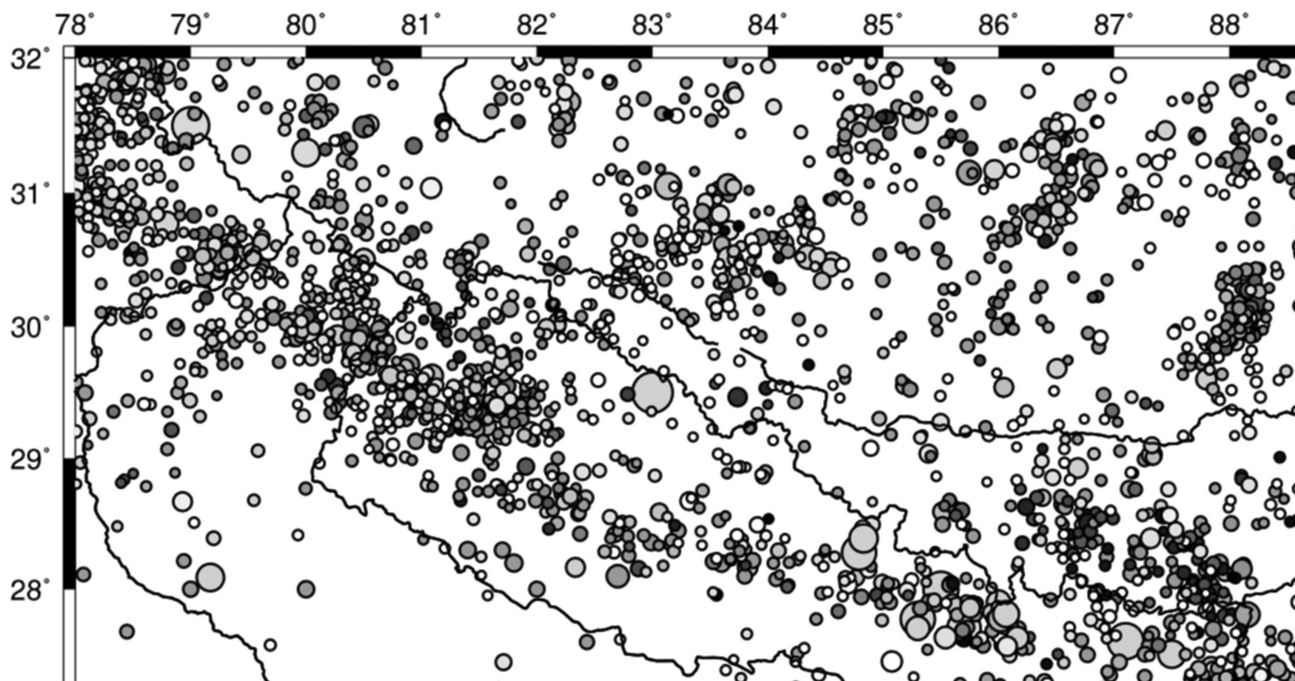
Fig. 5: Epicenter distribution after declustering of the compiled catalogue. Note that the clusters of aftershocks disappear after declustering. The scale stands for depth (km)
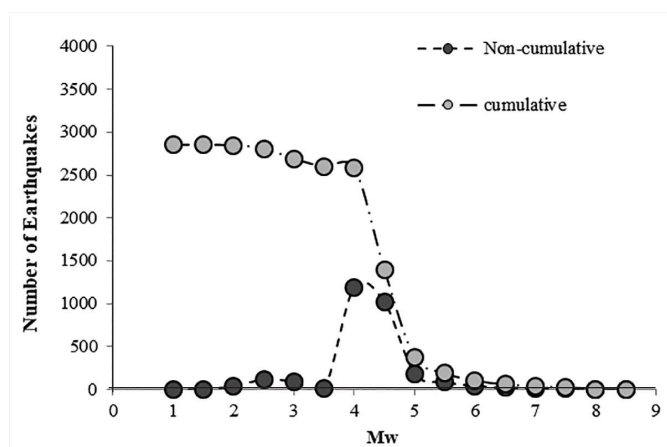
Fig. 6: Cumulative and non-cumulative distribution of earthquake for different magnitude ranges (ISC catalogue). The magnitude of completeness (Mc) for the study area is Mw 4.0
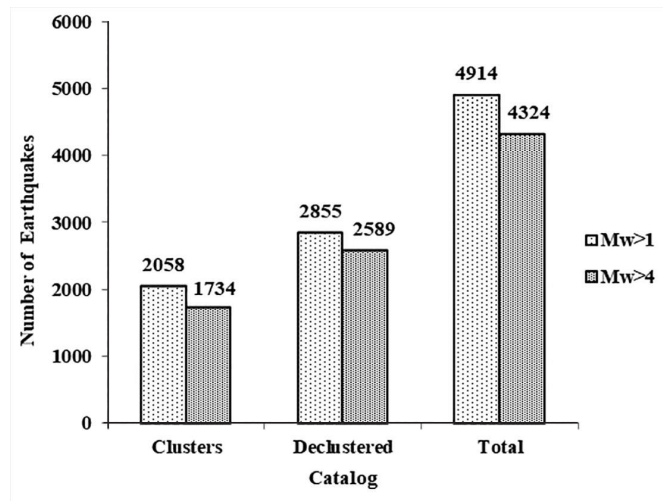
Fig. 7: The number of earthquakes in the catalogues before and after the declustering process is applied.

In order to determine the completeness levels for different magnitude classes, the catalogue was split into 8 time windows of 100-year length between 1100 (first data entry in the catalogue) before 1900 AD and 11 time windows of 10-year length after 1900 AD (Fig. 9). A summary of magnitude classes and their respective complete time intervals (T) are presented in Fig. 10.

Gutenberg-Richter relation

The Gutenberg-Richter relation is an empirical relation between the magnitude (m) of earthquake and number (N) of earthquakes with magnitude larger than 'm'. It is a remarkable feature of worldwide seismicity (Warner and Laura, 2003), which is used to describe seismic activity (Takeo and Shimazaki,
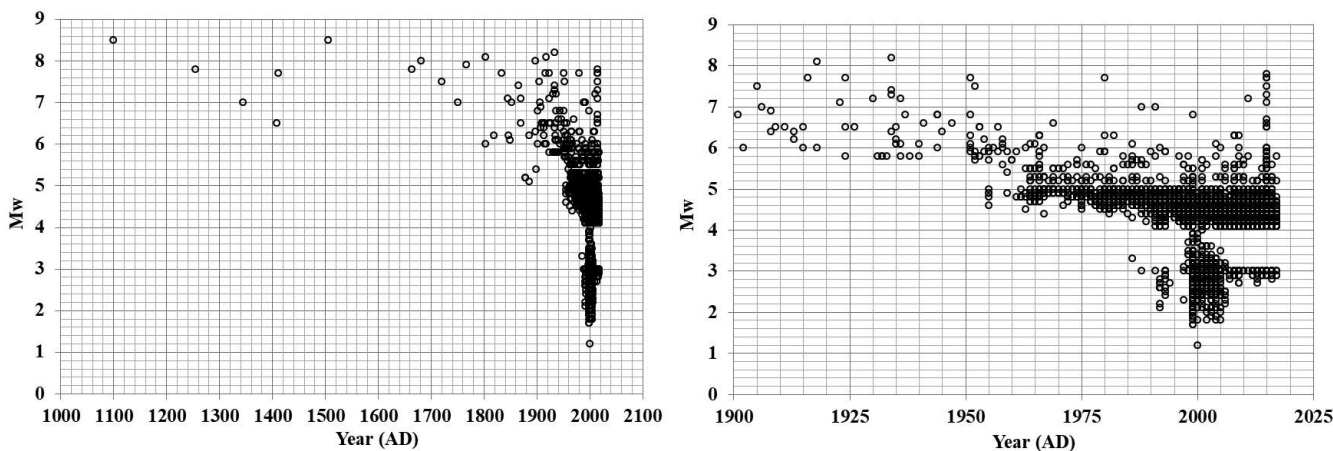
Fig. 8: Availability of earthquake size in different time
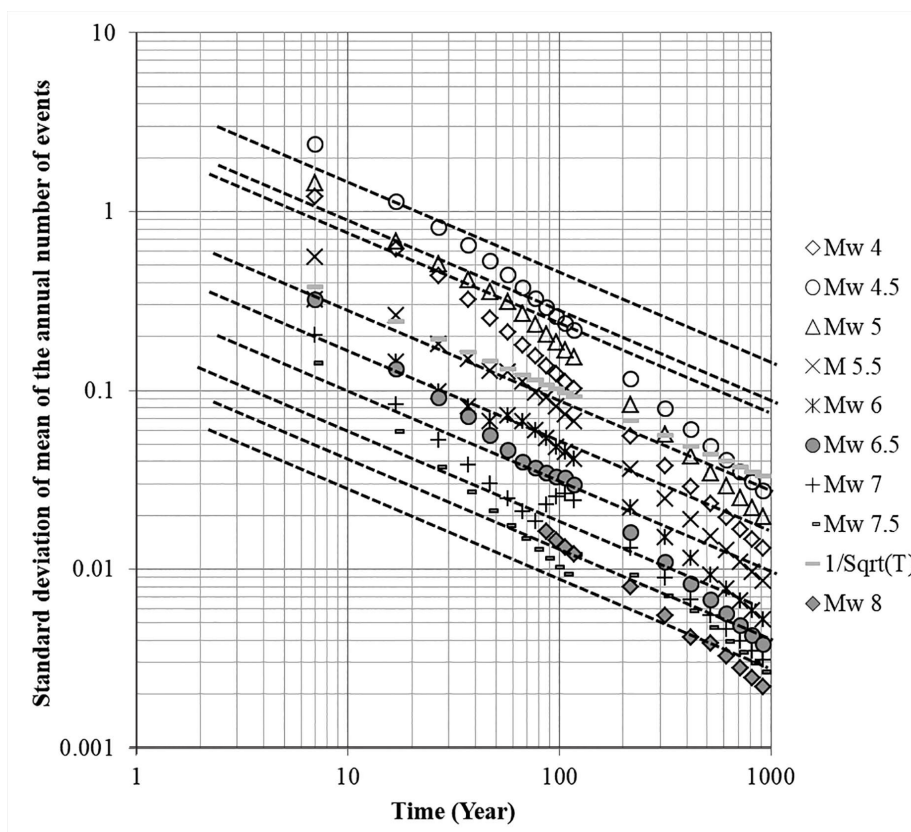
Fig. 9: Completeness test of homogenized composite catalogue following Stepp (1972) technique

2008). Ishimoto and Iida (1939) and Gutenberg and Richter (1944) proposed the relation in the following form.

$$Log_{10}(Nm) = a - b * m$$

Where 'N' is the number of earthquakes per year with magnitude equal to or larger than *m*. The *a* and *b* in the equation are coefficients called a value and b value respectively. The a-value' describes total activity of earthquakes in the region whereas the b value gives relative number of large and small earthquakes. When the *b* value increases, the number of large earthquakes decreases compared to the number of smaller magnitudes and vice versa. For active tectonic regions *b* value is about 1 and for volcanic regions it is up to 2 or higher. The a and b value are fundamental seismic parameters required in probabilistic seismic hazard analysis. The b value is estimated using least square method or the maximum likelihood method.
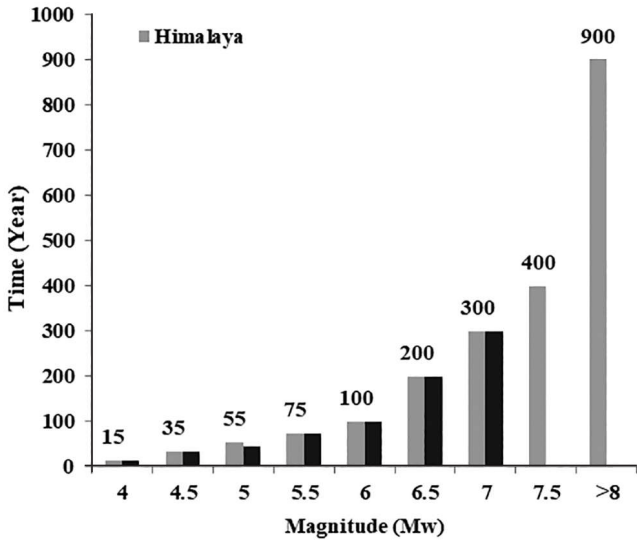
Fig. 10: Completeness of different magnitude classes for Himalaya and South Tibet

Fig. 11: Gutenberg-Richter relation for earthquakes in South Tibet

Table 2: Recurrence parameters for two tectonic zones (Himalaya and South Tibet)

Region	Method	'a' value	'b' value
Himalaya	Maximum likelihood	5.3	0.9
	Least square	5.2	0.95
South Tibet	Maximum likelihood	6.5	1.19
	Least square	5.9	1.1

The common technique to estimate b value is the least squares fit, which can lead to biased result and apparent errors may be much smaller than the real ones. The maximum likelihood method of Aki (1965) is the most accurate method to calculate 'b' value, but it requires large data sets. Monte Carlo simulations and equations from Aki (1965) indicate that a minimum of 2000 earthquakes are required to calculate 'b' to within 0.05 at 98% confidence.

In the Nepal Himalaya, the earthquakes in the south of the 3500 m elevation contour line, in majority, are overwhelmingly found to have thrust mechanism, whereas those in the north and above 3500 m contour line, in majority, have normal fault mechanism (e. g., Rajaure et al., 2013). Earthquakes in south Tibet, close to the Nepal-China border in north-east show strike-slip mechanisms (e. g., Rajaure et al., 2013). To estimate the a and b value the prepared catalogue was divided into two sub-regions (Himalaya and South Tibet) following the mechanism of deformation in the region. The recurrence parameters were estimated using the least square and maximum likelihood method (Table 2, Fig. 11, and Fig. 12) for the Himalaya and South Tibet, respectively.
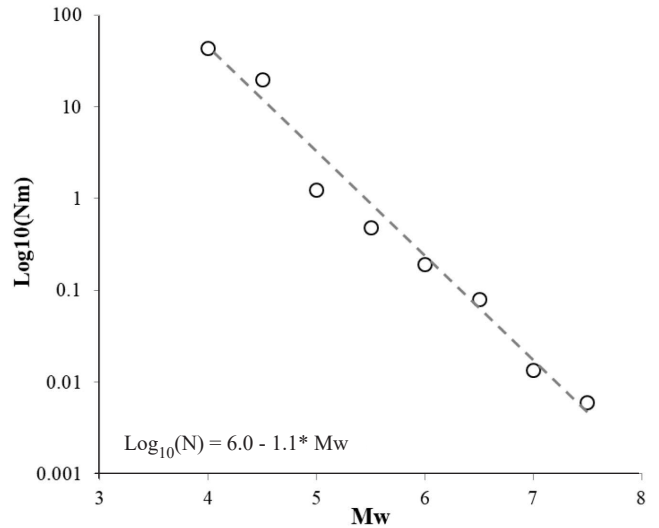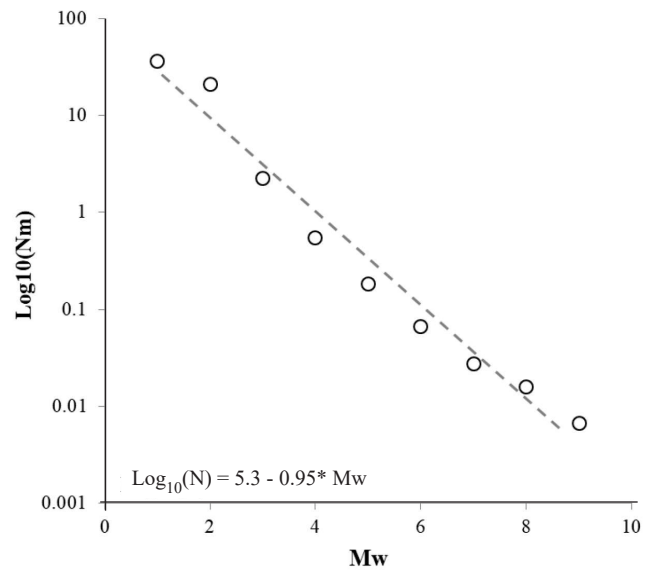
Fig. 12: Gutenberg-Richter relation for earthquakes in the Nepal Himalaya

CONCLUSIONS

A comprehensive and composite catalogue has been prepared for Nepal and its adjoining region between 25 N and 32 N latitude and 78 E and 92 E longitudes. The developed catalogue contains 2589 events with Mw between 4.0 and 8.5, for the period between 1100 AD and 2017 AD and the magnitude of completeness (Mc) is Mw 4.0.

A completeness test of the catalogue was performed for South Tibet and the Himalaya separately as they represent two types of stress regimes, i. e. extensive and compressive, respectively (e. g. Rajaure et al., 2013). The catalogue is

complete for large earthquakes (Mw>8.0) for the entire span of time (since 1100 AD) but is underreported for small magnitude earthquakes. The completeness of small earthquakes improved in the late 20th century, following the advent, continuous development and expansion of instrumental networks. The completeness test of the catalogue revealed that Mw 4, 4.5, 5, 5.5, 6, 6.5, 7, 7.5 and larger than Mw 8 are complete for 15, 35, 55, 75, 100, 200, 300, 400 and 900 years, respectively for the Himalaya and Mw 4, 4.5, 5, 5.5, 6, 6.5, 7 are complete for 15, 35, 55, 75, 100, 200, 300 years in their order for South Tibet.

Earthquake recurrence parameters are estimated in south Tibet and Himalaya separately; our analysis shows that strong earthquakes are more common in the Himalaya than in South Tibet.

The result of this work is expected to be useful in the study of seismotectonics, earthquake activity and seismic hazard assessments.

ACKNOWLEDGEMENTS

REFERENCES

Abrahamson, N A., 2006, Seismic hazard assessment: Problems with current practice and future developments. Proceedings of the First European Conference on Earthquake Engineering and Seismology, Geneva, p. 17.

Aki, K., 1965, Maximum Likelihood estimate of b in the formula logN = a - bM and its confidence limits. Bulletin of Earthquake Research Insttitute, v. 43, pp. 237–239.

Ambraseys, N. and Douglas, J., 2004, Magnitude calibration of north Indian earthquakes. Geophysics Journal International, v. 159, pp. 165–206.

Bilham, R., Bodin, P., and Jackson, M., 1995, Entertaining a great earthquake in western Nepal. Journal of Nepal Geological Society, v. 11 (1), pp. 73–78.

Chitrakar, G. R. and Pandey, M. R., 1986, Historical earthquakes of Nepal, Bulletin of the Nepal Geological Society, v. 4, pp. 7–8.

Gardner, J. K. and Knopoff, L., 1974, Is the sequence of earthquakes in Southern California, with aftershocks removed, poissonian? Bulletin of the Seismological Society of America, v. 64/5, pp. 1363–1367.

Gutenberg, B. and C. Richter, 1954, Seismicity of the Earth and Associated Phenomena (Princeton University Press, Princeton, New Jersey), 2nd edition, pp. 310.

Gutenberg, B., and C. F. Richter, 1944, Frequency of earthquakes in California. Bulletin of the Seismological Society of America, v. 34, pp. 184–188.

Hanks, T. C. and Kanamori, H., 1979. A moment magnitude scale. Journal of Geophysical Research, v. 84, pp. 2348–2350.

International Seismological Centre, 2015, On-line Bulletin, http://www.isc.ac.uk, International . Seismological. Centre., Thatcham, United Kingdom.

Ishimoto, M. and Iida, K. 1939, Observations sur les seims euregistr´e par le microseisograph construite dernierment (I). Bulletin of the Earthquake Research Institute-University of Tokyo, v. 17, pp. 443–478.

Kanamori, H., 1977, The energy release in great earthquakes. Journal of Geophysical Research, v. 82, pp. 2981–2987.

Lave, J., Yule, D., Sapkota, S. N., Basant, K., Madden, C., Attal, M., and Pandey, R., 2005, Evidence for a Great Medieval Earthquake (~1100 A.D.) in the Central Himalayas, Nepal. Science, v. 307, pp. 1302-1305. CHECK Pandey, M. R. or only R??? (Checked: it's a mistake in the article. It should have been Pandey M. R. in fact)

Ojha S., Bhattarai G. K., and Rajaure S., 2013, A catalog for Nepal Himalaya earthquakes from 1255 to 2012. International Journal of Landslide and Environment, v. 1, p 3.

Pandey, M. R., Tandukar, R. L. P., Lave, J. P., and Massot, J. P., 1995, Interseismic Strain Accumulation on the Himalayan Crustal Ramp, Nepal. Geophysical Research Letters, v. 22 (7), pp. 751–754.

Pandey, M. R., Tandukar, R. P., Avouac, J. P., Vergne, J., and Heritier, T., 1999, Seismotectonics of the Nepal Himalaya from a local seismic network. Journal of Asian Earth Sciences, v. 17, pp. 703–712.

Rajaure, S., Sapkota, S. N., Adhikari, L. B., Koirala, B., Bhattarai, M., Tiwari, D. R., Gautam, U., Shrestha, P., Maske, S., Avouac, J. P., Bollinger, L., and Pandey, M. R., 2013, Double difference relocation of local earthquakes in the Nepal Himalaya. Journal of Nepal Geological Society, v. 46, pp. 133–142

Scordilis, E. M., 2006, Empirical global relations converting MS and mb to moment magnitude. Journal of Seismology, v. 10, pp. 225–236.

Shearer, P. M. and Stark, P. B., 2011, Global risk of big earthquakes has not recently increased. Proceedings of the National Academy of Sciences, v. 109, pp. 717–721.

Stepp, J. C., 1972, Analysis of the completeness of the earthquake sample in the Puget Sound area and its effect on statistical estimates of earthquake hazards. Proceedings of International Conference on Microzonation for Safer Construction, Research, and Application, Seattle, Washington University, v. 2, pp. 897–909.

Szeliga, W., Hough, S., Martin, S., and Bilham, R., 2010, Intensity, Magnitude, Location, and Attenuation in India for Felt Earthquakes since 1762. Bulletin of the Seismological Society of America, v. 100 (2), pp. 570–584.

Takeo I., and Kunihiko S., (2008), The Gutenberg-Richter relationship vs. the characteristic earthquake model: effects of different sampling methods. Bulletin of Earthquake Research Insitute, Univeristy of Tokyo, v. 83, pp. 131–151

Thapa, D. R., and Wang G., 2013, Probabilistic seismic hazard analysis of Nepal. Earthquake Engineering and Engineering Vibration, v. 12 (4), pp. 577–586.

United States Geological Survey, On-line Bulletin, . United States Geological Survey, Golden, USA

Utsu, T., 1965, A method for determining the value of b in the formula logN=a-bM showing the magnitude-frequency relation for earthquakes. Geophysics. Bulletin of Hokkaido University, v. 13, pp. 99–103

Warner, M. and Laura, S., 2003, A review and new insights on the estimation of the b-value and its uncertainty. Annals of Geophysics v. 46 (6), pp. 1271–1282.

Woessner, J., and Wiemer S., 2005, Assessing the quality of earthquake catalogs: Estimating the magnitude of completeness and its uncertainty. Bulletin of the Seismological Society of America, v. 95, pp. 684–698.

APPENDIX 2

Participation in International Conferences

Appendix 2-1: The 10th ASC General Assembly (ASC 2014) Makati City, Philippines 17-20 November 2014- Conference

Appendix 2-2: The 11th Asian Regional Conference of International Association of Engineering Geology and Environment (IAEG), November 28–30, 2017, Kathmandu, Nepal.

APPENDIX 3

National earthquake hazards reduction program (NEHRP) (www.nehrp.gov) soil classification system. Where Vs_{30} stands for shear-wave velocity of upper 30 m thick soil profile.

NEHRP Class	Soil description	Shear-wave velocity
A	Hard rock	$Vs_{30} > 1500$
B	Firm to hard rock	$760 < Vs_{30} < 1500$
C	Dense soil and soft rock	$360 < Vs_{30} < 760$
D	Stiff soil	$180 < Vs_{30} < 360$
E	Soft soil	$Vs_{30} < 180$
F	Soil requiring site-specific evaluations	----

APPENDIX 4

Local earthquakes relocated usingdouble difference relocation technique (Waldhauser and Wellsworth (2000), (Rajaure *et al*.,2013). There are noticeable lateral variations in the seismicity belt. These variations correlate with geological structures (Appendix 8).

APPENDIX 5

Geological map of Nepal (Department of Mines and Geology, 1987).
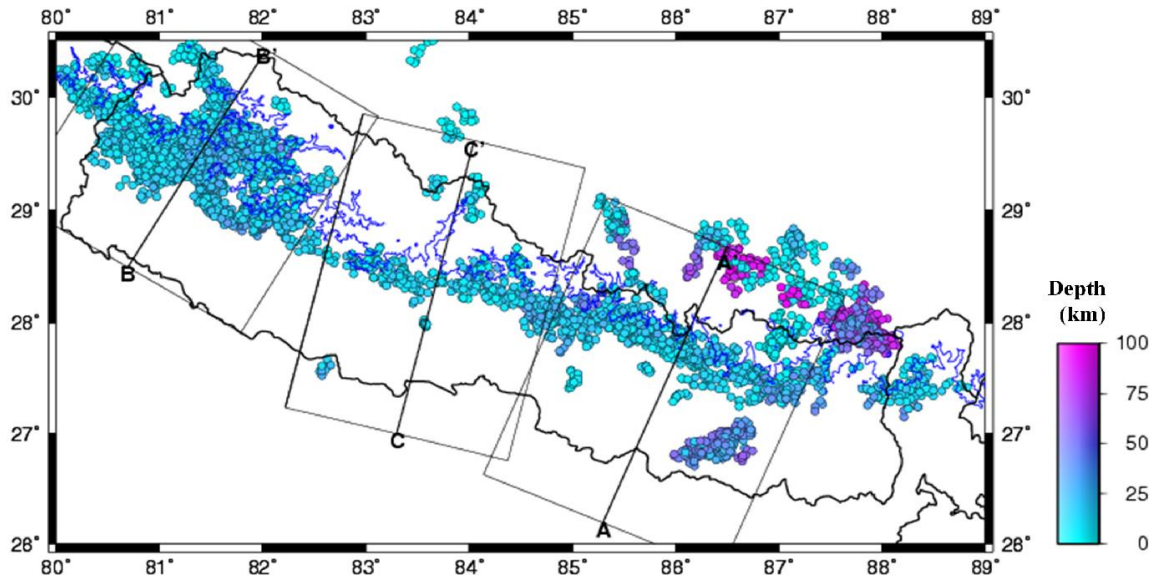
APPENDIX 6

Active fault distribution in Nepal (based on the work of Nakata, 1982, Nakata *et al*., 1984 and Nakata & Kumahara, 2000)
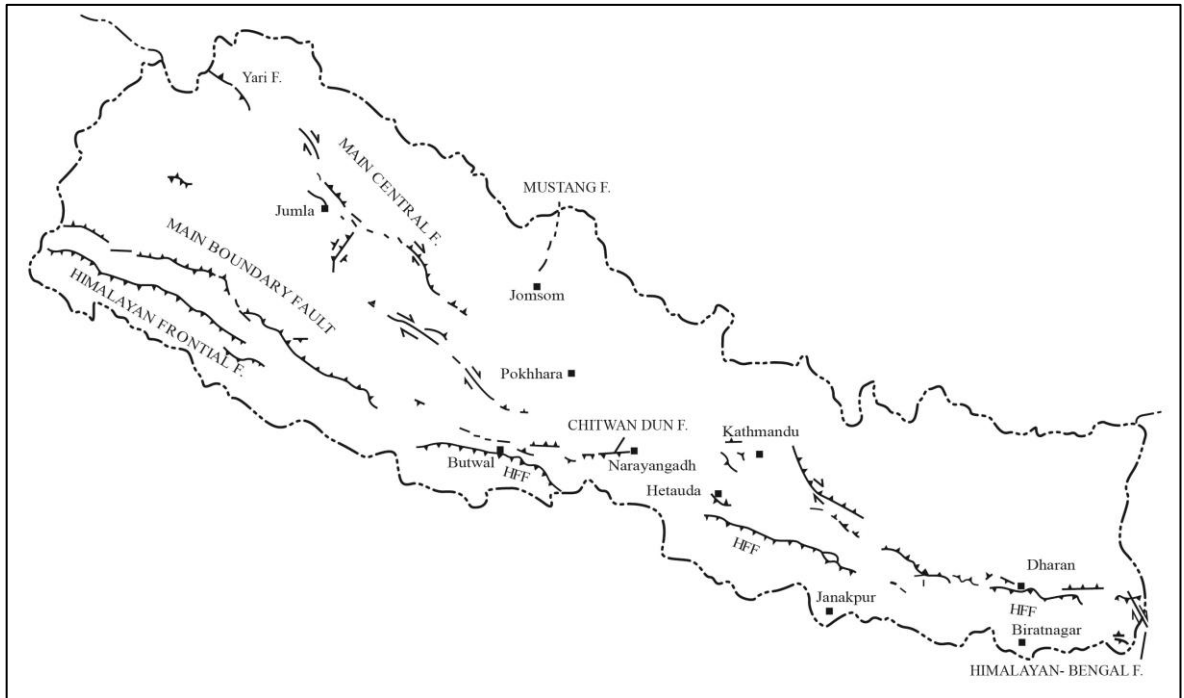
APPENDIX 7

Google Earth image of Nepal and surrounding region with relocated seismicity by Rajaure et al. (2013). Lineaments and some of the faults can be identified in this imageLateral variation (demarcated by NE-SW blue dashed line) in seismicity belt is very interesting and was used in the delineation of earthquake sources.
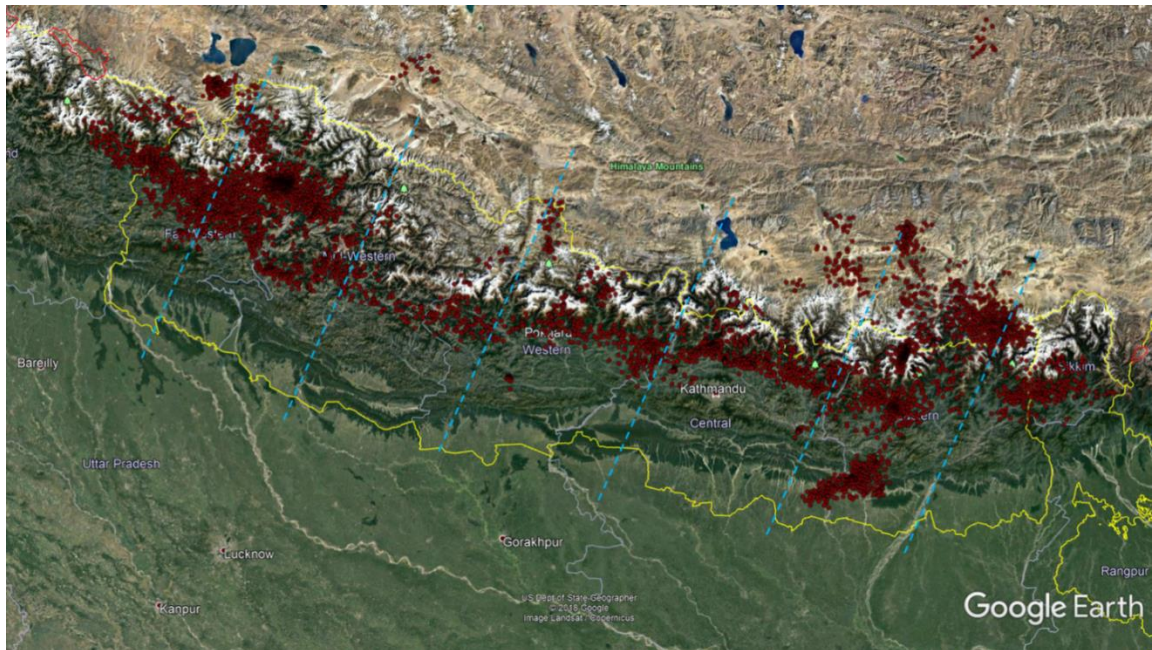
APPENDIX 8

Geological structures, fold axis and lineaments in the region, compiled by the author from different sources. The two stars are the 2015 Gorkha Earthquake (left) and Dolakha Earthquake (right). (Modified from Rajaure et al., 2013)
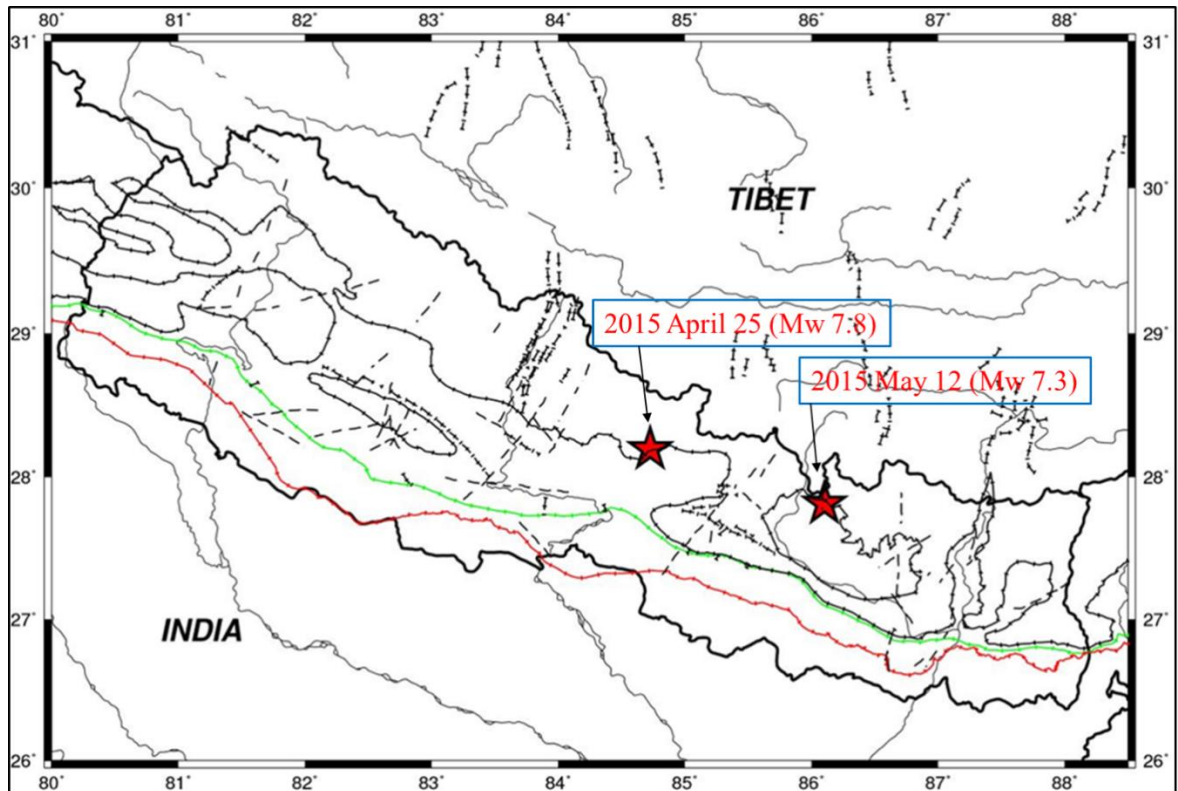
APPENDIX 9

Subsurface ridges in north India. These ridges are supposed to control the rupture size and maximum magnitude of earthquakes in the Himalaya (Gahalaut V. K. and Kundu B., 2012)
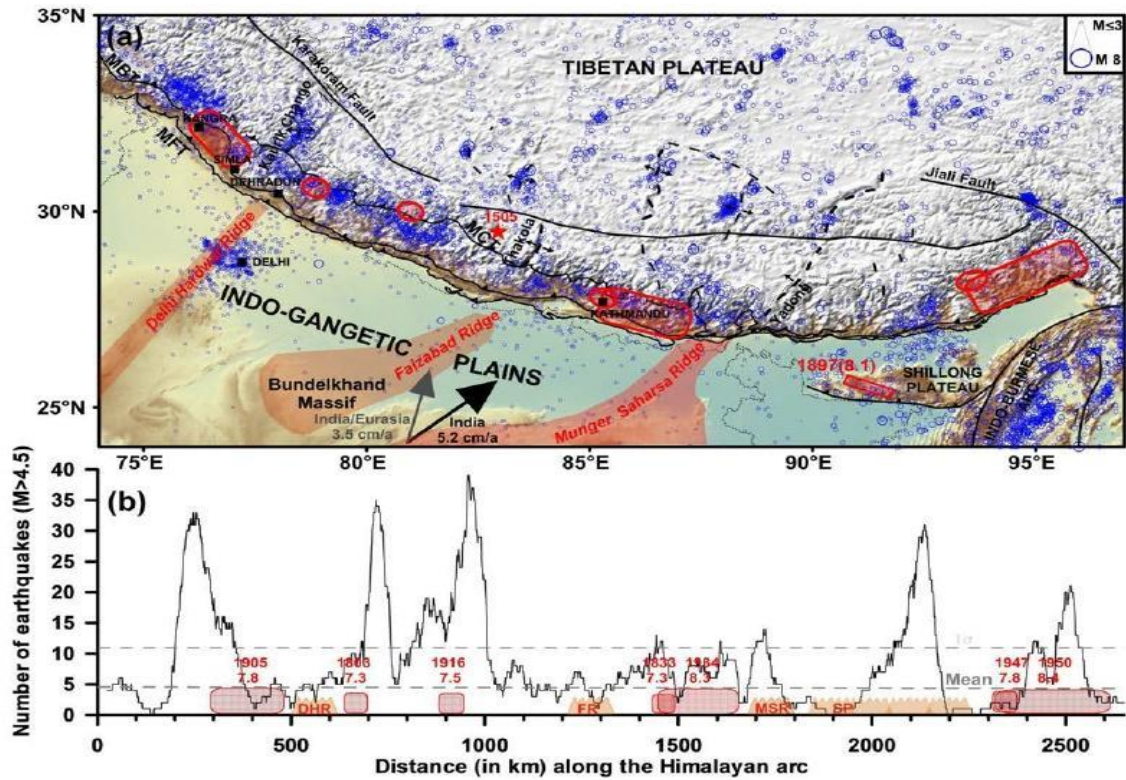
APPENDIX 10

Possible segments along the Himalaya and their potential magnitudes at the present (Bilham, 2019)
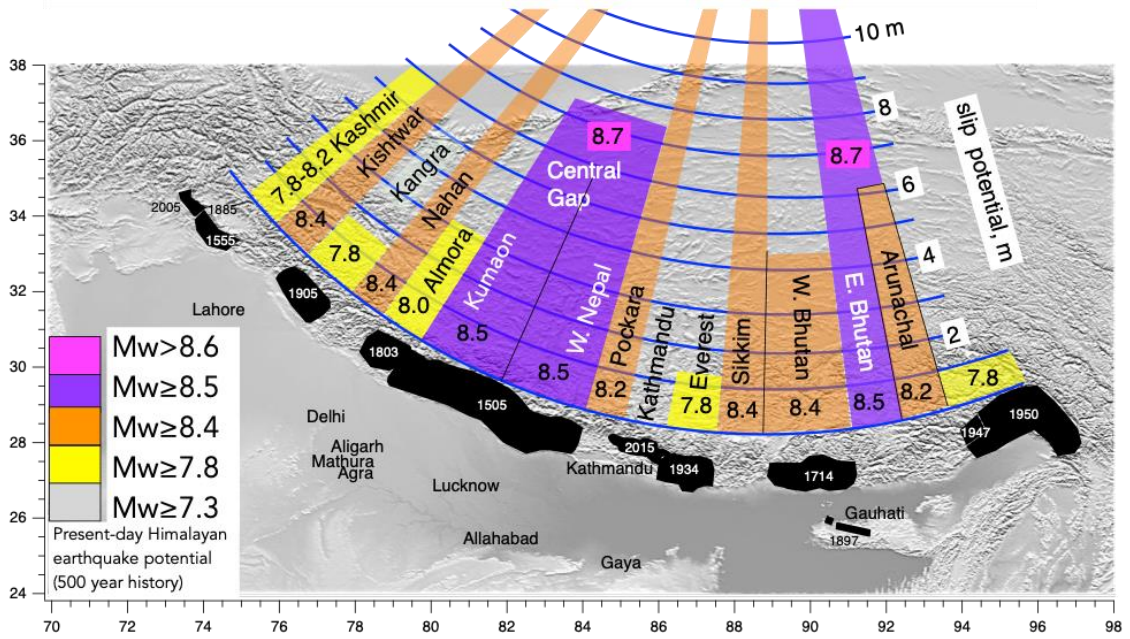
APPENDIX 11

Potential earthquake sources, identified in the present study. There are altogether nine source models (Appendix 11-1 to 11-9).

Appendix 11-1: This model (Model-1) contains segments of the MHT only. The northern border corresponds to the seismicity belt in Nepal Himalaya, which correlates with the boundary between locked part of MHT in the south and aseismically creeping part in the north. The model has seven sources, with maximum potential magnitude (Mw) between 8.0 and 8.2.
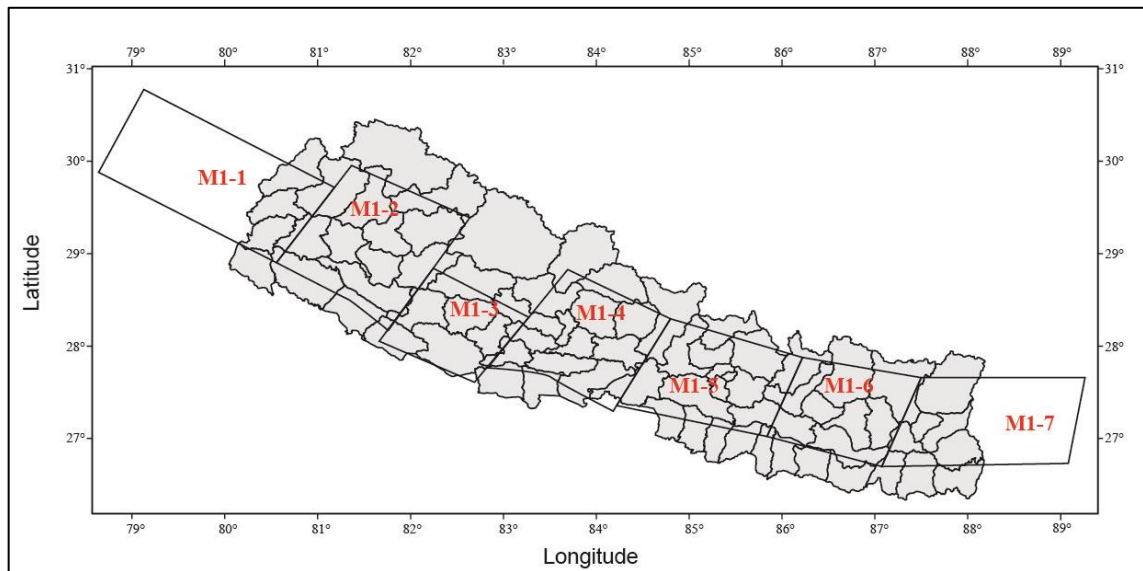
Appendix 11-2: This model (Model-2) also consists of seven sources. These sources represent the northern (half) rupture of Model-1. This model has been considered because earthquakes of Gorkha Earthquake size and rupture are believed to be common than Model-1. The maximum potential magnitude (Mw) ranges between 7.8 and 8.0.
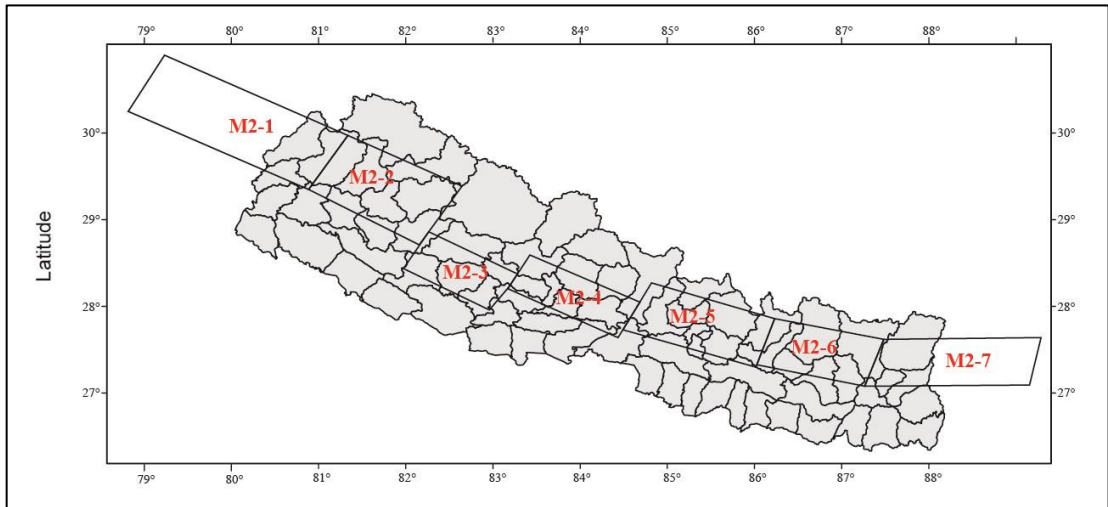
Appendix 11-3: This model (Model-3) also has seven sources. This model is considered to represent the southern ruptureof the sources in Model-1, which did not rupture during the 2015 Gorkha Earthquake. This model has 20 km depth in the northern border and 10 km in the south. The maximum potential magnitude of the sources rangesbetween Mw 7.8 and 8.0.
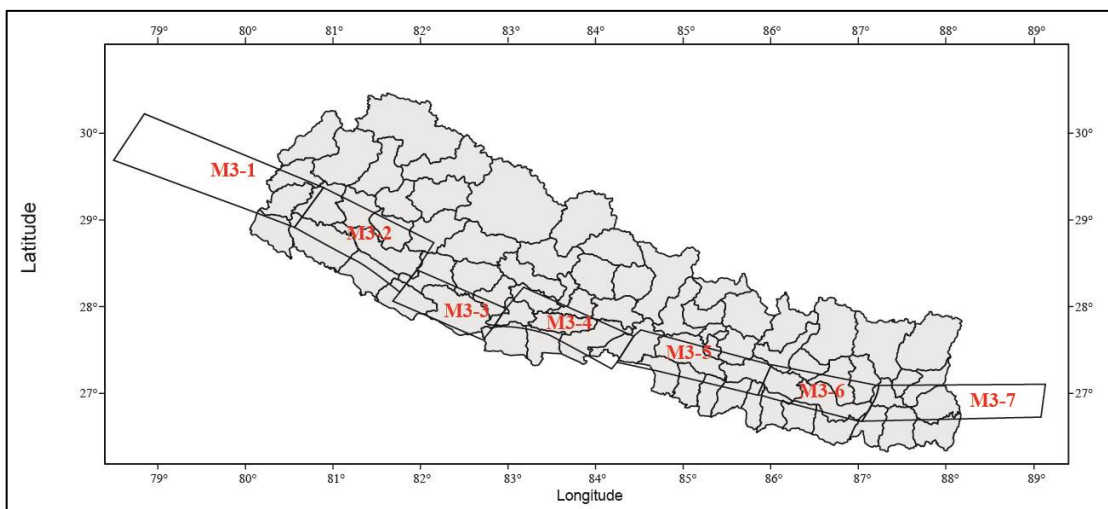
Appendix 11-4: This model (Model-4) has twenty sources. The depth of northern border of the sources (M4-4 to M4-12) is 10 km and 0 km in the south. The maximum potential magnitudes of the sources ranges between Mw 7.5 and 8.2.
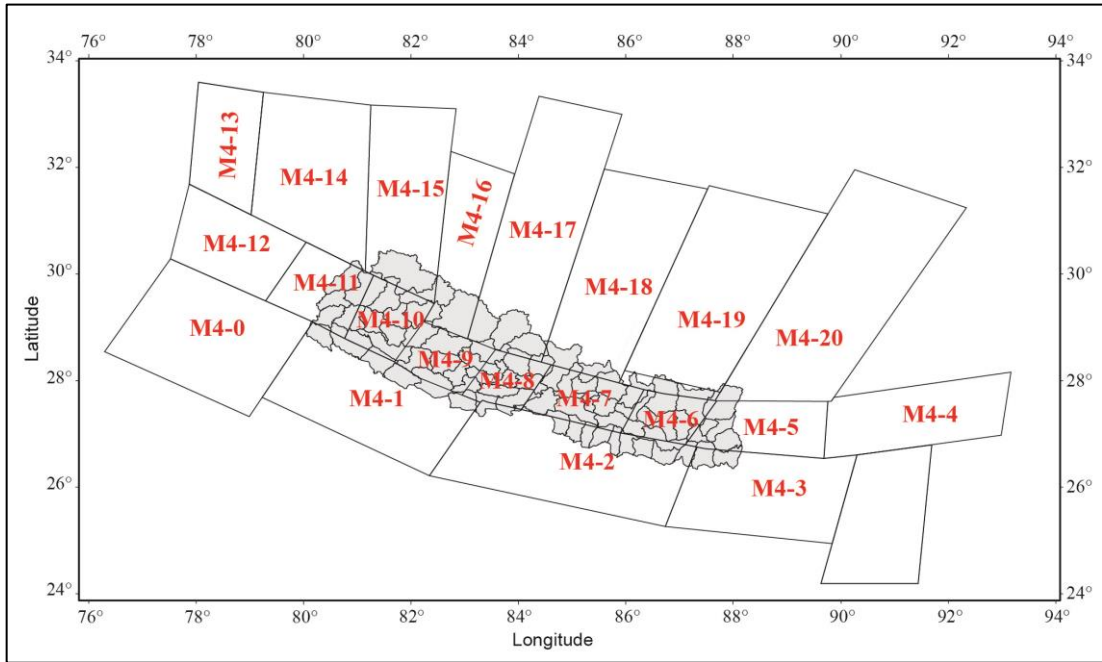
Appendix 11-5: This model (Model-5) considers sources from the Himalaya (MHT) as well as the surrounding region. There are altogether 21 sources with maximum potential magnitude between Mw 7.5 and 8.2.
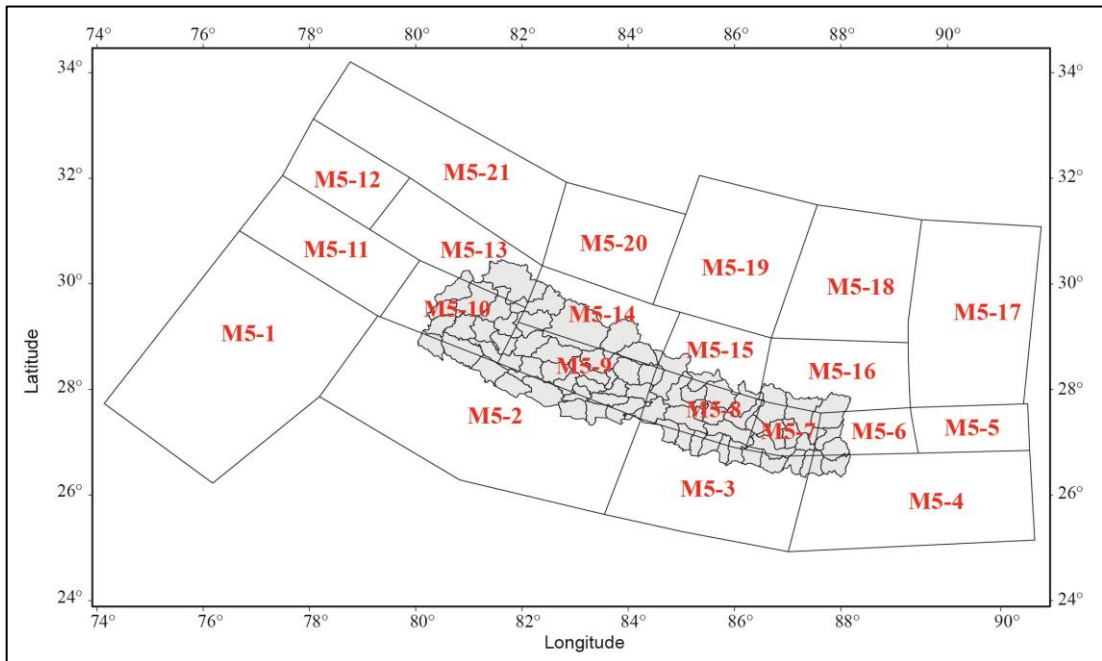
Appendix 11-6: This model (Model-6) has 24 potential sources from Himalaya and the surrounding region. The maximum potential magnitude of the sources is between 7.5 and 8.4.
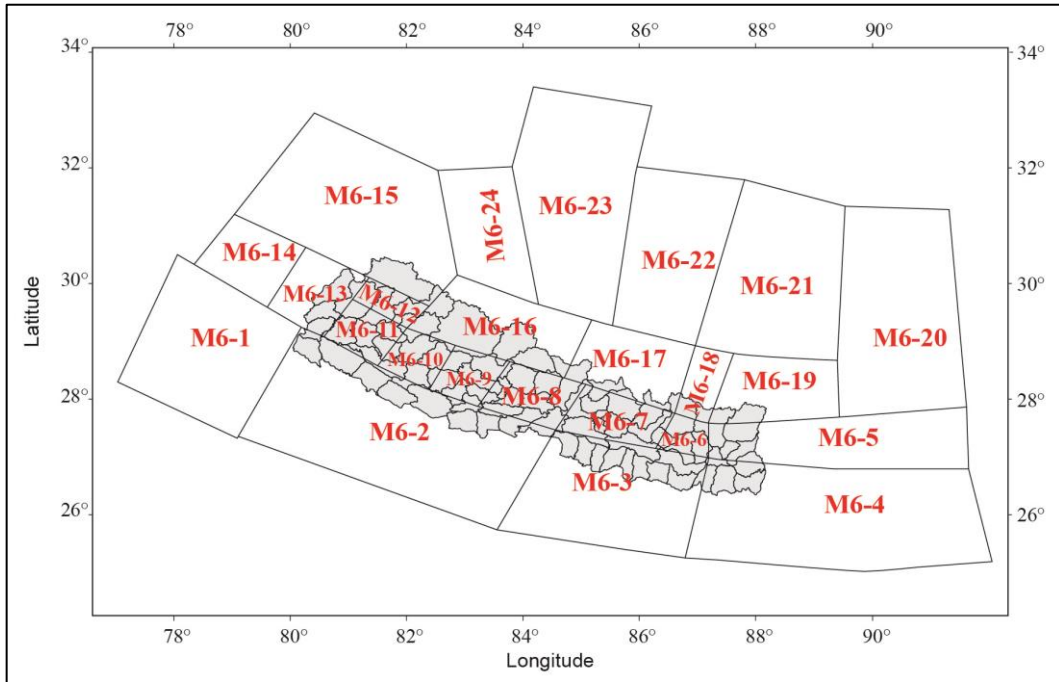
Appendix 11-7: There are altogether 15 sources in this model (Model-7). The maximum potential magnitude of the sources ranges between 7.5 and 8.3.
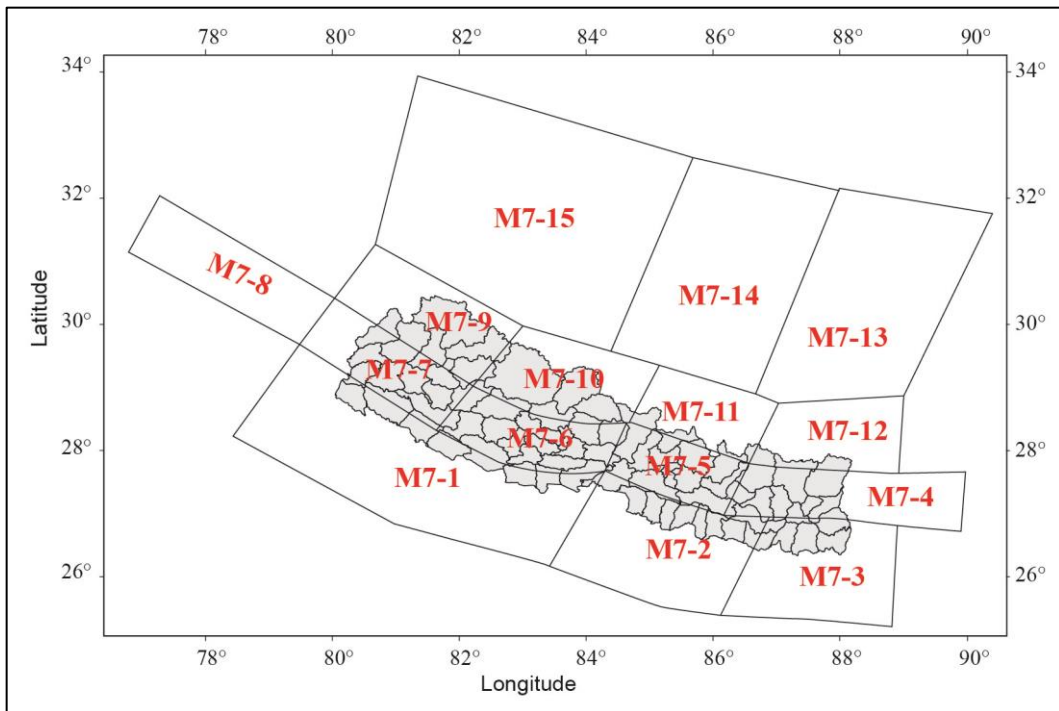
Appendix 11-8: This model (Model-8) has 18 sources from the Himalaya and the adjoining region. The maximum potential magnitude of the sources ranges between 7.5 and 8.5.
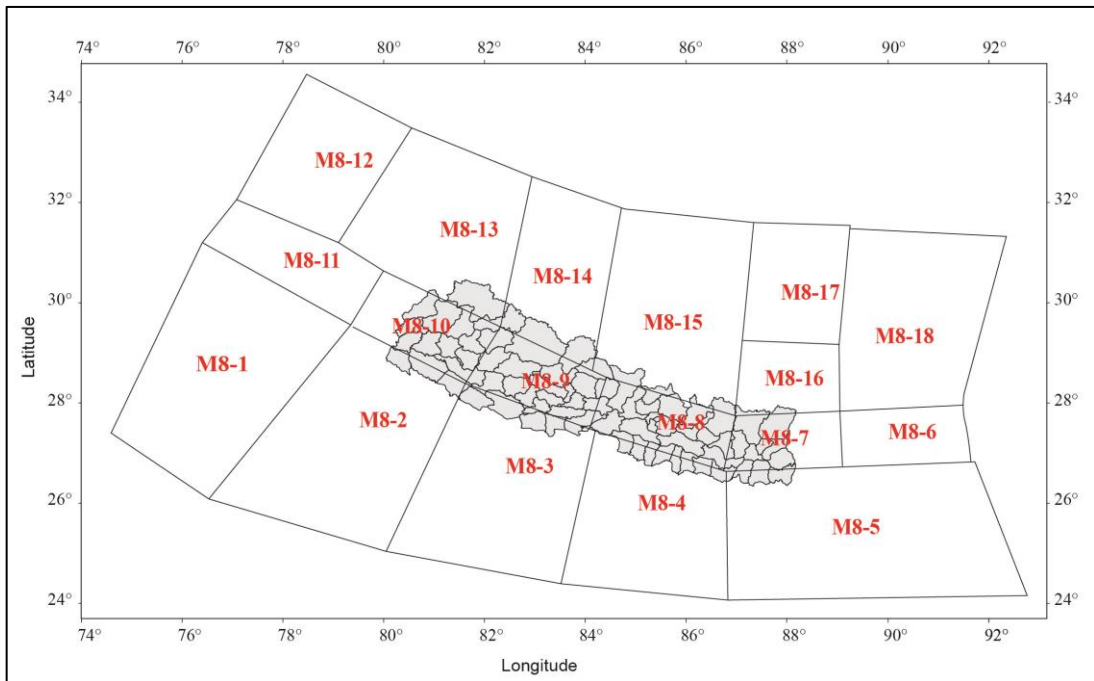
Appendix 11-9: This model (Model 9) has 24 earthquake sources. The maximum potential magnitude of the sources ranges between 7.5 and 8.5.
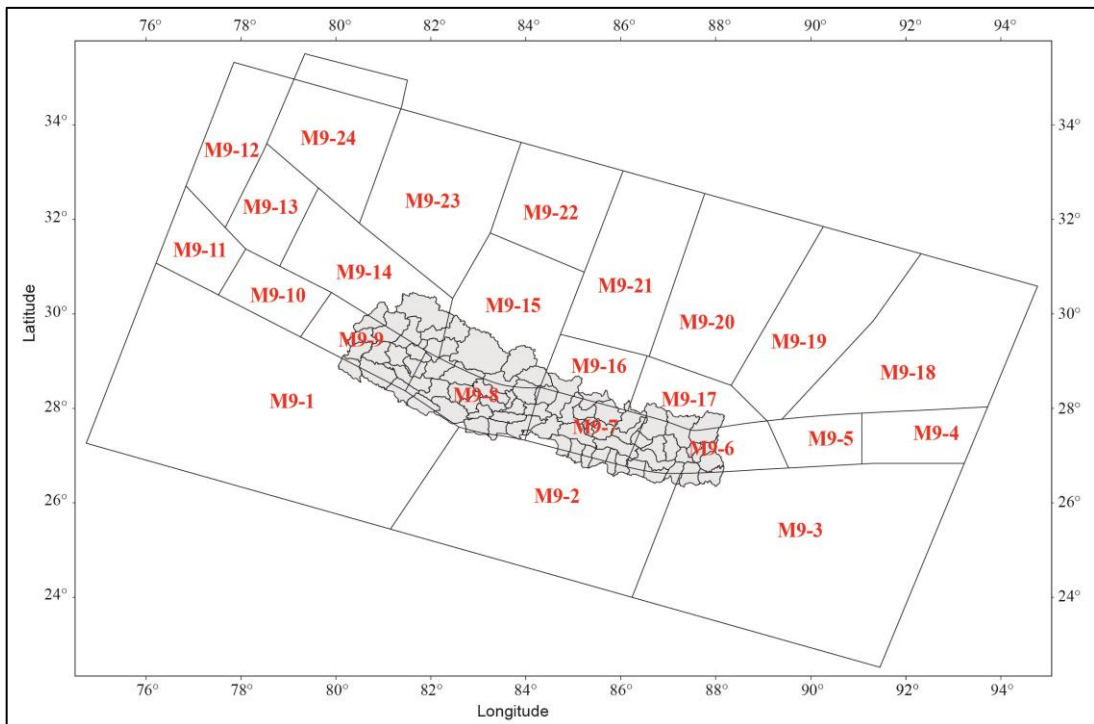
APPENDIX 12

Generalized section across the Himalaya (USGS poster). The Main Himalayan Thrust (MHT) is the detachment surface (MHT) on which slip occurs during earthquakes. The red line on MHT is the slip that occurred during Gorkha Earthquake. In the source models a simple model is assumed, where the depth of the source (segment of MHT) in the north correlates with the cluster of earthquakes and in the south it joins the MFT.
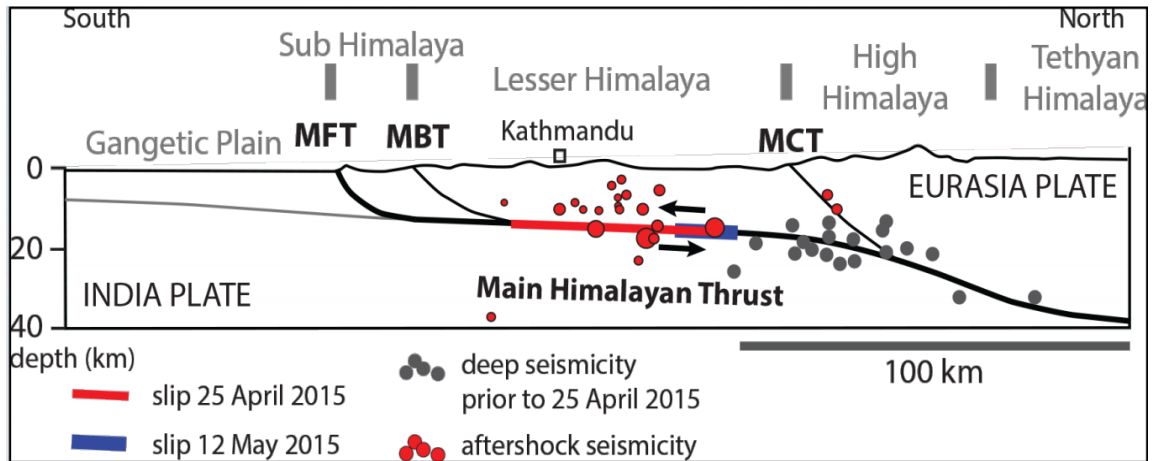
APPENDIX 13

Variation in PGA with variation in depth of source plane. Common source model, common attenuation relation, common earthquake recurrence parameters were used in this test.

Appendix 13-1: Seismic hazard map with 20 km depth fixed to all vertices of the sources in Model-1 (Appendix 11-1). The maximum PGA is about 0.5 g in the far-west.
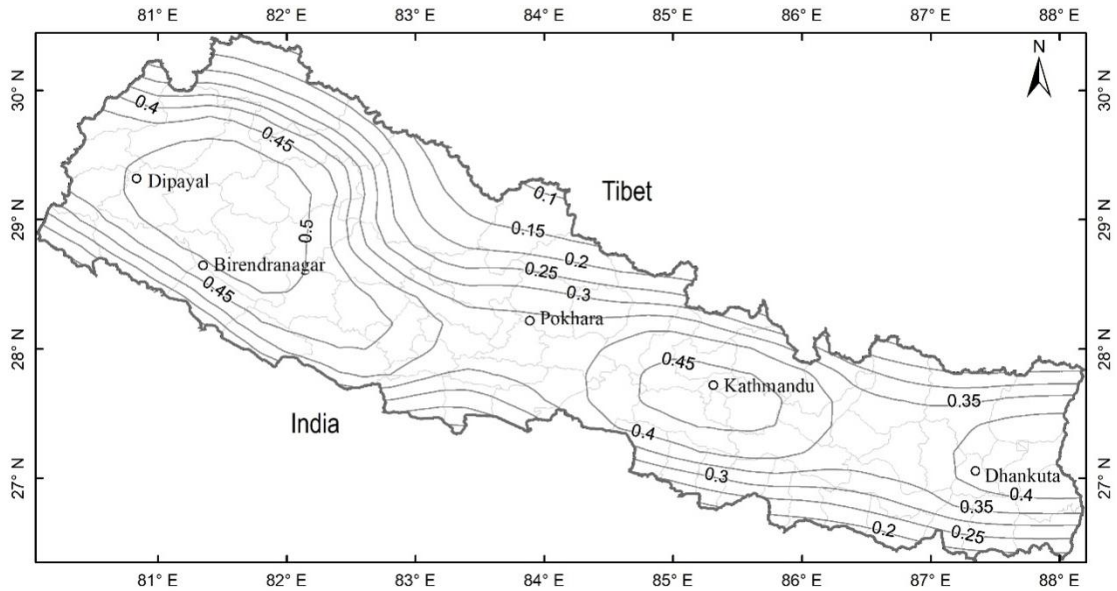
Appendix 13-2: Seismic hazard map with 5 km depth fixed to northern vertices of Model-1(Appendix 11-1). The maximum PGA is about 0.55 g in the far-west and the shapes of zones are in the middle of north-south stretch.
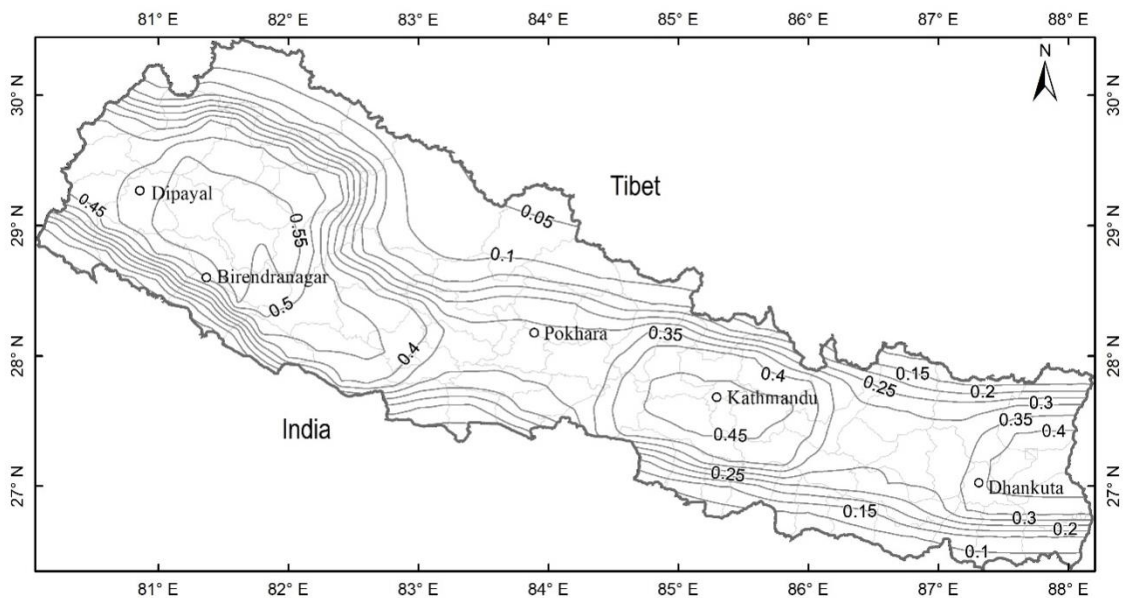
Appendix 13-3: Seismic hazard map with 10 km fixed depth to all vertices of the sources in Model-1 (Appendix 11-1). The maximum PGA is about 0.55 g. The shape of the PGA values got denser in the south on account of the hanging wall effect because of the geometry of the MHT.
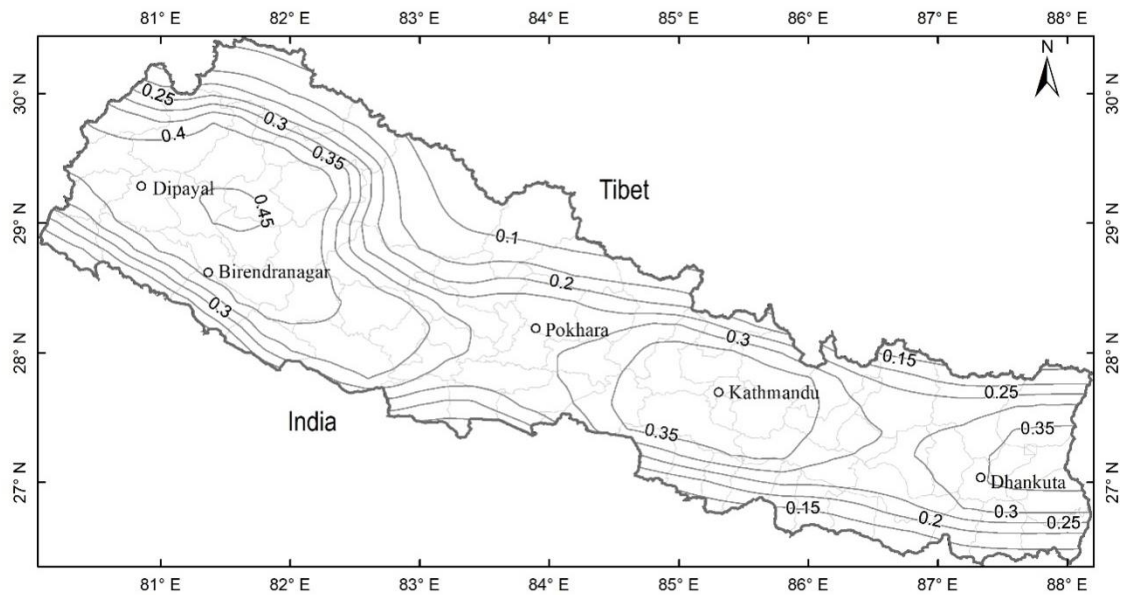
Appendix 13-4: Seismic hazard map with 20 km depth fixed to the vertices in the north of the sources in Model-1 (Appendix 11-1) and 0 km in the south. The maximum PGA is about 0.55 g in the far-west and the oval shapes of zones are getting shorter in the N-S direction because of hanging wall effect of the sources.
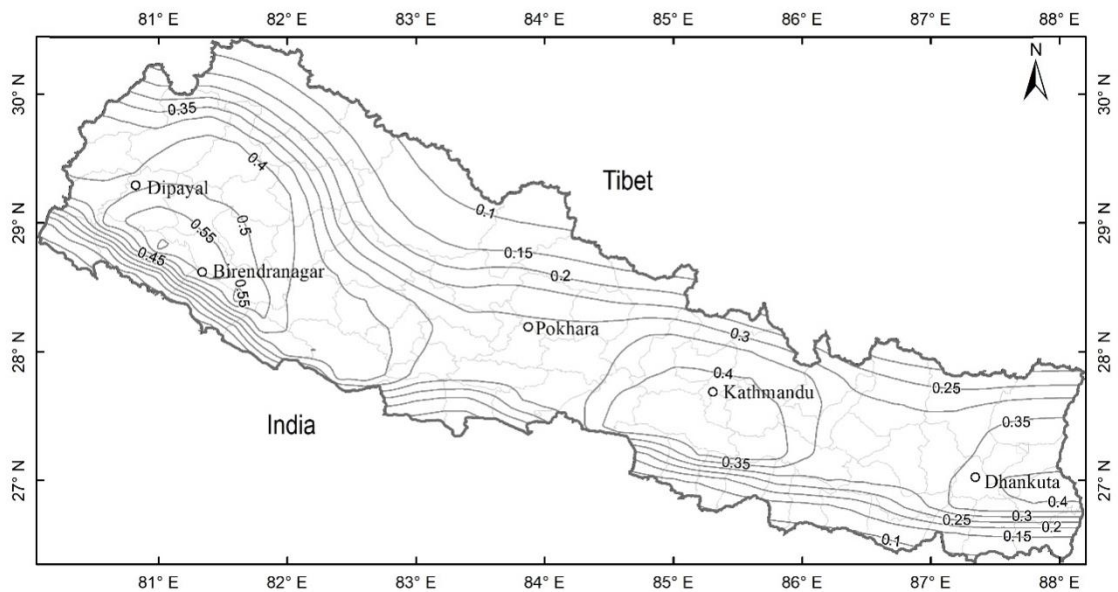
Appendix 13-5: Seismic hazard map with 50 km depth fixed to the vertices in the north.Model-1 (Appendix 11-1). The maximum PGA is about 0.5 g in the southern part of far-west. The change in the shape of the contours can be noticed between this map and the previous one. Because of hanging wall effect and depth > 50 km north, the higher PGA contours are concentrated in the southern part of Nepal.
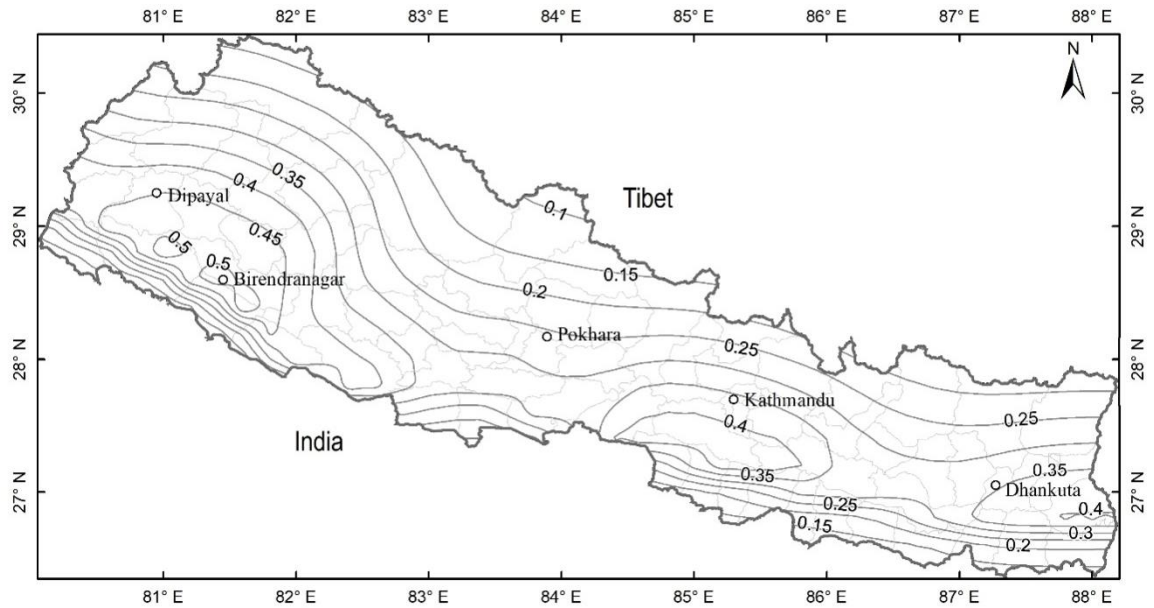
Appendix 13-5: Seismic hazard map with 50 km depth fixed to all vertices of the sources in Model-1 (Appendix 11-1). The maximum PGA is about 0.27 g in the southern part of far-west. The change in the shape of the contours can be noticed between this map and the previous one. Because of hanging wall effect and depth > 50 km north, the higher PGA contours are concentrated in the southern part of Nepal.
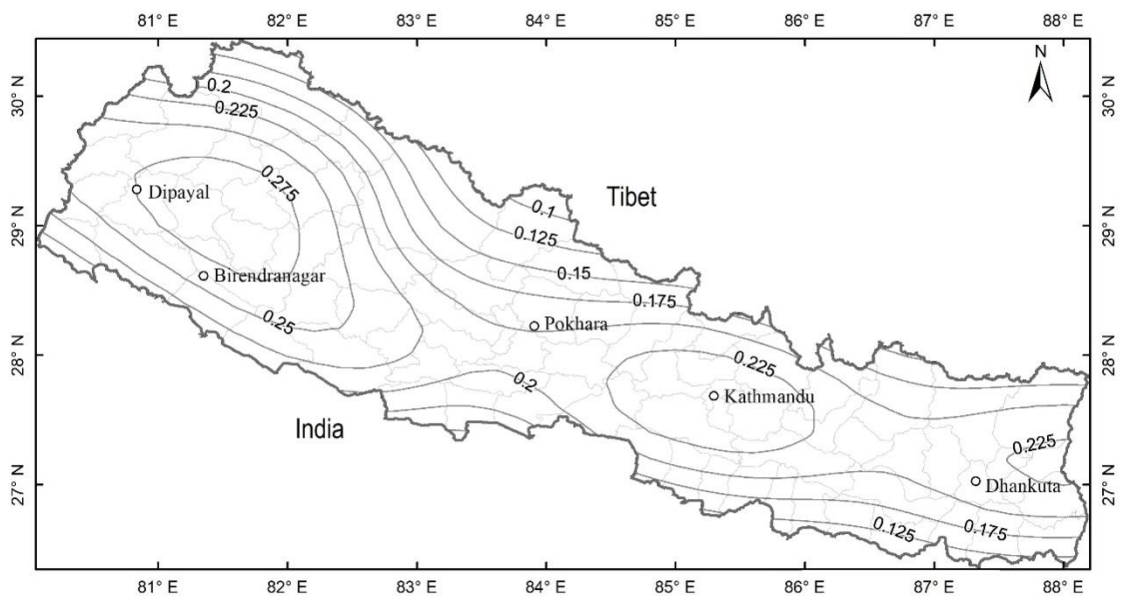
APPENDIX 14

Variation in seismic hazard with variation in maximum potential magnitude. Common model (Appendix 11-1), common attenuation relation and common recurrence parameters were used in this test.

Appendix 14-1: Seismic hazard map using maximum potential magnitude (Mw) 6.5. The maximum PGA is about 0.4 g in far-west and 0.3 g in Kathmandu Valley.
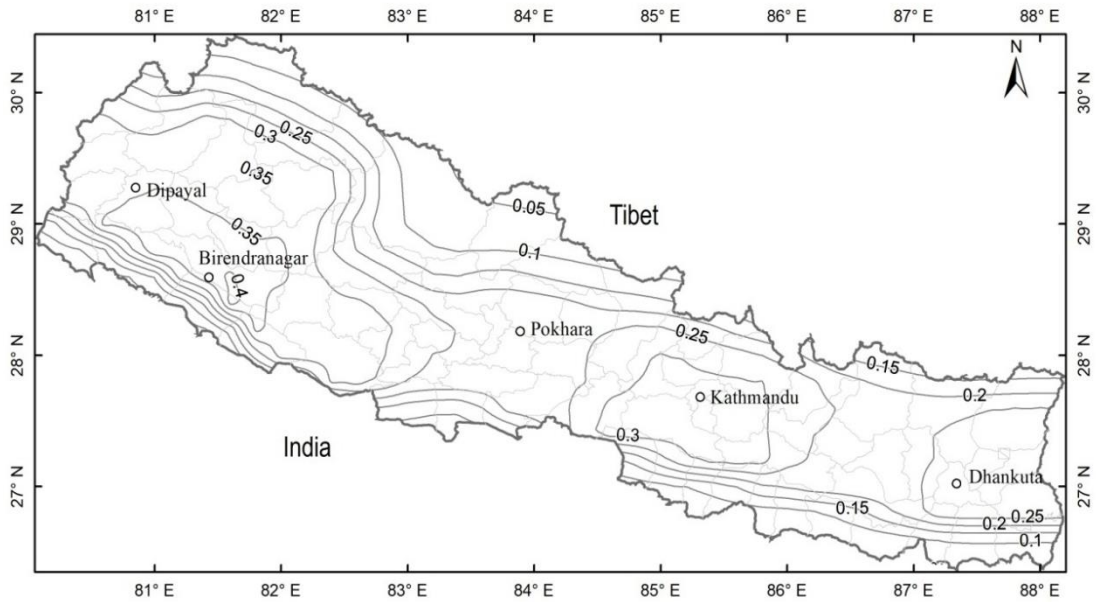
Appendix 14-2: Seismic hazard map using (Mw) 7.0 as maximum potential magnitude. The maximum PGA is about 0.45 g in a small area in far-west and 0.3 g in Kathmandu Valley.
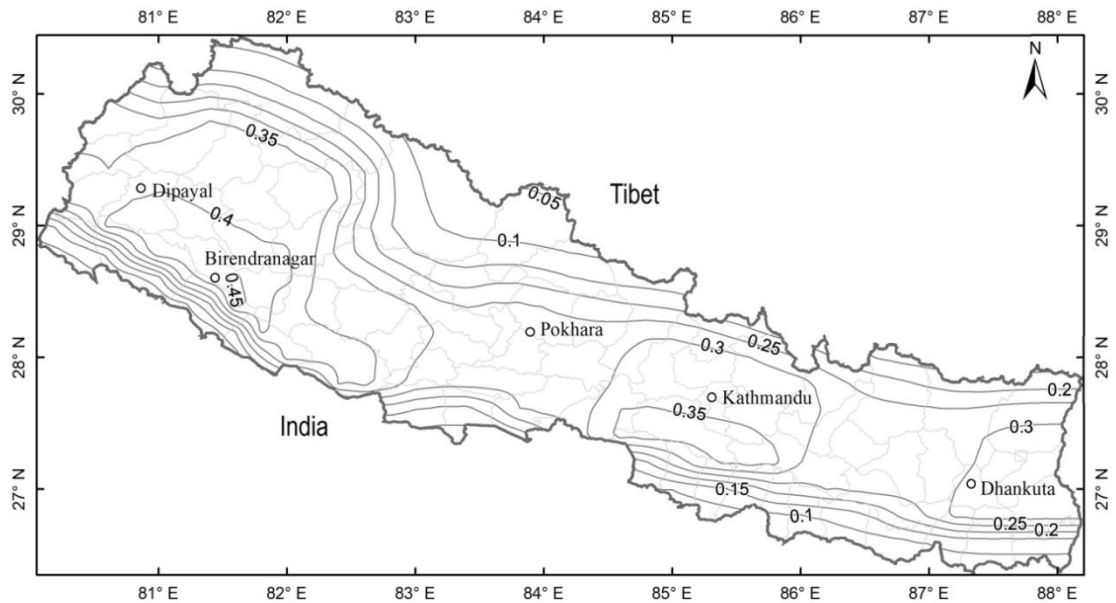
Appendix 14-3: Seismic hazard map using (Mw) 7.5 as maximum potential magnitude. The maximum PGA is about 0.5 g in a small area in far-west and 0.35 g in Kathmandu Valley.
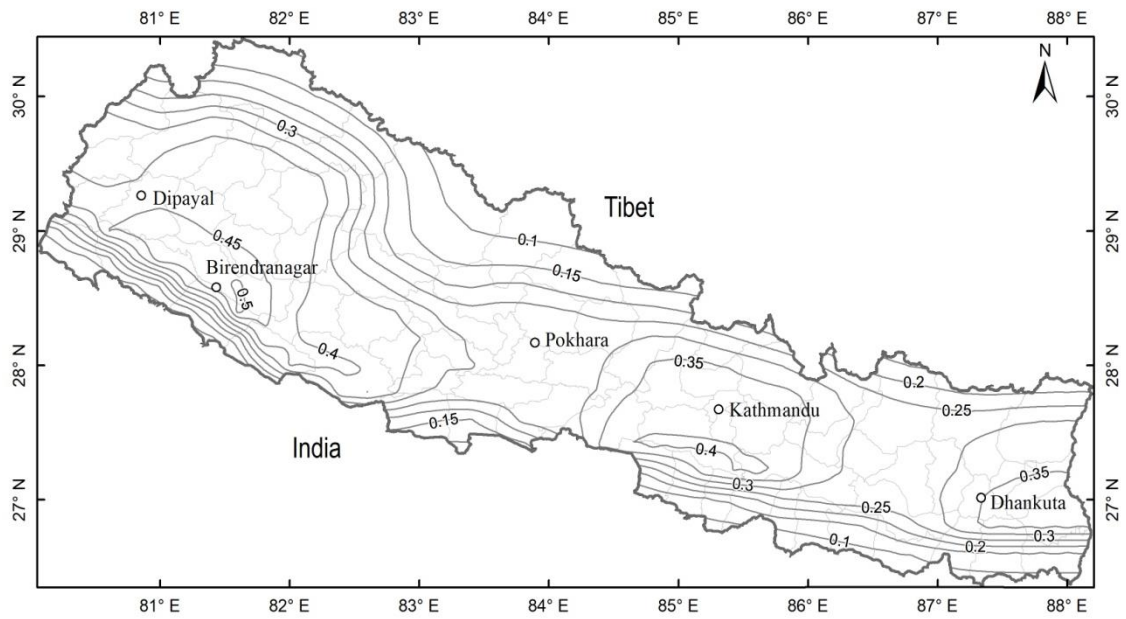
Appendix 14-4: Seismic hazard map using (Mw) 8.0 as maximum potential magnitude of sources. The maximum PGA is about 0.5 g in a small area in far-west and 0.4 g in Kathmandu Valley.
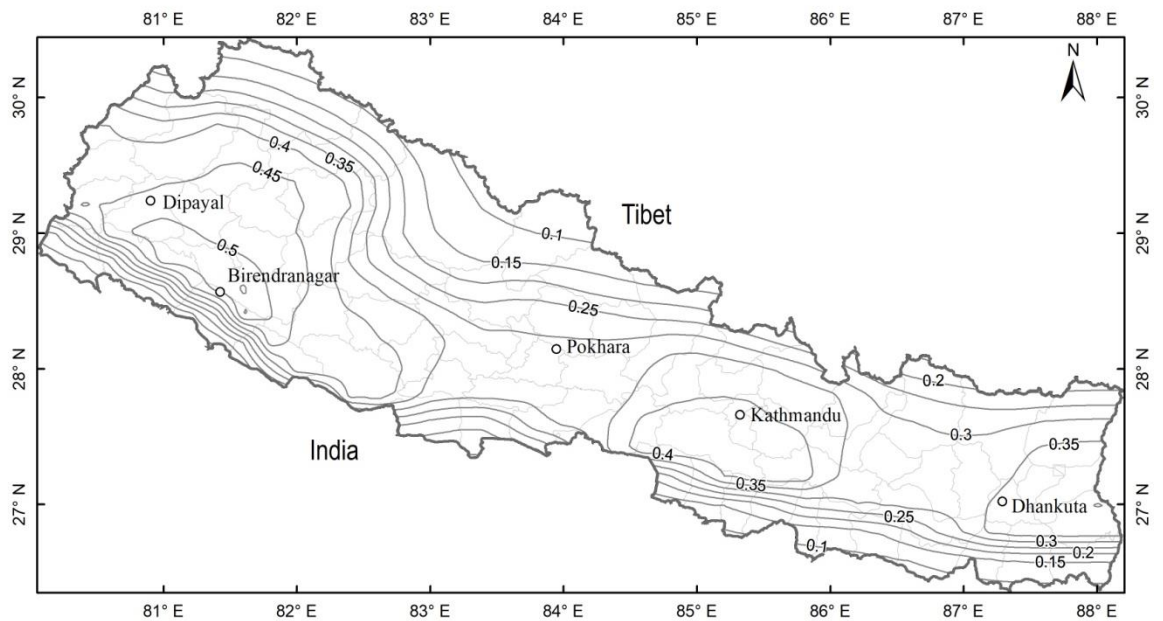
Appendix 14-5: Seismic hazard map using (Mw) 8.5 as maximum potential magnitude. The maximum PGA is about 0.55 g in a small area in far-west and 0.4 g in Kathmandu Valley.
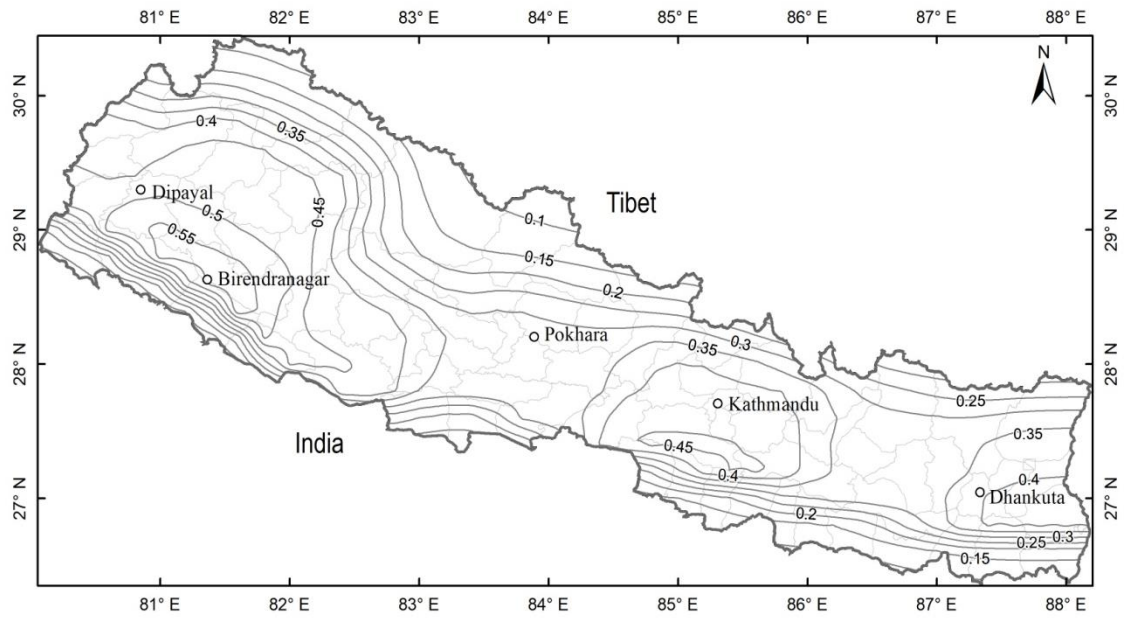
APPENDIX 15

Maximum potential magnitude and earthquake recurrence parameters of identified earthquake sources. The magnitudes of the earthquake sources, which are segments of the MHT were calculated using Equations 1, 2, 3, and 4. The magnitudes of other sources from South Tibet and north India were fixed to Mw 7.5 as we don't have data of large earthquakes and experience in those regions.

Appendix 15-1: Maximum potential magnitude and earthquake recurrence parameters of sources in Model-1 (Appendix11-1). The maximum potential magnitude of Model-2 and Model-3 were estimated assuming half rupture area of the corresponding sources in Model-1.

Source	a-value	b-value	λ	β	Max Mw
M1-1	4.3	0.95	0.37	2.19	8.2
M1-2	3.9	0.95	0.14	2.19	8.2
M1-3	4.2	0.95	0.27	2.19	8.2
M1-4	4.4	0.95	0.45	2.19	8.1
M1-5	4.4	0.95	0.40	2.19	8.2
M1-6	4.1	0.95	0.22	2.19	8.1
M1-7	4.1	0.95	0.23	2.19	8.3

Appendix 15-2: Maximum potential magnitude and earthquake recurrence parametersof sourcesin Model-2 (Appendix 11-2).

Source	a-value	b-value	λ	β	Max Mw
M2-1	4.3	0.95	0.37	2.19	7.9
M2-2	3.9	0.95	0.14	2.19	7.9
M2-3	4.2	0.95	0.27	2.19	7.9
M2-4	4.4	0.95	0.45	2.19	7.8
M2-5	4.4	0.95	0.40	2.19	8.0
M2-6	4.1	0.95	0.22	2.19	7.8
M2-7	4.1	0.95	0.23	2.19	8.0

Appendix 15-3: Maximum potential magnitude and earthquake recurrence parameters of sources in Model-3 (Appendix 11-3).

Source	a-value	b-value	λ	β	Mmax
M3-1	4.3	0.95	0.37	2.19	7.9
M3-2	3.9	0.95	0.14	2.19	7.9
M3-3	4.2	0.95	0.27	2.19	7.9
M3-4	4.4	0.95	0.45	2.19	7.8
M3-5	4.4	0.95	0.40	2.19	8.0
M3-6	4.1	0.95	0.22	2.19	7.8
M3-7	4.1	0.95	0.23	2.19	8.0

Appendix 15-4: Maximum potential magnitude and earthquake recurrence parametersof sourcesin Model-4 (Appendix 11-4).

Source	a-value	b-value	λ	β	Mmax
M4-1	4.2	1.1	0.05	2.53	7.5
M4-2	4.2	1.1	0.13	2.53	7.5
M4-3	4.9	1.1	0.26	2.53	7.5
M4-4	4.3	0.95	0.32	2.19	8.4
M4-5	4.3	0.95	0.39	2.19	8.2
M4-6	3.9	0.95	0.15	2.19	8
M4-7	4.2	0.95	0.30	2.19	8.2
M4-8	4.0	0.95	0.16	2.19	8
M4-9	4.2	0.95	0.25	2.19	8.1
M4-10	4.5	1	0.34	2.30	7.5
M4-11	4.5	0.95	0.60	2.19	5.2
M4-12	4.4	0.95	0.50	2.19	8.3
M4-13	5.3	1.1	0.64	2.53	7.5
M4-14	5.1	1.1	0.44	2.53	7.5
M4-15	4.9	1.1	0.28	2.53	7.5
M4-16	5.1	1.1	0.44	2.53	7.5
M4-17	5.3	1.1	0.59	2.53	7.5
M4-18	5.2	1.1	0.50	2.53	7.5
M4-19	5.1	1.1	0.40	2.53	7.5
M4-20	5.0	1.1	0.32	2.53	7.5

Appendix 15-5: Maximum potential magnitude and earthquake recurrence parametersof sourcesin Model-5 (Appendix 11-5)

Source	a-value	b-value	λ	β	Mmax
M5-1	4.4	1.1	0.07	2.53	7.5
M5-2	4.5	1.1	0.11	2.53	7.5
M5-3	4.6	1.1	0.11	2.53	7.5
M5-4	5.0	1.1	0.32	2.76	7.5
M5-5	3.7	0.95	0.09	2.19	8.3
M5-6	4.4	0.95	0.48	2.19	8.2
M5-7	3.8	0.95	0.11	2.19	7.9
M5-8	4.0	0.95	0.20	2.19	8.1
M5-9	4.8	1	0.56	2.53	8.1
M5-10	4.3	0.95	0.35	2.19	7.9
M5-11	4.1	0.95	0.20	2.19	7.9
M5-12	4.4	0.95	0.50	2.19	7.5
M5-13	4.2	0.95	0.28	2.19	7.7
M5-14	4.6	1	0.44	2.19	8.2
M5-15	4.9	1.1	0.26	2.53	7.5
M5-16	5.2	1.1	0.50	2.53	7.5
M5-17	4.9	1.1	0.23	2.53	7.5
M5-18	4.9	1.1	0.27	2.53	7.5
M5-19	4.7	1.1	0.14	2.53	7.5
M5-20	5.0	1.1	0.29	2.53	7.5
M5-21	5.2	1.1	0.51	2.53	7.5

Appendix 15-6: Maximum potential magnitude and earthquake recurrence parametersof sourcesin Model-6 (Appendix 11-6).

Source	a-value	b-value	λ	β	Mmax
M6-1	3.3	1.1	0.04	2.53	7.5
M6-2	3.7	1.1	0.08	2.53	7.5
M6-3	3.8	1.1	0.13	2.53	7.5
M6-4	4.6	1.1	0.72	2.53	7.5
M6-5	4.1	0.95	0.21	2.19	8.2
M6-6	4.2	0.95	0.30	2.19	8.1
M6-7	3.9	0.95	0.13	2.19	8
M6-8	4.2	0.95	0.30	2.19	8.3
M6-9	4.0	0.95	0.18	2.19	8.1
M6-10	4.1	0.95	0.20	2.19	8
M6-11	4.5	0.95	0.56	2.19	8.4
M6-12	4.4	0.95	0.49	2.19	8.5
M6-13	3.9	1.1	0.14	2.53	7.5
M6-14	4.6	1.1	0.14	2.53	7.5
M6-15	4.2	1.1	0.05	2.53	7.5
M6-16	4.1	1.1	0.04	2.53	7.5
M6-17	4.5	1.1	0.10	2.53	7.5
M6-18	4.5	1.1	0.09	2.53	7.5
M6-19	4.7	1.1	0.17	2.53	7.5
M6-20	4.6	1.1	0.13	2.53	7.5
M6-21	4.6	1.1	0.14	2.53	7.5
M6-22	3.9	1.1	0.03	2.53	7.5
M6-23	4.5	1.1	0.17	2.53	7.5
M6-24	4.1	1.1	0.16	2.53	7.5

Appendix 15-7: Maximum potential magnitude and earthquake recurrence parametersof sourcesin Model-7 (Appendix 11-7).

Source	a-value	b-value	λ	β	Mmax
M7-1	3.8	0.95	0.12	2.19	7.5
M7-2	4.0	0.95	0.20	2.19	7.5
M7-3	3.9	0.95	0.15	2.19	7.5
M7-4	4.5	0.95	0.54	2.19	8.2
M7-5	4.0	0.95	0.17	2.19	7.9
M7-6	4.4	0.95	0.42	2.19	8.2
M7-7	4.4	0.95	0.50	2.19	8.2
M7-8	4.8	1	0.57	2.30	8.3
M7-9	4.5	0.95	0.61	2.19	8.3
M7-10	4.8	1.1	0.19	2.53	7.5
M7-11	4.2	1.1	0.05	2.53	7.5
M7-12	4.3	1.1	0.07	2.53	7.5
M7-13	4.6	1.1	0.12	2.53	7.5
M7-14	5.0	1.1	0.28	2.53	7.5
M7-15	5.0	1.1	0.28	2.53	7.5

Appendix 15-8: Maximum potential magnitude and earthquake recurrence parametersof sourcesin Model-8 (Appendix 11-8).

Source	a	b	λ	β	Mmax
M8-1	3.5	0.95	0.06	2.19	7.5
M8-2	2.7	0.95	0.01	2.19	7.5
M8-3	2.7	0.95	0.01	2.19	7.5
M8-4	2.6	0.95	0.01	2.19	7.5
M8-5	4.8	0.95	1.19	2.19	7.5
M8-6	4.3	0.95	0.40	2.19	8.4
M8-7	4.4	0.95	0.54	2.19	8.4
M8-8	4.4	0.95	0.51	2.19	8.5
M8-9	4.4	0.95	0.56	2.19	8.5
M8-10	4.9	0.95	1.45	2.19	8.5
M8-11	4.5	0.95	0.62	2.19	8.6
M8-12	4.1	0.95	0.22	2.19	7.5
M8-13	5.3	1.1	0.79	2.53	7.5
M8-14	5.6	1.1	1.47	2.53	7.5
M8-15	5.7	1.1	1.87	2.53	7.5
M8-16	5.3	1.1	0.67	2.53	7.5
M8-17	5.6	1.1	1.42	2.53	7.5
M8-18	4.8	1.1	0.5	2.53	7.5

Appendix 15-9: Maximum potential magnitude and earthquake recurrence parametersof sourcesin Model-9 (Appendix 11-9).

Source	a	b	λ	β	Mmax
M9-1	4.3	0.95	0.34	2.18	8.4
M9-3	4.7	1.10	0.18	2.53	7.5
M9-4	4.3	1.10	0.06	2.53	7.5
M9-5	3.6	1.00	0.04	2.303	7.5
M9-6	4.3	0.95	0.35	2.18	8.3
M9-7	4.8	1.10	0.22	2.53	7.0
M9-8	4.8	1.10	0.2	2.53	7.5
M9-9	4.8	1.10	0.2	2.53	7.5
M9-10	4.0	0.95	0.2	2.18	8.1
M9-11	4.6	1.10	0.14	2.53	7.5
M9-12	4.7	1.10	0.16	2.53	7.5
M9-14	4.2	1.10	0.05	2.53	7.5
M9-15	4.7	1.10	0.15	2.53	7.5
M9-16	5.6	1.20	0.38	2.76	7.5
M9-17	3.8	0.95	0.12	2.18	8.0
M9-18	4.2	0.95	0.31	2.18	8.2
M9-19	5.6	1.20	0.39	2.76	7.5
M9-20	4.3	0.95	0.39	2.18	8.3
M9-21	4.3	0.95	0.4	2.18	8.4
M9-22	5.0	1.20	0.1	2.76	7.5
M9-23	4.5	1.10	0.1	2.53	7.5
M9-24	4.0	0.95	0.2	2.18	8.3

APPENDIX 16

Variation of seismic hazard with variation in b-value. The b-value was changed from 0.7 to 1.2 successively with the increment of 0.1. Common attenuation relation, common source model (Model-1) and common earthquake recurrence parameters were used in the following tests.

Appendix 16-1: Seismic hazard map prepared using b-value 0.7. The PGA is as high as 0.75 in the far-west and 0.6 in the Kathmandu Valley.
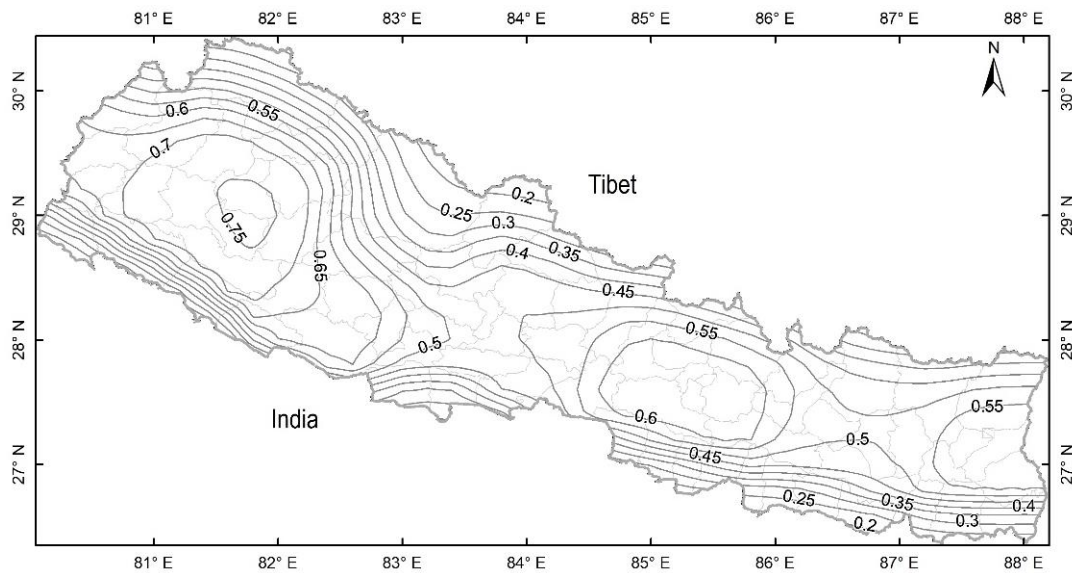
Appendix 16-2: Seismic hazard map prepared using b-value 0.8. The PGA is as high as 0.6 g in the far-west and 0.5 g in the Kathmandu Valley.
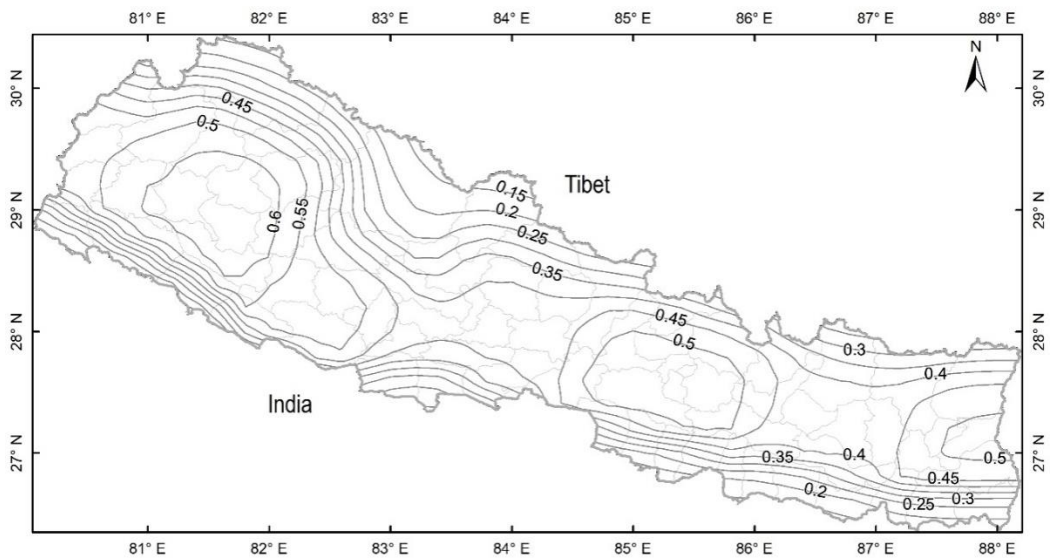
Appendix 16-3: Seismic hazard map prepared using b-value 0.9. The PGA is as high as 0.5g in the far-west and 0.45 g in the Kathmandu Valley.
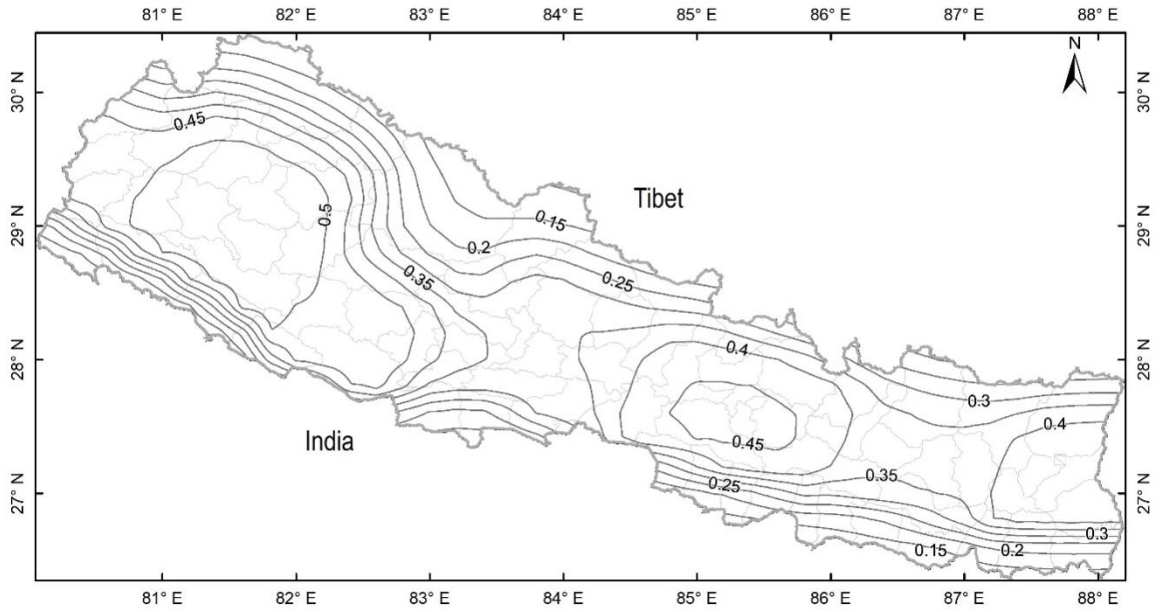
Appendix 16-4: Seismic hazard map prepared using b-value 1.0. The PGA is as high as 0.4 g in the far-west and 0.35 g in the Kathmandu Valley.
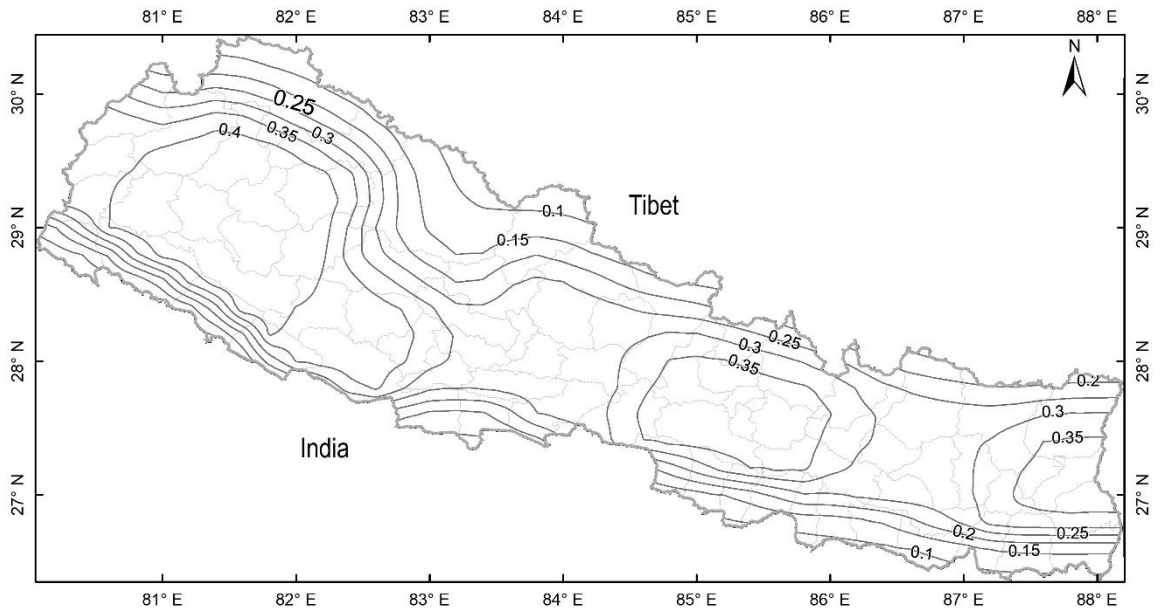
Appendix 16-5: Seismic hazard map prepared using b-value 1.1. The PGA is as high as 0.35 g in the far-west and 0.3 g in the Kathmandu Valley.
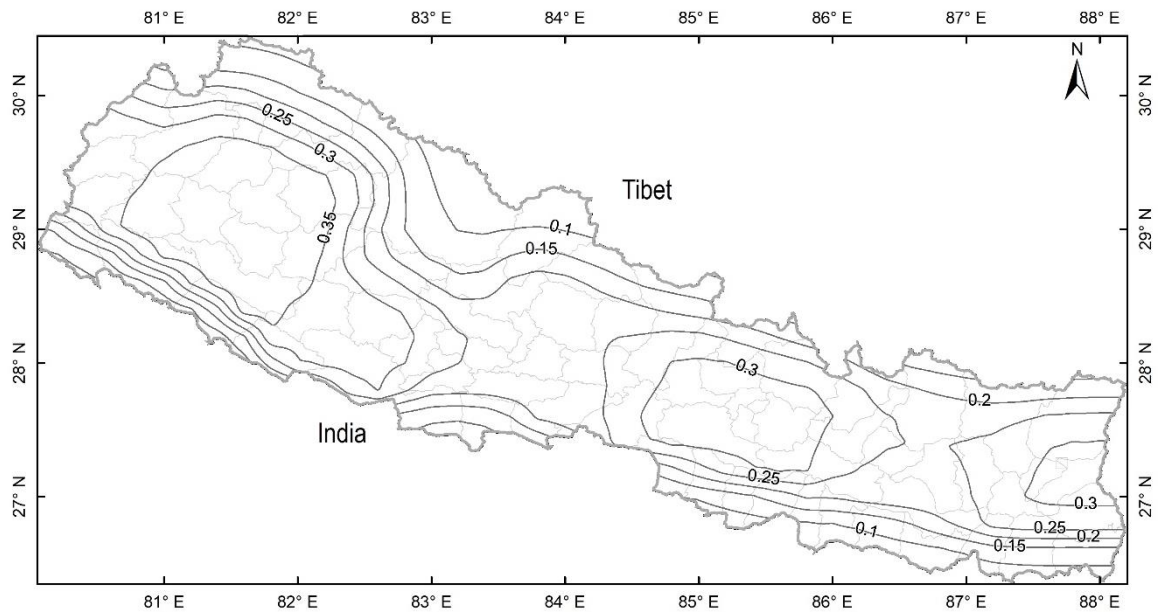
Appendix 16-6: Seismic hazard map prepared using b-value 1.2. The PGA is as high as 0.3 g in the far-west and 0.25 g in the Kathmandu Valley.
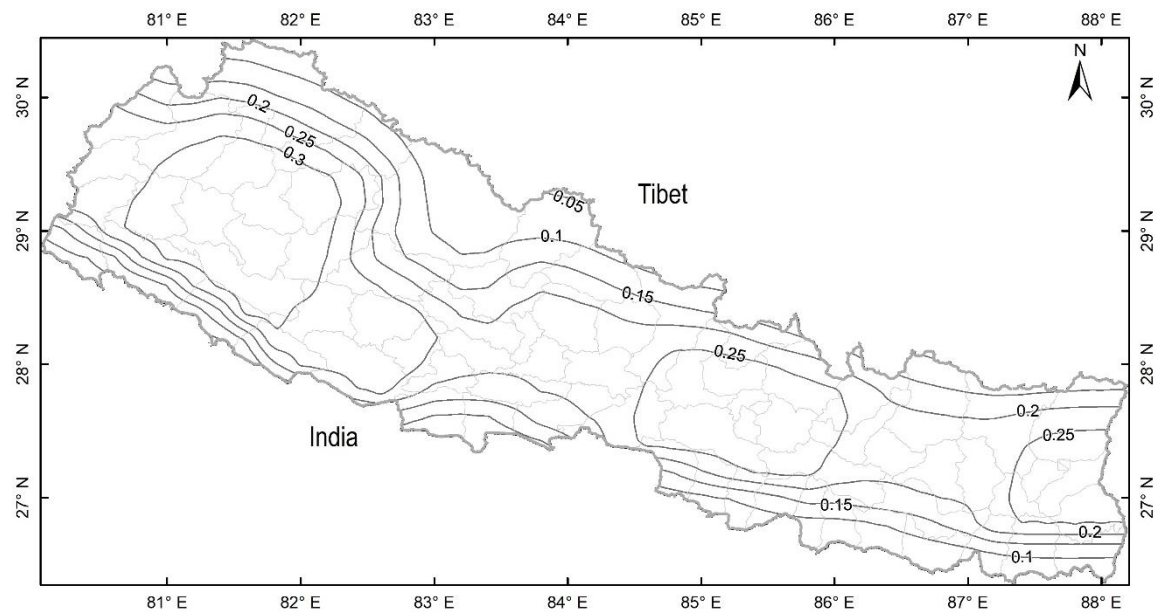
APPENDIX 17

Variation in seismic hazard with different catalogues and differently estimated a- and b-values.

Appendix 17-1: Seismic hazard map prepared using an earthquake catalogue, which contains data since 1900 AD. The a- and b-values of the sources (Appendix 11-1) were calculated applying least square method.
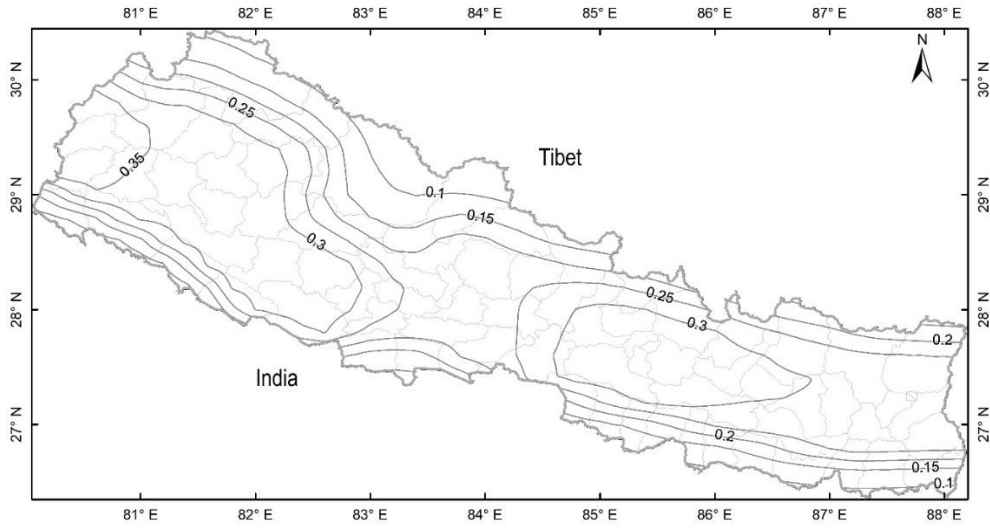
Appendix 17-2: Seismic hazard map prepared using data since 1900 AD. A fixed b-value f (0.95) was applied to all sources (Appendix 11-1) and a-values were calculated from the data.
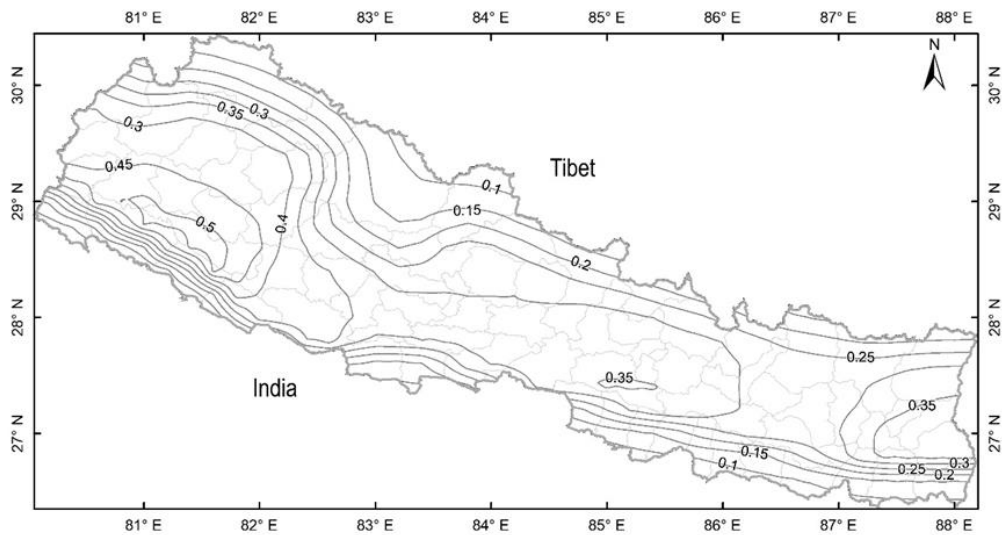
Appendix 17-3: Seismic hazard map prepared using data since 1100 AD. The a- and b-values of the sources (Appendix 11-1) were calculated applying least square method. The maximum PGA is larger than that in Appendix 17-2.
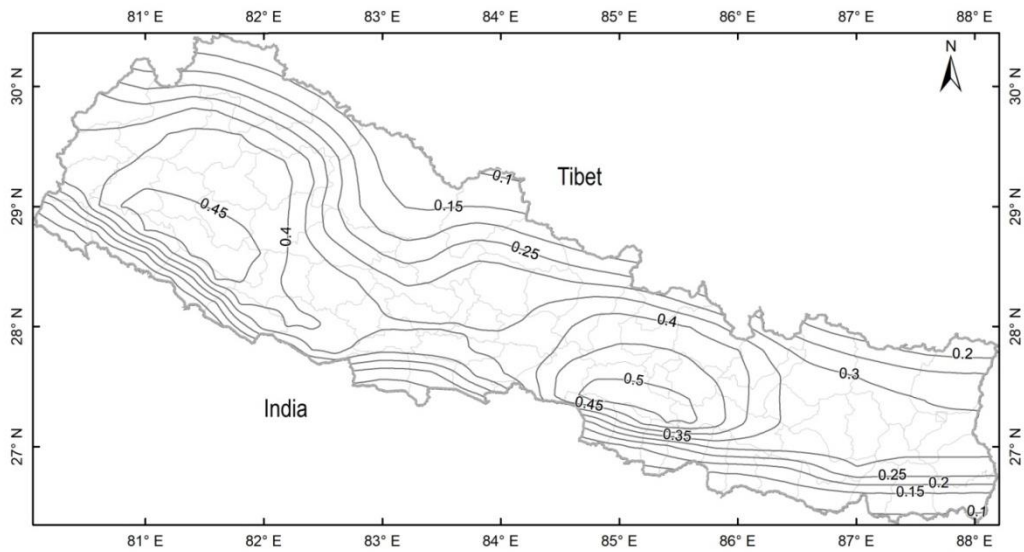
Appendix 17-4: Seismic hazard map prepared using earthquake parameters from the instrumental data available since 1100. A fixed b-value (0.95) was used to recalculate the a-values of the sources (Appendix 11-1). The maximum PGA is larger than that in Appendix 17-3.
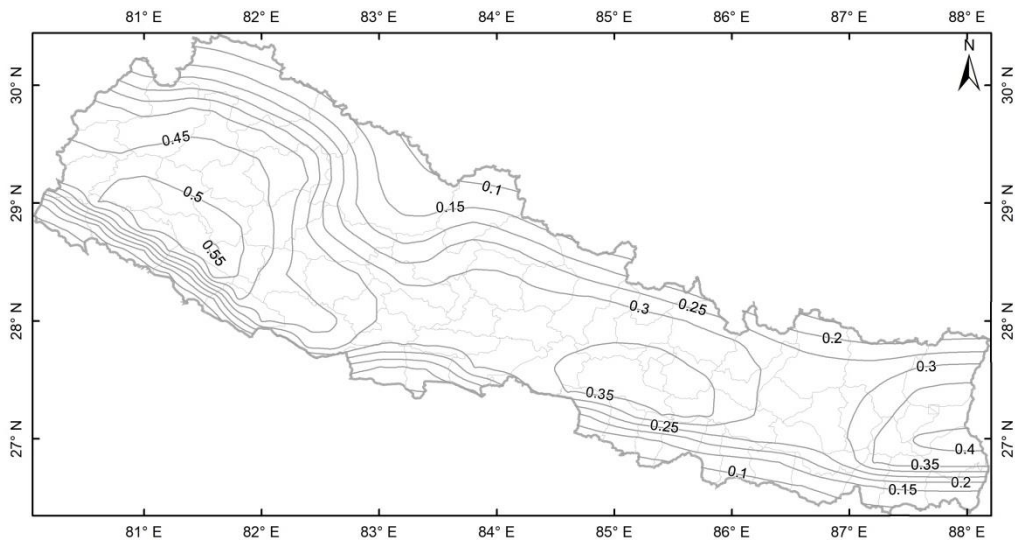
Appendix 17-5: Seismic hazard map prepared using data since 1964. After 1964, there is regular reporting of earthquakes up to Mw 4.0. The b-value was fixed to 0.95 and a-values were recalculated from data. The maximum PGA is comparable to Appendix 17-4.
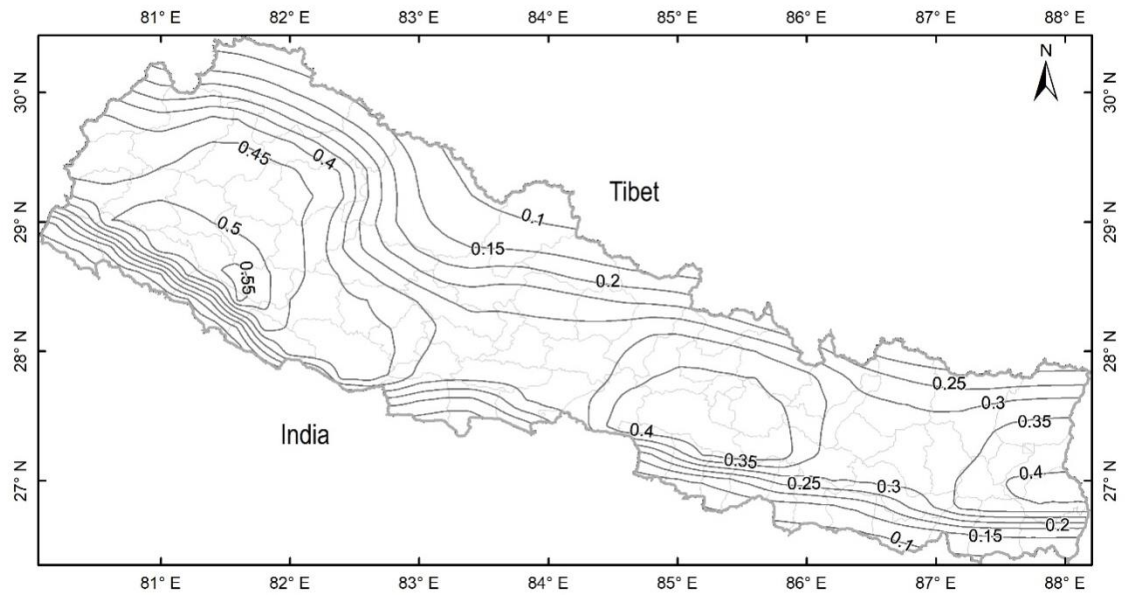
APPENDIX 18

Attenuation relations (also called ground motion prediction equation (GMPE)), which were used in this study.

Appendix 18-1: Attenuation relations for subduction zone. The Atkinson and Boore (2003) relation was not used in hazard calculations because it produces considerably small hazard (Appendix 19-2)
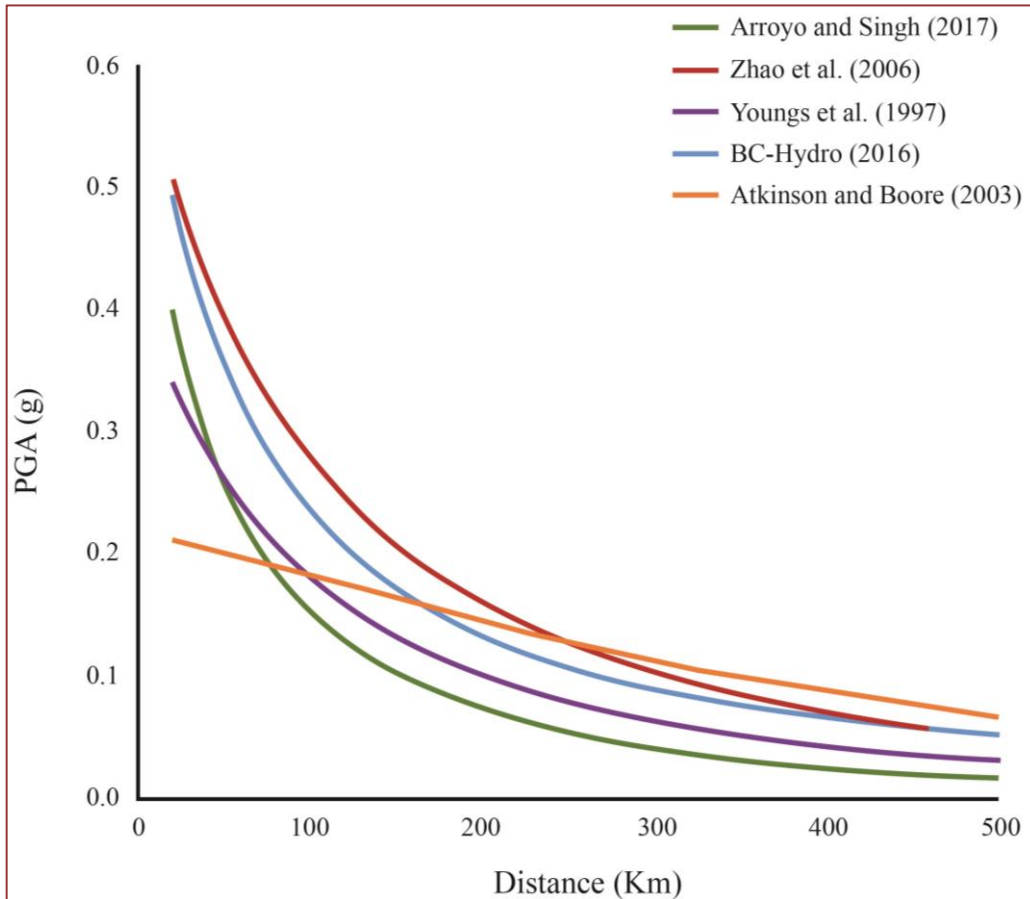
Appendix 18-2: Description of attenuation relations for subduction zone.

Features	Attenuation relations				
	Zhao *et al*. (2006)	Young's *et al*. (1997)	BcHydro(2016)	Atkinson And Boore (2003)	Arroyo and Singh (2017)
Database	USA and Iran	Global	NGA-Westt-2	Cascadia, Japan, Mexico, Central America	India and Nepal
Valid Distance (Km)	0-300	10-500	10-300	1-300	0-1000
Distance metric	Rrup	Rrup	Rrup	Rup	Rrup
Spectral Period (s)	0-5	0-5	0-10	0-3	0.01-6
Magnitude (Mw)	5-8.3	5-8.5	6-8.4	5-8.5	5-8.0
Unit	gal	gal	g	gal	gal

Appendix 18-3: Attenuation relation for shallow-active crustal earthquakes (normal fault earthquakes).
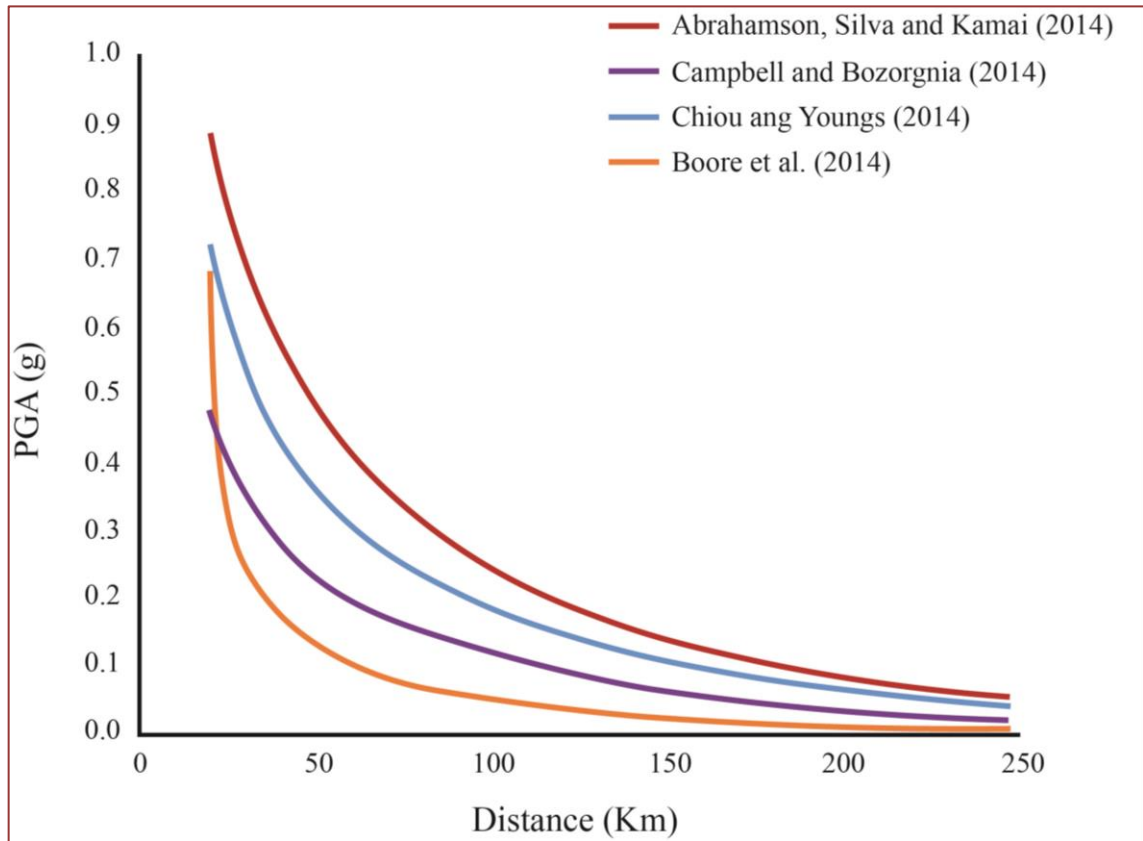
Appendix 18-4: Attenuation relations for subduction zone. The Atkinson and Boore (2003) relation produces the smallest PGA, therefore was not used. The other four relations were used in this study using a logic tree with equal weight for earthquake sources in the Himalaya (MHT).

Features	Attenuation relations			
	Abrahamson, Silva and Kamai (2014)	Boore *et al.* (2014)	Chiou and Youngs (2014)	Campbell and Bozorgnia (2014)
Database	NGA-West-2	NGA-West-2	NGA-Westt-2	NGA-Westt-2
Valid Distance (Km)	0-300	0-400	0-300	0-300
Distance metric	Rrup	Jyb	Rrup	Rup
Spectral Period (s)	0-10	0-10	0-10	0-10
Magnitude (Mw)	3-8.5	3-8.5	3.5-8	3-8.5
Unit	g	g	g	g

APPENDIX 19

Common earthquake recurrence parameters to different attenuation relations, common attenuation relation and common source models were applied to different attenuation relations.

Appendix 19-1: Seismic hazard map prepared using Youngs *et al*. (1997) attenuation relation. This relation is for subduction region. The maximum PGA is larger than 0.85 g in the far-west and over 0.6 g in the Kathmandu Valley.
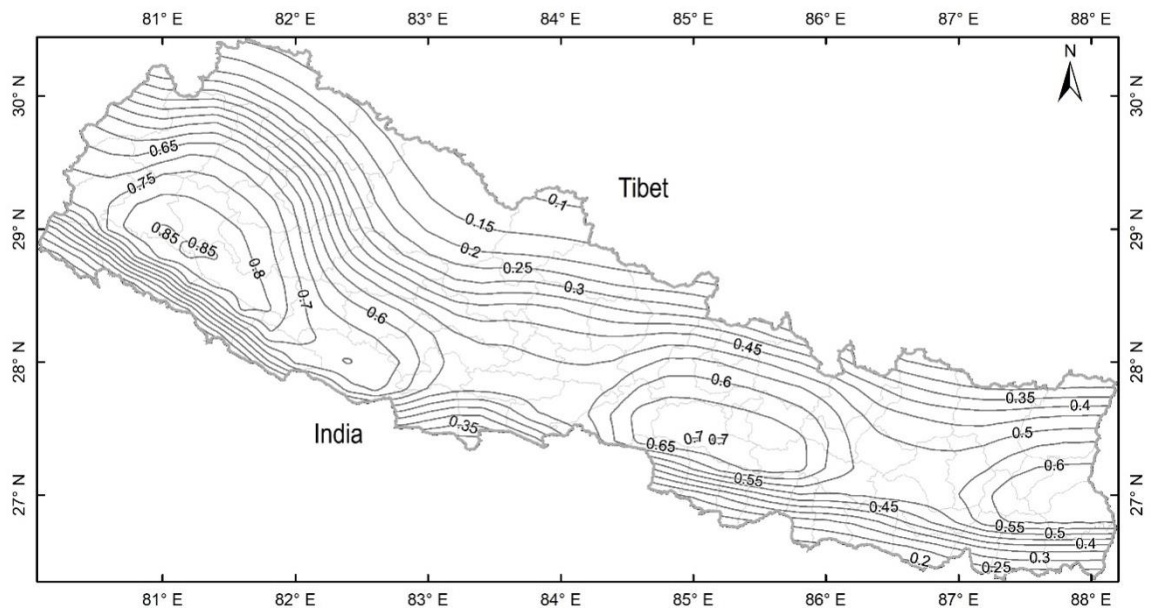
Appendix 19-2: Seismic hazard map prepared using Atkinson and Boore (2003) attenuation relation. This relation is for subduction region. The maximum PGA is very small (0.8 g) in the far-west and 0.14 g in the Kathmandu Valley in comparison to other relations.
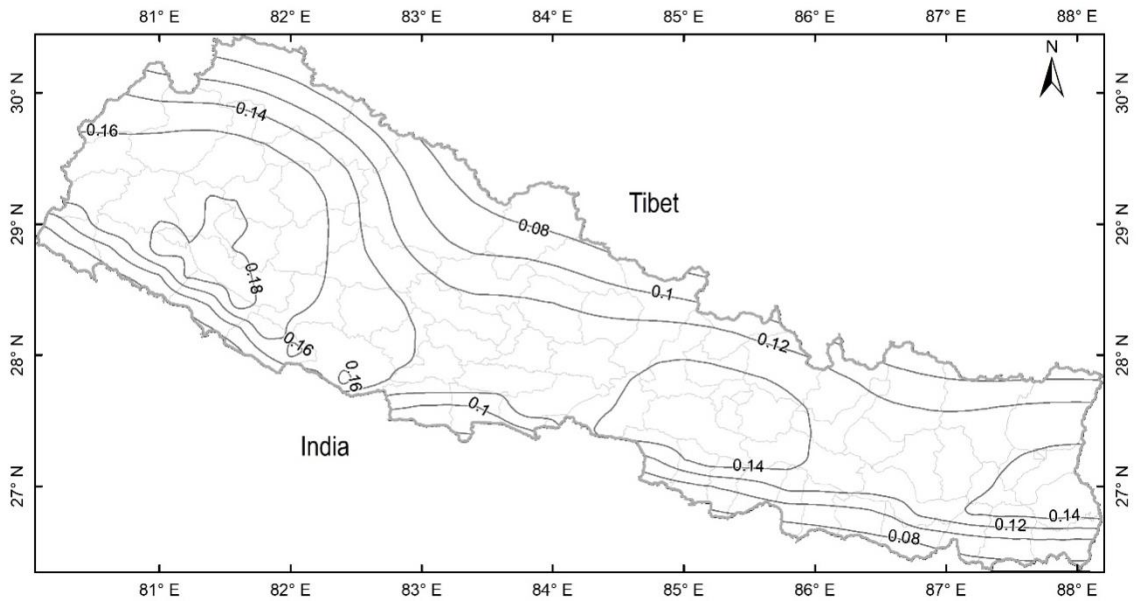
Appendix 19-3: Seismic hazard map prepared using Zhao *et al*. (2006) attenuation relation. The maximum PGA is larger than 0.5 g in the far-west and over 0.3 g in the Kathmandu Valley.
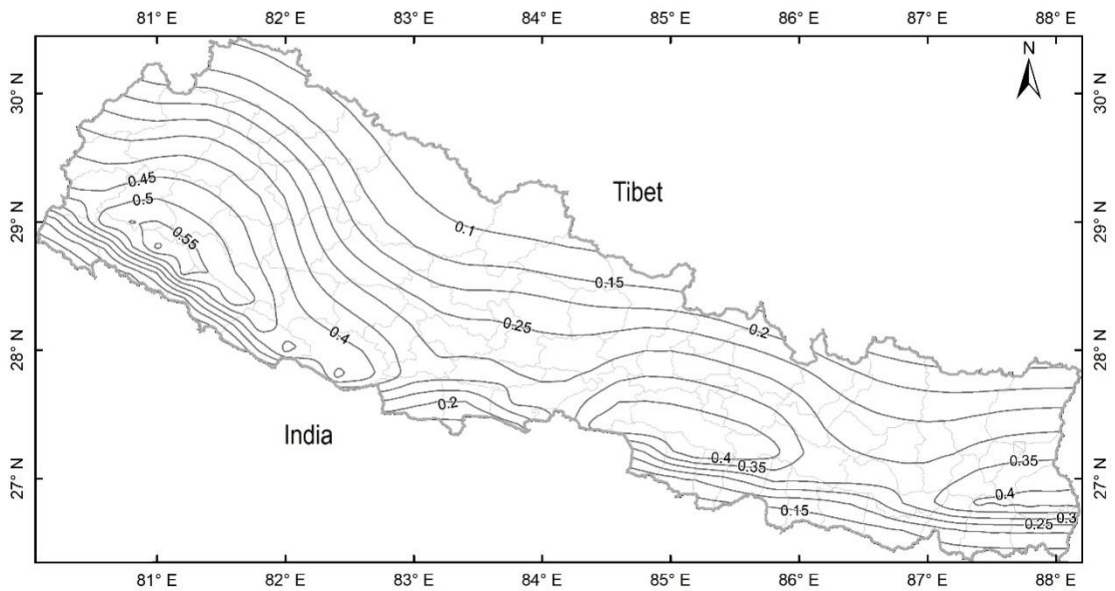
Appendix 19-4: Seismic hazard map prepared using BC-Hydro (2016) attenuation relation. The maximum PGA is larger 0.4 g than in far-west and over 0.25 g in the Kathmandu Valley.
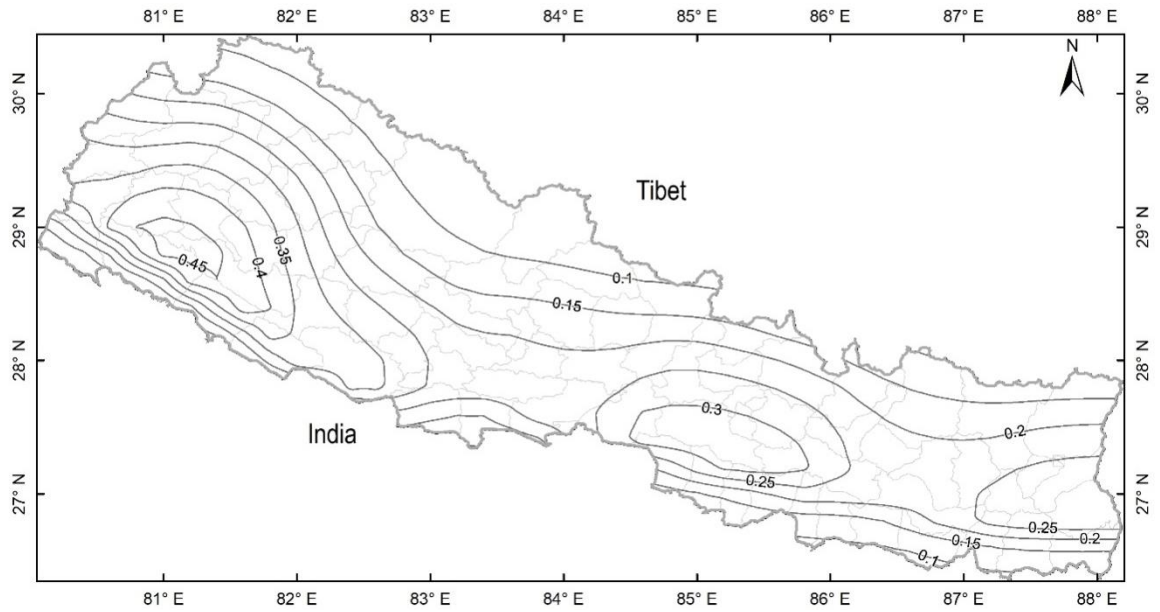
Appendix 19-5: Seismic hazard map prepared using Arroyo and Singh (2017) attenuation relation. The maximum PGA is larger than 0.28 g in the far-west and over 0.22 g in the Kathmandu Valley.
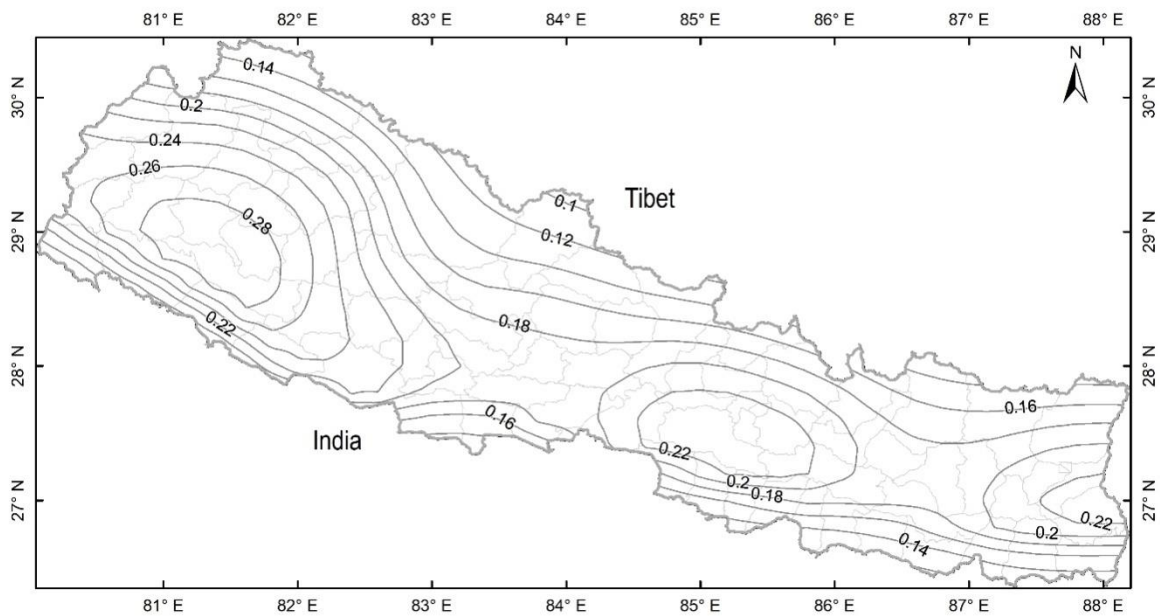
Appendix 19-6: Seismic hazard map prepared using Atkinson, Silva and Kamai (2014) attenuation relation. This relation and other relationsonwards are for active shallow crustal earthquakes. The maximum PGA is larger than 0.5 g in the far-west and over 0.4 g in the Kathmandu Valley.
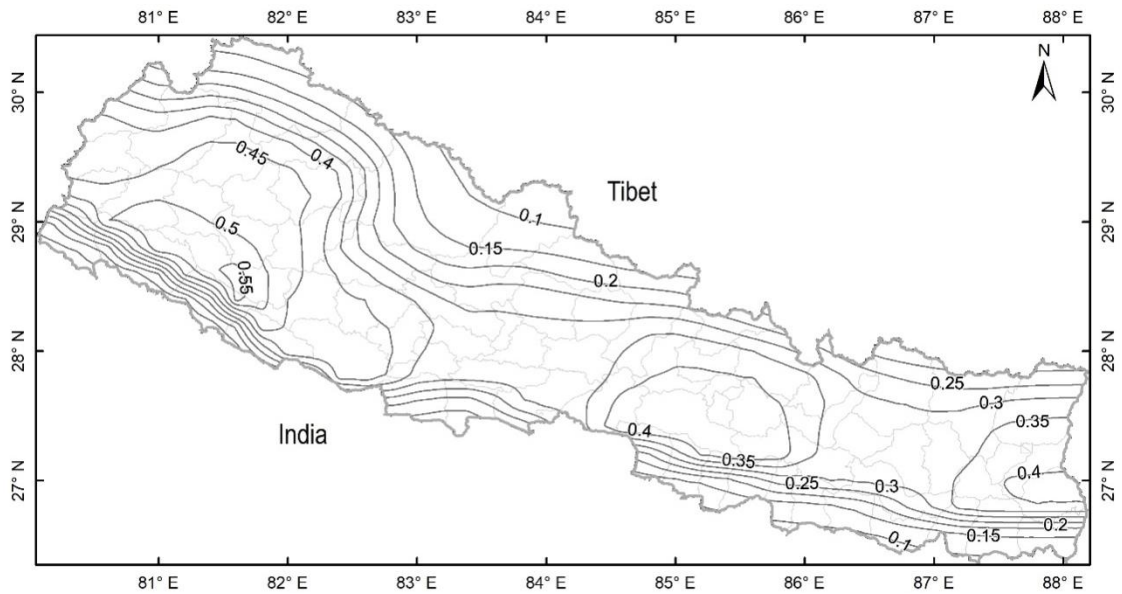
Appendix 19-7: Seismic hazard map prepared using Boore *et al*. (2014) attenuation relation. The maximum PGA is larger than 0.55 g in the far-west and over 0.35 g in the Kathmandu Valley.
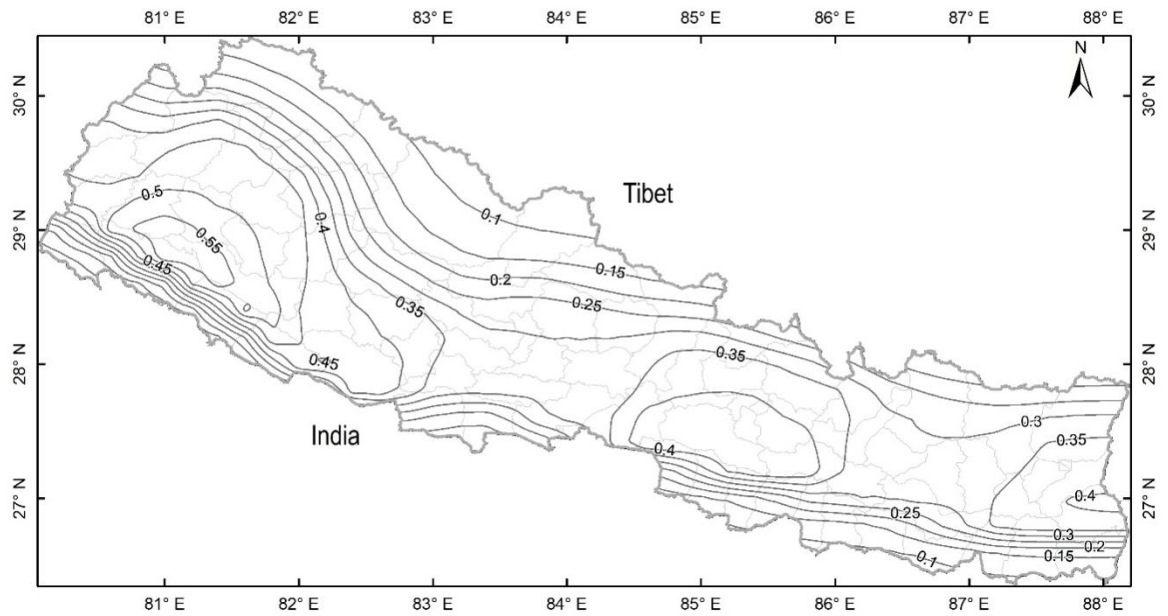
Appendix 19-8: Seismic hazard map prepared using Campbell and Bozorgnia (2014) attenuation relation. The maximum PGA is larger than 0.55 g in the far-west and over 0.35 g in the Kathmandu Valley.
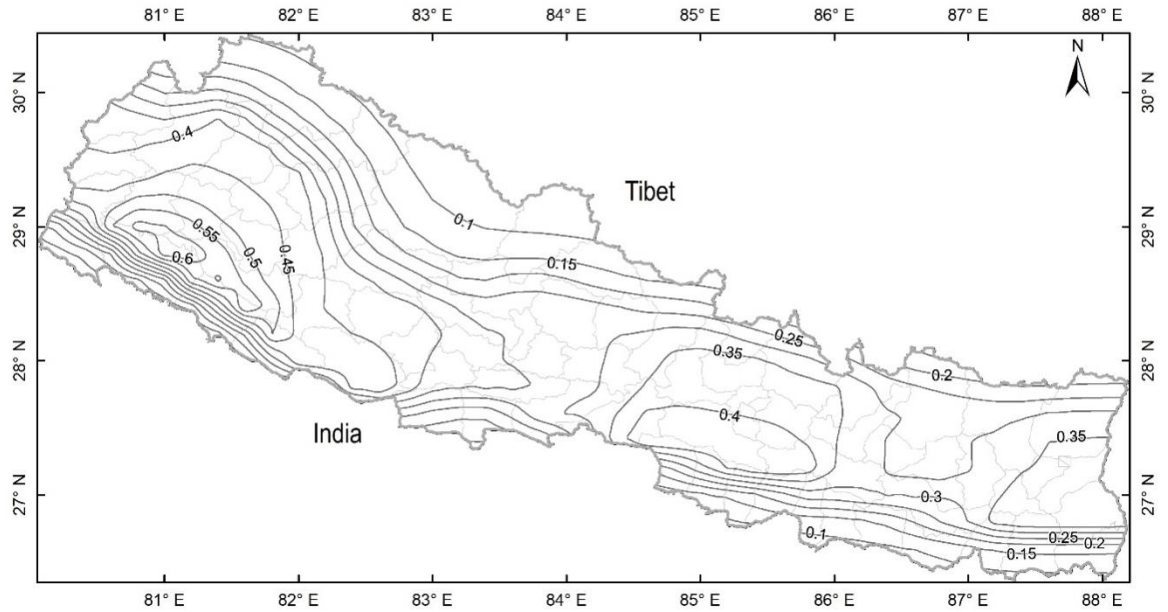
Appendix 19-9: Seismic hazard map prepared using Chiou and Youngs (2014) attenuation relation for active shallow crustal earthquakes. The maximum PGA is larger than 0.5 g in the far-west and over 0.35 g in the Kathmandu Valley.
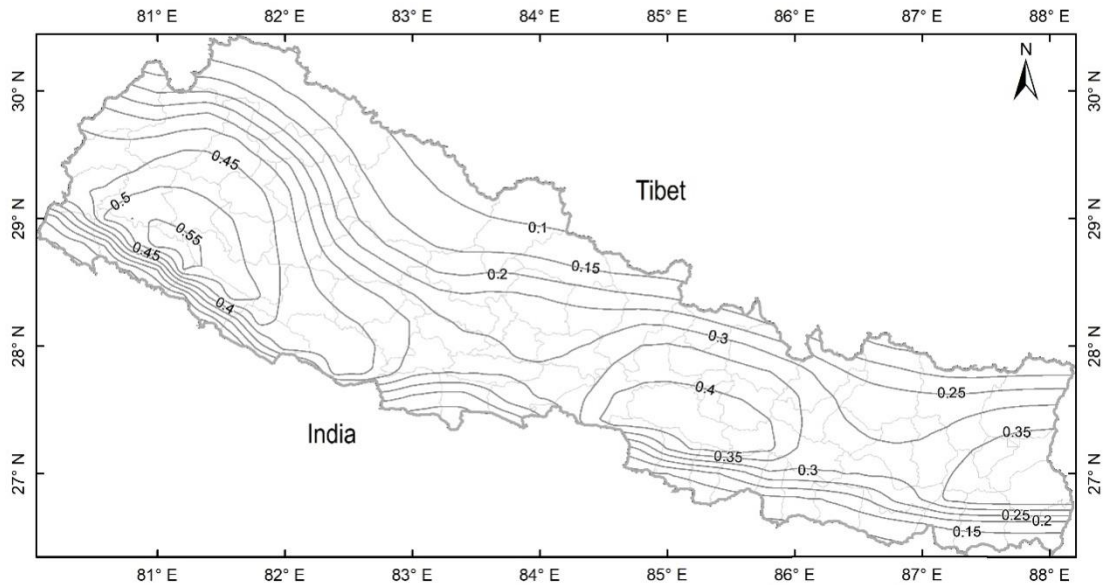
APPENDIX 20

Seismic hazard maps prepared using different source models. Nine different source models were used with common attenuation relation and common earthquake recurrence parameters.

Appendix 20-1: Seismic hazard map prepared using Model-1 (Appendix 11-1).. The largest PGA is 0.55 g in the far-west.
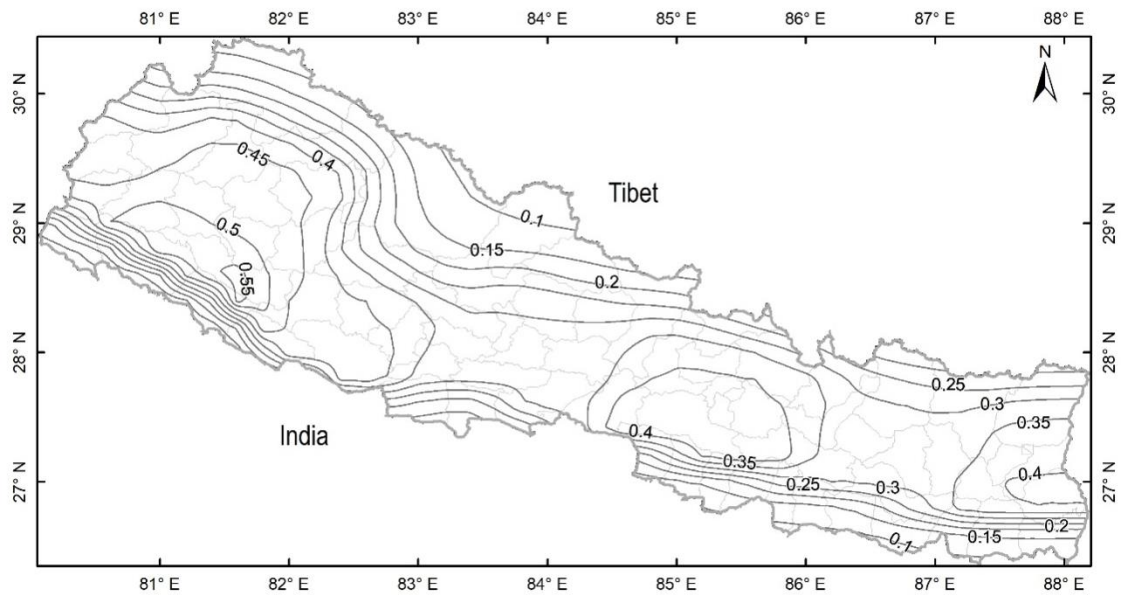
Appendix 20-2: Seismic hazard map prepared using Model 2 (Appendix 11-2). The high hazard is in the middle part because northern half area (rupture scenario) of Model-2 (Appendix 11-2) was used as a source. The sources have 20 km fixed depth in the north and 10 km in their southern part. The largest PGA is 0.5 g in the far-west and larger than 0.4 in the Kathmandu Valley.
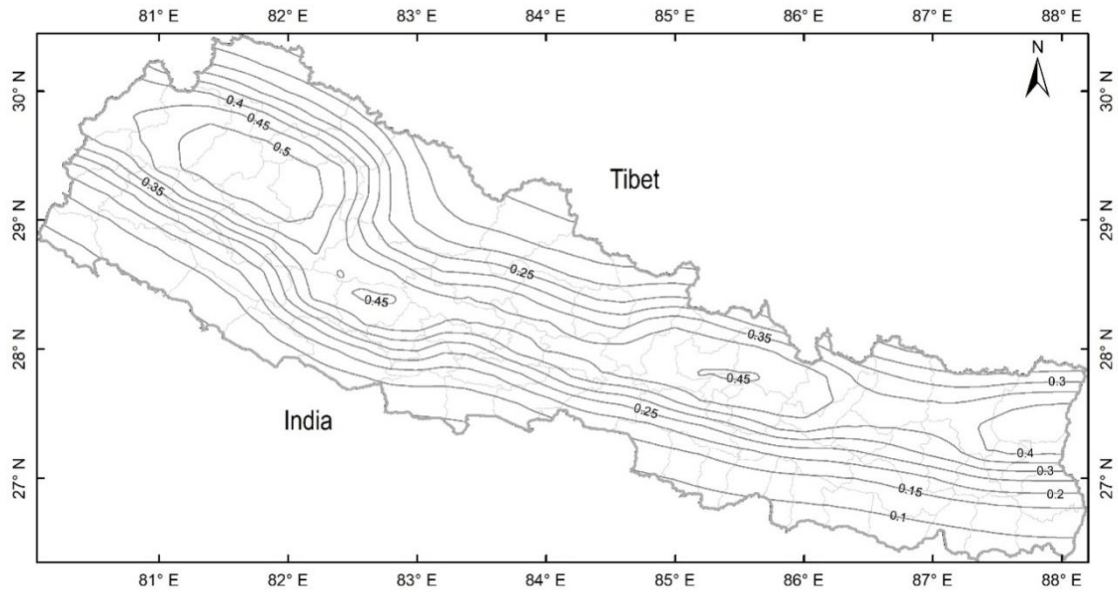
Appendix 20-3: Seismic hazard map prepared using Model-3 (Appendix 11-3). The sources have 10 km fixed depth in the north and 0 km in their southern border, where MHT emerges to the surface along MFT. The largest PGA is 0.7 g in the far-west and larger than 0.3 in the Kathmandu Valley.
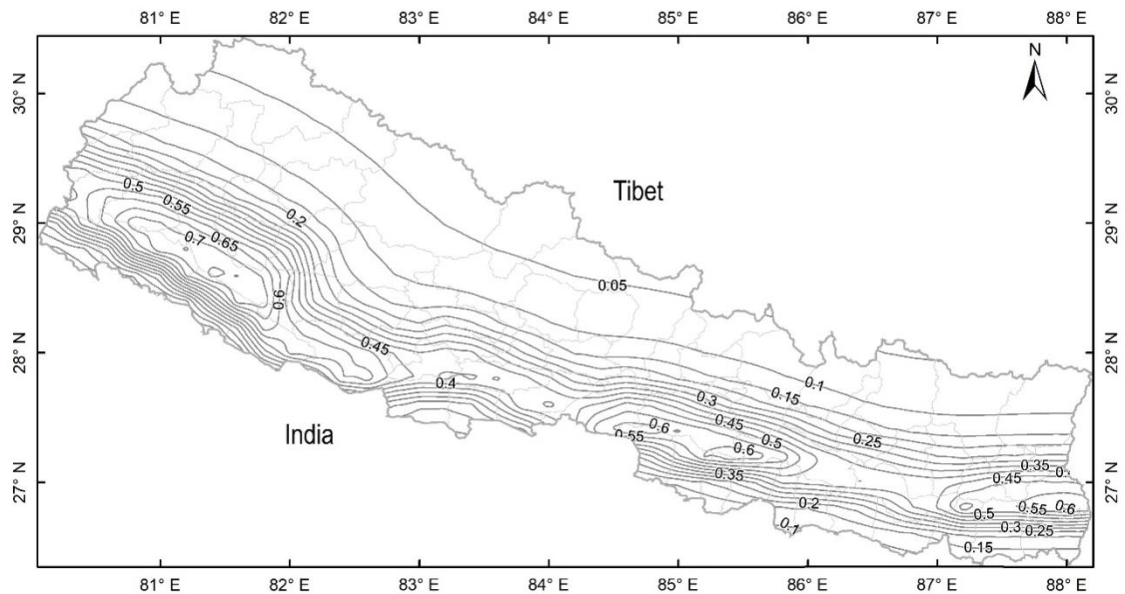
Appendix 20-4: seismic hazard map prepared using Model 4 (Appendix 11-4). The high hazard is in the southern part because of the geometry of the earthquake sources. The largest PGA is larger than 0.5 g in the far-west and larger than 0.4 in the Kathmandu Valley.
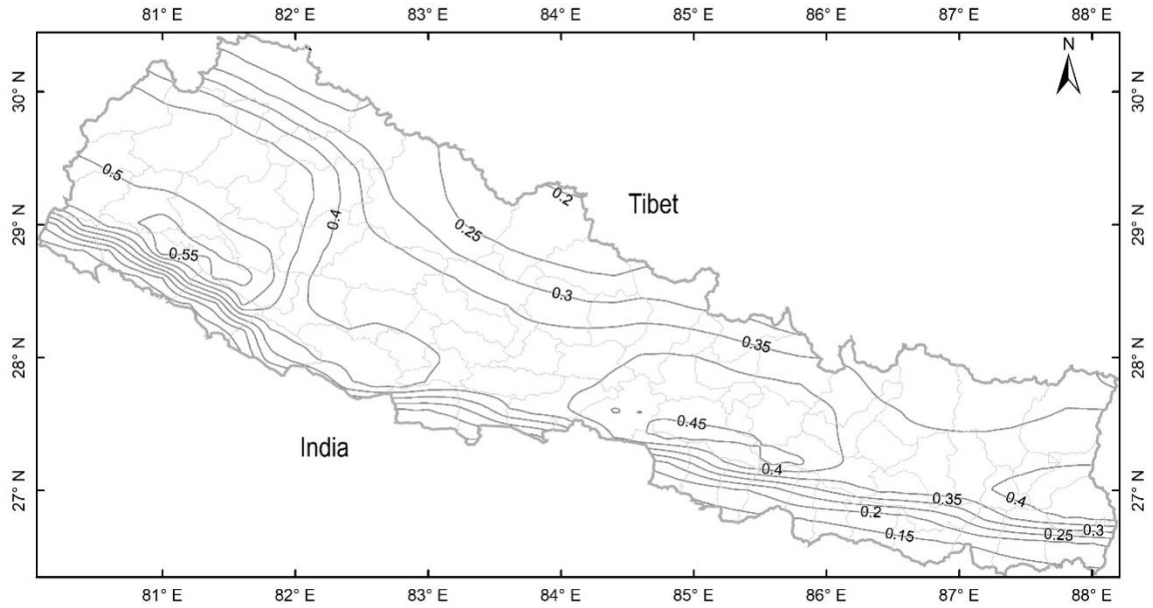
Appendix 20-5: seismic hazard map prepared using Model 5 (Appendix 11-5). The largest PGA is 0.4 g in the far-west and larger than 0.4 in the Kathmandu Valley.
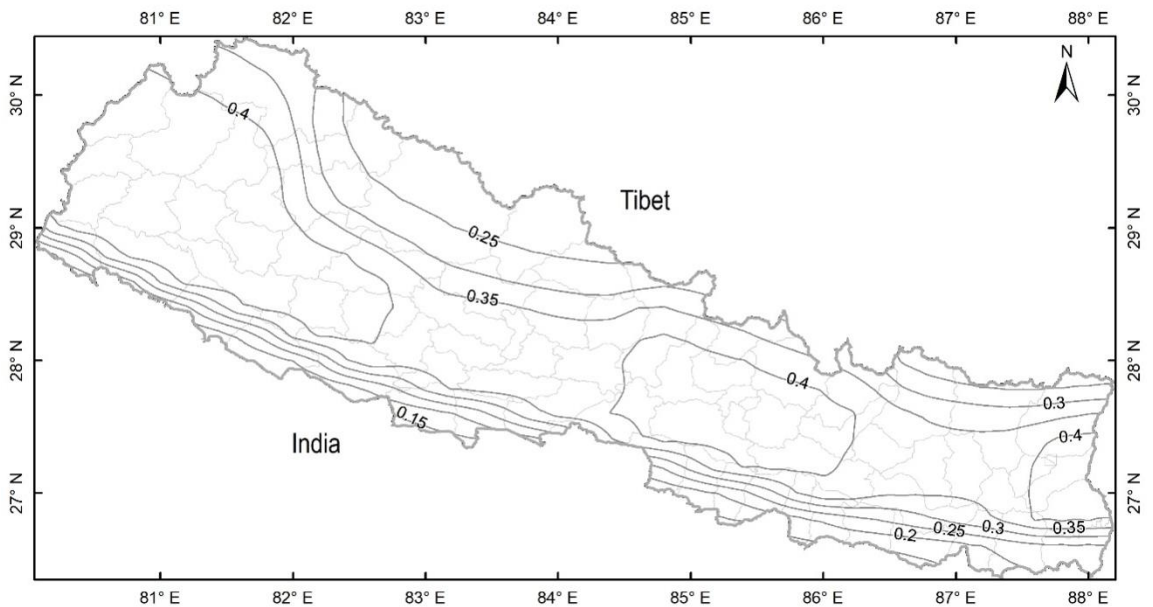
Appendix 20-6: seismic hazard map prepared using Model 6 (Appendix 11-6). The largest PGA is larger than 0.5 g in the southern part of far-west and larger than 0.4 in the Kathmandu Valley.
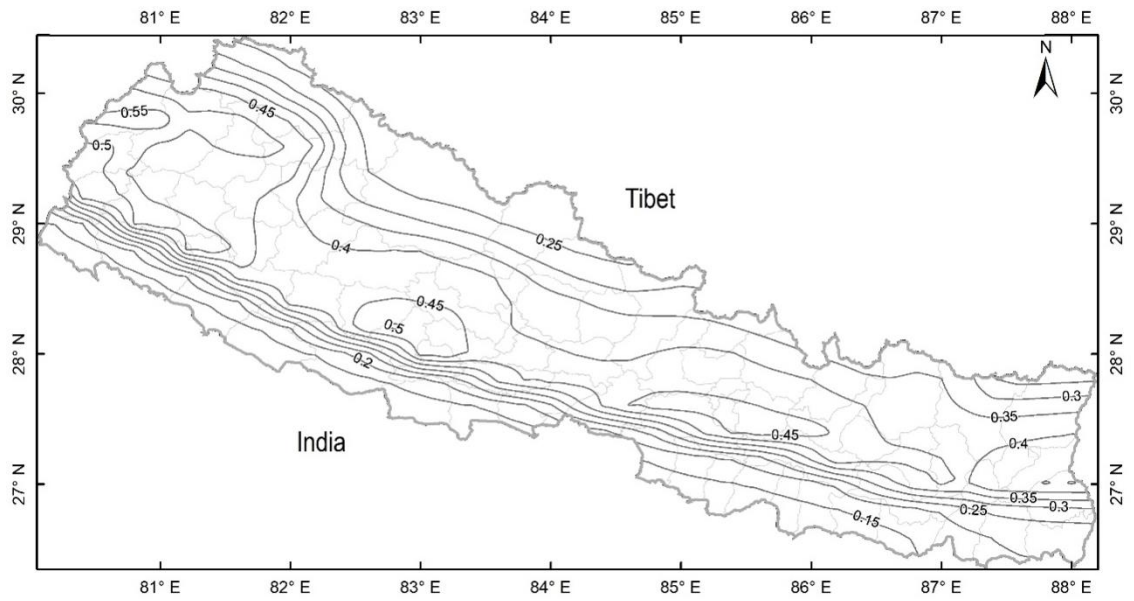
Appendix 20-7: seismic hazard map prepared using Model 7 (Appendix 11-7). The largest PGA is larger than 0.45 g in the southern part of far-west and larger than 0.35 in the Kathmandu Valley.
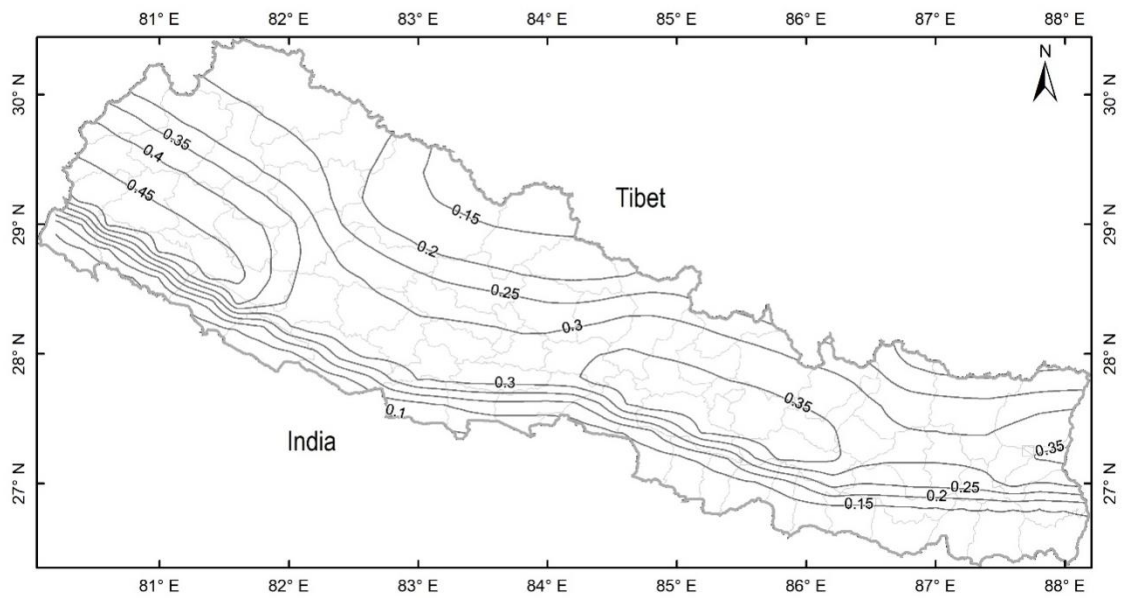
Appendix 20-8: Seismic hazard map prepared using Model 8 (Appendix 11-8). The high hazard is in the southern part because of hanging wall effect. The sources have 20 km fixed depth in the north and 10 km in their southern border. The largest PGA is 0.5 g in the far-west and larger than 0.4 in the Kathmandu Valley.
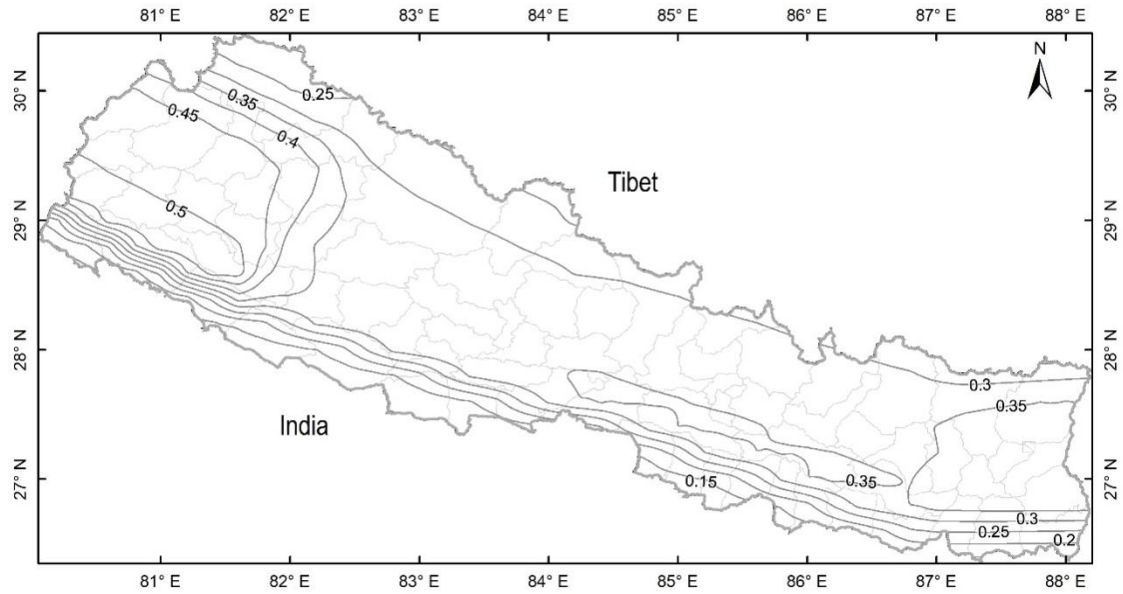
Appendix 20-9: seismic hazard map prepared using Model-9 (Appendix 11-9). The high hazard is in the southern part because of hanging wall effect. The largest PGA is 0.5 g in the far-west and larger than 0.4 in the Kathmandu Valley.
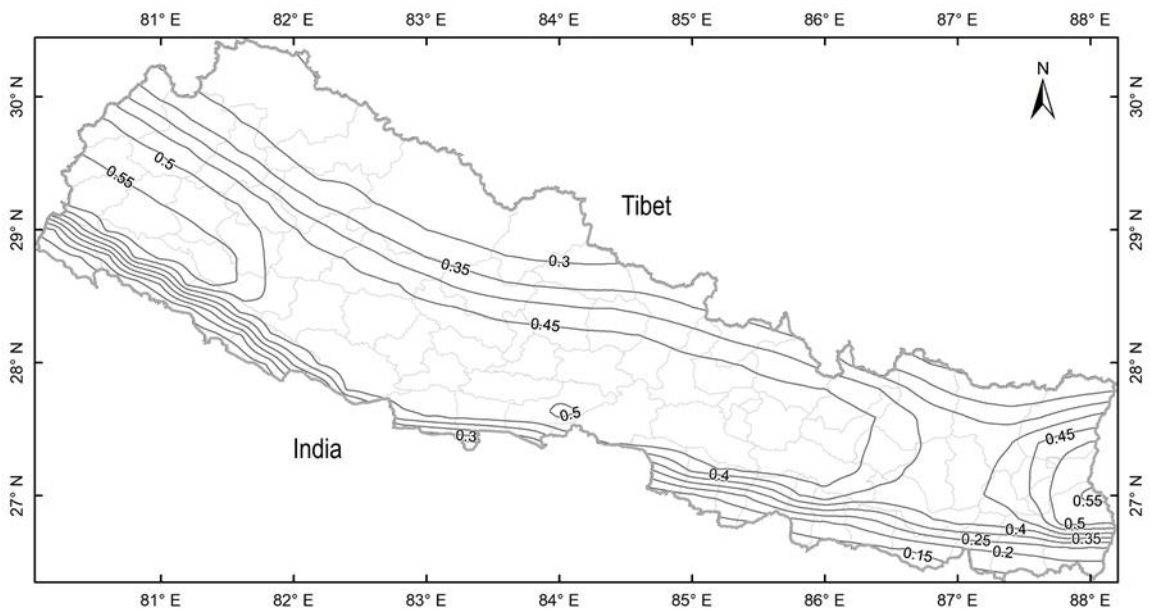
APPENDIX 21

Seismic hazard maps prepared using logic tree method.

The seismic hazard map (Appendix 21-1) was prepared using two sets of attenuation relations (Appendix 18-1 and 18-2). Attenuation relations as described in Appendix 18-1 were applied to segments of the MHT and its adjacent area in the south. The sources in South Tibet were applied the second sets of attenuation relation (Appendix 18-2). The six source models and two sets of attenuation relations, each were given equal weight to produce the final map (Figure 50). Fixed b-value and recalculated a-value were applied to prepare Appendix 21-1 utilizing earthquake catalogue since 1100 AD.

Appendix 21-2 is an example of seismic hazard map prepared ignoring Young's 1997 attenuation relation in Appendix 21-1.

Appendix 21-3 is another example of seismic hazard map, which was prepared using earthquake sources in South Tibet and North India. In this map the sources from the MHT were not used.

Appendix 21-1: Seismic hazard map applying logic tree method as mentioned above. The maximum PGA reaches 0.45 g in the far-west.
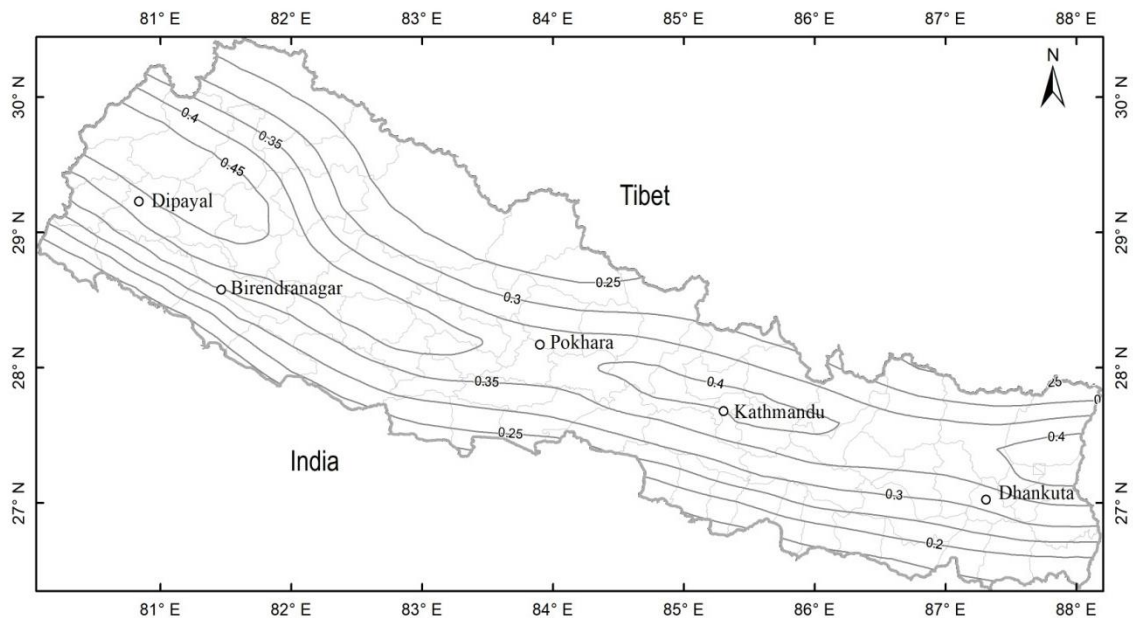
Appendix 21-2: Seismic hazard map applying logic tree method as mentioned above. This map was prepared following the process explained in Appendix 21-3, using Zhao *et al*. (2006) and BcHydro (2016) attenuation relations (Young's *et al*., 1997 attenuation relation was not used). The largest PGA is smaller than that in Appendix 21-3.
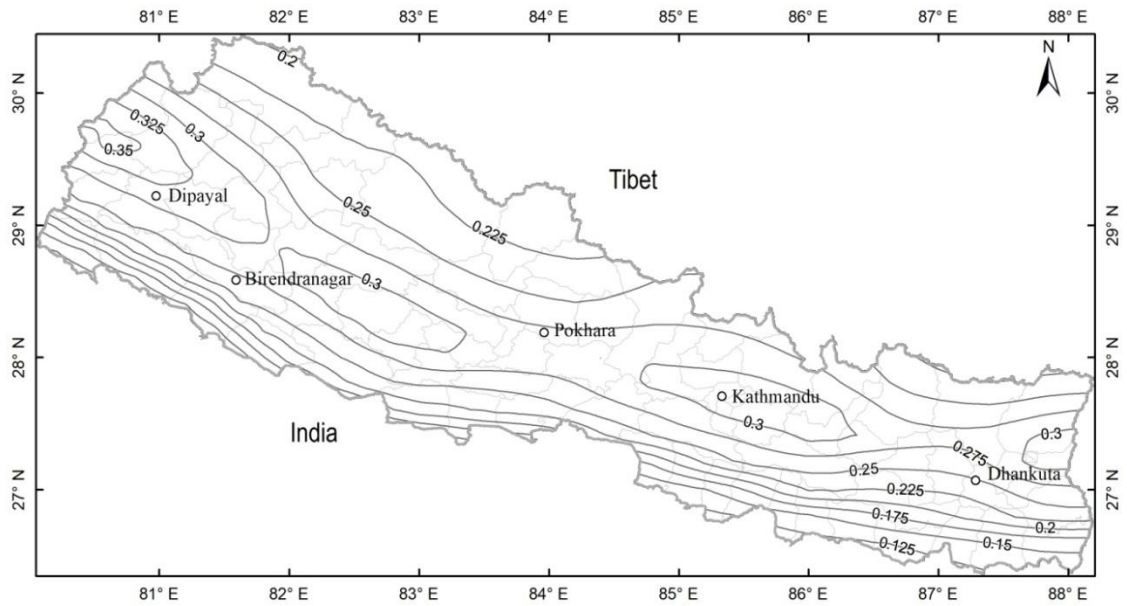
Appendix 21-3: Seismic hazard map applying logic tree method as mentioned above. This map was prepared without considering the sources from MHT in order to check the influence of other sources in Nepal.
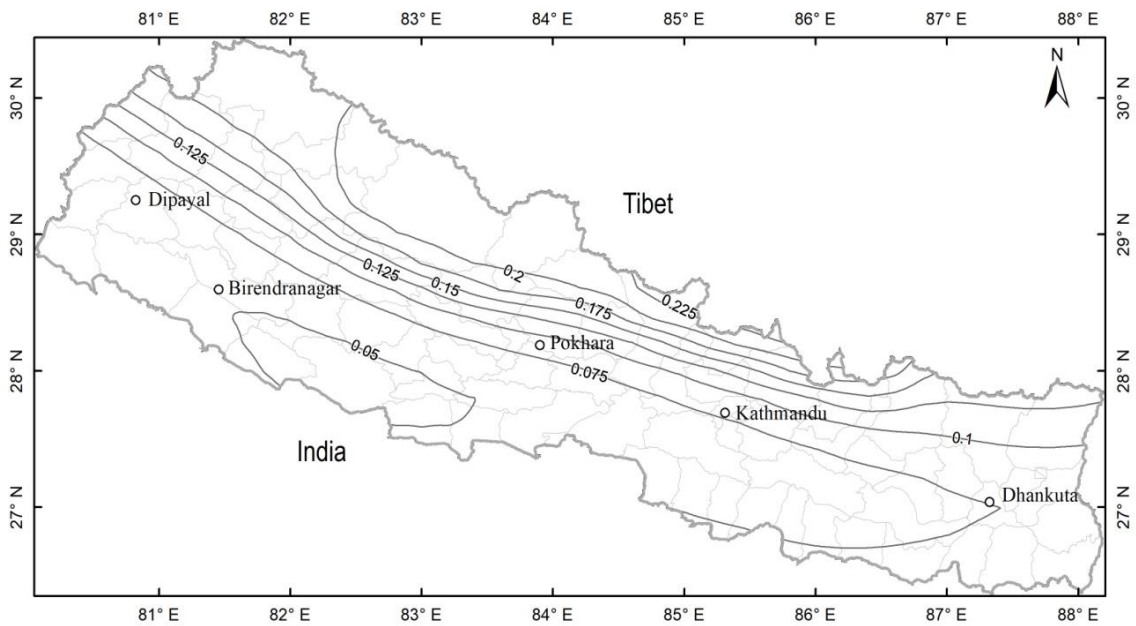
APPENDIX 22

Earthquake catalogue (Mw ≥ 5.5) compiled in this study

Year	Month	Day	Hour	Minute	Second	Latitude	Longitude	Depth	Mw
1100	1	15	8	43	25.6	26.885	86.589	NA	8.5
1255	6	7	NA	NA	NA	27.77	85.3	NA	7.8
1344	9	14	NA	NA	NA	27.5	87.5	NA	7
1408	8	0	NA	NA	NA	27.9	86	NA	6.5
1411	9	29	NA	NA	NA	30	90.2	NA	7.7
1681	1	0	NA	NA	NA	27.6	87.1	NA	8
1505	6	6	NA	NA	NA	29.5	83	NA	8.5
1664	0	0	NA	NA	NA	25	90	NA	7.8
1720	7	25	NA	NA	NA	30	80	NA	7.5
1751	0	0	NA	NA	NA	31.3	80	NA	7
1767	7	0	NA	NA	NA	28	85.5	NA	7.9
1803	9	1	NA	NA	NA	31.5	79	NA	8.1
1803	9	4	NA	NA	NA	29.6	87.8	NA	6
1819	6	27	NA	NA	NA	30.5	80.5	NA	6.2
1833	8	26	NA	NA	NA	27.7	85.7	NA	7.7
1845	8	6	NA	NA	NA	26.09	90.89	NA	7.1
1846	10	18	NA	NA	NA	25.07	90.37	NA	6.2
1849	1	22	NA	NA	NA	25.97	90.07	NA	6.1
1852	3	31	NA	NA	NA	28.09	79.17	NA	7
1866	5	23	NA	NA	NA	27.12	85.26	NA	7.4
1869	7	7	NA	NA	NA	27.7	85.3	NA	6.5
1869	1	9	NA	NA	NA	25.5	91.5	NA	7.1
1885	5	14	NA	NA	NA	30.5	91	NA	6.2
1897	6	12	NA	NA	NA	25.5	91	NA	8
1897	8	2	NA	NA	NA	25	90	NA	6.3
1944	10	29	NA	11	35	31.051	83.135	20	6.8
1945	6	4	12	8	59.7	30.218	80.082	15	6.4
1947	2	10	4	2	3.7	31.537	85.278	15	6.6
1951	5	28	15	59	23.7	28.926	86.685	15	5.9
1951	11	17	4	46	2.7	30.908	91.498	15	6.1
1951	11	18	9	26	37.3	30.799	91.413	15	6.8
1951	11	18	9	35	54.7	31.056	91.261	30	7.7
1951	12	26	10	7	0.4	31.244	90.784	15	6.3
1952	6	15	15	16	3.3	31.373	90.919	15	5.9
1952	8	17	16	2	14.5	30.648	91.601	25	7.5
1952	10	7	18	2	19.9	31.464	87.446	15	5.7
1952	11	19	10	23	32	29.682	86.506	15	5.8

1953	2	23	0	46	10.8	29.529	81.382	10	5.8
1953	8	29	1	58	29.2	28.168	82.333	15	5.8
1953	12	3	14	54	11.4	31.151	85.743	30	6.5
1954	2	23	6	40	35.9	27.672	91.605	15	6.2
1954	9	4	6	43	49.4	28.169	83.825	15	5.9
1955	3	27	14	38	48.2	29.671	90.166	15	5.9
1955	8	4	6	40	49.5	30.675	86.43	15	5.7
1955	9	20	20	21	13	27.5	90	15	5.9
1955	12	29	8	25	35.4	29.845	90.189	15	6
1956	6	12	3	12	30.4	25.029	90.853	15	6
1957	4	14	7	11	58	30.521	84.348	15	6.5
1957	4	22	1	42	22.9	30.841	84.297	15	5.9
1958	1	23	5	30	13.4	30.622	84.133	15	6
1958	10	28	10	46	33.7	30.472	84.553	15	6.2
1958	11	3	14	31	39.3	30.44	84.54	15	5.6
1958	12	28	5	34	41	29.926	79.9	15	6
1959	2	22	3	30	44.6	28.949	91.925	20	5.9
1960	7	29	10	42	47.6	26.488	90.297	15	5.7
1960	8	21	3	29	4.9	27	88.5	29	5.7
1961	12	24	7	13	27.6	29.512	80.806	15	5.9
1963	4	12	0	41	29.3	31.885	78.781	30	6
1963	11	27	21	10	25	30.8	80.5	33	5.5
1964	2	18	3	48	34.4	27.4	91.18	22	5.5
1964	4	13	3	19	57.3	27.52	90.17	1	5.5
1964	9	26	0	46	2.6	29.96	80.46	50	6
1964	10	6	20	19	32.1	29.4	80.98	11	5.5
1964	12	20	3	31	32.1	29.35	81.1	9	5.5
1965	1	12	13	32	24.1	27.4	87.84	23	6
1965	6	1	7	52	25.1	28.59	83.06	20	5.5
1966	3	6	2	10	52	31.51	80.55	5	5.6
1966	3	6	2	15	57.2	31.49	80.5	50	6.1
1966	6	27	10	41	8.1	29.62	80.83	33	6.1
1966	6	27	10	47	45.1	29.55	80.99	43	5.5
1966	6	27	10	49	51	29.5	80.9	72	5.6
1966	6	27	10	59	18.1	29.71	80.89	36	6.1
1966	6	27	13	55	49.3	29.62	80.93	18	5.5
1966	8	15	2	15	28	28.67	78.93	5	5.8
1966	12	16	20	52	16.3	29.62	80.79	19	5.9
1966	12	21	22	10	59.3	29.65	80.79	21	5.5
1967	9	15	10	32	44.2	27.42	91.86	19	6
1969	2	11	22	9	57	28.1	82.7	33	6.3
1969	2	13	10	23	54	28.2	81.8	33	5.5

1969	6	22	1	33	23	30.5	79.4	15	5.5
1970	2	12	1	51	48.4	29.24	81.57	25	5.5
1971	5	3	0	33	24.6	30.789	84.328	27.1	5.5
1972	7	22	16	41	2.1	31.377	91.414	17.3	5.6
1974	3	3	4	53	17.3	30.745	86.318	28.6	5.6
1974	3	24	14	16	1.1	27.664	86.003	20.4	5.6
1974	9	27	5	26	33.6	28.594	85.512	19.9	5.7
1975	1	19	8	12	9.8	31.937	78.525	48.6	6
1976	9	14	6	43	51.6	29.808	89.568	75.4	5.6
1977	2	19	6	15	25	31.797	78.432	40	5.6
1978	2	10	17	29	47.1	28.033	84.698	0	5.5
1979	5	20	22	59	11.6	29.932	80.27	15.8	5.9
1980	2	22	3	2	44.8	30.552	88.646	14.2	5.9
1980	7	29	12	23	7.7	29.339	81.214	3	5.9
1980	7	29	14	58	41.6	29.628	81.091	23.3	6.2
1980	11	19	19	0	44.6	27.402	88.797	1.3	6.1
1982	1	22	4	29	55.9	30.891	89.867	2.6	5.5
1982	1	23	17	37	29.2	31.675	82.284	25	6.1
1982	1	23	17	48	1.9	31.563	82.208	30.9	5.5
1984	5	18	4	28	52.2	29.52	81.793	0	5.8
1984	11	18	22	4	35.5	28.674	83.319	0	5.6
1985	1	7	16	13	5.4	27.14	91.958	12	5.6
1986	1	10	3	46	30.9	28.653	86.563	63.4	5.7
1986	6	20	17	12	47.2	31.216	86.824	33	6
1986	7	16	22	3	6.5	31.051	78.002	4.4	5.8
1986	9	9	16	24	21.8	31.54	85.046	0	5.6
1987	8	9	21	15	2.7	29.465	83.739	73.6	5.7
1988	4	20	6	40	25.8	27.017	86.721	55	5.6
1988	8	20	23	9	10.1	26.72	86.626	64.6	6.5
1988	10	29	9	10	52.7	27.866	85.637	18	5.7
1989	2	3	17	50	0.2	30.187	89.944	18.7	5.6
1990	1	9	2	29	21.8	28.154	88.108	35.5	5.9
1991	10	19	21	23	14.8	30.77	78.791	13.2	6.5
1991	12	9	1	2	42.5	29.512	81.611	2.9	5.8
1992	7	30	8	24	49.2	29.566	90.18	31.4	6
1993	1	18	12	42	4.5	30.844	90.378	10	5.9
1993	3	20	14	51	59.7	29.027	87.328	12.2	5.9
1993	3	20	18	13	26.4	25.88	90.68	19	5.9
1996	7	3	6	44	41.5	30.106	88.191	8.2	5.8
1997	1	5	8	47	24.5	29.874	80.565	24.9	5.6
1997	11	3	2	29	48.1	29.036	85.392	8.3	5.6
1998	7	20	1	6	1.1	30.175	88.245	57.9	5.5

1998	9	3	18	15	52.1	27.863	86.95	2.6	5.8
1999	3	28	19	5	12.3	30.511	79.421	22.9	6.4
1999	10	5	17	4	48	26.26	91.926	33	5.5
1999	10	8	14	52	12.9	31.286	79.437	15	5.5
2001	11	27	7	31	51.6	29.691	81.716	22.6	5.7
2001	11	27	8	53	53.8	29.641	81.704	25.7	5.5
2002	6	4	14	36	2.6	30.566	81.42	10	5.6
2004	7	11	23	8	41.8	30.719	83.666	8.1	5.8
2004	10	26	2	11	31	31.036	81.082	4	6
2005	4	7	20	4	40.2	30.517	83.655	14.7	6
2006	2	14	0	55	24.8	27.387	88.416	28.7	5.5
2006	2	23	20	4	54.5	26.958	91.712	14.9	5.6
2008	8	25	13	22	1.5	31.061	83.652	25.5	6.1
2008	9	25	1	47	12.2	30.84	83.586	10	5.6
2008	10	6	8	30	45	29.844	90.379	6.4	6.1
2008	10	8	14	7	15.4	29.768	90.336	2.4	5.5
2008	12	8	8	59	8.8	29.99	82.085	15.3	5.5
2009	7	24	3	11	57	31.169	85.963	13.3	6
2009	9	21	8	53	6.2	27.369	91.46	16.1	6.1
2009	11	7	20	8	49.2	29.539	86.045	21.4	5.8
2009	12	31	9	57	31	27.332	91.48	18.5	5.6
2010	2	26	4	42	38.1	28.507	86.776	79	5.7
2010	11	30	8	39	57.5	29.797	90.317	13.8	5.6
2010	11	30	12	40	27.6	29.688	91.248	0	5.6
2011	4	4	11	31	41.1	29.626	80.729	17.4	5.8
2011	9	18	12	40	49.6	27.804	88.154	29.6	6.6
2014	3	30	17	10	14.7	31.345	86.472	12.6	5.5
2014	3	30	17	17	23.8	31.518	86.585	0	5.5
2014	3	30	17	40	31.4	31.294	86.269	10	5.5
2015	4	25	6	11	26.3	28.28	84.79	15	7.8
2015	4	25	6	11	33	27.794	85.339	8	6.8
2015	4	25	6	15	3.1	27.443	85.074	0	6
2015	4	25	6	15	22.9	27.628	85.54	10	6.2
2015	4	25	6	17	57.4	27.641	85.758	0	5.5
2015	4	25	6	18	10.9	27.686	86.021	10	5.8
2015	4	25	6	20	40.3	28.205	84.492	10	5.6
2015	4	25	6	45	22.1	28.39	84.83	15	7.1
2015	4	25	6	45	29.3	27.86	84.93	21	6.7
2015	4	25	6	56	33.9	27.882	85.751	10	5.7
2015	4	25	8	55	56	27.587	85.506	10	5.5
2015	4	25	9	17	2.3	28.39	87.317	10	5.9
2015	4	25	17	42	50.9	28.238	85.829	10	5.6

2015	4	25	23	16	15.5	27.82	84.89	9	5.7
2015	4	26	7	9	10.7	27.771	86.017	22.9	6.7
2015	4	26	7	9	24.2	26.923	87.064	10	6.2
2015	4	26	16	26	5	27.856	85.753	17	5.9
2015	5	12	7	5	19.7	27.809	86.065	15	6.8
2015	5	12	7	5	34.2	26.861	87.136	10	6.6
2015	5	12	7	17	20.6	27.714	86.218	13	5.7
2015	5	12	7	34	22.6	27.746	86.245	10	5.6
2015	5	12	7	36	54.5	27.625	86.162	15	6.3
2015	5	12	7	37	5.1	26.917	86.895	10	6
2015	5	16	11	34	10	27.56	86.073	7	5.9
2015	5	16	11	34	24	26.696	87.031	10	5.6
2015	6	28	1	5	28.6	26.638	90.41	26	5.7
2015	9	8	13	27	19.6	26.485	85.964	326	5.6
2015	12	18	22	16	56.5	29.399	81.654	10	5.6
2016	11	27	23	35	21	27.802	86.532	10	5.6